

**DIRECT- AND
RECIPROCAL SPACE
STRUCTURE MODELLING**
CONTRIBUTIONS TO THE ADVANCED
UNDERSTANDING OF INCLUSION
COMPOUNDS

by

STIAN PENEV RAMSNES



Thesis submitted in fulfilment of the
requirements for the degree of
philosophiae doctor

Department of Mathematics and Physics
Faculty of Science and Technology
UNIVERSITY OF STAVANGER

MMXXII

University of Stavanger
NO-4036 Stavanger
NORWAY

www.uis.no

© 2022 Stian Penev Ramsnes

ISBN 978-82-8439-081-9

ISSN 1890-1387

PhD: Thesis UiS No. 644

In memory of my dear grandmother, «babo»,



Jivka Peneva

1931-08-17 — 2019-04-08

Table of contents

Table of contents	v
Preface	vii
Acknowledgements	xi
Summary	xiii
I The Thiourea-Ferrocene Inclusion Compound	15
1 Structure and phases	19
1.1 The history of ferrocene	19
1.2 Structure and phase transitions of ferrocene	20
1.2.1 Challenges regarding the centrosymmetry	20
1.2.2 Eclipsed and staggered conformations	21
1.3 Host-guest inclusion complexes	22
1.4 Thiourea as a host	23
1.4.1 Connection between temperature and disorder	24
1.4.2 The honeycomb lattice	24
1.5 Dynamics and phases of thiourea-ferrocene	25
1.5.1 Possible orientations of the guest molecules	25
1.5.2 Fluctuations of the orientations	26
1.5.3 Temperature-induced phase transitions	27
1.5.4 Comparison with similar structures	28
2 Reciprocal space	33
2.1 Experimental details	33
2.2 Qualitative investigation of single crystals	35
2.2.1 Sample 1 – Obverse-reverse twin ($\Sigma 3$)	36
2.2.2 Sample 2 – Untwinned crystal	42
2.2.3 Sample 3 – Plesiotwin ($\Sigma 7$)	47
2.3 Summary of observations	53
3 Structure solutions	57
3.1 Pure ferrocene	57
3.2 Thiourea-ferrocene inclusion compound	59
3.2.1 Data analysis of the TFICs	60
3.2.2 Structure solution statistics and conclusions	69
II The Mathematica X-ray Diffraction Package	75
4 The MaXrd package	79
4.1 The beginning	79
4.1.1 Why Mathematica?	79
4.1.2 The initial purpose and vision	80
4.1.3 A quick tour of the package	82
4.2 Model utilities	83
4.2.1 Perturbation options	85
4.2.2 Domains	86
4.2.3 Simulation of diffraction patterns	87
5 Simulations	91
5.1 Category A: Simple models	94
5.2 Category B: Literature models	97
5.3 Category C: Particular orderings	102
5.4 Category D: Models of twinning	108
5.5 Category E: Domains	112
5.6 Summary of the modelling results	127
6 Concluding remarks	131
6.1 Discussion and results	131
6.1.1 Information conveyed by the data	131
6.1.2 The main phase transition event	132
6.2 Future work	134
Appendix	137
A Oriented crystal associations	138
B MaXrd Change log	144
C Poster contribution at ECM ₃₂	154
Publications	155
Publication 1	156
Publication 2	161
References	167
List of symbols	171
Index	173

Preface

The compound

«If you had more time, what would you continue working on?» is one of those typical questions following the end of a project, and something along the line of what I was asked in my master's examination. The master's project was initially centred around dynamical diffraction, and beamtime at the ESRF was granted for a three-beam diffraction study in addition to a thiourea-ferrocene temperature study. Findings in the latter experiment intrigued us, and the remainder of my master's thesis became dedicated to examination of the collected data. Afterwards, it was clear that a lot of questions were still unanswered; a complete and satisfactory understanding of the thiourea-ferrocene system was not yet realised. The first chapter in this document covers the host and guest in question.

With the PhD position secured, the study on the compound's structural phase transitions could be continued. In fact, this project unintentionally became the only actual material-specific study in my PhD research, if we consider the programming to be categorised as «method development». I remember one meeting with my supervisors and David Graham Nicholson in particular. It was in the autumn of 2016, very early in my PhD employment. Optimism was high. David was drawing parallels between the elusive thiourea-ferrocene and the pioneering work on the DNA structure. Much of the work has since been thoroughly revisited numerous times to ensure all the measured data will have the chance to «tell its story». This brings us to the opening question: in my answer, I mentioned something along the lines of simulations being one of the crucial paths forward in order to cut through the complexity and to delve deeper into understanding this compound. Continued development on the Mathematica package has been very gratifying and educational to me. Today, simulation capabilities are in place and countless models have been put to the test. Yet, there is always something to reach for and investigate.

Since a large portion of the thesis has been committed to the thiourea-ferrocene inclusion compound, each chapter in the main body starts with an image related to the crystal. These depict *ab*-planes in reciprocal space at various temperatures, converted to greyscale to mimic traditional X-ray film recordings. The reciprocal planes shown, all taken at 100 K, are of:

Chapter 1	(<i>hk</i> 0) plane for TFIC-2
Chapter 2	(<i>hk</i> 3) plane for TFIC-3
Chapter 3	(<i>hk</i> 1) plane for TFIC-1
Chapter 4	(<i>hk</i> 2) plane for TFIC-1
Chapter 5	(<i>hk</i> 3) plane for TFIC-1
Chapter 6	(<i>hk</i> 4) plane for TFIC-1

where the TFICs denote three different samples. Hopefully, these images may serve to inspire the reader, and be a reminder of the intricacy at play.

Note that in the digital version of this thesis, clicking the page numbers in the footer or the chapter name in the header will redirect the reader back to the Table of contents.

The package

In the era we live in, much of the abstract work takes place in digital domains, with a lot of the equations and ideas being conveyed in form of computer code instead. This thesis is therefore devoid of much mathematics; being implicitly contained «under the hood» in the change log (Appendix B) of the Mathematica package instead. A short story about the package is found in Section 4.1.

Arguably, I may have spent too much time sharpening the pencils when I should have been drawing. It is important to find a balance between writing more code, and spending time actually trying to solve the problem at hand. The only ready articles to date are about the tool, and the final article, concerning its application to a real case, is «on the way». As the case is when scientists program instead of computer engineers, the code is susceptible to shortcomings, but the package has become something I am proud and fond of. One can always hide behind the great saying:

*Premature optimization is the root
of all evil (or at least most of it) in
programming.* — Donald Knuth

written by the famous computer scientist Donald Knuth,^[43] referring to the pitfall of spending too much time improving parts before they have actually proven their usefulness.

The procrastination

In retrospect, I may have been struck with some type of «analysis paralysis» and «impostor syndrome», causing a seemingly endless drain of motivation and lack of concrete results. Or perhaps I have always been a talented procrastinator, and have just taken it to a «PhD level». In any case, after spending a year and a half overtime on this endeavour, I am fairly certain I cannot recommend it to anyone.

Maybe it is as founding member of Queen and astrophysicist Brian May put it:

*Astronomy is much more fun when
you're not an astronomer.* — Brian May

(He has truly mastered the art of procrastination, technically taking 36 years to complete his PhD.^[73])

If I could give my past self just one piece of advise (and quitting was not an option), it would have to be: *strike while the iron is hot.*

A handwritten signature in black ink, reading "Stian Penev Ramsnes". The script is cursive and elegant, with the first letters of each name being capitalized and prominent.

Stian Penev Ramsnes
Stavanger, 2022-02-22

Acknowledgements

I am very thankful to the University of Stavanger and the Norwegian Research Council for the opportunity to pursue this assignment, and for being able to spend plenty of time to code and to bring the thesis to completion. It has been an experience with a lot of freedom and room for personal growth.

I am also grateful for the chances to travel abroad and participate at conferences and workshops in France, Spain and Austria, from which I have only fond memories. In the course of this thesis, the meetings with Gunnar Thorkildsen, Helge Bøvik Larsen and David Graham Nicholson were always a pleasure, and they always left me inspired and ambitious—without exception. An extra acknowledgement is in order for my supervisor, Helge, whose patience and support during this thesis has been remarkable. Helge has truly been a stable and inexhaustible dispenser of motivation. Finally, I am glad for the good memories with my colleagues, both inside and outside the office.

There are of course some very important people outside the university who deserve some praise: I thank my parents for being my favourite role models, and my brothers for being around and helping me take breaks. I have nonetheless saved the greatest thanks to the end: to my wife and dearest companion, Lena, whose support and love I am eternally grateful for.

Summary

The main content of this thesis falls naturally into one of two parts. The chapters come in an order which follows the research development, but encapsulates single topics enough to allow the reader some flexibility. In short, this work concerns the study of one particular inclusion compound, and all the programming utilities that have been developed in an attempt to tackle this structure as well as others like it. We have sought to gather more details about what happens to the structure in the midst of a chaotic phase transition. This has been done by a non-standard approach of diligent entity construction, seeking to bring a model to perfection by invoking direct space modelling with reciprocal space validation. The idea is simple, but has proven more difficult to conduct to an end.

Part I comprises the structural information and data analysis of the central analysis subject: the thiourea-ferrocene inclusion compound (TFIC). It is divided into chapters with a logical progression: starting with a background on host-guest inclusion complexes and details on the TFIC from the literature in Chapter 1. Then, our experimental details and qualitative investigation is compiled in Chapter 2. The next step is data reduction and structure solutions, covered in Chapter 3. Some background theory and information on twinning is covered in Appendix A.

Part II starts off with a presentation of the developed Mathematica package in Chapter 4. The reader will learn what it is and how it may serve as a utility in the field of crystallography. Its origin, functionality and purpose will be examined in a summary of its two articles. The subject of model construction will be emphasised, and the thesis will culminate with demonstrations of its capability in Chapter 5 where models are tailored to the specific TFIC system. The associated simulations of the diffraction patterns are compared with experimental counterparts in order to ascertain what characteristics may be ascribed to the structure during the prominent phase transition; discussions that bring the separate topics together are made in the concluding Chapter 6, which summarises the most important findings on the TFIC.

The following work (published, or to be published) comprises this thesis, listed chronologically:

- I Stian Ramsnes, Helge Bøvik Larsen and Gunnar Thorkildsen. ‘Using *Mathematica* as a platform for crystallographic computing’. In: *Journal of Applied Crystallography* 52.1 (Feb. 2019), pp. 214–218. DOI: [10.1107/S1600576718018071](https://doi.org/10.1107/S1600576718018071) (see page 156)
- II Stian Penev Ramsnes, Helge Bøvik Larsen and Gunnar Thorkildsen. ‘*MaXrd* updated with emphasis on model construction and reciprocal-space simulations’. In:

Journal of Applied Crystallography 53.6 (Dec. 2020), pp. 1620–1624. DOI: [10.1107/S160057672001328X](https://doi.org/10.1107/S160057672001328X) (see page 161)

III Stian Penev Ramsnes et al. ‘Complementary Synchrotron Diffraction and Simulation Studies on a Ferrocene:Thiourea Inclusion Compound’. To be published. 2022

The first paper concerns the release of the Mathematica X-ray diffraction package (MaXrd). In essence, it contains point- and space group information from the International Tables for Crystallography and tabulated data on scattering factors and cross sections, required for calculations related to X-ray physics. Included are also functions to utilise this data, with a documentation demonstrating their usage. Highlighted functionality includes extraction of symmetry data, data import from cif files, calculations of structure factors, linear absorption coefficients and unit cell transformations.

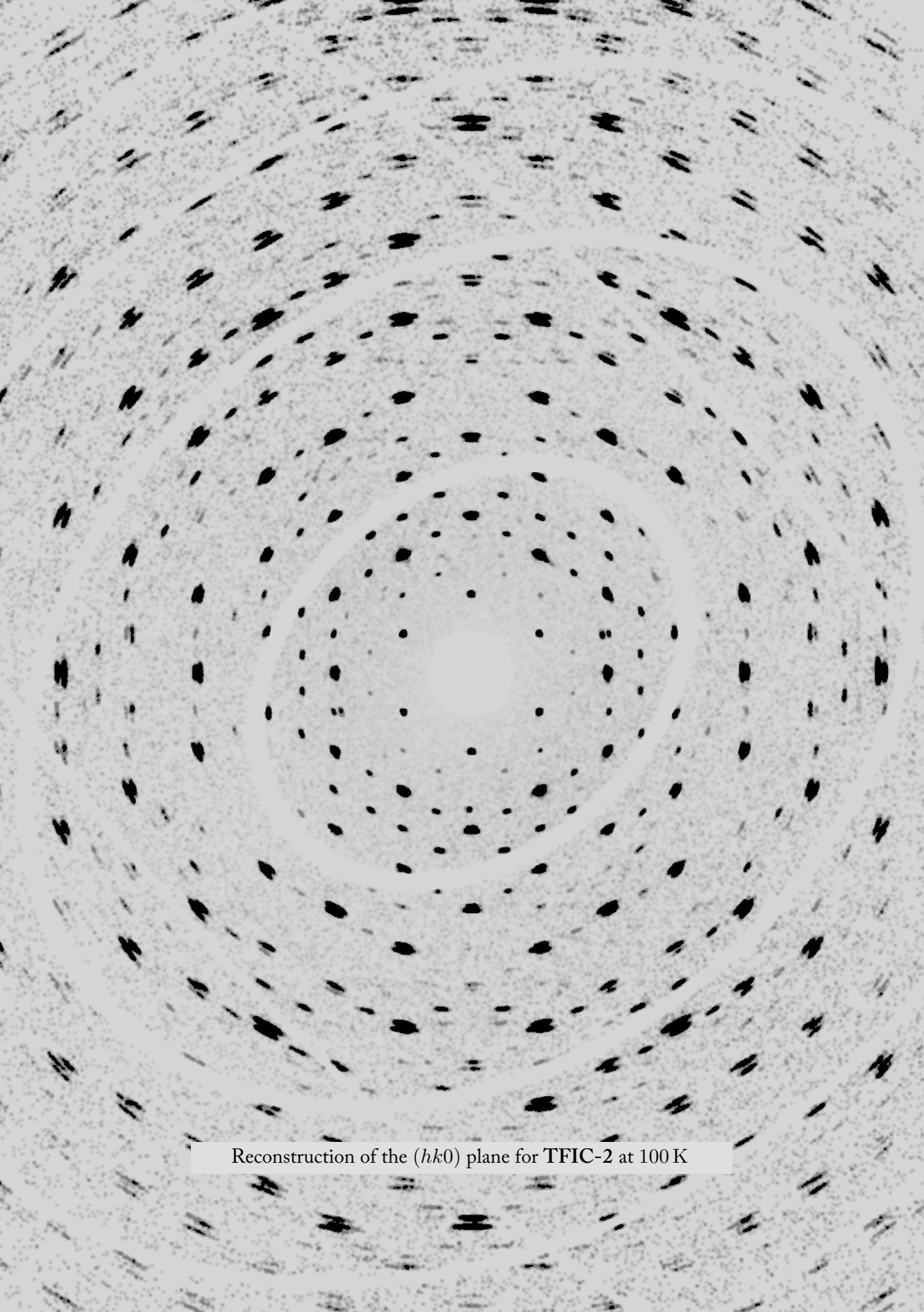
The second article was submitted once a practical structure modelling extension had been sufficiently generalised. The imported cif data could now be employed to create and visualise crystal structures. Many additions depended on the original symmetry-related foundation, but a few brought novel concepts into the package, such as the function for making domains. The focus on model construction was motivated by the study of a host-guest complex, hence the ability to embed one crystal entity into another. With the possibility to simulate the diffraction patterns (reciprocal space maps), a way of comparing a customised structure with experimental data was realised.

The third article conveys our findings on the thiourea–ferrocene inclusion compound. Complementary studies have been conducted in three areas: qualitative exploration of reciprocal space, quantitative structure solutions of synchrotron data and various model investigations with the MaXrd utility package in Mathematica. We discuss both supporting evidence and shortcomings of the prevalent high- and low-temperature phases of the TFIC structure.

It is said that if you’re unable to provide a clean and short explanation on a subject, you don’t understand it well enough. In any case, capturing the thesis in a single sentence is a good exercise. Since the first part is about method development, a conclusive remark does not fit as much as for the second part, for which a fitting and simplistic one-liner conclusion for the layman may be:

*The cold makes the guest molecules inside the
honeycomb network halt their motion and shatters the
neat pattern, but heating it makes everything fine
again, even if the crystal was a twin to begin with.*

Part I
*The Thiourea-Ferrocene
Inclusion Compound*



Reconstruction of the $(hk0)$ plane for TFIC-2 at 100 K

Structure and phases

1.1 The history of ferrocene

As with many things in science, the discovery of *ferrocene*, $\text{Fe}(\text{C}_5\text{H}_5)_2$, happened by accident. Peter Pauson and his student Tom Kealy were to make pentafulvalene—two five-membered carbon rings connected by one carbon–carbon double bond—but were surprised by the stability of the resulting orange compound. In their proposed planar/linear structure an iron atom was situated between the two rings. Pauson and Kealy were the first to publish on this new compound at the end of 1951^[40] (although another team submitted a report on this first^[49]). Figuring out the correct structure of ferrocene is ascribed to two other independent groups:^[9,68] One being led by Geoffrey Wilkinson and Robert Woodward at Harvard University^[97] the other by Ernst Otto Fischer at the Technical University of Munich.^[59] From an infrared absorption spectrum Wilkinson et al. deduced that only one type of C–H bond was present. Moreover, they found the crystal to be diamagnetic and that it had zero dipole moment. With X-ray analysis carried out in 1952 by Eiland and Pepinsky^[24] and Dunitz and Orgel in 1953^[19] and 1955,^[20] the characteristic hourglass shape seen in Figure 1.1 was ascertained.

Fischer used the term *double cone* (*doppelkegel*) structure^[61] while the two at Harvard and Jack Dunitz used the term *sandwich structure*, which stuck. We refer to sandwich compounds as a subclass of organometallic compounds where a metal atom is positioned between two organic rings that are planar and parallel. If the rings are five-membered we can specify them further as *metallocenes*. It is Woodward who coined the name ferrocene, using the suffix *-ene* to betoken its aromatic character.^[61]

Fischer and Wilkinson shared the 1973 Nobel Prize in Chemistry for pioneering work with sandwich compounds.

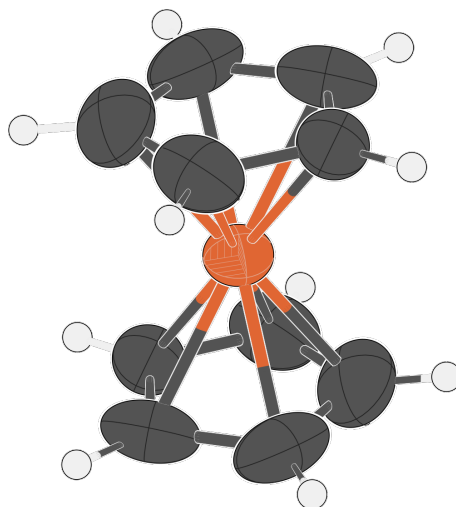


Figure 1.1: Rendering of the ferrocene molecule. The asymmetric unit is grown to show both cyclopentadienyl rings, appearing centrosymmetric due to the space group symmetry. See Section 3.1 for more details on the structure solution.

1.2 Structure and phase transitions of ferrocene

Ferrocene is found in a monoclinic cell ($P2_1/a$) at ambient conditions. When cooled it becomes triclinic ($P\bar{1}$) at 164 K and orthorhombic ($Pnma$) below 110 K to 90 K, with the lattice parameters changing continuously.

The crystal is deep orange at room temperature, becomes light orange when it approaches the triclinic transition before turning lemon yellow in this phase[†], and from there it becomes more greenish with lower temperature^[85] and finally turning brownish in the orthorhombic phase.^[62] Disintegration of the crystal has been observed in the interval 108 K to 125 K; the exact temperature of fracture depends on the crystal size^[60] and the cooling rate.^[6]

Ascertaining whether the two cyclopentadienyl rings are eclipsed, staggered or something in between has proven to be challenging with conflicting evidence. For an isolated molecule the energetically favoured conformation is eclipsed, which is about 4 kJ/mol lower than staggered.^[10,63]

Subjecting ferrocene to a pressure of 3.24 GPa will transition it into a phase where the molecules are crammed into staggered configurations. The space group remains the same (also up to the end of measurement at 11.6 GPa), but the structure is now ordered. A discontinuity in the unit cell c parameter is observed.^[63]

See Section 3.1 for our own structure solution.

1.2.1 Challenges regarding the centrosymmetry

Dunitz et al.^[20] first concluded with a staggered conformation at room temperature. A noticed smearing of the electron density was explained by a combination of experimental error and slight deviations of the ligands' average positions. Besides, it was the choice compatible with the molecular inversion centre required by the space group. 23 years later Seiler and Dunitz published a new interpretation of this structure, also taking into account other propositions in the literature.^[83]

The revised conclusion is that the monoclinic high-temperature phase is disordered. A long-range order of the cyclopentadienyl rings that the triclinic lattice possesses is lost. Only one such ring is seen in the asymmetric unit; the average of four symmetry-independent (from two molecules) in the triclinic phase.

In 1959 Edwards et al.^[23] measured a peak in heat capacity at about 164 K indicating a phase transition, found to be triclinic by Seiler and Dunitz.^[83] Below this temperature all the cell lengths double; molecules are no longer exactly related in terms of (the monoclinic) lattice translations. The two independent ring pairs in the asymmetric unit differ

[†]The change in colour of the thiourea–ferrocene inclusion compound matches that of pure ferrocene (at least down to 100 K).

slightly in their orientations as well as their centres, which causes the mentioned smearing. Studies with single crystal neutron diffraction confirm the rotationally disorder in addition to revealing that the hydrogens are displaced slightly (5° ^[7]; $1.6(4)^\circ$ ^[92]) out of the cyclopentadienyl plane towards the central iron atom[†].^[92]

Below 110 K the orthorhombic lattice is formed, which is practically isomorphous to that of ruthenocene.^[84] It appears to be possible to skip the intermediate triclinic phase when warmed, reaching the monoclinic phase in the range 242 K^[60] to 275 K.^[62]

1.2.2 Eclipsed and staggered conformations

Measurements of how much the couple of cyclopentadienyl rings are twisted in relation to each other are also reported. If 0° marks the eclipsed conformation and 36° staggered, they are perfectly eclipsed in the coldest, orthorhombic phase. The amount is circa 9° in the triclinic phase, increasing by one degree when it approaches 148 K,^[5,85] arriving at around 24° in the monoclinic state.^[63,92] As stated previously, all molecules are staggered in the pressure-induced phase, becoming truly centrosymmetric.

Since the barrier height for internal rotation is relatively small, intermolecular packing forces have been suggested to dominate the configurations.^[29,85] At 400°C , in gas phase, this barrier is practically zero.^[82]

[†]Willis^[98] placed the hydrogens in plane with the carbons, but Takusagawa and Koetzle^[92] comment that the neutron data were somewhat limited in resolution.

1.3 Host–guest inclusion complexes

Since this part of the thesis concerns the study of a particular inclusion compound, it would be a good idea to start with a few definitions. We will conform to the nomenclature used in Herbstein’s book *Crystalline Molecular Complexes and Compounds, volume 1*.^[34]

We consider two-component compounds where one component is contained within the other: an *inclusion compound*, and refer to the distinct parts as *host* and *guest*. If each component is relatively easily discernible and mostly retain their individual properties it can be called a *binary adduct*. A binary adduct can be further subdivided into two groups depending on which type of interaction plays the dominant role in the structure’s integrity: *molecular compounds* are governed by host–guest interactions, whereas the structure of *molecular complexes* is primarily determined by interactions between components of the same type.

Inclusion complexes are considered a subtype of molecular complexes where host–host couplings are dominant. They can be symbolised on the form {host·[guest]}, so our compound of interest becomes {3(thiourea) · [ferrocene]} or {3 SC(NH₂)₂ · [Fe(C₅H₅)₂]}, although spelling out the name or using the acronym TFIC (thiourea–ferrocene inclusion compound) will be preferred in this text. Simply using «guest/host», e.g. ferrocene/-thiourea, is also common.

The main connection mechanism between all combinations of hosts and guests is van der Waals forces. Hydrogen bonding may also occur in the host framework, and guest-to-guest interactions can typically be neglected, though it is noted that two parallel ferrocenes would have an intermolecular distance of just 2.88 Å.^[37]

Finally, we discern subtypes of inclusion complexes based on the dimensionality of the void for the entrapped guest phase. Guest molecules can be «caged» at fixed points throughout the crystal (dimensionality zero) being enclosed by the host lattice in every direction. This is known as a *clathrate*. If the guests are unobstructed in one dimension, we have a *tunnel inclusion complex* (*channel* is also used), as is the case with thiourea–ferrocene. Guest molecules may also be situated between two-dimensional layers of host molecules; a famous example is intercalation of potassium into graphite.

Inclusion compounds are diverse with matching usability. Catalysis is a frequent application, and those with tunnel networks can function as separators, e.g. divide linear molecules from branched ones, filter different enantiomers of the guest, or confinement in general. There is also potential for new composite materials where polymers are embedded to make wires.^[3, p. 227] With appropriate organometallic guests thiourea inclusion compounds can also have optical applications through so-called second-harmonic generation (doubling of the light frequency passed through) or as a dichroic filter for polarised

X-ray radiation.^[3, p. 1505] Combination of linear shaped guests and host channels of perhydrotriphenylene have produced nonlinear optical systems.^[38]

1.4 Thiourea as a host

The room temperature structure of *thiourea* was solved as far back as in the early 1930's.^[99] Its use for tunnel inclusion compounds was first discovered in 1947,^[34, p. 205] and the first publication on inclusion of ferrocene seems to be from 1974.^[14]

Pure thiourea, SC(NH₂)₂, crystallises in an orthorhombic lattice with space group *Pnma* (number 62) above 202 K and *Pmc2₁* (number 26) below 169 K.^[2,45] There are three intermediate phases between the two temperatures in which the polarisation characteristics change. It is ferroelectric in the coldest phase and paraelectric at room temperature.^[91] There is also a high-pressure superstructure phase around 0.35 GPa with a threefold *c*-axis.^[2] Another transition at 0.54 GPa has been proposed, but not confirmed.^[93]

In general, and in the case of urea and thiourea, the crystal structure of inclusion complexes are different from what the pure host structure normally is and do not necessarily maintain the structure when the guests are removed (then referred to as a *soft host*). The size and shape of the molecules constituting the guest phase determine the formation of inclusion complexes.^[96] Too large and they won't fit; too small and they «fall through». As an example of suitable guests for thiourea, consider the metallocenes ferrocene, nickelocene and ruthenocene. Despite all being metal ions sandwiched between a couple of cyclopentadienyl ligands and having similar bond distances[†], ferrocene forms an inclusion while the other two do not. Nickelocene can be clathrated with thiourea if mixed with ferrocene (up to Ni/Fe \approx 0.4),^[35] but clathration of ruthenocene will not happen.^[14]

At room temperature it is common for thiourea to form rhombohedral structures with guests that are shaped isotropically, typically with space group *R $\bar{3}c$* and $a = 15.5\text{--}16.2 \text{ \AA}$ and $c = 12.5 \text{ \AA}$ in a hexagonal description. See Figure 1.2.

Comparing this range with thiourea–ferrocene's $a = 16.36 \text{ \AA}$ ^[18] it seems that the ferrocene guests give the thiourea host a discernible push in the planar direction.

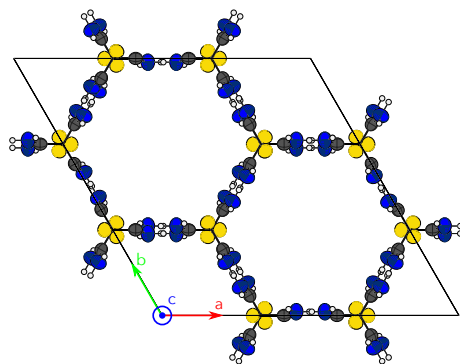


Figure 1.2: The unit cell of the characteristic honeycomb shape of thiourea as a host in the high-temperature phase, here with guests evicted for clarity.

[†]Fe–C = 2.064 Å, Ni–C = 2.196 Å, Ru–C = 2.21 Å.^[14]

1.4.1 Connection between temperature and disorder

A property tunnel inclusion complexes have in common is that guest molecules tend to be disordered in the tunnels at room temperature and undergo phase transformations upon cooling, through interaction with and distortion of the host framework.^[34, p. 203] For thiourea–ferrocene in particular, there is a monoclinic phase (space group $P2_1/c$) where the deformation of the tunnels lead to a greater ordering of the guests. Molecules that are planar in shape are more likely to crystallise in this monoclinic system at ambient conditions,^{[3, p. 1501][32]} but it is usually a low-temperature phase with an order–disorder type transition and accompanied by twinning (even triplets^[46]). More details on the structural phases in Subsection 1.5.3.

Harris advises to study powdered forms of urea and thiourea inclusions to overcome twinning complications arising in the low-temperature transition.^[32] In a study of the thiourea–cyclohexane inclusion compound at ambient temperature, the positions of the guest molecules were not actually determined by X-ray diffraction.^[32]

1.4.2 The honeycomb lattice

Both urea and thiourea are able to construct the characteristic or conventional «honeycomb» lattice as hosts (see Figure 1.3a). The tunnels of urea have cylindrical force fields, whereas the thiourea tunnels vary significantly in diameter—from 5.8 Å to 7.1 Å compared to 5.5 Å to 5.8 Å for urea—making the internal surface resemble something like an egg carton.^[81] This provides «pockets» for the guests to be locked into, and is presumably why these inclusion compounds mostly are commensurate and behave somewhat more like a clathrate.^[3, p. 1501] With urea, the tunnel structure is formed only with compatible long alkane chain guest molecules, and generally not those with benzene or cyclohexane rings, which are probably too wide. Most urea inclusion compounds have incommensurate host–guest repeat distances (contrary to thiourea), and with guest–guest interactions being repulsive.^[32]

Thiourea will usually enclose two guest molecules for every unit cell length of the host in the tunnel direction, and give a host–to–guest molar ratio of 3 : 1 with guests located at sites of 32 symmetry. All of the hydrogen bonding capacity is spent on constructing the host network and interaction between that and the guest is weak.^[3, p. 223]

When looking down the tunnels we find the thiourea molecules aligned to the corners of the «honeycombs». Traversing along an arbitrary column, each molecule we pass will be rotated 120° compared to the previous one, and they will always go in just one of the two possible directions. In the case of thiourea, neighbouring columns always have the opposite handedness, and one of the two possibilities is shown in Figure 1.3b. This makes the tunnel walls layered in contrast to urea which has a spiral structure as a result of having the same handedness everywhere.^[34, pp. 210, 231]

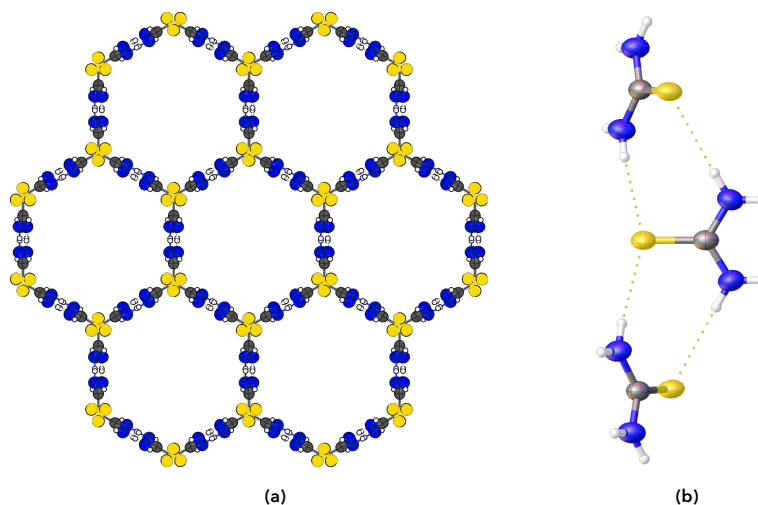


Figure 1.3: (a) Thiourea host cells together (cf. a single cell in Figure 1.2). (b) Depicts three thiourea molecules as seen perpendicular to the tunnel axis. Note that they are rotated 120° from each other, and that the sulphur atoms make a «clover» when seen from above, as seen in the «hexagon corners» in (a).

1.5 Dynamics and phases of thiourea–ferrocene

Before examining the overall structure of the system as a function of temperature, we should keep our attention on the scale of the guest molecules and learn their roles in the big picture. How the ferrocenes are oriented inside the system is crucial, and there is also the question of how they are distributed.

1.5.1 Possible orientations of the guest molecules

From Mössbauer spectroscopy Gibb^[27] had found that the five-fold molecular axis of the ferrocenes lie either *parallel* with the tunnel axis (which coincides with the trigonal c direction) or *perpendicular* to it. This makes sense from a packing efficiency standpoint, but it is not obvious whether there are any preferable combinations or long-range patterns.

Sorai et al.^[90] considered four possible orientations of the ferrocene molecules. There are three perpendicular orientations, all rotated effectively 60° from each other, and one parallel case. They are confident in that the ferrocenes play a vital role in all transitions, and that the driving mechanisms differ between the transitions.

Lowery et al.^[47] and others have suggested that the latter orientation is an approximation; the ferrocenes are actually tilted about 17° off the tunnel axis[†] due to repulsion from other ferrocenes. They also operate with three rotated sub-variants of the parallel type as well.

[†]Lorson et al.^[46] report this tilt to be 16.2° while the perpendicular guests are 87.0° away from the tunnel axis, with a change to 18.4° and 87.6° , respectively, in the monoclinic phase.

Recall that a couple of neighbouring ferrocenes in parallel orientations would have an unreasonably short space between them (page 22). The repulsions arising could be driving the tilting.^[37]

1.5.2 Fluctuations of the orientations

At room temperature the molecules show sign of being disordered and of reorienting themselves rapidly between the various configurations, appearing isotropic.^[18,35] Even at 221 K this description of the system is given by Lowery et al.^[47] The considerable delocalisation of the electron density belonging to the cyclopentadienyl rings suggests an overall disorder of the molecule.^[37]

Lowering the temperature impairs the process in which the molecules «flip» or «jump» between the parallel and perpendicular orientations. A decline is particularly noticed in the 225–160 K range.[†] Changing internally among the three parallel orientations, or the three perpendicular orientations, requires less energy, but abruptly below 160 K the ferrocenes are no longer changing to such sub-variants.^[47]

Lowery et al.^[47] have observed an entropy gain close to $R \ln 4$ at the main transition, 160 K. They interpret this to mean there is appreciable correlation between stacked ferrocenes, since a value of $R \ln 6$ would indicate independency between the six different orientations.

The ratio of parallel-to-perpendicular configurations varies a little with temperature, but estimates are never very far from equal proportions, at most 3:2. An overview is given in Table I.I.

	300 K	260 K	215 K	190 K	160 K	145 K	100 K
Gibb ^[27]	33 %		45 %	42 %	50 %	35 %	41 %
Nakai et al. ^[52]	37 %		47 %	47 %	47 %	47 %	
Lowery et al. ^[47]					40 %	45 %	48 %
Heyes et al. ^[35]	35.5 %						
Lorson et al. ^[46]		44.5 %				48.4 %	
average	35 %	45 %	46 %	45 %	46 %	44 %	45 %

Table 1.1: Percentages showing the relative proportion of ferrocene molecules aligned parallel to the tunnel axis at various temperatures. Some entries do not match the column temperature exactly, but have been moved to the closest bin (within ± 10 K).

[†]Lowery et al.^[47] find that the percentage of parallel-oriented ferrocenes being *static* increases from about 8.7 % at 210 K to 34 % at 160 K.

1.5.3 Temperature-induced phase transitions

A calorimetric study by Sorai et al.^[90] divided thiourea–ferrocene into six phases in the temperature range 13 K to 280 K. Transitions were registered at: 147.2 K, 159.79 K, 171.4 K, 185.5 K and 220 K.

Starting at top and going down in temperature we pass three minor anomalies in the heat capacity measurements (at 220 K, 185.5 K and 171.4 K) which are classified as continuous (second-order) transformations. These are all believed to be transitions intrinsic to the coupled system of thiourea and ferrocene.

Continuing further down to 159.8 K triggers the phase transition with the largest enthalpy change. It is volume-changing and a first-order transformation, and was the only one found by Clement et al.^[14] (at 162 K) using differential thermal analysis. There has been reporting of reversible twinning taking place when crossing this temperature.^[37] Some sources assert that the molecules are *not* tilted anymore,^[52] while others don't use this limitation in their modelling.^[46]

Although slower than before, reorientation among the possible perpendicular variants remains operative until we reach 153 K where also this process is slowed down. This point marks the start of the inhomogeneous, but hysteresis-free transition described by Gibb,^[27] taking place between 153 K and 141 K. This is presumably connected with the final peak in the calorimetric profile at 147.2 K. Sorai et al.^[90] describe the two lowest transitions events as two steps of a reorientational process in which the ferrocene molecules are more «independent» and permitted to flip between the parallel and perpendicular orientations. At the coldest transition temperature, units of three adjacent ferrocenes are reoriented together as a unit.

Orientation changes eventually come to a stop at 141 K, below which all molecules are practically frozen in place.^[27] Even though the five-fold molecular axes are now locked, the cyclopentadienyl rings do not cease to turn.^[35] Ring dynamics are limited to the plane they trace out for temperatures below 150 K.^[47]

The thiourea host molecules remain stationary from room temperature all the way down to 140 K.^[47] Sorai et al.^[90] point out that the phase transition at 171.4 K, despite being very close to one of the intermediate transitions of pure thiourea (171.20 K), is unrelated. They argue that the molar ratio of 3 : 1 is still correct, that the ferroelectric property is absent, and that the transition entropies do not add up.

The low-temperature structure of urea inclusion compounds are orthorhombic and perturbed versions of the orthohexagonal description of the high-temperature phase. A coupling between transverse acoustic phonons of the host and the orientation of the guest molecules has been suggested to indirectly shape the low-temperature phase. There is still much to learn about these phase transition mechanisms.^[32]

1.5.4 Comparison with similar structures

The main features of the thiourea inclusion complex is also seen with other guests, e.g. cyclohexane^[15,66], cycloheptane, cyclooctane and cyclooctanone^[48], bromocyclohexane^[65] and fluorocyclohexane.^[100] Listed in Table 1.2 are structural parameters from the literature.

Table 1.2: Lattice parameters for the TFIC and a selection of other thiourea inclusion compounds, listed chronologically. See also Table 1 in Drew et al.^[18].

Source	Guest	Temperature	Space group	Lattice parameters [Å and °]			
				<i>a</i>	<i>b</i>	<i>c</i>	β
Clement et al. ^[14]	ferrocene		$R\bar{3}c$	16.40		12.50	
Hough et al. ^[37]	ferrocene	295 K	$R\bar{3}c$	16.360		12.395	
Jones et al. ^{[39]†}	chlorocyclohexane	289 K	$R\bar{3}c$	16.481 5		12.899 7	
		85 K	$P2_1/a$	9.651 1	15.963 6	12.478 4	114.222
Yeo et al. ^[100]	fluorocyclohexane	293 K	$R\bar{3}c$	15.971		12.495	
		111 K	$P2_1/n$	27.52	15.718	12.33	90
Maris et al. ^[48]	cycloheptane	293 K	$R\bar{3}c$	16.012		12.447	
		150 K	$P2_1/c$	12.406	15.535	10.140	114.27
	cyclooctane	293 K	$R\bar{3}c$	16.225		12.488	
		150 K	$P2_1/c$	12.416 0	30.918 0	10.371 0	113.848
	cyclooctanone	293 K	$P2_1/c$	12.236 5	15.631	10.360 3	111.82
Pan et al. ^[66]	cyclohexane	293 K	$R\bar{3}c$	15.835 9		12.455 8	
		100 K	$P2_1/a$	10.213 3	14.979 4	12.407 3	115.176
Palmer et al. ^[65]	bromocyclohexane	110 K	$P2_1/a$	9.663 7	15.962	12.488	114.047
Lorson et al. ^[46]	ferrocene	260 K	$R\bar{3}c$	16.319 4		12.363 0	
		135 K	$P2_1/a$	10.129 5	16.168 3	12.403 5	114.037

† Lattice parameters transformed from rhombohedral setting.

The structural behaviour is similar with the various guests: the high-temperature phase having the conventional honeycomb tunnels and the guest molecules being highly disordered. Being rhombohedral crystals, twinning by reticular merohedry is known to occur. If so, the twinning remains after the transition to a monoclinic cell. Inclusion compounds are also prone to become twinned when entering the low-temperature regime, regardless of prior twinning (i.e., ending up with twins formed by both growth and transformation). In a case with bromocyclohexane, the twinning and detwinning that accompanied the transition was found to be reversible.^[65]

In the low-temperature phase, around 150 K,^[15] the tunnels are deformed to a lower, monoclinic symmetry, so that there are two distorted types of hexagons.^{[100]†} This phase is a superstructure of the previous, displaying new diffraction spots in the diffraction pattern, which are likely due to displacement of the host molecules from their equivalent positions.

† Note also by the determinant of the transformation matrix in Equation (1.1) on the next page that the monoclinic cell has twice the volume of the rhombohedral cell.

The glide plane parallel to \mathbf{c} is also lost,^[15] but the repeat distance along the tunnel (c) stays mostly the same.^[65]

The transformation in question from rhombohedral (r) to monoclinic (m) lattice may be executed with:^[15,39]

$$\begin{pmatrix} \mathbf{a}_m & \mathbf{b}_m & \mathbf{c}_m \end{pmatrix} = \begin{pmatrix} \mathbf{a}_r & \mathbf{b}_r & \mathbf{c}_r \end{pmatrix} \begin{pmatrix} 1 & 0 & \bar{1} \\ 0 & \bar{1} & \bar{1} \\ 0 & 1 & \bar{1} \end{pmatrix} \quad (\text{I.1})$$

See Clément et al.^[15] or Desmedt et al.^[16] for more details on this relation between the rhombohedral and monoclinic cells.

In the case of thiourea–cyclohexane, the transition from rhombohedral to monoclinic cell occurs at practically the same temperature, but there is a third isosymmetric phase below 130 K, characterised by lattice parameter discontinuity, believed to be a result of guest molecule rearrangements.^[15,16,66] Clément et al.^[15] note that the volume declines relatively quickly in the second phase.

With chlorocyclohexane as guest, the transition is observed around 190 K instead.^[39] The guests cycloheptane and cyclooctane experience intermediate transitions to a final low-temperature monoclinic cell, but cyclooctanone stands out as possessing the ordered and distorted structure already at room temperature without any transitions encountered upon cooling.^[48]

The guest molecules may remain substantially disordered also at the lower temperatures. Examples of exceptions are noted for chlorocyclohexane—the guests actually have well-defined positions in the low-temperature phase^[39]—and for bromocyclohexane, which is also characterised by two well-defined guest orientations (when sufficiently cold: 110 K).^[65] The guests appear to prefer an orientation along the longest internal diameter of the distorted tunnels.^[100]

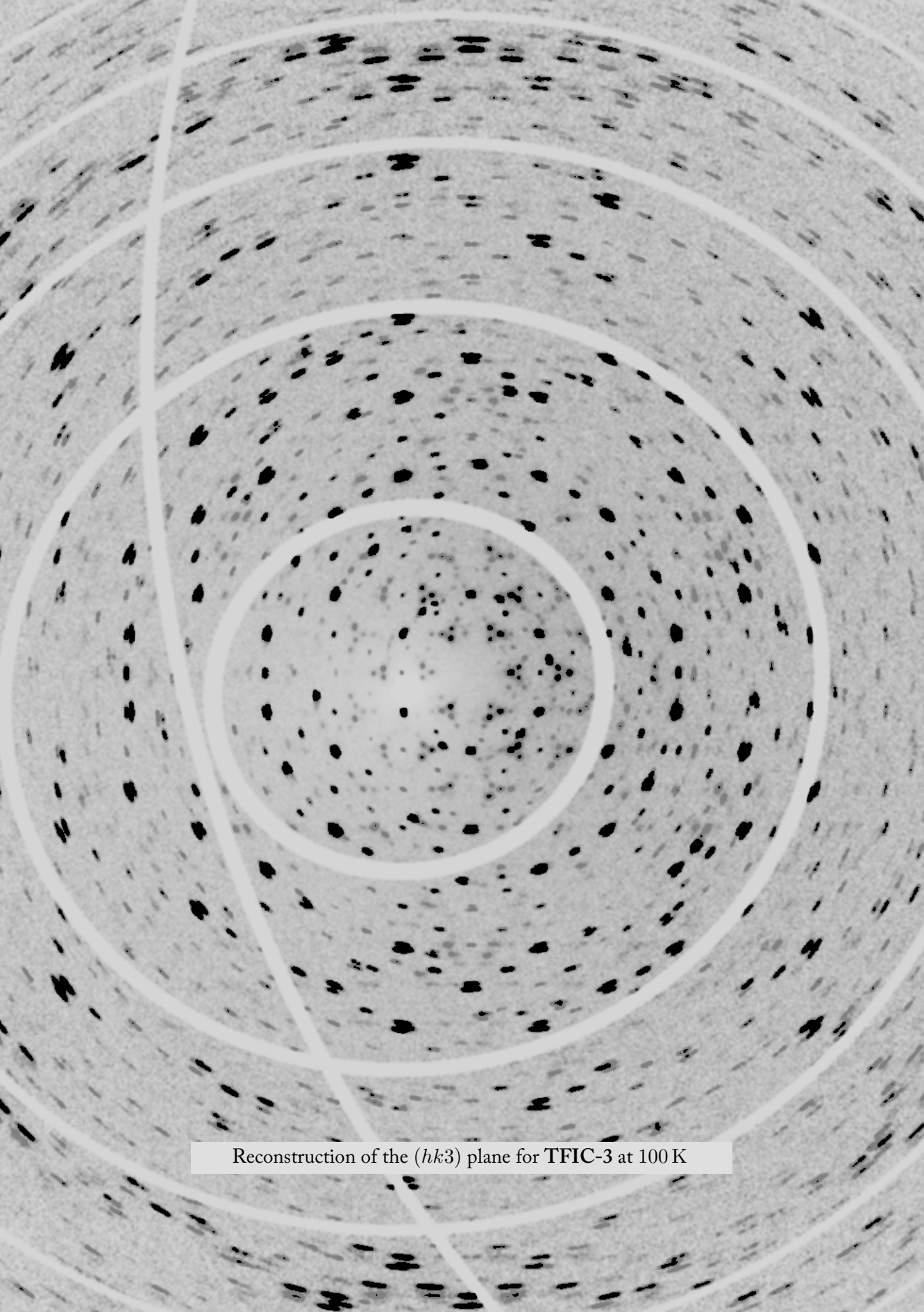
A measure of deviation from the hexagonal shape ($D = 1$) of the high-temperature may be quantified using the following formula:^[65]

$$D = \frac{b_m}{\sqrt{3} a_m \cos(\beta_m - 90^\circ)} \quad (\text{I.2})$$

where a_m , b_m and β_m are lattice parameters of the monoclinic structure. There are two modes of distortion: if $D > 1$, one of the corner-to-corner distances is compressed while the perpendicular edge-to-edge distance is stretched (examples: bromocyclohexane, chlorocyclohexane). Cases with $D < 1$ have an opposite description with regard to compression/stretching (example: cyclohexane).^[65]

On a final note, X-ray irradiation has been known to make decomposition products of thiourea inclusion compounds, leaving signatures of pure thiourea and pure guest struc-

tures in the powder patterns.^[16,33,66] This structural degradation does not infer the existence of empty thiourea tunnels, of which there are no indications to be found.



Reconstruction of the $(hk3)$ plane for TFIC-3 at 100 K

Reciprocal space

In this chapter, the reciprocal space of the TFIC will be explored. The raw data and initial analysis is also presented here. An effort has been made to intercept any changes or features of characteristic importance. Some background information is given shortly in Section 2.1, then findings on each of the three TFIC samples are elaborated upon in Section 2.2.

2.1 Experimental details

A research project at the ESRF was conducted in November 2015 to elucidate the dynamics of the TFIC. Data were collected at temperatures between the critical values (T_1 to T_5) pointed out by Sorai et al.^[90], see Figure 2.1 (cf. Subsection 1.5.3).

Most temperatures were recorded twice in the experiments: first when cooling the sample with a liquid nitrogen blower, and again when returning to room temperature. The TFIC is predominantly devoid of hysteresis effects, although an exception is found for TFIC-3.

The main part of the author's master's thesis^[74] concerned the analysis of this data. Focus was largely on obtaining refined instrument parameters for the CrysAlis software and on extracting all available information about reciprocal space. A vast collection of «unwarps» (two-dimensional reconstruction images of reciprocal space) were generated and organised.

Data reductions were carried out and attempts were made to solve the structure of the TFICs, but the ferrocene molecules could not be modelled in a reasonable manner due to high disorder. A renewed effort has however been made since the master's: see Section 3.2 for details on the updated structure solution, and Chapter 5 for details on model simulations.

In our making of the TFICs, four out of ten crystals were unsuccessful at forming a clathrate. These were recognised to be pure ferrocene by preliminary analyses. Complete scans were nevertheless acquired for these samples and only one of them was of

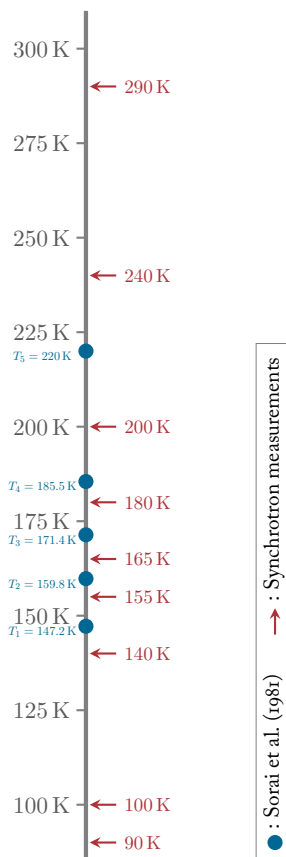


Figure 2.1: A temperature scale which indicates where Sorai et al.^[90] found phase transitions of the TFIC (blue points), and where our synchrotron measurements have taken place (arrows).

poor quality. The three remaining data sets, labelled **TFIC-1**, **TFIC-2** and **TFIC-3**,[†] have been used to solve the structure, albeit with a poor account of the cyclopentadienyl rings. All data sets could be analysed and used to solve the structure, but a more thorough revision has since been made.

Sample and instrumentation details

Crystals were prepared according to the procedure described by Hough et al.^[37]. That is, by mixing hot solutions of commercially available ferrocene (0.93 g) in benzene (10 cm³) and commercially available thiourea (1.5 g) in methanol (40 cm³). Upon slow evaporation needle-shaped crystals were formed. In addition, another batch was prepared using methanol exclusively—i.e, the thiourea (1.5 g) was resolved in hot methanol (50 cm³) and ferrocene (0.93 g) was added directly. Here, envelope-formed crystals appeared upon slow evaporation.

The two procedures thus yielded samples of distinct morphology, indicating a dependence of the solvent. It turned out that only the benzene-based procedure gave the wanted intercalation effect, whereas the crystals from pure methanol showed themselves to be simply ferrocene.

Recordings were made using a Dectris Pilatus 2M area detector at the Swiss–Norwegian beamline (SNBL-BM01A) at the ESRF. Interface with the hardware was through the program Pylatus^[22]. Exposure times were 0.25 s and angle increments $\Delta\phi = 0.1^\circ$ on a Huber 515 series κ -goniometer. For all measurements the wavelength was $\lambda = 0.69804 \text{ \AA}$ and a liquid nitrogen cryostat was used to control the temperature. Output were crystallographic binary files (.cbf), which were run through SNBL ToolBox^[22] in order to make a parameter file compatible with CrysAlis^[80], where all the main data processing were done. Quantitative details will follow in Subsection 3.2.1.

Only **TFIC-2** was measured with a filter between the incoming radiation and the sample.

[†]Labelled crystal 1, -4 and -9, respectively, in the master's thesis,^[74] reflecting the chronological sample order.

2.2 Qualitative investigation of single crystals

All recordings were performed going from room temperature down to 100 K or 90 K, then back again. Changes in reciprocal space influenced by temperature will be described in this section. Samples 1 and 3 are twinned crystals; see Appendix A for a summary of the relevant twin nomenclature.

Reciprocal space has been mapped in two primary directions: the basal hk -plane, with varying

$$l \in \{0, 1, 2, 3, 4, 5, 6\}$$

and perpendicular to this, i.e. in the $h0l$ -plane. Figure 2.2 shows «azimuthal variations» of the $h0l$ plane (A_1) tested. No directions were found to be favourable, so the simplest was chosen in the further analysis. The directions have been labelled A and B to signify similarities in the diffraction patterns: families $\{10\bar{1}0\}$ and $\{11\bar{2}0\}$, respectively.

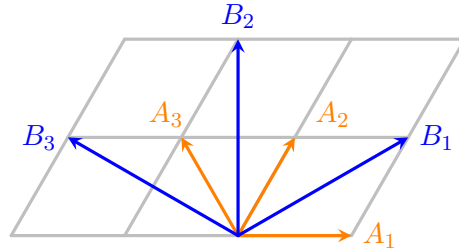


Figure 2.2: Schematic figure of the reciprocal hk -plane. A_1 is parallel with \mathbf{a}^* and A_2 with \mathbf{b}^* . Planes spanned by the vectors shown and the direction normal to the plane, have been investigated.

The next three subsections contain descriptions of each of the TFIC specimens. Their describing names, «Obverse-reverse twin ($\Sigma 3$)», «Untwinned crystal», and «Plesiotwin ($\Sigma 7$)» were not used in the preliminary part of the research, but nevertheless attached as descriptors at this point. A summary of the main observations is presented in Section 2.3 at the end of this chapter.

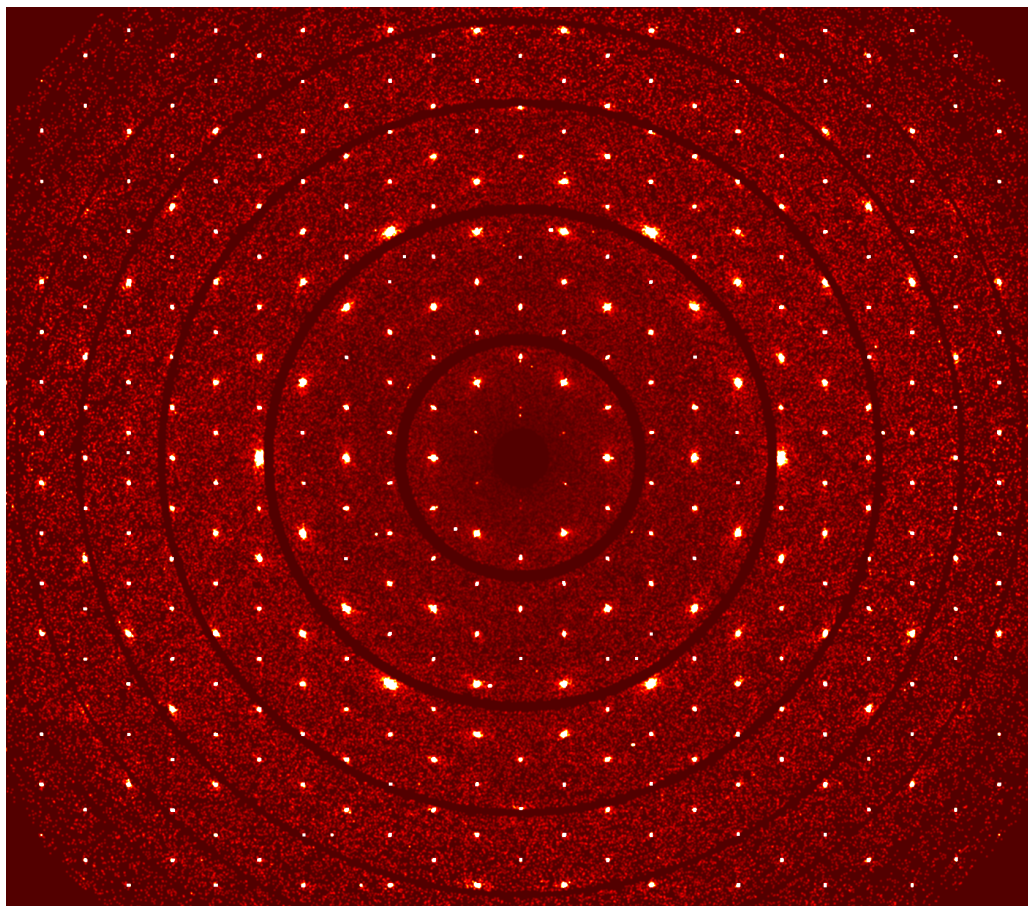
2.2.1 Sample 1 – Obverse–reverse twin ($\Sigma 3$)

In the hk -planes nothing worth mentioning happens until 165 K is reached, but changes in the $h0l$ -plane are detected—see Figure 2.5 and the surrounding figure text for a run-down.

In the temperature range 290 K to 240 K there are no obvious changes seen anywhere, which is to expect according to Sorai et al.^[90] who measured a minor anomaly in the heat capacity first at 220 K. Nevertheless, a few, faint and diffuse bands can be seen to coalesce very slightly towards nodes of indices $(1, 0, 3 \pm 0.2)$ and $(3, 0, 3 \pm 0.2)$ and their symmetric counterparts about the \mathbf{a}^* - and \mathbf{c}^* -axes.

At 200 K inspections of the $h0l$ plane reveal a materialisation of reflections at ± 0.2 units away from integral l values. This form remains at 180 K. Some indications of change can be seen in $hk1$ at this temperature with a few, low-index reflections appearing. The

Figure 2.3: Reconstruction of the $hk0$ layer of TFIC-1 at 290 K.

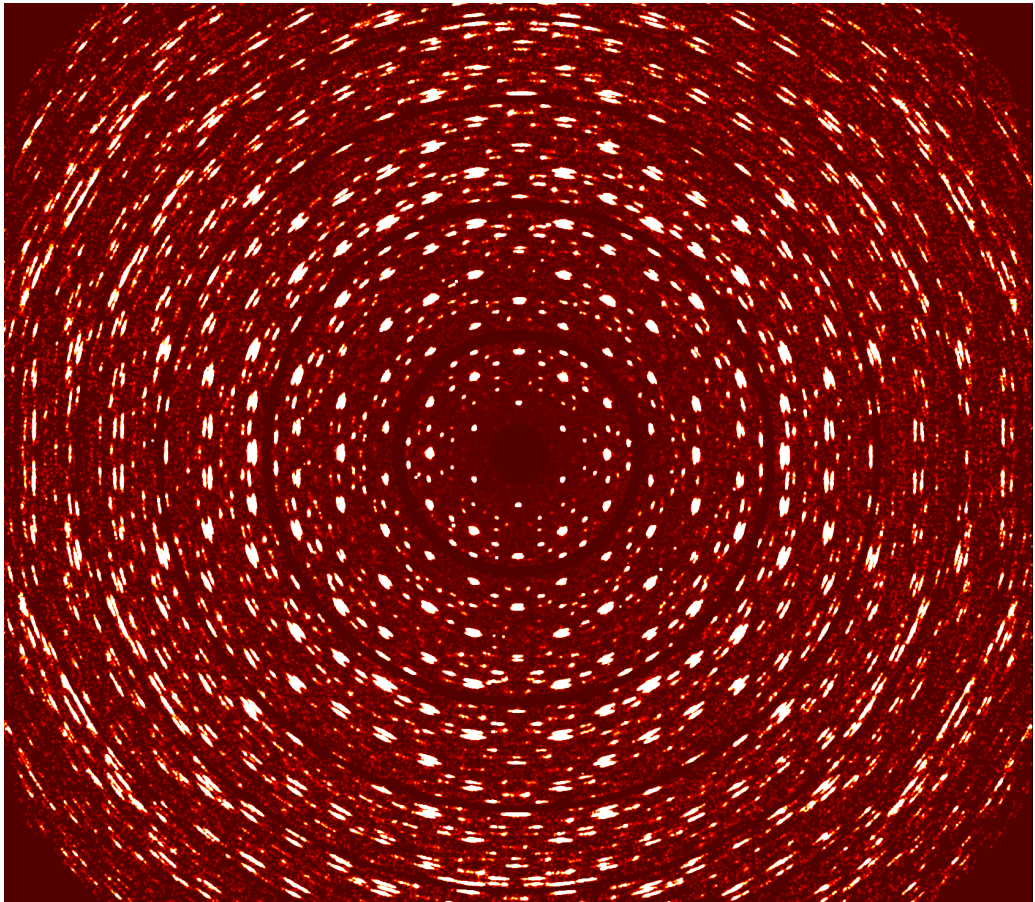


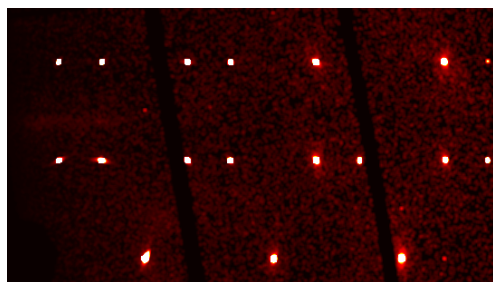
other hk -layers are seemingly still unaffected at 180 K.

Stepping down to 165 K, a third phase of **TFIC-1** is instigated. New reflections appear at non-integer values of h , allowing them to be seen in the hk -planes as well. In the $hk1$ - and $hk3$ planes they seem to organise themselves into smaller hexagons (for small indices). Faint reflections also appear in the other planes, although a recognisable pattern is not obvious. No changes noted at 155 K.

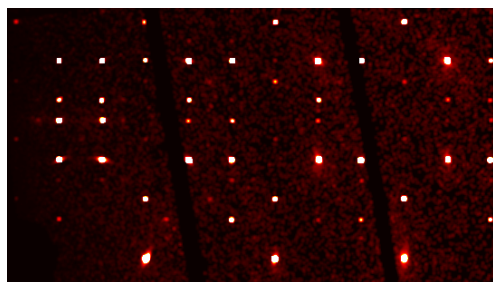
The biggest transformation occurs when passing $T_1 = 147$ K. At 140 K there are three particular events to be noted: The reconstructed images are considerably brighter as each and all reflections are (1) elongated and (2) split into two or three fragments. Moreover (3), new reflections appear in the hk -planes, between existing nodes in way to resemble new, smaller hexagons, at least for small indices, perhaps signalling a doubling of a lattice parameter.

Figure 2.4: Reconstruction of the $hk0$ layer of **TFIC-1** at 90 K.

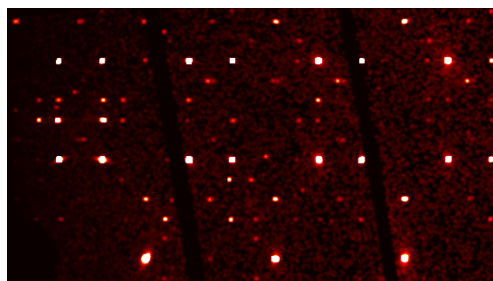




(a) Phase 1: 290 K to 240 K (here: 290 K)

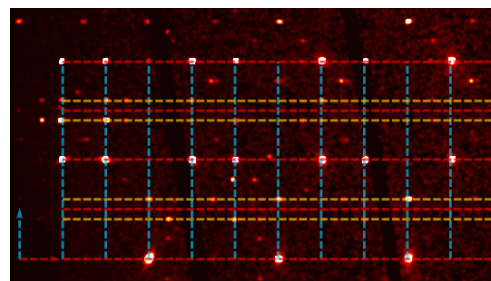


(b) Phase 2: 200 K to 180 K (here: 180 K)

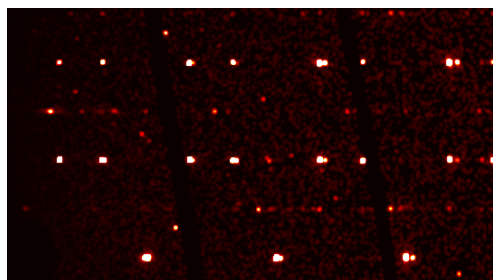


(c) Phase 3: 165 K to 155 K (here: 165 K)

The are four conspicuous phases of the **TFIC-1** structure seen in the $h0l$ -plane as the temperature drops (here labelled with Arabic numerals to avoid confusion with Sorai et al.^[90]). The first phase looks like (a) and is only present between 290 K to 240 K. The interval 200 K to 180 K is characterised by new reflections as seen in (b). From 165 K to 155 K we see mostly the same pattern, but more reflections appearing along \mathbf{a}^* . The final phase is marked by a «collapse» of the recent reflections of phases 2 and 3 to an integral l layer. Also, the strong, «original» reflections from the first phase are now split. This is more pronounced with higher indices, but can be seen well in for example the (900), (10, 0, 2) and (10, 0, 4) reflections in (e).



(d) Same as (c)



(e) Phase 4: 140 K to 90 K (here: 90 K)

The subfigure shown above is a duplicate of (c) with a grid overlay for the reciprocal lattice. Its origin is at the intersection of the \mathbf{a}^* (abscissa, red) and \mathbf{c}^* (ordinate, blue) axes in the bottom left corner. The yellow lines are located at $l = 1 \pm 0.2$ and $l = 2 \pm 0.2$.

Figure 2.5: A selected area in the $h0l$ -plane of **TFIC-1** across four chronological data series.

Examining images from 140 K, 100 K and 90 K at any plane makes it clear that they all belong to the same, fourth phase exhibited by **TFIC-1**. One can still see, however, minor changes between 140 K and 100 K: in the same way «secondary» reflections emerged,

now a «tertiary» set appears between those (or intensify if they barely made appearance at 100 K). This could indicate a quadrupling of the repeating unit in the planar direction. Nothing distinguishes the structure at 90 K from 100 K.

Investigation of hysteresis

Despite the seemingly dramatic alterations of the reciprocal lattice, as the sample returns to room temperature every step seems to retain the overall structure the crystal possessed at the original temperature, devoid of any genuine signs of hysteresis. To check this, pairs of images from the same temperatures on either «side» of the decent and ascent in temperature were compared[†] for all available temperatures and hk -planes with l varying from 0 to 6. Even with a few weak and non-integral reflections lingering on from past states, the overall impression from the measurements is that a highly reversible transition takes place.

Some reflections also vanish, but in general we are left with a little more reflections when the **TFIC-1** returns to room temperature than before it went down. This effect is not substantial, but seems to be most notable at 200 K and 180 K.

Among the two data sets at 140 K, it appears that the transition was still ongoing when the first measurements were recorded, but nothing more is noted here. Compare the image in front of Chapter 5 with Figure 2.8.

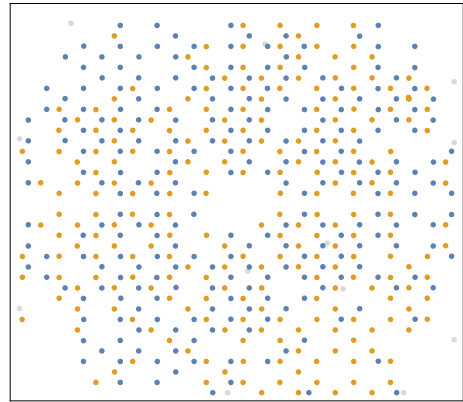


Figure 2.6: Output from `ReciprocalImageCheck` applied to an $(hk1)$ image of **TFIC-1** at 290 K. Blue nodes belong to the obverse domain and orange nodes to the reverse.

Hexagonal symmetry?

Although the correct space group was suggested

by `CrysAlis` upon data reduction, the lattice symmetry was given to be $6/m$. After initial analysis of **TFIC-2**, which lattice symmetry was visibly trigonal and truly $\bar{3}$, it became clear that **TFIC-1** was twinned. A type of twinning by reticular merohedry combines the obverse and reverse possibilities of the rhombohedral cell (see page 141 of Appendix A). Obverse–reverse twinning has been observed before in fluorocyclohexane/thiourea.^[100]

The ad-hoc Mathematica function `ReciprocalImageCheck` was written to investigate the relations (A.obv) and (A.rev). It works by overlaying a lattice on reconstructed image, which is analysed automatically to detect Bragg reflections. In the code below four inputs are provided.

[†]Comparison was done visually with the `Blend` function in Mathematica.

```
ReciprocalImageCheck[image,
  {16.1503, 16.1503, 12.3512, 90, 90, 120},
  coordinateData, {h_, k_, l_} /; Divisible[h - k + l, 3]]
```

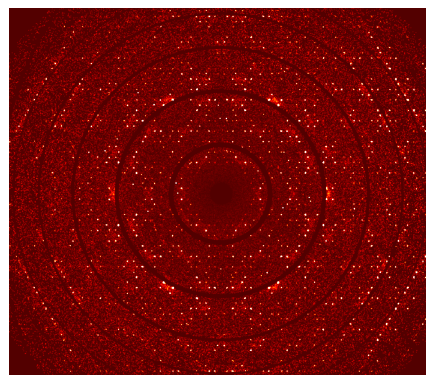
The first two arguments are self-explanatory. The variable `coordinateData` is list of data with entries of an arbitrary length[†]. Each entry is on the form $\{x, y, h, k, l\}$, indicating a correspondence between the pixel location and Miller indices of a reflection. These points are used to optimise the overlay by non-linear least squares. The final argument is a condition to gather those reflections belonging to the reverse domain; these are orange in Figure 2.6. The twin operation at work, $2_{[001]}$, may also be applied directly to one set of reciprocal nodes. (Such nodes may be acquired with the `ReciprocalSpaceSimulation` function.)

Satellite reflections

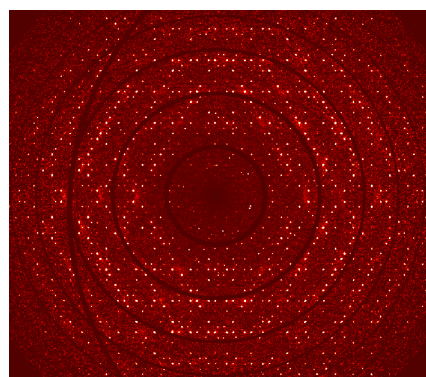
In Figure 2.5 we saw the emergence of satellite reflections in the range 200 K to 155 K. Four phases were distinguished of which number 2 and 3 exhibit these ordered layers with $l \pm 0.2$ away from integral values of l . (In the fourth phase these disappeared as new reflections with odd l values emerged.) Figure 2.7 depicts this phenomenon in various $(h, k, l + 0.2)$ layers.

Without exception, the same process unfolds in all layers: reflections form a pattern during the transition across $T_5 = 220$ K, then, through the next two transitions, $T_4 = 186$ K and $T_3 = 171$ K, this pattern is made more «complete» at each step with additional reflections coming into view. There seems to be no fundamental changes from 165 K to 155 K, although the structure seems to «settle» a bit in this 10 K range, with some reflections becoming sharper.

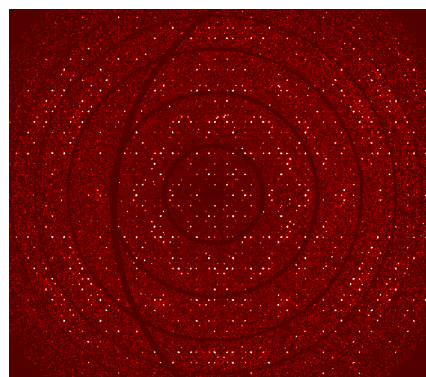
[†]Truthfully, at least two points must be provided since two scaling factors are minimised in the underlying Gauss–Newton algorithm.



(a) The $(h, k, 0.2)$ -plane of TFIC-1 at 155 K.



(b) The $(h, k, 2.2)$ -plane of TFIC-1 at 155 K.



(c) The $(h, k, 3.2)$ -plane of TFIC-1 at 155 K.

Figure 2.7: Satellite reflections in TFIC-1 only present in the temperature range 200 K to 155 K (and seemingly exclusive to this specimen). Here seen for $l \in \{0.2, 2.2, 3.2\}$. They are clearly existent in all layers with $l \pm 0.2$; sometimes also for $l \pm 0.4$.

With the aforementioned `ReciprocalImageCheck` function the majority of nodes were indexed when halving the reciprocal lattice used by `CrysAlis`.

Trefoil pattern at $hk3$

Although the diffraction patterns of **TFIC-1** are quite extraordinary at all basal planes, additional attention is still given $hk3$ here due to a fascinating display (see also the image in front of Chapter 5). As in planes with other values of l , we see new reflections appearing in the basal plane midway between existing ones. The $hk3$ -plane stands out as the one with the largest splitting of these new nodes, although $hk1$ -sections display a resembling pattern. This «trefoil» pattern arises in all three TFIC samples.

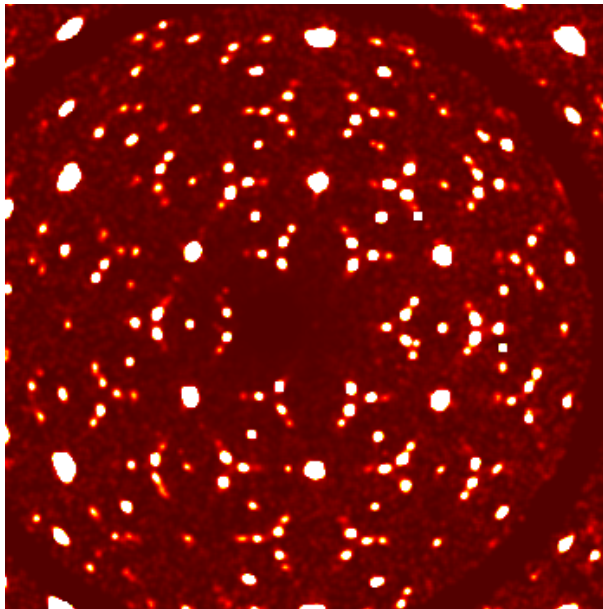


Figure 2.8: The $hk3$ -plane of **TFIC-1** at 140 K (first occurrence).

2.2.2 Sample 2 – Untwinned crystal

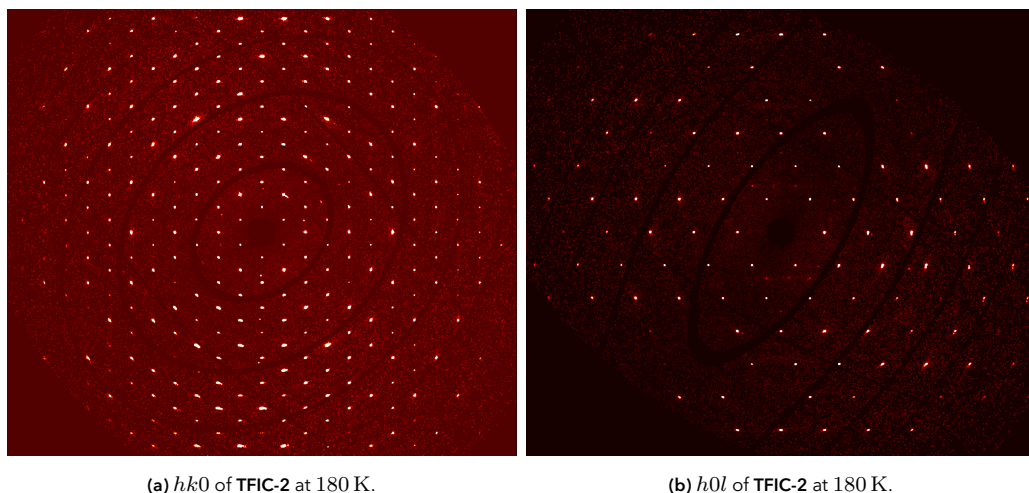


Figure 2.9: Comparison of the $hk0$ - and $h0l$ -planes of TFIC-2 at 180 K. The plane shown in (a) is practically the same at room temperature. The horizontal arrays of reflections in (b) correspond to even values of l .

No perceivable differences observed between 290 K and 240 K.

Passing the alleged transition temperature $T_5 = 220$ K, we observe nothing in particular in the hk -plane, and barely a formation of «diffuse streaks» in the hl -plane.

Going down to 200 K, this diffuse streak conglomerates into three, weak Bragg peaks that seem to take coordinates $(\bar{2}, 0, 2.8)$, $(\bar{0.5}, 0, 2.8)$ and $(1, 0, 2.8)$ (also their Friedel pairs). These six reflections are faintly visible in Figure 2.9b, standing out as they do not belong to a «proper array» of reflections. An inspection of the $(h, k, 2.8)$ plane shows nothing of monumental interest, but there are few, non-integer peaks appearing between 200 K and 155 K, being clearest at this last temperature.

Going from 200 K to 180 K crosses $T_4 = 186$ K. We note a minor intensifying of the three pairs of mentioned reflections, and barely two more pairs of the same fashion appearing, but with $l = 4.8$ instead (and shifted one unit of $-\mathbf{a}^*$).

The step from 180 K and 165 K yields no visible change in neither the $hk0$ - nor the $h0l$ -plane. This passes a reported transition, albeit a small one, at temperature $T_3 = 171$ K.

The structure crosses $T_2 = 160$ K in the next step from 165 K to 155 K. Recall that Sorai et al.^[90] report this to be a first-order transition that involves a volume change (see page 27). No abrupt changes are seen in the lattice parameters, and there is still nothing to report about the $hk0$ - or $h0l$ -planes. In fact there are no discernible changes to be observed at all in the hk -plane between 290 K and 140 K.

Main transition event (below 150 K)

The most obvious and dramatic transition takes place when crossing $T_1 = 147$ K. The reciprocal space is altered in three primary ways: (1) Nodes are elongated radially relative to the origin, (2) nodes are split into two or three streaks, (3) new reflections emerge midway between the existing ones, indicating a doubling of the lattice (repeating unit) in the ab -plane. See Figure 2.12 and compare with Figure 2.9. The first effect bears a resemblance to mosaicity.^[79]

Considering now the $h0l$ -plane shown in Figure 2.12b, we observe the same features, too, although nodes do not really extend much more than their original shape. The slanted arrays of reflections seen in the $h0l$ -layer before the transition (see Figure 2.9b) repeat every unit of h and every even unit of l . The weaker nodes that appear between the original lattice are situated midway between, i.e. at half-integer values of h and odd values of l . Satellites along a^* seem to be related to the mentioned Bragg reflections; appearing to «slide» to the nearest integral value of l .

A particular observation at $hk3$ is worth noting: a selection of low-index reflections are split into a «trefoil» pattern. It was found that these nodes are actually best visible at $(h, k, l \pm 0.05)$. Figure 2.10 demonstrates this at $(h, k, 2.95)$, where the reflections (023) , $(\bar{2}03)$, (103) , $(0\bar{1}3)$, $(\bar{1}13)$ and $(2\bar{2}3)$ are split in this way. Compare the same plane of **TFIC-1** in Figure 2.8 (where the trefoil actually is best at $l = 3$ precisely).

For the **TFIC-2** sample, we have performed two measurements at 100 K, a couple of hours apart, with the reason being that the cooling caused the crystal to crack into two pieces. Nothing substantial differentiates them—there are a few more satellite reflections present in one of the series. In all other regards, the structure looks the same at 100 K as it did at 140 K. This is an accordance with Sorai et al.'s findings, who measured down to 13 K but found no other anomalies which could indicate another phase.^[90]

The sample's journey back to room temperature reveals nothing new nor any different observations.

Satellite reflections

Despite the remarkable reflections at non-integer values of l seen in Figure 2.7, the most noticeable equivalent plane for **TFIC-2** is shown in Figure 2.11.

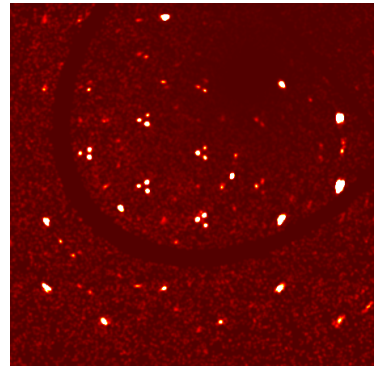


Figure 2.10: $(h, k, 2.95)$ of **TFIC-2** at 140 K.

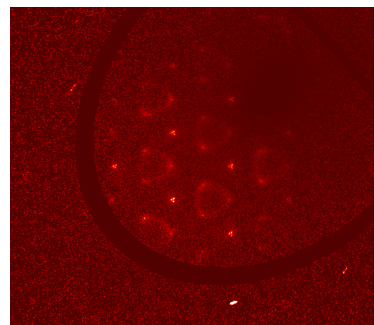
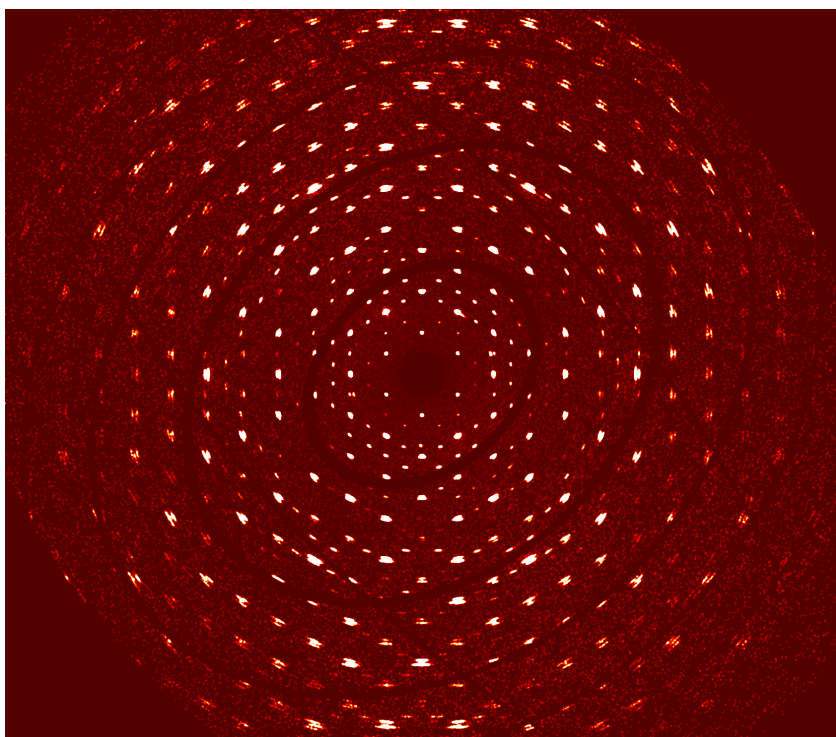
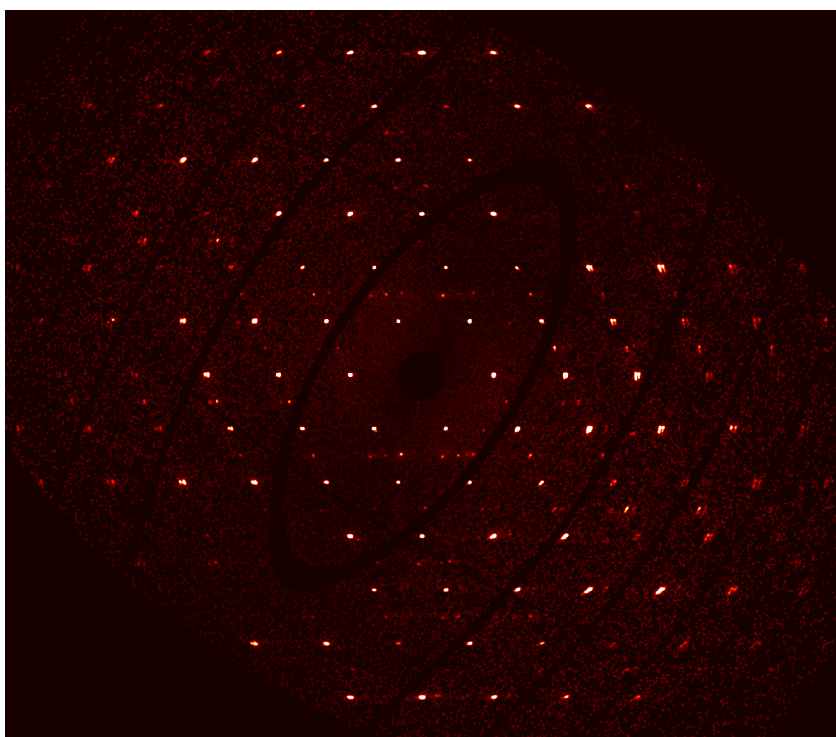


Figure 2.11: $(h, k, 2.8)$ of **TFIC-2** at 155 K.

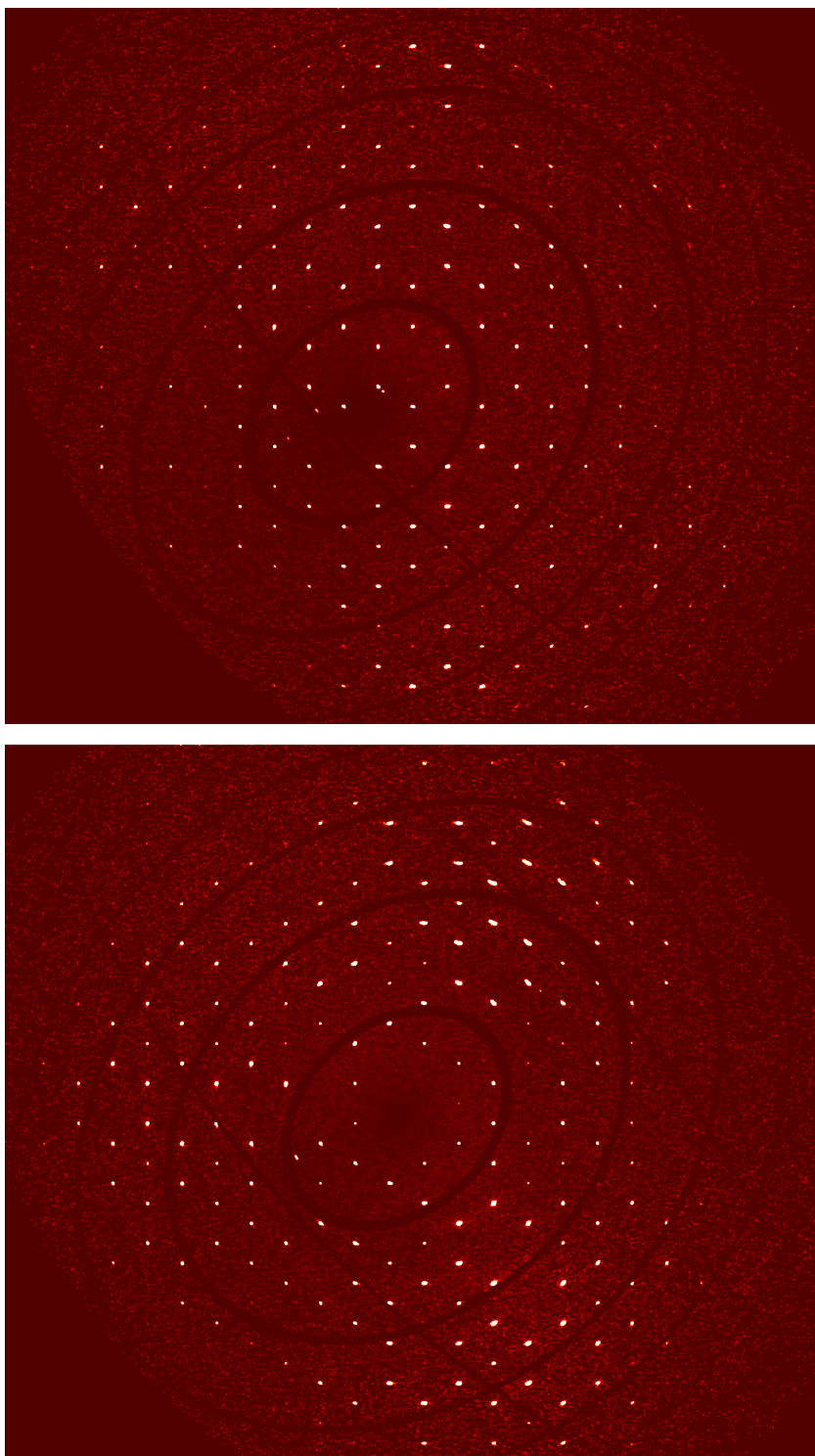


(a) $hk0$ at 140 K.



(b) $h0l$ at 140 K.

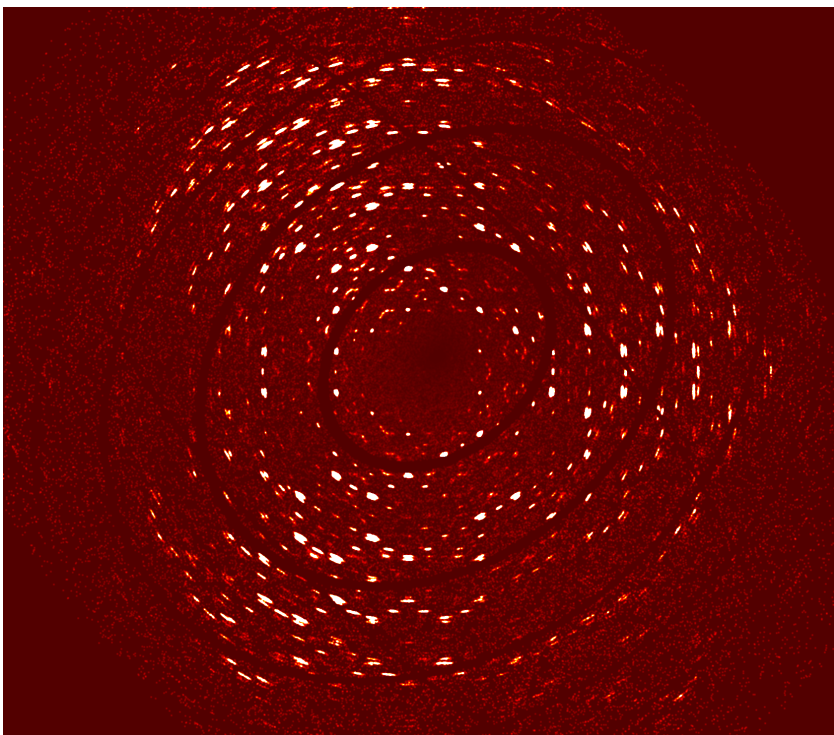
Figure 2.12: Reconstructions of the perpendicular planes $hk0$ and $h0l$ of **TfIC-2** at 140 K.



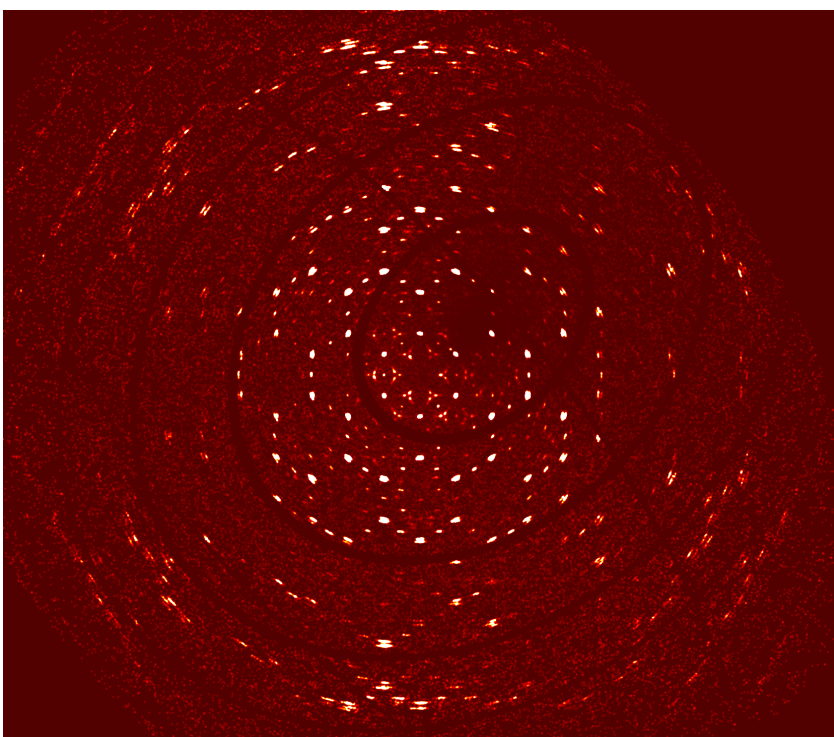
(a) $hk1$ at 290 K.

(b) $hk3$ at 290 K.

Figure 2.13: Reconstructions of the planes $hk1$ and $hk3$ of **TFIC-2** at 290 K.



(a) $hk1$ at 100 K.



(b) $hk3$ at 100 K.

Figure 2.14: Reconstructions of the planes $hk1$ and $hk3$ of TFC-2 at 100 K.

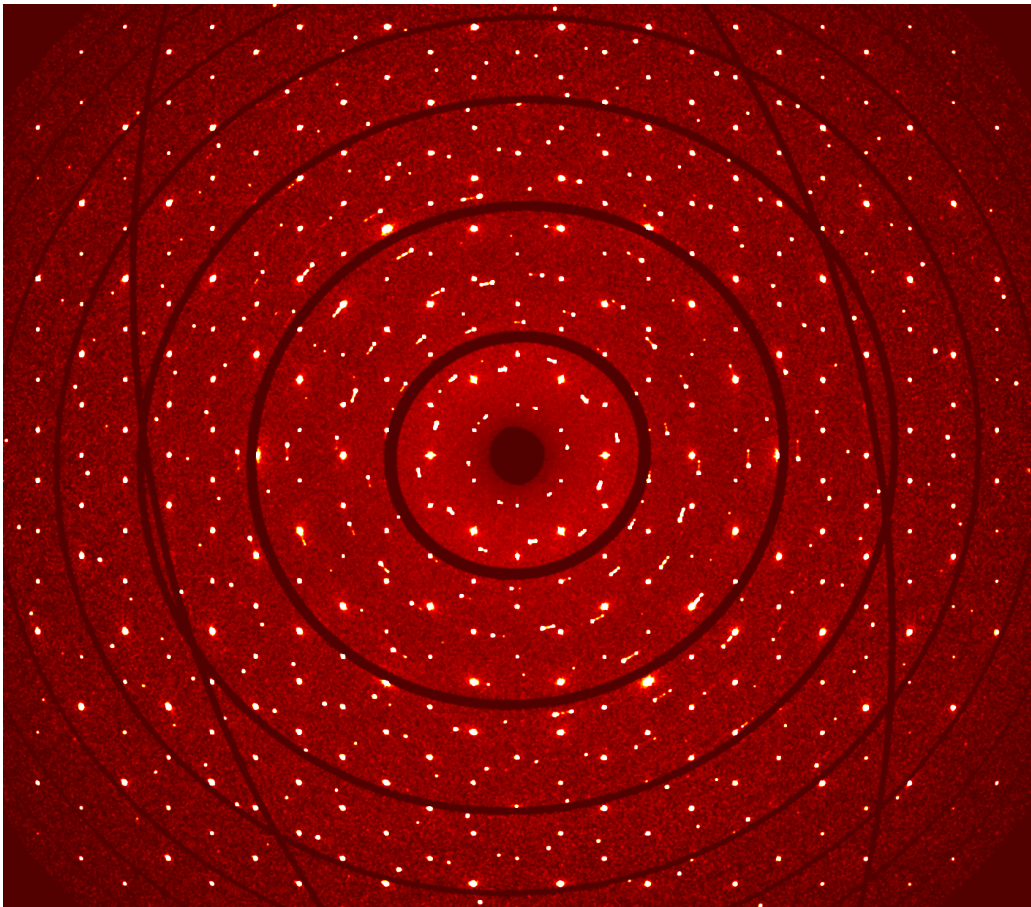
2.2.3 Sample 3 – Plesiotwin ($\Sigma 7$)

Despite being a twin, this crystal carries great significance as the sample with the best signal-to-noise ratio. See for instance the chapter image of Chapter 2.

The CSL patterns

Immediate observations of this sample signify twinning, especially when we know from sample 2 how a «regular structure» should look like. A striking feature is the appearance of «circular» patterns as seen in the $hk0$ -plane in Figure 2.15. Such patterns are typical of coincidence site lattices (CSL)[†]. Figure 2.16 shows a schematic drawing of how a single circle appears.

Figure 2.15: Reconstruction of the $hk0$ -layer of TFIC-3 at 290 K.



[†]See page 142 in Appendix A for more about coincidence site lattices.

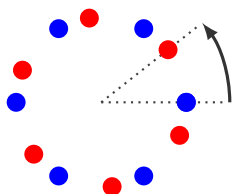


Figure 2.16: Simplified drawing showing the circular patterns of reflections observed in the basal ab -plane in the reciprocal space of **TFIC-3** due to the rotation of twin domains. The red points are rotated 38.2° anticlockwise from the blue.

A straightforward analysis of the peaks in CrysAlis indicate two identical lattices that are rotated 38.2° [†] relative to each other about the c -axis.

With the lattice parameters obtained, `ReciprocalSpaceSimulation` of `MaXrd` may be used to make a basic simulation of the diffraction pattern. Rotating this lattice will create interesting CSL patterns up to $\varphi = 30^\circ$, from where the same patterns emerge in reversed order until $\varphi = 60^\circ$, completing one period. What values of φ these CSLs appeared at is given in Table 2.1 below, and Figure 2.17 shows selected examples.

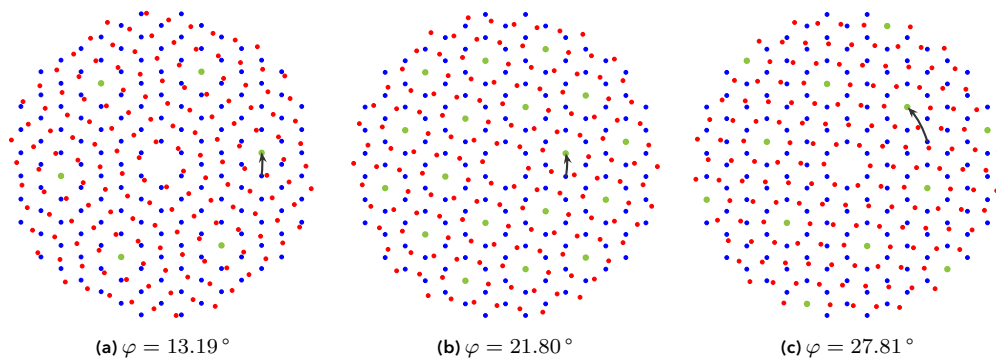
$(9.4 \pm 0.4)^\circ$	$(15.2 \pm 0.4)^\circ$	$(21.8 \pm 0.4)^\circ$
$(13.2 \pm 0.5)^\circ$	$(17.9 \pm 0.4)^\circ$	$(27.8 \pm 0.4)^\circ$

Table 2.1: Rotation angles φ marking where other CSLs were discovered in a quick simulation with $0^\circ \leq \varphi \leq 30^\circ$.

The pattern we happen to be see in our crystal is the same as in Figure 2.17b, equivalent since the emerging patterns are symmetric around 30° .

CrysAlis registers **TFIC-3** as a non-merohedral twin. Since the rotation angle is non-crystallographic, produces a CSL and this particular value of rotation has been reported in the literature before,^[50,54] we believe this to be a plesiotwin (see page 143). The same angle 38.2° also occurs in Klapper and Hahn’s analysis of $\Sigma 7$ twins of hexagonal and trigonal

Figure 2.17: Simulated CSLs, all of the same TFIC lattice, but with different rotation angles φ . Blue dots make up the original, single crystal lattice (same in all subfigures), while the red dots represent the rotated lattice. Coincident nodes are coloured green, and each subfigure includes an arrow showing one example of a node being transferred to a such position.



[†]The internal procedure of CrysAlis often finds different, but equivalent angles.

crystals.^[41] Performing a change of basis using one of their transformation matrices,

$$P = \begin{pmatrix} -5/7 & -3/7 & 0 \\ 3/7 & -8/7 & 0 \\ 0 & 0 & 1 \end{pmatrix}$$

we achieve a rotation about the c -axis that is equivalent to the angle in question. When simulating this twin it is necessary to «cut out» a 7×7 block in order to obtain a proper repeat unit for the structure. See the modelling of the plesiotwin on page 108.

Changes in reciprocal space influenced by temperature

As noted for TFIC-1 and TFIC-2, there are no substantial structural changes to report about the basal hk -plane from 290 K down to 140 K. The course of events in the $h0l$ -plane starts like the other two crystals: a diffuse line coalesces into the same «central», weak peaks, which are «shifted» or «collapsed» in the main phase transition.

Main transition event (below 150 K)

Figure 2.18 below show four pairs of segments from the $hk0$ -plane of TFIC-3 at various temperatures for focused comparison.

There are a few unique observations to be registered here: first (1), the initial arrival at 140 K does not show a clear transformation of the structure, in contrast to TFIC-1 and

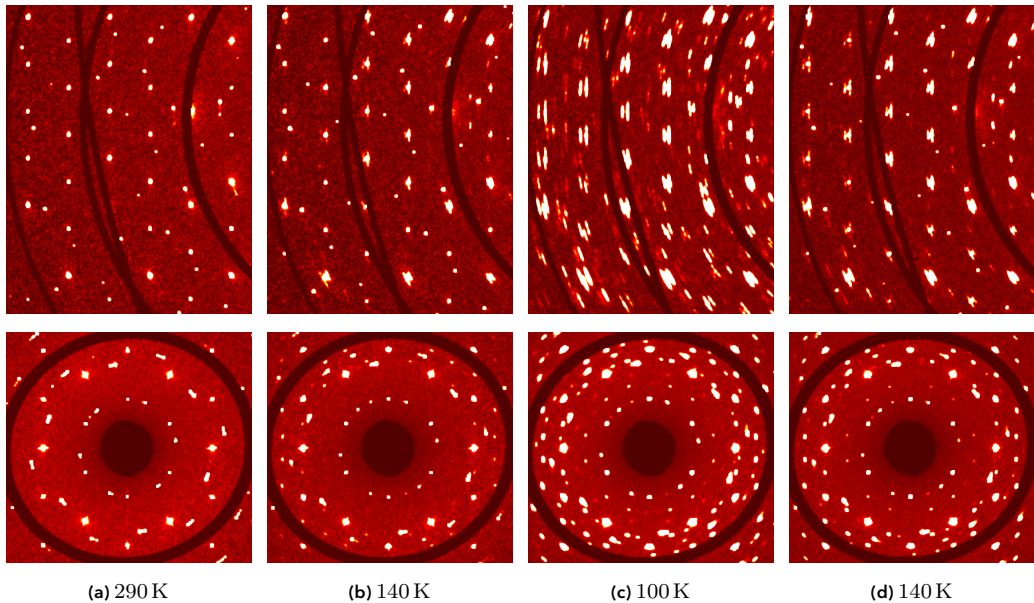
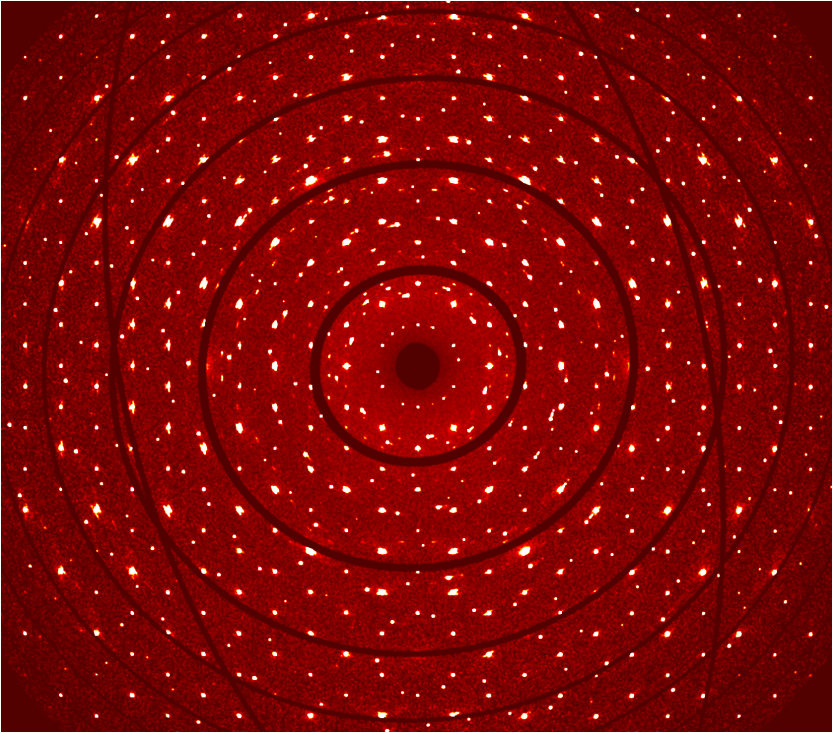
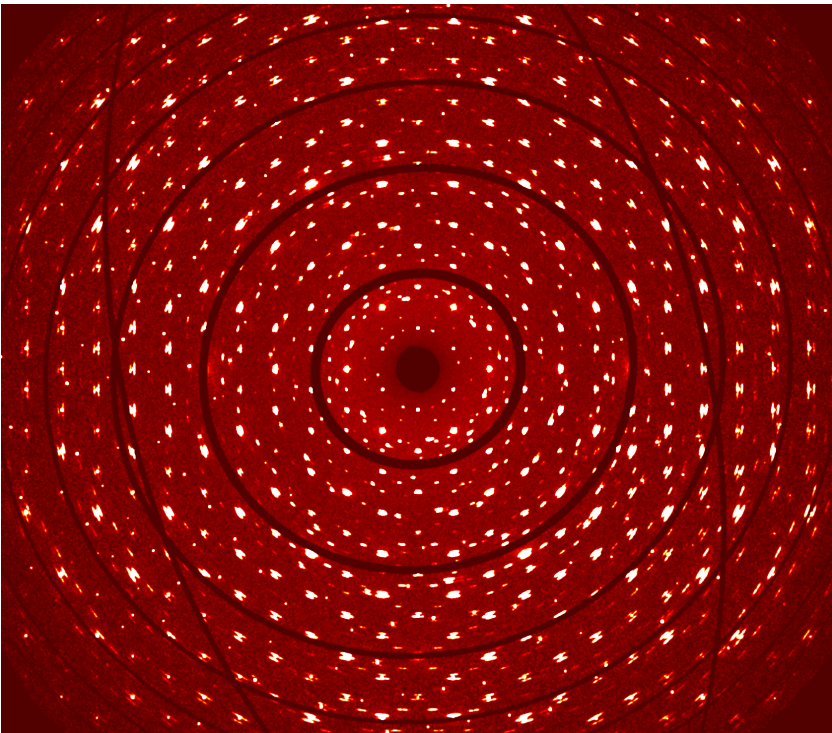


Figure 2.18: A selected area in the $hk0$ -plane of TFIC-3 across four data series, shown in chronological order from left to right. The bottom row shows low-index reflections.

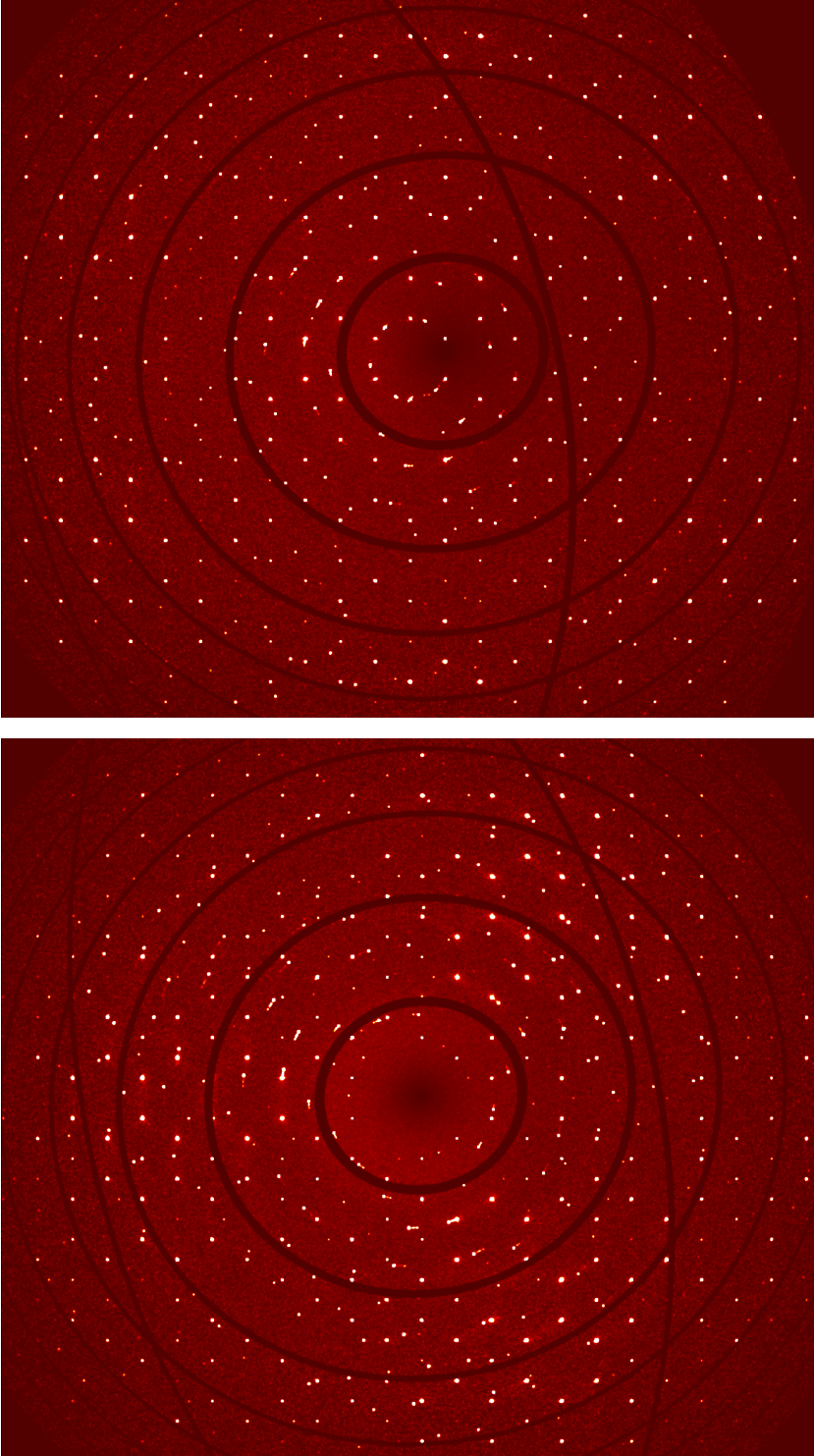


(a) First occurrence (decreasing temperature).



(b) Returning occurrence (increasing temperature).

Figure 2.19: Reconstructions of **TFIC-3** at the same temperature, 140 K, and of the same plane, $hk0$, but chronologically different.



(a) TFIC-3 at 180 K, reconstruction of $hk1$.

(b) TFIC-3 at 180 K, reconstruction of $hk3$.

Figure 2.20: Reconstructions of TFIC-3 at the same temperature, 180 K, but of different planes: $hk1$ and $hk3$.

TFIC-2. In fact, the attained phase seems metastable, as we see a tendency to the (now expected) broadening and splitting of nodes. (2) Still considering Figure 2.18, note that only one twin component seems to be properly affected by the structural changes at 140 K. Looking at the top row of images, the minor (weaker) twin component appears to «give in» to elongation and fragmentation somewhere between 140 K and 100 K. At 100 K we see the characteristic signs of both components being in the low-temperature phase. (3) The two sections at 140 K are noteworthy different, and indeed the closest indication of hysteresis in our measurements.

Another observation, common with the other TFICs, is the emergence of «secondary» reflections at 140 K, and a «tertiary» set at 100 K. An exclusive remark for **TFIC-3** is that diffuse spots intensify from 200 K to the main phase transition, positioned where several of the «secondary» reflections come out. The good image quality is likely why this is resolved in this sample only.

An isolated observation **TFIC-3** is that some permanent satellites are seen in $h0l$, particularly visible for (300) , (600) , $(40\bar{2})$, $(70\bar{2})$, $(10, 0, \bar{2})$ and $(13, 0, \bar{2})$ (plus the Friedel pairs). These are all along c^* , and are also split at the main transition, which is affected along a^* like the others.

Satellite reflections

Inspection of $(h, k, 2.8)$ -layers reveal the same type of patterns as seen in Figure 2.11. Another unique observation for **TFIC-3** is that this shape is still visible at 140 K. It is still strongest at 155 K.

Trefoil patterns

At $hk3$ we observe much the same as seen with **TFIC-1** (Figure 2.8).

2.3 Summary of observations

A review of the observations concerning the TFIC crystals is presented in Table 2.2.

No concrete evidence of hysteresis was observed, although the two twins (TFIC-1 and TFIC-3) both had indications of a slightly delayed transition going down to 140 K. A remark that holds true for all TFIC samples is that those reflections that are present at room temperature remain more or less fixed throughout the whole endeavour. When reflections split, the new part appears next to the original reflection (with slightly greater Bragg angle).

As mentioned on page 43, we believe the overall shape of reflections below the main transition event may be ascribed to a high degree of mosaicity or some similar structural effect. For all three samples, we ascribe three common changes in reciprocal space when transitioning to the low-temperature phase: (1) reflections are «smeared» tangential to circles centred at the origin; (2) reflections are split into two or three fragments; (3) new reflections appear between old ones, as if we have a doubling of the cell dimensions.

Differences among the TFIC samples

There are obvious dissimilarity among the crystals due to twinning. The satellite reflections at $l = \pm 0.2$ and $l = \pm 0.4$ are most predominant for TFIC-1, even if the phenomenon exists for the other two as well. In the study of the $h0l$ -layers, TFIC-2 and TFIC-3 resemble each other more than the first crystal, since they only exhibit two distinct phases. TFIC-1, as shown in Figure 2.5, have four distinguishable phases. In the basal planes, there are still just two main phases, although the appearance of additional, low-index peaks at 165 K (not so visible in the $hk0$ -plane) could count as a metastable phase.

Structural phases

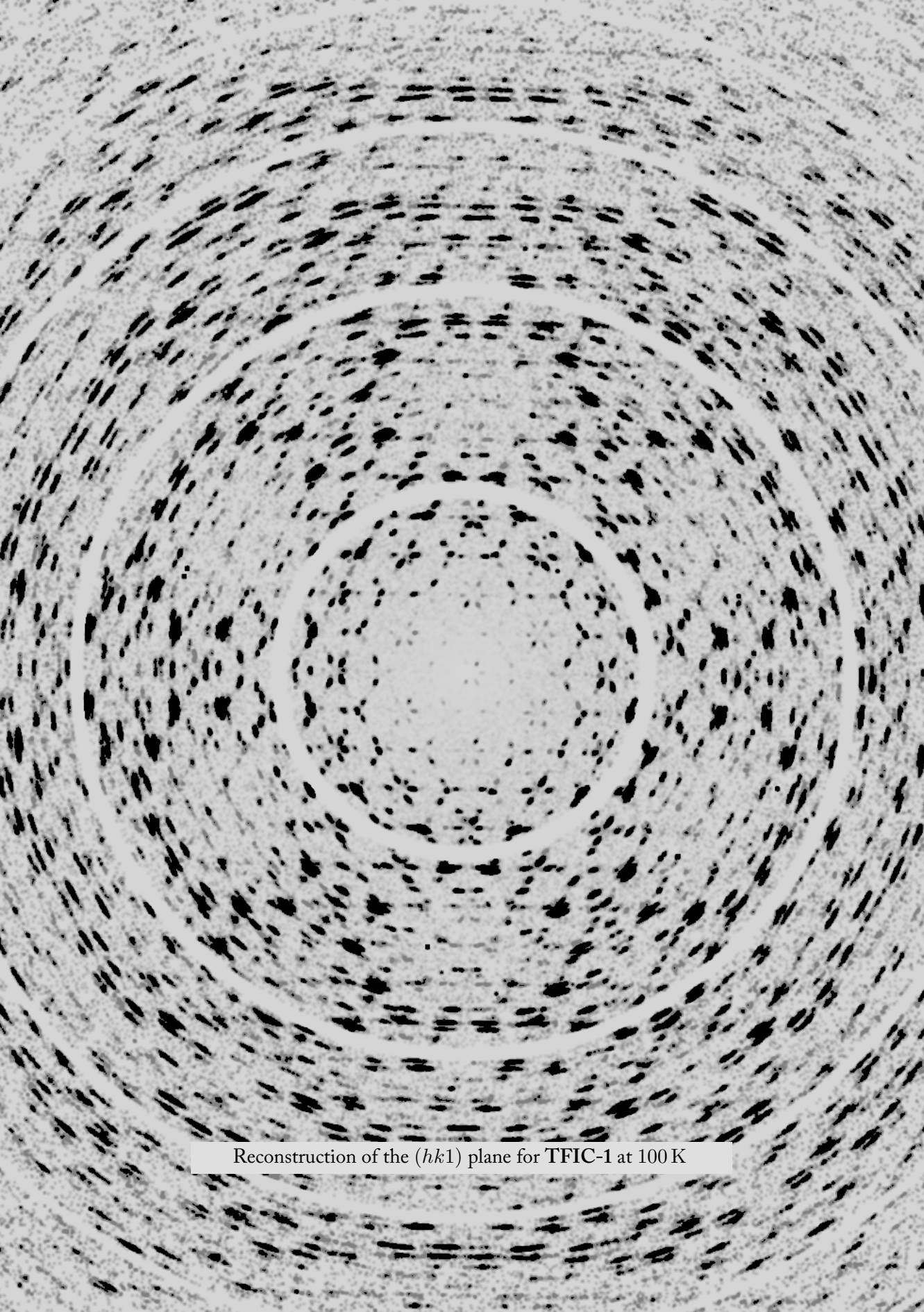
We do not see any new or missed phase transitions compared to Sorai et al.^[90]. Perhaps most puzzling of all is that the crossing of $T_2 = 160$ K, having the greatest enthalpy change according to Sorai et al.^[90] (see Subsection 1.5.3), yields nothing to register about the structure in any of our samples. As T_1 appears to be the main transition event in all three TFICs, it is improbable that we simply see a delayed response of the T_2 transition.

When considering just the intersection of the observations, the conclusion is that there exists two noticeable phases of TFIC: a rhombohedral above approximately 150 K and something resembling the same structure below this temperature, but «broken» in some regard—a topic that will be continued in Chapter 5

Table 2.2: 290 K is our reference point at ambient conditions. Long dashes indicate temperatures not used on that particular sample. The crossing temperatures refer to Sorai et al.^[90]

Temperature	Crossing	TFIC-1 notes	TFIC-2 notes	TFIC-3 notes	Common observations
240 K		Nothing in $hk0$; Diffuse band formation in $h0l$	Nothing in $hk0$; Diffuse band formation in $h0l$	Nothing in $hk0$; Diffuse band formation in $h0l$	Diffuse band formation in $h0l$
200 K	$T_5 = 220$ K	Diffuse streaks «conglomerate»; «Phase 2» in $h0l$; $l \pm 0.2$ satellite reflections appear	Diffuse band turns into three «central» Bragg peaks with $l = 2.8$	Diffuse band turns into three «central» Bragg peaks with $l = 2.8$	A few, weak reflections appear with $l \pm 0.2$
180 K	$T_4 = 186$ K	New low-index reflections in $hk1$	Minor intensifying of «central» peaks, and similar appearing at $l = 4.8$	Nothing new to report	Nothing particular
165 K	$T_3 = 171$ K	A few low-index satellites emerge in basal planes; «Phase 3» in $h0l$	Nothing new to report	Slight intensifying of diffuse spots	Nothing particular
155 K	$T_2 = 160$ K	Nothing new to report	Nothing new to report	Nothing new to report	Nothing particular
140 K	$T_1 = 147$ K	Elongated and split nodes; new midway reflections; «Phase 4» in $h0l$; Delayed transition first; «Trefol pattern»; « $l \pm 0.2$ satellites» disappear	Elongated and split nodes; new midway reflections; «collapse» of the «central» reflections; «trefol» reflections at $hk3$ « $l \pm 0.2$ satellites» disappear	Elongated and split nodes; new midway reflections; only one twin component affected; First occurrence transitioned late; «collapse» of the «central» reflections; «trefol» reflections at $hk3$	Elongated nodes; Split nodes; new midway («secondary») reflections; «collapse» of the «central» $h0l$ reflections; «trefol» reflections at $hk3$
100 K		New or intensified «tertiary» reflections	Slight «settling» of the phase; New «tertiary» reflections	Both twin components transitioned	Slight «settling» of the phase; New, weak midway («tertiary») reflections
90 K		Nothing new to report	—	—	—

The «central reflections» here are the six peaks emerging from diffuse scattering around 200 K: (2, 0, 2.8), (0.5, 0, 2.8) and (1, 0, 2.8) (and Friedel pairs).



Reconstruction of the $(hk1)$ plane for TFIC-1 at 100 K

Structure solutions

3.1 Pure ferrocene

As mentioned before, four of the samples tested were unsuccessfully clathrated, revealed after initial data collection at room temperature. Most of them were pure, but well-developed ferrocene crystals. They served as «training data» for solving structures in the author's master's thesis, but there is nonetheless opportunity for attaining a detailed, synchrotron-based solution. This may serve as a «benchmark» or reference for the experimental setup, giving an indication of the overall achievable quality.

In continued mentioning of the ferrocene crystal, only the most promising crystal candidate[‡] from the previous analysis will be regarded.

Structure solution

Recall from Subsection 1.2.2 that the twist angle between the two cyclopentadienyl ligands is about 24° from an eclipsed state at room temperature. This was modelled with the following procedure: After solving the structure with SHELXS^[87], only the iron atom was initially fitted. The subsequent three greatest peaks were used to fit a cyclopentadienyl ring with the FragmentDB utility in Olex2^[17], assigning this ring to part 1 of the structure and giving the carbon atoms an occupancy of $\frac{1}{2}$. To model the disorder, this ring was split and rotated to fit the three next largest «*Q* peaks». The new ring is regarded as part 2. See Figure 3.1. Thereafter a regular refinement process followed with inclusion of hydrogens, switching on anisotropic parameters for the atoms and adjusting the weighting scheme automatically.

Table 3.1: Structure solution data for pure ferrocene at 290 K.

Property	Value
Sample name/label	Ferrocene
Space group	$P2_1/n$ (#14)
Temperature	290 K
Lattice parameters	$a = 5.928\ 60(17)\ \text{\AA}$ $b = 7.612\ 00(10)\ \text{\AA}$ $c = 9.041\ 10(10)\ \text{\AA}$ $\beta = 93.156\ 0(10)^\circ$
Cell volume V	$407.392(14)\ \text{\AA}^3$
Mass density ρ	$1.517\ \text{g/cm}^3$
Chemical formula	$\text{C}_{10}\text{H}_{10}\text{Fe}$
Formula units Z	2
Wavelength	$0.698\ 0(1)\ \text{\AA}$
Number of reflections	total: 3 360; unique: 1 126
Reflection indices limit	$\pm\{8, 11, 10\}$
Refinement factors	$R_{\text{int}} = 1.23\ \%$ $R_1 = 2.77\ \%$ $wR_2 = 8.36\ \%$ $\text{Goof} = 1.090$
Mean signal-to-noise ratio	$\langle I/\sigma(I) \rangle = 84.7$

[‡]The decision was based on completeness of the reciprocal mapping, signal-to-noise ratio and common refinement/goodness parameters.

It is customary to use the alternative $P2_1/n$ setting (unique axis b ; cell choice 2), presumably since this choice yields a complete molecule in the centre of the unit cell instead of splitting it at the edges. In Olex2, this was done with the command «sgs b2». The structure solution data and quality indicators are presented in Table 3.1

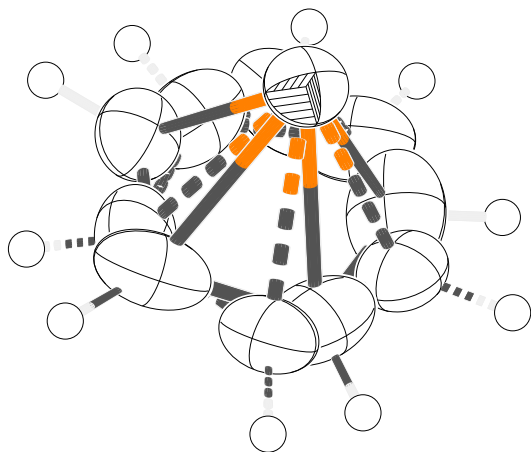


Figure 3.1: Asymmetric ferrocene unit. One part is shown with dotted bond lines, the other with solid lines. The iron atom is present in both (PART 0), while the two parts share occupancy 50:50. Ellipsoids are displayed at 50% probability.

The structural data obtained were useful in a couple of ways: they provided coordinates for construction of a so-called *fragment* in Olex2 (see the next section), and the angular displacement between the two parts could be found and compared with the literature. Determination of the latter was done by considering the vectors to each pair of neighbouring hydrogen atoms from the centre of the ring, then the same was done with pairs of carbon atoms. The weighted mean was found to be $(23.0 \pm 1.2)^\circ$, in close agreement with other findings (cf. Subsection 1.2.2).

Fragment

After countless unsuccessful attempts at solving the structure with the cyclopentadienyl rings falling in place to stationary positions, or even obtaining reasonable atomic displacement parameters (ADPs) for the carbon atoms, the coordinates of the ferrocene molecule were added to a new fragment in the FragmentDB utility in Olex2. The restraints SADI, FLAT and SIMU were put on each ligand, by the following:

1	5.9286	7.6120	9.0411	90	93.1560	90
2						
3	Fe	0.0000	0.0000	0.0000		
4	C1-A	-0.1104	-0.0458	-0.2028		
5	H1-A	-0.1108	0.0244	-0.2754		
6	C2-A	0.0745	-0.1499	-0.1546		
7	H2-A	0.2352	-0.1516	-0.2154		
8	C3-A	0.0168	-0.2515	-0.0349		
9	H3-A	0.1142	-0.3346	0.0116		
10	C4-A	-0.2064	-0.2103	-0.0082		
11	H4-A	-0.2848	-0.2666	0.0666		
12	C5-A	-0.2834	-0.0824	-0.1118		
13	H5-A	-0.4308	-0.0456	-0.1084		
14	C1-B	0.0601	0.0621	0.2238		
15	H1-B	0.0315	-0.0162	0.3068		
16	C2-B	-0.0975	0.1772	0.1562		
17	H2-B	-0.2447	0.1967	0.1829		
18	C3-B	0.0117	0.2577	0.0397		
19	H3-B	-0.0530	0.3415	-0.0244		
20	C4-B	0.2321	0.1928	0.0345		
21	H4-B	0.3382	0.2251	-0.0324		
22	C5-B	0.2624	0.0695	0.1500		

```

23 H5-B      0.3994  0.0008  0.1740
24
25
26 SADI  0.02 C1-A C2-A C2-A C3-A C3-A C4-A C4-A C4-A C5-A C5-A C1-A
27 SADI  0.04 C1-A C3-A C1-A C4-A C2-A C4-A C2-A C5-A C3-A C5-A
28
29 SADI  0.02 C1-B C2-B C2-B C3-B C3-B C4-B C4-B C5-B C5-B C1-B
30 SADI  0.04 C1-B C3-B C1-B C4-B C2-B C4-B C2-B C5-B C3-B C5-B
31
32 FLAT  C1-A > C5-A
33 SIMU  C1-A > C5-A
34 RIGU  C1-A > C5-A
35
36 FLAT  C1-B > C5-B
37 SIMU  C1-B > C5-B
38 RIGU  C1-B > C5-B

```

One of the ligands have been moved to the other side of the iron atom to make a proper ferrocene molecule. The result was seen in Figure 1.1.

3.2 Thiourea-ferrocene inclusion compound

Of the three TFIC crystals studied, the first sample was found to be twinned by reticular merohedry (obverse–reverse twinning). The second was normal, but the application of a filter appears to have diminished the signal-to-noise ratio in the data. The final sample has the best quality, but is also twinned.

At first, much attention was given to study the reciprocal space and the characteristics of TFIC-1. Below the main transition temperature 150 K, the overall diffraction patterns appeared to remain rhombohedral with the chaotic effects (splitting and elongation of reflections) believed to result from a combination of reversible twinning and modulation. Thus, all reconstructions of reciprocal space presented in Chapter 2 are based on a rhombohedral lattice (using hexagonal axes and ensured to have the same orientation). We now know that the hexagonal «honeycombs» become distorted and lose symmetry, but going through the analysis with a monoclinic lattice was overlooked at that time. The challenge with the distorted ferrocene molecules was never properly overcome, but the work has been helpful in narrowing down which data sets to focus on. See Ramsnes^[74] for details on the early solution attempts.

This upcoming subsection contains details and comments on the practical analysis. Discussion and conclusion will be presented in another subsection thereafter. Categorized and in order we have analysis of the:

- TFIC-2 high-temperature phase
- TFIC-2 low-temperature phase
- TFIC-3 high-temperature phase
- TFIC-3 low-temperature phase
- TFIC-1 high-temperature phase
- TFIC-1 «phase 2» (at 180 K)
- TFIC-1 «phase 3» (at 165 K)

3.2.1 Data analysis of the thiourea–ferrocene inclusion compounds

Treatment of data from raw images through data reduction was performed with CrysAlis Pro version 171.40.84a^[80], and further processed in Olex2 1.3^[17] to obtain structure solutions. The structures were solved with the SHELXT program and refined with SHELXL.^[88,89] From experience, the automated peak finding routine in CrysAlis is satisfactory without making adjustments. The next step of ascertaining the unit cell may, however, render incorrect lattice suggestions if the instrument model parameters (detector distances and rotation offsets etc.) are inaccurate, even if roughly the same number of reflections are found. To ensure a good starting point, the instrument model parameters were set to the best average found in the master's thesis. This was accomplished by handling all the room temperature data, manually correcting the peak tables, refining instrument parameters and finally weighting the resulting values by the residual factors (R_{int}). To automate the process, the parameter file (.par) was exported with the WD P command in CrysAlis. A script was made which first reads in this file with the RD P command. After this, the following code was executed:

```
1 XX CHEMFORM "C13 H22 Fe N6 S3" 6
2 PH SNOGUI
3 UM TTT
```

This first sets the chemical formula, searches for peaks, then indexes the reflections.

Analysis of the TFIC-2 high-temperature phase

The first data set at 290 K was processed by the common routine stated above. The reduced data indicated a reasonable internal consistency (merging residual) of $R_{\text{int}} = 6.31\%$ and signal-to-noise ratio of $\langle I/\sigma \rangle = 26.2$. The host structure is straightforward to fit, and after placing the iron atom at the Wyckoff position $6a$ and refining all non-hydrogen atoms with anisotropic displacement parameters, the R_1 factor is around 12% and the largest electron density peak at $2.5 \text{ e}/\text{\AA}^3$. Naïvely placing carbon atoms at the next two maximum peaks and performing subsequent refinement (anisotropic parameters, free occupancy, automatically added hydrogen and automatic weighting scheme), one obtains $R_1 = 7.24\%$ and maximum peak $1.8 \text{ e}/\text{\AA}^3$. Unrealistic it may be—see Figure 3.2a—but we now have a benchmark with which to compare future models. Note also that there is one carbon atom too many in each of the cyclopentadienyl rings in this model. In the asymmetric unit, there are two carbon atoms belonging to a single guest molecule, both in general positions. What we see is an interpretation based on the underlying space group and recorded data; the ferrocene molecule itself has non-crystallographic symmetry. In addition, the molecule has a relatively high rotational freedom, and we have seen that this crystal is prone to twinning, both of which could explain the observed disorder.

We now attempt to model the guest molecule by inserting a ferrocene fragment based

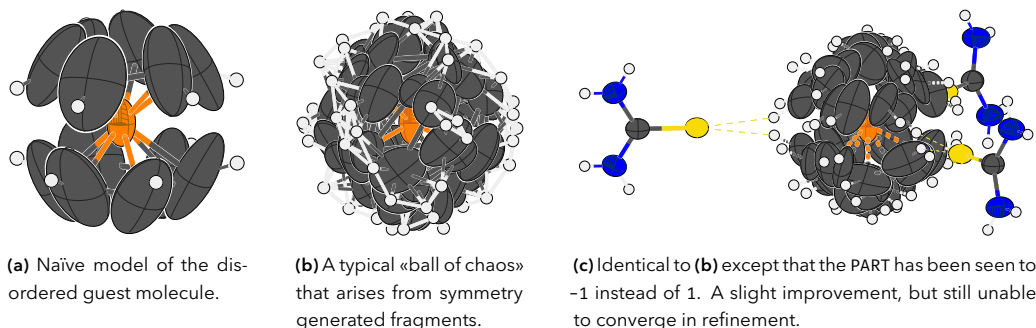


Figure 3.2: Trial models of disordered ferrocene using data of **TFIC-2** at 290 K. Rendered with Olex2.

on the pure ferrocene structure solution (see page 58). An immediate challenge is that a myriad of guest molecules are generated when having a single ferrocene molecule at the special position of the iron, see Figure 3.2b. Although the chaotic unit cell gains an isotropic «ball» of ferrocenes that could be said to model ultimate disorder, this structure is unable to settle during refinement, and at no better values compared to the previous model. This will also cause a mismatch between the cell content and the (true) chemical formula listed in the instructions file.

Assigning a negative PART number was tried to avoid bonding between symmetry-equivalent atoms.^[51, p. 62] The result is seen in Figure 3.2c. Neither this model would settle, and the parameters were $R_1 \approx 8\%$ and maximum peak $2.0 \text{ e}/\text{\AA}^3$ at best.

After some more trial and error with fitting the ferrocene molecule, a somewhat reasonable and converging model was acquired. Here, the thiourea molecule and the iron atom belongs to PART 0 while there are two cyclopentadienyl rings, each assigned to be PART -1 and PART -2, respectively. They were both placed to fit the observed Q peaks as best as possible, but two of the halves were removed to «regain control» of the structure development. Optimal occupancy factors seem to be $\frac{1}{2}$ for one of the remaining carbon rings, and $\frac{1}{4}$ for the other. Neither of them stabilised with anisotropic refinement. See Figure 3.3 for the asymmetric unit of this final model of **TFIC-2** at 290 K ($R_1 = 7.64\%$; maximum peak at $1.7 \text{ e}/\text{\AA}^3$). The largest share of electron density of the carbon atoms is found in the plane perpendicular to the tunnel axis.

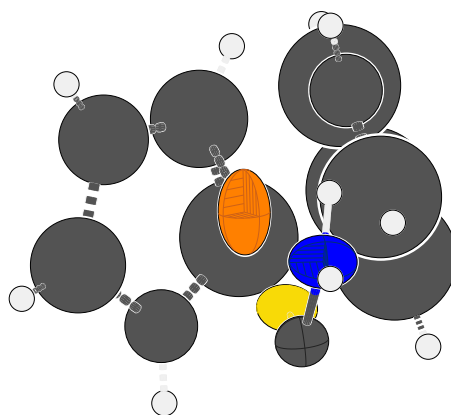


Figure 3.3: The final model of **TFIC-2** at 290 K.

Next, we tried with the coldest high-temperature phase available, 155 K, in the hope that the guest molecules are «calmer» while still retaining the undistorted host framework.

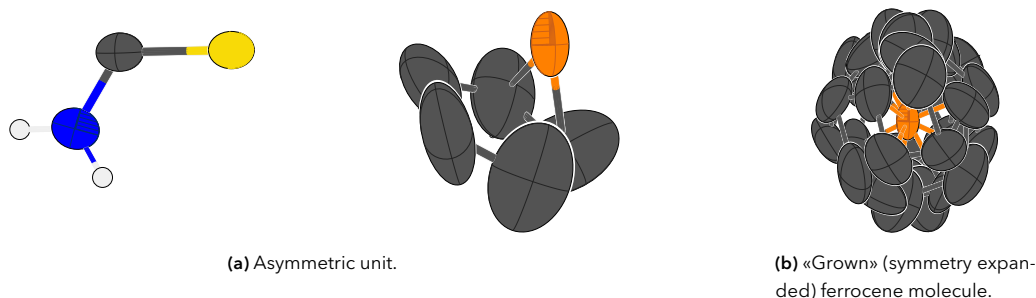


Figure 3.4: Final model of TFIC-2 at 155 K.

Despite a drop of 135 K in temperature, we were still unable to ascertain a clear positioning of the ferrocene molecule. One of the cyclopentadienyl rings was again deleted, as the refinement rapidly diverged with the whole molecule in place. After trying various models, a real improvement could not be obtained. A different approach with only one of the carbon rings was carried out. No disorder component was enabled (all constituents in PART 0), and the occupancy of most of the carbon atoms were refined freely, which rendered quite different values (0.322, 0.444, 0.411, 0.250 (fixed), 0.512). This time, the program was able to converge on a model with anisotropic displacement parameters, but no hydrogens could be automatically added. See Figure 3.4a. There is a notable inclination of the cyclopentadienyl ligand in Figure 3.4a, but the accuracy of this is dubious. Final R_1 factor for this solution is 7.56 % and maximum electron density difference $0.9 e/\text{\AA}^3$.

Analysis of the TFIC-2 low-temperature phase

The same initial procedure was followed in CrysAlis, except that the number of formula units was changed to $Z = 4$ prior to script execution. After the search for peaks was completed, a hR lattice was assigned with a 75 % match. A rerun of unit cell search immediately found a mI lattice matching 81 % of the reflections. No further convincing twin components were discovered, so the subsequent analysis of this data set at 140 K proceeded as a single crystal experiment. Automatic data reduction procedure gave the expected space group $P2_1/c$, but suffered a greater loss in signal strength than expected: $\langle I/\sigma \rangle = 6.7$. Switching off the lattice extinctions filter did not help. Modelling the ferrocene in this data set seemed hopeless.

Before giving up on this data set, reprocessing it as a two-component (rhombohedral-monoclinic) multi-crystal was tried, but this only produced worse structure files. A last check at the coldest temperature, 100 K, was also conducted, but without any workable

results. It seems more constructive to work with **TFIC-3** which has a superior signal quality.

Analysis of the TFIC-3 high-temperature phase

The common initial procedure was commenced with the data set at 290 K. A 74 % match with a hR lattice (8 683 peaks) was found, but the cell parameter $a \approx 43.15 \text{ \AA}^\dagger$. Another automatic unit cell indexation gave the anticipated cell, but now with only 988 (33 %) peaks matching. Some fiddling with twin components landed at a 58 : 23 ratio (of separate reflections), where the two components were rotated 38.23° around the c -axis. After this, 19 % (2 197) peaks were unindexed. Still, the remaining peaks without an attachment to any lattice were comparatively weak and unable to fit another component by more than 6–7 %. We therefore simply proceeded with the structure as a twin.

The results from the data reduction were promising. A refined mass fraction of 79.23 : 20.77 and $R_{\text{int}} = 2.62\%$; $\langle I/\sigma \rangle = 67.5$ of the largest component, contrary to $R_{\text{int}} = 7.01\%$; $\langle I/\sigma \rangle = 21.7$ for the other, suggested we continue the structure solution with the primary component.

Despite a better starting point, the best model obtained was one similar to that shown in Figure 3.4, with the same electron density difference, and a slightly improved $R_1 = 6.68\%$. The hydrogens on the cyclopentadienyl ligands hindered the refinement convergence here as well. The carbon atoms could all be free here without any issues: (0.208, 0.410, 0.583, 0.613, 0.018), although the significance of this is vague.

We now investigate the last data set before the main phase transition, at 155 K, in the same manner. Two twin components were found in CrysAlis with a rotation of 38.23° again. The mass fraction was refined to 74.18 : 25.82. Superb indicators were attributed the primary component—a merging residual of $R_{\text{int}} = 2.68\%$ and $\langle I/\sigma \rangle = 85.0$,

Table 3.2: Structure solution data for **TFIC-3** at 155 K.

Property	Value
Sample name/label	TFIC-3_06_155K_twin1
Space group	$R\bar{3}c$ (#167)
Temperature	155 K
Lattice parameters	$a = 16.176\ 10(10) \text{ \AA}$ $c = 12.354\ 1(2) \text{ \AA}$
Cell volume V	$2\ 799.56(6) \text{ \AA}^3$
Mass density ρ	1.475 g/cm^3
Chemical formula	$\text{C}_{13}\text{H}_{22}\text{FeN}_6\text{S}_3$
Formula units Z	6
Wavelength	$0.698\ 0(1) \text{ \AA}$
Number of reflections	total: 6 583; unique: 961
Reflection indices limit	$\pm\{24, 24, 13\}$
Refinement factors	$R_{\text{int}} = 2.68\%$ $R_1 = 5.97\%$ $wR_2 = 19.99\%$ GooF = 1.111
Mean signal-to-noise ratio	$\langle I/\sigma(I) \rangle = 85.0$

[†]This corresponds to a seven-fold increase in unit cell volume. The cell height, c , remained the same.

while the second component had $R_{\text{int}} = 5.02\%$ and $\langle I/\sigma \rangle = 28.4$.

Using SHELXT to gain a solution to work with, the thiourea molecule and the iron atom were refined a few times anisotropically. In the emerging Q peaks, we are able to discern five in which a cyclopentadienyl ring is suitable. The ligand on the other side, however, is rotated too much for a good fit. We therefore proceed using individual rings instead. Placing the first one generates the other one automatically. The second fragment was placed in a similar manner to five Q peaks, becoming almost perpendicular to the first ring. The occupancy of the couple of cyclopentadienyl rings were fixed at $\frac{1}{2}$ to compensate for multiplication by the space group symmetry. The refinement now settled without any difficulties or with the guest atoms becoming unreasonable, but reaching relatively poor refinement parameters: $R_1 = 5.97\%$; goodness of fit: 1.111; and maximum electron density peak difference of $1.5 \text{ e}/\text{\AA}^3$. An illustration of the final solution is presented in Figure 3.5.



Figure 3.5: Final model of TFIC-3 at 155 K.

Attempts were made at having the two cyclopentadienyl parts share two common, diametrically opposite carbon atoms (like Lorson et al.^[46]), but without great success. This could point to more disorder in our data, but when the structure is «grown» it looks as chaotic as Figure 3.5b regardless of whether the two ligands were connected at common carbon atoms, if we use $\frac{1}{2}$, or use one or two ligands in the asymmetric unit.

Analysis of the TFIC-3 low-temperature phase

Let us first consider the data set at 140 K. Recall from Subsection 2.2.3 that there were two peculiar observations at this temperature; (1) the splitting/elongation of nodes indicated that perhaps only one of the components had initiated the main phase transition, and (2) when returning to 140 K the transition seemed significantly more «completed». It appears that both components have transitioned at 100 K.

With the regular procedure in CrysAlis, the program still insists on an hR lattice (71 % match), but it could be transformed to a metric with recognised monoclinic cell parameters (discussed on page 72). After this, we were able to find a twin component rotated

141.74° (which is supplementary to 38.2°). The remaining 16.7% of peaks were unindexed, but comparatively weak.

Twin analysis by CrysAlis reported a 88:12 mass ratio; $R_{\text{int}} = 3.5\%$ and 5.2% ; and $\langle I/\sigma \rangle = 77.3$ and 22.9 , for the two components respectively. However, the wrong space group $R\bar{3}c$ was automatically set. Redoing the data reduction with a manual space group inspection yielded a mass ratio of 89:11, $R_{\text{int}} = 2.83\%$ and $\langle I/\sigma \rangle = 48.3$ for the major component.

SHELXT located all atoms but the cyclopentadienyl members. Trying to fit a ferrocene fragment results in the same story as at 155 K—and the same remedy attempted. Pentagons of Q peaks were spotted a bit easier at this temperature. Although a satisfactory fit was found for four cyclopentadienyl rings, and the structure was able to settle with anisotropic refinement on all non-hydrogen atoms, a maximum electron density difference of $1.8 \text{ e}/\text{\AA}^3$ and $R_1 = 8.97\%$ signifies an imperfect solution. Contrary to Lorson et al.^[46] the two cyclopentadienyl parts do not share any carbon atom positions, only the iron position, in this particular solution at 140 K.

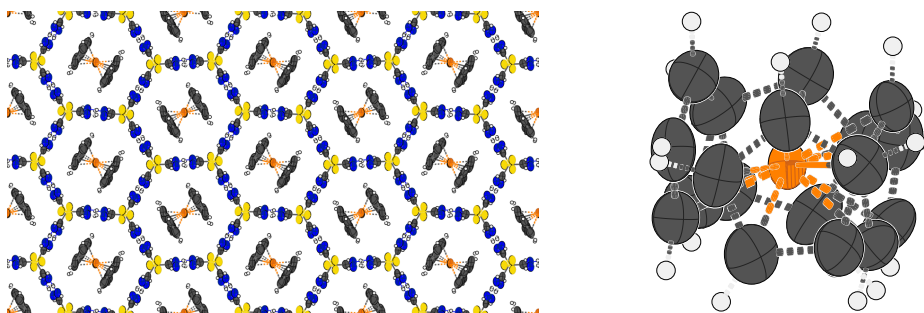
Before leaving the first data set at 140 K, another analysis was carried out with a multi-crystal assumption, i.e. one twin domain being monoclinic, while the other still being rhombohedral. From the intensities seen in Figure 2.18, it seems that the largest component is the one transitioning first (and retaining its monoclinic cell longest when increasing in temperature). The result from CrysAlis was an unusable monoclinic part, and a great rhombohedral component ($R_{\text{int}} = 2.29\%$; $\langle I/\sigma \rangle = 95.7$). Analysis of the latter lead to an identical «clamshell» solution as the final model of **TFIC-3** at 155 K.

The twinning issue escalates at 100 K, as it is hard to tell whether any extra (transformation) twins have been created in addition to the two «original» (growth) twin components. Recall that at this stage, both twin individuals appear fully transitioned in the diffraction patterns.

Table 3.3: Structure solution data for **TFIC-3** at 140 K.

Property	Value
Sample name/label	TFIC-3_07_140K_twin1
Space group	$P2_1/c$ (#14)
Temperature	140 K
Lattice parameters	$a = 10.19220(10) \text{ \AA}$ $b = 16.1501(2) \text{ \AA}$ $c = 12.3515(3) \text{ \AA}$ $\beta = 113.823(2)^\circ$
Cell volume V	$1859.89(6) \text{ \AA}^3$
Mass density ρ	1.480 g/cm^3
Chemical formula	$\text{C}_{13}\text{H}_{22}\text{FeN}_6\text{S}_3$
Formula units Z	4
Wavelength	$0.6980(1) \text{ \AA}$
Number of reflections	total: 15 116; unique: 5 127
Reflection indices limit	$\pm\{15, 24, 13\}$
Refinement factors	$R_{\text{int}} = 2.83\%$ $R_1 = 8.97\%$ $wR_2 = 32.05\%$ Goof = 1.078
Mean signal-to-noise ratio	$\langle I/\sigma(I) \rangle = 48.3$

Initially, an hR lattice was proposed by CrysAlis matching 24 % of the 42 479 peaks found. Two components were found rotated 98° from each other about the (direct) c -axis. These indexed 34.2 % and 15.2 %, respectively. With half still unindexed and the remaining peaks appearing strong, a search for additional twins was conducted. Eventually, four components whose indexations were all above 10 % were selected. The 27 % still unindexed were still medium in strength. Unfortunately, after data reduction all components had an $R_{\text{int}} > 10\%$. The best case was the primary component with $R_{\text{int}} = 11.2\%$ and $\langle I/\sigma \rangle = 37.6$. Surprisingly, SHELXT was able to create the main framework of the structure (some incorrect elements were chosen), and for the first time pentagon patterns clearly emerged in the distribution of Q peaks surrounding the iron atom. Thus, the same model as Lorson et al.^[46] could easily be resolved, i.e. two quasi-perpendicular cyclopentadienyl pairs which share two nearly diagonally opposite[†] carbon atoms in common.



(a) View down the tunnels in the monoclinic regime. Note that the ferrocenes (and hexagonal cavities) are shown in two different conformations, and that the thiourea edges are nearly horizontal, but not exactly. Only one part is shown here—the parallel part is hidden.

(b) The two ferrocene parts at 100 K superimposed in Olex2. Two of the carbon atoms are shared by both parts. The remaining carbon atoms are fixed at 50 % occupancy.

Figure 3.6: Final model of TFIC-3 at 100 K.

Going back to CrysAlis, an analysis with just two monoclinic components was carried out in an attempt to improve the data reduction results. Two mP twin components were found indexing 36.9 % and 14.5 %, respectively. They are rotated 22.33° from each other about the c -axis (in direct space). After data reduction, the result for the main component was $R_{\text{int}} = 5.7\%$ and $\langle I/\sigma \rangle = 47.4$. (The second component was inapt: $R_{\text{int}} = 23.5\%$; signal-to-noise: 11.0.) The same structure was obtained. Despite appearing reasonable—see Figure 3.6—goodness parameters are quite unsatisfactory ($R_1 = 17.15\%$ and maximum peak $3.3 e/\text{\AA}^3$).

Finally, the returning 140 K data set was analysed. Recall from Figure 2.18 that the two individuals appear to be captured on either side of the phase transition. This was

[†]Considering a single ferrocene molecule (one «PART»), then one of the shared atoms is neighbouring the inversion of the other.

observed for the first 140 K data set, too, but the low-temperature component seems more «complete» in this case. In *CrysAlis*, an *hR* lattice is first proposed which accounts for 38 % of the peaks. Considering it as a multi-crystal twin with both phases present was first attempted, in which a *mP* lattice indexed 46.2 % and an *hR* 16.5 %, but the results turned out unusable. Then two monoclinic cells, rotated around the *c*-axis and with very similar indexation fractions, was tried, but unfortunately did not produced better results.

Analysis of TFIC-1 high-temperature phase (at 240 K)

Recall from Subsection 2.2.1 that the **TFIC-1** is an obverse–reverse twin, quite typical of rhombohedral specimens. Immediately after acquiring the peak table, we notice a different lattice symmetry of $6/m$ (instead of $\bar{3}$). The diffraction pattern, which we now know is of a merohedral nature, looks very «clean» without much noise. This is reflected in the 98.03 % match between the found peaks and the *UB* matrix.

One is able to divide the obverse and reverse reflections into separate groups in *CrysAlis*. We find 5 091 peaks belonging to the obverse domain and 2 980 to the reverse, which is close to a $\frac{2}{3}$ fraction for the primary component. Unable to make *CrysAlis* distinguish the two components as separate, we continue the analysis with the smaller domain hidden and use a filter for lattice extinctions (letting through the obverse reflections).

This resulted in a data reduction with indicators $R_{\text{int}} = 4.96\%$ and $\langle I/\sigma \rangle = 57.2$. Since this was not better than previously obtained values (as with **TFIC-3**), we tried something else. Going back to *CrysAlis* we performed another reduction of data, but this time without any lattice extinction filters nor any outlier rejection procedures. *CrysAlis* would be oblivious to the twinning, but we might have had luck with configuring that in the structure solution step. Unfortunately, the results were poorer: $R_{\text{int}} = 11.16\%$ and $\langle I/\sigma \rangle = 24.4$.

Analysis of TFIC-1 low-temperature phase (at 90 K)

An initial *C*-centred $2/m$ lattice was suggested by *CrysAlis* with a 47.40 % match (9 325 of 19 672 reflections). The reciprocal space is quite chaotic, so four reasonable components were investigated (percentages include overlap):

- *hR* lattice: $a \approx 16.0 \text{ \AA}$; $c \approx 12.45 \text{ \AA}$; 55.9 %
- *mI* lattice: $a \approx 10.2 \text{ \AA}$; $b \approx 16.1 \text{ \AA}$; $c \approx 12.45 \text{ \AA}$; $\beta \approx 114.1^\circ$; 19.2 %
- *oC* lattice: $a \approx 10.2 \text{ \AA}$; $b \approx 22.7 \text{ \AA}$; $c \approx 16.26 \text{ \AA}$; 15.9 %
- *oC* lattice: $a \approx 10.1 \text{ \AA}$; $b \approx 22.7 \text{ \AA}$; $c \approx 16.23 \text{ \AA}$; 9.0 %

Results from the data reduction were unworkable.

If one searches for a matching unit cell repeatedly, the program seems to cycle through all of these and other «candidates» (including *mP* and *mC*, *hP*), each matching around

47 % alone. Attempt with a triplet mP crystal was futile. Then a twin mP lattice was tried, then a single monoclinic cell, also without success. An $mC-hR$ multi-crystal indexing in total 59.4 %, but the results were very poor. Finally a single mI cell, single hR , and a single mC lattice were tried, just for comparison. In all cases studied, the obtained data do not have any practical usefulness. The same goes for the 140 K data sets.

Analysis of TFIC-1 «phase 2» (at 180 K)

Separating out the new reflections observed in Figure 2.5b, we find that they fit a superlattice: $c_{180\text{K}} \approx 61.79 \text{ \AA} \approx 5c$, where c is the «conventional» repeat length of the tunnel axis. Also these reflections are mixed between the obverse and reverse individuals, but the intensity distribution can be described as generally weaker and more random than the regular peaks. About 2–3 times more reflections are indexed in the main lattice, compared to the superlattice.

While a twinning approach failed, going through the analysis assuming the crystal to be a superstructure, with a modulation vector $\mathbf{q} \approx 1/5 \mathbf{c}^*$ appeared to better describe the circumstances. A merging residual of $R_{\text{int}} = 5.25 \%$ is not bad in comparison with the previous results, but the reduced data files were not refining satisfactorily in JANA2020^[70].

Analysis of TFIC-1 «phase 3» (at 165 K)

At this temperature, we notice a minor «expansion» of satellites along the \mathbf{a}^* -plane (see Figure 2.5c). Using the Ewald Explorer of CrysAlis, we are able to fit 89 % of the reflections when using a two-dimensional modulation vector: $\mathbf{q}_1 \approx 1/5 \mathbf{c}^*$ and $\mathbf{q}_2 \approx 1/2 \mathbf{a}^* + 1/2 \mathbf{b}^* + 1/5 \mathbf{c}^*$. The satellites account for approximately 19 % of the total reflections.[†] The merging residual was similar for this modulated structure, $R_{\text{int}} = 5.95 \%$, but the signal was very poor at only $\langle I/\sigma \rangle = 2.9$.

[†]1 996 satellites and 8 351 of the main lattice. These figures combine the obverse and reverse settings.

3.2.2 Structure solution statistics and conclusions

Refinement parameters and the relevant details are found in the three preceding tables in this chapter. Ideally we would have one solution for both phases of all three TFIC samples, but not enough converging results derived from our endeavours. Besides the pure ferrocene (Table 3.1) solution, only the best candidates for the high-temperature rhombohedral phase (Table 3.2) and low-temperature low-temperature monoclinic phase (Table 3.3) are considered to be of satisfactory quality, as the numbers in Table 3.4 show. Even with the prepared ferrocene fragment, a straightforward solution was difficult to achieve all the same.

Table 3.4: A collection/overview of all the three structure solutions presented in the previous section.

	Ferrocene at room temperature	TFIC high-temperature	TFIC low-temperature
Sample name/label	Ferrocene	TFIC-3_06_155K_twin1	TFIC-3_07_140K_twin1
Space group	$P2_1/n$ (#14)	$R\bar{3}c$ (#167)	$P2_1/c$ (#14)
Temperature	290 K	155 K	140 K
Lattice parameters	$a = 5.928\,60(17)\text{ \AA}$ $b = 7.612\,00(10)\text{ \AA}$ $c = 9.041\,10(10)\text{ \AA}$ $\beta = 93.156\,0(10)^\circ$	$a = 16.176\,10(10)\text{ \AA}$ $c = 12.354\,1(2)\text{ \AA}$	$a = 10.192\,20(10)\text{ \AA}$ $b = 16.150\,1(2)\text{ \AA}$ $c = 12.351\,5(3)\text{ \AA}$ $\beta = 113.823(2)^\circ$
Cell volume V	$407.392(14)\text{ \AA}^3$	$2\,799.56(6)\text{ \AA}^3$	$1\,859.89(6)\text{ \AA}^3$
Mass density ρ	1.517 g/cm^3	1.475 g/cm^3	1.480 g/cm^3
Chemical formula	$C_{10}H_{10}Fe$	$C_{13}H_{22}FeN_6S_3$	$C_{13}H_{22}FeN_6S_3$
Formula units Z	2	6	4
Wavelength	$0.698\,0(1)\text{ \AA}$	$0.698\,0(1)\text{ \AA}$	$0.698\,0(1)\text{ \AA}$
Number of reflections	total: 3 360; unique: 1 126	total: 6 583; unique: 961	total: 15 116; unique: 5 127
Reflection indices limit	$\pm\{8, 11, 10\}$	$\pm\{24, 24, 13\}$	$\pm\{15, 24, 13\}$
Refinement factors	$R_{\text{int}} = 1.23\%$ $R_1 = 2.77\%$ $wR_2 = 8.36\%$ $\text{Goof} = 1.090$	$R_{\text{int}} = 2.68\%$ $R_1 = 5.97\%$ $wR_2 = 19.99\%$ $\text{Goof} = 1.111$	$R_{\text{int}} = 2.83\%$ $R_1 = 8.97\%$ $wR_2 = 32.05\%$ $\text{Goof} = 1.078$
Mean signal-to-noise ratio	$\langle I/\sigma(I) \rangle = 84.7$	$\langle I/\sigma(I) \rangle = 85.0$	$\langle I/\sigma(I) \rangle = 48.3$

In Table 3.4 above we see a copy of three mentioned tables, repeated here for easier comparison.

TFIC-1 summary

Our first TFIC crystal is twinned by reticular merohedry (see pages 140 and 141) in a typical obverse–reverse fashion. The primary component is estimated to be twice as massive as the minor domain. Although we do not seem to learn much from the structure solutions of TFIC-1, this sample exhibits great complexity and unique traits, as discussed in Subsection 2.2.1. Recall that at 180 K and 165 K we described structural changes which

appear exclusive to **TFIC-1**. Despite unavailing data reductions, we got indications that the emerging superlattice may be resulting from a modulation along the tunnel axis, extending the repeat distance five-fold. At 165 K, an additional modulation vector was proposed by CrysAlis to fit the diffraction spots. To account for this extra dimension, one could imagine a helical-shaped modulation description, shifting or orienting the molecules in a fashion similar to the steps of a spiral staircase. This idea has not been pursued further at the present time.

We were unable to properly instruct CrysAlis about this particular nature of twinning. The twin law is therefore not found in the `cif` file, but the typical obverse–reverse twinning can be achieved with the operation $2_{[001]}$ (cf. Subsection 2.2.1, page 39).

TFIC-2 summary

Even though **TFIC-2** is the only non-twinned crystal at our disposal, it has the poorest signal-to-noise ratio among our samples. This is likely due to a filter being used with this measurement series. Despite being the simplest candidate, solution attempts were challenged by unstable atoms of cyclopentadienyl ligands. Reasonable models were obtained for the high-temperature phase, albeit with no parameter triumphing above the other samples. Below the critical temperature 150 K, the noise is apparently too overwhelming for any constructive work.

TFIC-3 summary

The plesiotwin falls in the «non-merohedral» classification, with an approximate 4 : 1 mass fraction ratio, where the minor component is rotated about the *c*-axis by 38.2°. The mass fractions determined by CrysAlis are found in Table 3.5.

An interesting discrepancy was found among data series number 7 and 9: the two at 140 K, cf. Figure 2.18 on page 49 for an exposition in reciprocal space. Looking closely at Figure 2.5 as the temperature progresses downwards, note how all the reflections from the first room temperature phase become (1) flattened along \mathbf{a}^* and (2) split in the same direction.

In the second data set, four crystal components were suggested by the program: two belonging to the rhombohedral system, indexing 50.2% and 20.9%, respectively. The other two being monoclinic, indexing 14.3% and 12.0% of the reflection peaks, respectively. All four components are mutually rotated in the *ab*-plane.

Using equation (1.2) we obtain a value of $D = 1.017$

Table 3.5: Twin mass fractions for **TFIC-3**.

Temperature	Major component
290 K	79.23 %
155 K	74.18 %
140 K	88.72 %
100 K	88.80 %

for the so-called «distortion parameter».[†] The fact that $D > 1$ tells us that the hexagonal honeycomb cross-sections are «squeezed» at a pair of opposing edges.^[65] Other similar values to compare with are: 1.009 (thiourea–ferrocene at 135 K)^[46] and 1.044 (thiourea–bromocyclohexane at 110 K).^[65]

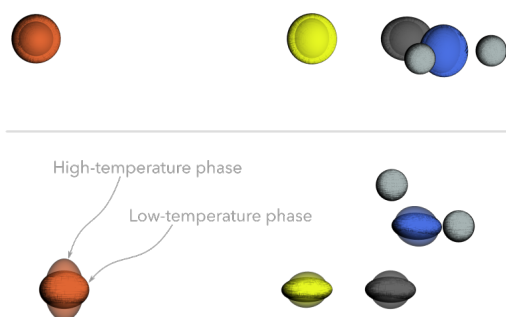


Figure 3.7: Comparison of the atomic displacement parameters between the high- and low-temperature phases, seen from above (top) and from the side (bottom). Only the asymmetric unit is shown, and the carbon atoms of the ferrocene are omitted. Transparent atoms represent the high-temperature case; the solid atoms are copies with the ADPs changed to those of the low-temperature phase. The cold phase structure was «solved» in the trigonal crystal system.

Although it had proven to be difficult attaining any meaningful insight from the disordered cyclopentadienyl rings, a common observation that distinguishes the two phases is a noticeable «flattening» of the ADPs (atomic displacement parameters) when transitioning to the colder structure, see Figure 3.7. This affects both the host network and the iron atom of the ferrocene. Regardless if the low-temperature structure should be assigned a monoclinic or rhombohedral cell, this observation supports the idea of a distorted honeycomb structure with the positioning of the same elements varying more in the horizontal plane from one cell to another.

Combined conclusion on the high-temperature rhombohedral phase

It is evident that ascertaining the positions of the thiourea atoms is straightforward, while the ferrocenes never seem to fit well in a single unit cell. A refined charge difference at around $1.4 e/\text{\AA}^3$) coupled with substandard R_1 factors at circa 7% signal that our model is imperfect. Typical measures for dealing with disorder, such as splitting the unit into different parts and adjusting occupancy, have been attempted to no avail. Despite this, the attained model may indicate that there are two main orientations, as stated in the literature.

Combined conclusion on the low-temperature monoclinic phase

The low-temperature phase is afflicted by a fragmentation of reflections, likely due to the notorious, multiple twinning, making most of the reduced single crystal data impractical

[†]The distortion parameter quantifies the deviation from a perfect hexagonal symmetry. Since we have used an alternative space group representation, we have used lattice parameter c in place of a .

for further research. Our best chance was with the already twinned sample **TFIC-3**, whose great signal quality delivers a model which is recognisable to the other literature models. Despite appearing realistic, and similar to e.g. the model of Lorson et al.^[46], the poor refinement values suggest that also this phase may require further research outside the conventional unit cell scheme. We have chosen to let the first 140 K data set represent this phase since it nonetheless has the best qualifiers, and note that there are no common carbon positions in that solution, contrary to that at 100 K.

Commentary on commensurability

From the inspected reconstructions in Chapter 2, we find no supporting evidence for incommensurability between then host and guest. Commensurability is the expected configuration (see Subsection 1.4.2).^[32,65] Although an exception has been found with 1-*tert*-butyl-4-iodobenzene as guest, the incommensurability between the host and guest repeat distances along the tunnel axis results in two distinguishable diffraction layers.^[64] We do not find such systematic features (nor extra Bragg spots), at least not in the untwinned **TFIC-2** crystal sample, and the separated reflection seen in **TFIC-1** are explained by twinning. Split reflections in the low-temperature phase are still considered to belong to the main lattice.

Investigating the shape of the iron atom's atomic displacement parameters (see Figure 3.7) we observe that the spatial dimensions change from extending along the tunnel to a «flattened» shape across the tunnel cross section instead. This description goes for all atoms except the elusive cyclopentadienyl carbons. Regardless, the iron atoms do not seem to possess continuous disorder, suggesting that the ferrocene molecules are still fitted by steric forces at special positions in the thiourea tunnels, and that twinning causes the variation across the tunnel axis.

Orthohexagonal relations

The unit cell determination procedure in CrysAlis usually recommends the same rhombohedral variant instead of the expected monoclinic cell, even at the lower temperatures. It is, however, possible to use the «Lattice reduction» tool to transform to alternative cells. One will recognise the monoclinic lattice ($a = 10.25 \text{ \AA}$, $b = 16.25 \text{ \AA}$, $c = 12.37 \text{ \AA}$, $\beta = 113.7^\circ$) among the suggested alternatives, although with often with *I*-centring.

It was found that combining the (inverse transpose of the) matrix for advancing the cell choice of monoclinic cells with unique axis b , P_1 , with the (transpose of the) matrix from converting a hexagonal cell to orthohexagonal C_2 centred cell, P_2 , one of the suggested

transformations was obtained:

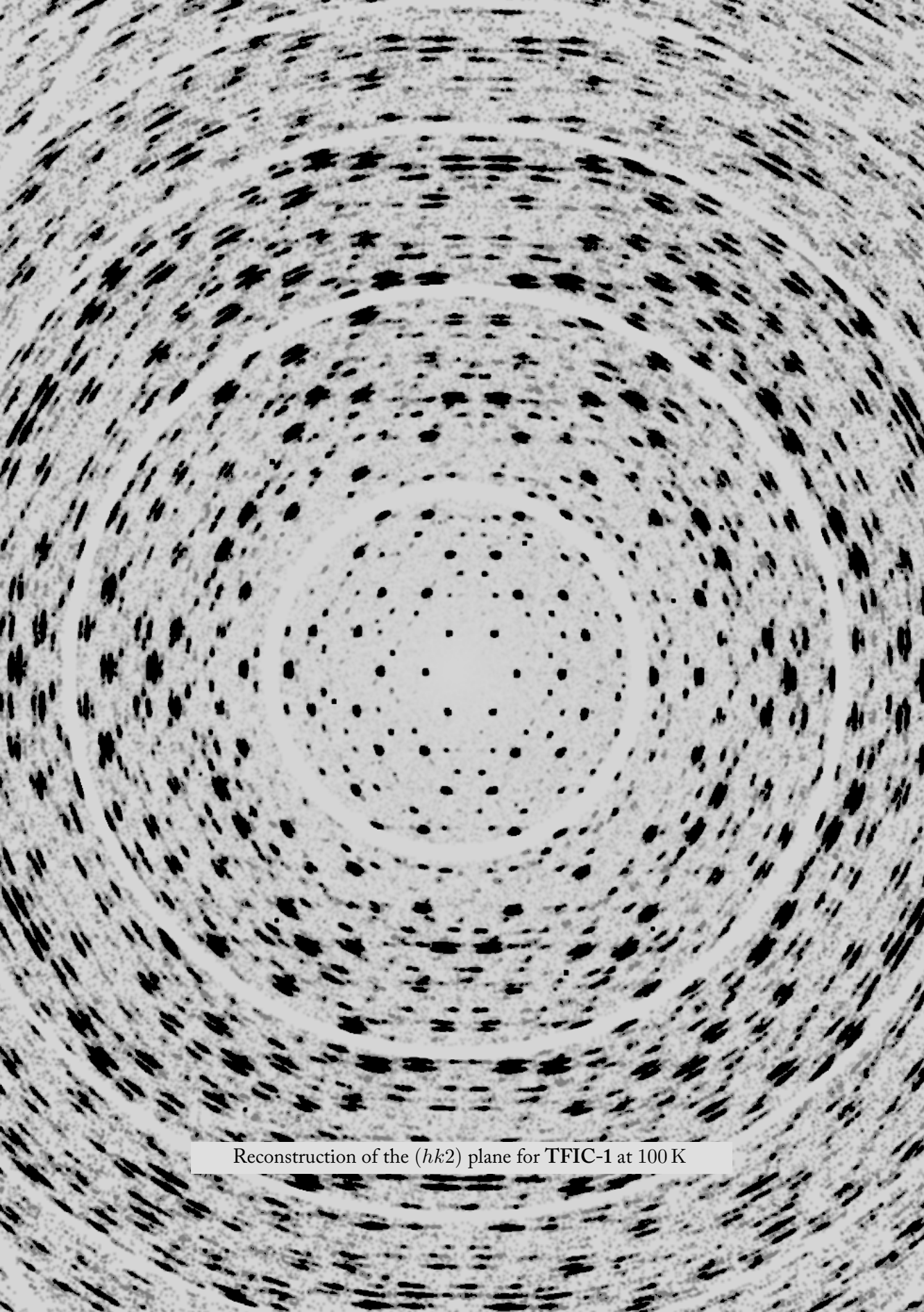
$$P_1 = \begin{pmatrix} \bar{1} & 0 & 1 \\ 0 & 1 & 0 \\ \bar{1} & 0 & 0 \end{pmatrix}, \quad P_2 = \begin{pmatrix} 1 & \bar{1} & 0 \\ 1 & 1 & 0 \\ 0 & 0 & 1 \end{pmatrix}, \quad P_1^{-\text{T}} \cdot P_2^{\text{T}} = \begin{pmatrix} 0 & 0 & 1 \\ \bar{1} & 1 & 0 \\ \bar{1} & \bar{1} & \bar{1} \end{pmatrix}$$

The conversions from rhombohedral to monoclinic cells given in Table 5.1.3.1 in volume A in the International Tables for Crystallography^[30] yield a different monoclinic unit cell.

Jones et al.^[39] mention that the monoclinic structure is very close to that derived by the same transformation provided by Clément et al.^[15] (see equation (1.1)).

Part II

*The Mathematica
X-ray Diffraction Package*



Reconstruction of the $(hk2)$ plane for TFIC-1 at 100 K

The MaXrd package

4.1 The beginning

4.1.1 Why Mathematica?

A common question about the *MaXrd* (Mathematica X-ray diffraction) package is why we have chosen to write it in this particular language. Surely, scientific software ought to be completely free, and Mathematica is a commercial software made by **Wolfram Research**. It comes down to one's work preferences, and the justification is subjective. Our research group happens to have a long history with Mathematica and plentiful of scripts and notebooks in our archives. The source code is nonetheless open and available for review and collaboration on **GitHub**.

An essential part of Mathematica is of course the notebook interface.[‡] This concept is intuitive and convenient for drafting and working with research. A free and equivalent system is IPython^[69], which drives the more popular Jupyter^[42] notebook interface. Still, Mathematica differs by having a more unison experience, since it is delivered with practically everything that is needed. The greatest advantage is nonetheless the built-in documentation of Mathematica. It is truly the best way of browsing and learning about the existing library of functions. This enables the researcher to program in a relatively streamlined and high-level code environment, with functional relations stretching across most areas of science and engineering, including state-of-the-art technologies such as artificial intelligence, especially machine learning capabilities. It is thus a robust work environment for an age where data is constantly increasing in size and complexity.

Given the choice again, however, I am not sure whether Python is the preferred answer. Once the project had grown to a certain point, it would perhaps have been better to use a statically typed language—a migration to another language can always be done in the future.

A final point to consider, regarding the time ahead, is that the usability is likely to survive for a great while, as the Wolfram Language is known to be compatible with legacy code written in many versions back. Also, Mathematica is quite flexible in terms of linking to other languages, and working via Wolfram Script is possible for those who prefer working without a graphical frontend. Many neat applications do not stand the test of time and end up in the **Crystallography Source Code Museum**. By relying on Wolfram to continue their work with Mathematica, *MaXrd* will likely survive for many years to come, even without maintenance from our side.

[‡]Mathematica is technically the kernel and the front end, and the code is written in the *Wolfram Language*.

4.1.2 The initial purpose and vision

During the author's master thesis, access was given to old routines used to calculate structure factors. The engagement in that work was useful to get familiar with all the pieces required in such computations, and it also sparked a yearning for factorising the code and make things more general. At this point, most of the symmetry information on point groups and space groups had been reproduced in a format to be used with Mathematica. For completion, this «data base» was later reorganised and expanded to include all non-conventional space groups as well as more entries, such as reflection conditions. With the addition of scattering cross section data and atomic form factors the core concept began to take form.

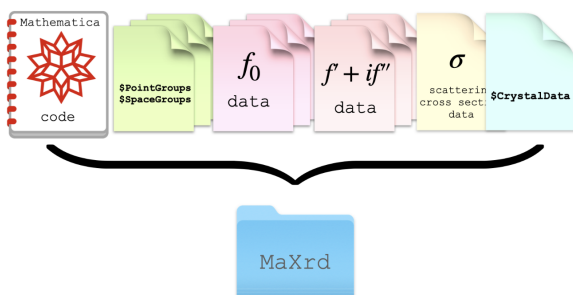


Figure 4.1: Illustration of the package's core contents. The first block represents all the Wolfram code behind the functions and documentation. The next four represent tabulated or incorporated data from external sources, which are essential to some calculations. The final piece, `$CrystalData`, denotes the interface with crystallographic data—a default set of «demo crystals» is included, and new structures can be added through cif files.

At this stage, the toolkit was regarded to be a supporting tool to lectures in introductory courses to crystallography and scattering physics, where topics such as Miller indices, reciprocal space, Bragg's law, symmetry operations, structure factors, etc. are central to the curriculum. Throughout the development our goal has been to make it as user-friendly as possible, requiring only the minimum from the user and no expertise in the Wolfram Language.

The project eventually branched into the area of inclusion compounds, aspiring to prove useful in the research of host–guest systems; particularly the TFIC in our case. Most of the new functions in version 2.3.0 were built on the symmetry foundation of the original package. Among the more valuable additions are the abilities to create and plot the crystal structures, and the interface with programs for simulating reciprocal space (diffraction patterns). This represents the key to analysing crystal structures by the means of combined direct–reciprocal space modelling. The modelling results may be compared to relevant experimental data.

A static version of the documentation may be found at ux.uis.no/~stianr. A complete change log may be found in Appendix B.

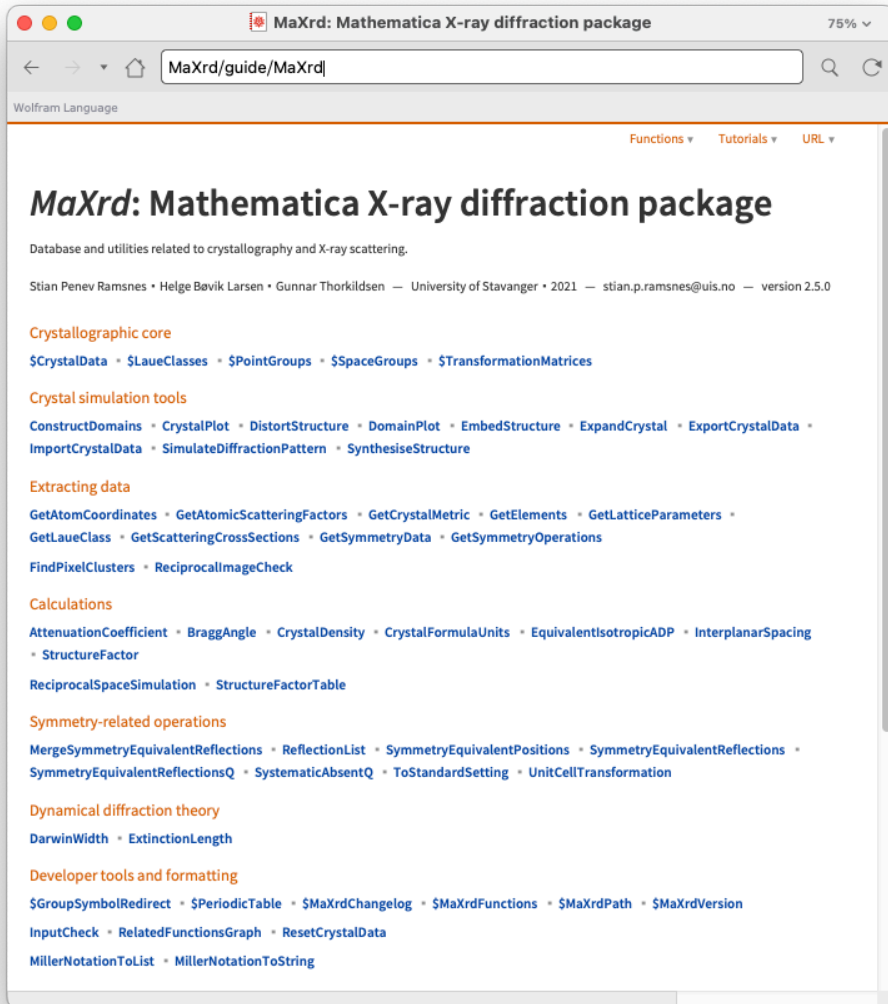


Figure 4.2: Screenshot of the main guide page in the documentation. Functions have been divided into likely associated application areas. On each page, closely related functions are listed as well.

4.1.3 A quick tour of the package

Once the package had been thoroughly generalised and tested, the first article^[75] was written, giving the package an official and—more importantly—a peer-reviewed launch. While acknowledging that MaXrd is by no measure revolutionary, it is a simple, practical and helpful tool, which has received warm responses by the people whose interest happens to intersect both crystallography and Mathematica.

The primary method of user interaction with the package's content is via code expressions. In the following example,

```
1 BraggAngle["Nickel", 1.5418, {1, 1, 3}] (* Output: 46.5202 Degree *)
```

the arguments are the crystal label, wavelength in ångströms, and reflection indices, respectively. When accessing the documentation page of `BraggAngle`, one will see that the wavelength can be omitted if was included in the `cif` file at import. The output here is a `Quantity`, i.e. some unit accompanies the number. This goes for the similar, basic «calculating» functions—see other functions in this section on the guide page (Figure 4.2). We believe such measures are suited to avoid confusion, especially in a teaching environment, but this may be switched off with the Boolean `"Units"` option.

Another category of functions on the guide page are those used for «Extracting data», most of which start with `Get-`. The majority of these are «shortcut» procedures for obtaining information stored either in the data sources accompanying MaXrd or in crystallographic data imported by the user.

For more details on the essentials of MaXrd, consult the Mathematica documentation or see Ramsnes et al.^[75].

Importing crystallographic data

Structural data can naturally be inputted via `cif` files with `ImportCrystalData`. All such data is stored in the variable `$CrystalData` in memory, and may be accessed either directly as shown in Figure 4.3 or via auxiliary functions (e.g., `GetSymmetryData` or `GetAtomCoordinates`).

Since many of the tools mutate the crystal data, one may find it useful to run:

```
2 ResetCrystalData[]
3
4 (* Output: *)
5 {"Aluminium", "Austenite", "CalciumFluoride", "Cobalt(II)Fluoride", "Copper", "CopperTungstenOxide",
6 "Corundum", "Diamond", "Ferrite", "GalliumArsenide", "Germanium", "Glycyl-L-alanine", "Ice",
7 "LanthanumHexaboride", "LithiumCobaltate", "LithiumManganesePhosphate", "ManganeseSilicon",
8 "Nickel", "OxalicAcid", "Perovskite", "Polonium", "PrussianBlue", "Quartz", "Silicon", "Silver",
9 "Sodalite", "SodiumChloride", "Sphalerite", "Tungsten", "Zinc"}
```

in order to restore to the default «demo library» of crystal structures. These are mainly useful for demonstration purposes.

ChemicalFormula	C ₁₀ H ₁₀ Fe	
FormulaUnits	2	
SpaceGroup	P2 ₁ /n	
LatticeParameters	a	5.9286 Å
	b	7.612 Å
	c	9.0411 Å
	α	90°
	β	93.156°
	γ	90°
Wavelength	0.69804 Å	
AtomData	{ ... ₂₁ }	

(a) Main data entry.

Figure 4.3: Crystal data entry example, here of ferrocene. (a) shows the result of using the built-in Database function on `$CrystalData["Ferrocene"]`. (b) may be obtained by clicking on the disclosure bracket on the last row, or using `$CrystalData["Ferrocene", "AtomData"]` directly.

Element	OccupationFactor	SiteSymmetryOrder	FractionalCoordinates	DisplacementParameters	Type
Fe	1	2	{0., 0., 0.}	{0.0519, 0.03973, 0.0487, -0.0014, -0.00096, -0.00683}	Uani
C	0.5	1	{-0.0057, 0.0956, 0.2025}	{0.144, 0.083, 0.058, -0.033, 0.033, -0.024}	Uani
H	0.5	1	{-0.084122, 0.044844, 0.277861}	0.113	Uiso
C	0.5	1	{0.2152, 0.0583, 0.1706}	{0.115, 0.061, 0.057, 0., -0.033, -0.005}	Uani
H	0.5	1	{0.312073, -0.021032, 0.2199}	0.095	Uiso

(b) Content of the "AtomData" sub-entry of (a). The table has been truncated.

4.2 Model utilities

After an initial study of the TFIC, it occurred to us that simulating the structure was likely the best chance we had at «unwinding» the great complexity on display. A cornerstone of the «model construction» revision of MaXrd is the `CrystalPlot` function. It renders a three-dimensional graphical image of the structure, and is well-suited for up to a few thousand atoms. All the labels in the default crystal data base (listed in lines 5–9) contain only the atoms of the asymmetric unit, as one would expect in a `cif` format. Thus, using for instance `CrystalPlot["Sodalite"]` will only show five atoms.

```
10 CrystalPlot["Sodalite", "StructureSize" -> {1, 1, 1}, "AtomRadius" -> 0.4]
```

What happens in line 10 is that the "Structure-Size" option invokes another function, `ExpandCrystal`, which applies the symmetry operations of the crystal's space group to complete a unit cell, and duplicates this to a desired size. Leaving the "AtomRadius" option to its default value will make it look up tabulated atom radii instead (choices are atomic-, covalent- and van der Waals radius).

`CrystalPlot` is invaluable in the process of evaluating models, since it can be used with the basic «building blocks» up to large supercells. We use the word *entity* in this context as a collective term for generic atomic constructs. In practice, this means an entity can be any collection of atoms that constitute the structural model—ranging from a single atom to thousands of dif-

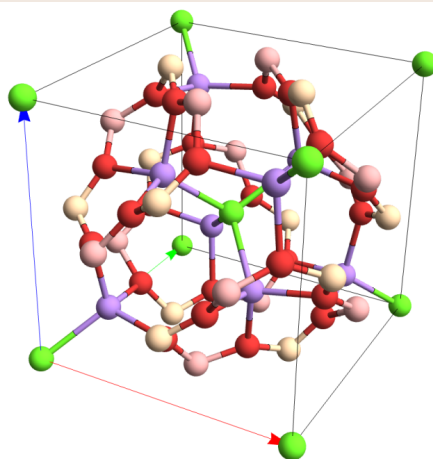


Figure 4.4: Image of the sodalite ($\text{Na}_8\text{Al}_6\text{O}_{24}\text{Si}_6\text{Cl}_2$) structure produced by line 10 above. The "StructureSize" option instructs the creation of a single unit cell; otherwise only the asymmetric unit of the mineral would have been displayed. Bonds and opacity may be configured as well. The red, green, and blue vectors denote the crystallographic *a*-, *b*-, and *c*-axes, respectively.

ferent unit cells (or whole crystals)[†]—and the starting point is usually cif files, although manual specification of a crystal is also possible.

The modelling utilities of MaXrd allow entities to be duplicated and assembled in manners that mimic both random and systematic perturbations. `EmbedStructure` has been written targeted towards host–guest complexes, but is nonetheless quite general and flexible.

One operates with two notions: a host and a guest. The host is an entity in which we are going to embed the guests. The guest input can be on one of three main forms: (i) a list of entities (crystals, chemical elements or the special label "Void"), (ii) such a list with an associated probability weight, or (iii) a list of conditions to constrain the placement. When using plain lists, the contained guest entities will be repeatedly «drawn», and one has the option to do so either randomly or sequentially.

The final missing input parameter is of course the embedding positions. At least one triplet of fractional coordinates (relative to the host entity) is required. These will be expanded to match the size of the host by default. Note that the host has a fixed size, while the guest entities are to be immersed in the host. One is therefore advised to use `ExpandCrystal` as a starting point in the «preparation» of the host entity.

The remainder of this chapter will concern the manipulation options that will be frequently used in Chapter 5, and a brief exposition of the simulation capabilities. Once more, the reader is encouraged to learn more from the accompanying article^[75] and the Mathematica documentation of MaXrd.

Table 4.1: Examples of perturbation introduced with the "Distortions" and "Rotations" options.

<code>"Distortions" -> {0, {2, 5}, 3}</code>	Distorts each embedded structure by a random amount between 2–5 Å in the y -direction and a constant amount by 3 Å in the z -direction.
<code>"Rotations" -> { {x_, y_, z_} /; y > 2 -> {90, 0, 25} Degree }</code>	Rotates all embedded structures placed at a position where $y > 2$ by 90° about the x -axis and 25° about the z -axis.
<code>"Rotations" -> {{0}, {60}, {120}}, 0, 0} Degree</code>	Rotates each embedded entity by either 0°, 60°, or 120° about the x -axis (randomly chosen each time).
<code>"Distortions" -> { "GuestEntityA" -> {0, 0.25, 0}, "GuestEntityB" -> {0, {0.4, 0.6}, 0} }</code>	Shifts all entities with the first label 0.25 Å in the y -direction, and all entities of the second label by a random amount in the given range.

[†]In our notation, the terms *block* and *fragment* are synonymous; they are arbitrarily large entities.

4.2.1 Perturbation options

The mentioned guest input forms of `EmbedStructure` instruct *what* is to be inserted, and allow for a wide range of systematic and random placement patterns. In addition, «fine-tuning» may be performed with the options "Distortions" and "Rotations". These adjust the guest entities *after* placement at the designated positions. For both of these, one may specify magnitudes as (i) fixed values, (ii) ranges of uniform randomness, (iii) list of discrete values to randomly choose from, or (iv) conditional expressions based on the insertion coordinates. Consult Table 4.1 for some examples.

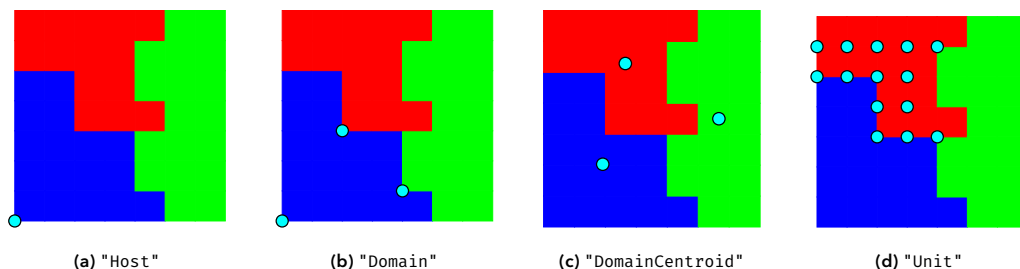


Figure 4.6: Indication of the available anchor reference settings, here shown on a $7 \times 7 \times 1$ structure representation with three domains. The cyan dots show the rotation anchors in each case—(d) shows only those of the red domain for clarity.

Rotations also require an anchor point and a rotation axis. In this context, up to three rotations are permitted in each embedding event. The axes are the a -, b -, and c -axes of the guest system by default. When using `EmbedStructure` the default setting of "RotationAnchorReference" is "Unit" (see Figure 4.6d), which means that the origin in each of the guest entity will be used as the rotation anchor. If one is working with domains (to be discussed shortly) it might be more natural to specify anchors relative to the domains instead. The functions that currently employ rotation options—`DomainPlot`, `EmbedStructure`, `SynthesiseStructure`—all use this common framework.

Lastly, there is a `DistortStructure` function that can be used to execute a global distortion field on the atoms of a crystal entity. The

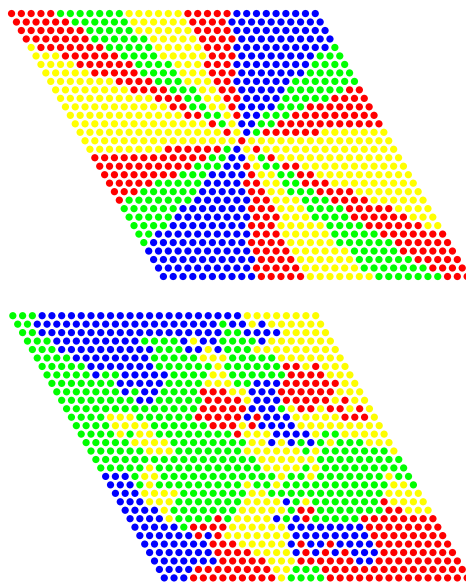


Figure 4.5: Two $32 \times 32 \times 1$ domain representations portrayed with the `DomainPlot` function. Both have been visually customised to depict a crystal of hexagonal symmetry, and each cell being a disk. There are four domains (colours) present. The instance on top is made with the "SectorRegions" mode, while the lower is created with the default Monte Carlo mode.

user only inputs a $\mathbb{R}^3 \mapsto \mathbb{R}^3$ map. A suitable application could be to create a *supercell*, i.e. a set of unit cells where subtle defects are introduced, generally of a periodic nature. Since one would typically use this on the host, there is a "DistortHost" option in EmbedStructure in which the map can be expressed inline. The advantage of doing this is that the target positions will then follow the distortions.

4.2.2 Domains

So far the tools have meticulously concerned the lowest level of customisation. In order to bring another layer of realism to the models, the notion of domains may be invoked—these have already been seen in Figure 4.6 and Figure 4.5. We loosely use the term *domain* to describe a collection of identical entities that emerge as a substructure in a larger model. These elements represent grains or subgrains in our structure models.

Each domain object consists of a stated three-dimensional size and a set of integer identifiers—one for each of the abstract cells that are to be replaced by some entity later. One can use ConstructDomain to generate such objects, and pipe the output to DomainPlot to make figures where each colour represents a single domain. As seen in Figure 4.5 there are two primary modes of operation for this function: either specifying the number and widths of sector-like domains, or generic Monte Carlo technique which traverses the abstract cells a given number of times to change the identifiers according to some probability schema (which is a customisable option).

The domain objects are realised as structure models with SynthesiseStructure, a function that assembles a selection of given entities into a designated domain pattern. One only needs to provide an association that defines the mapping between identifiers and entities. It is worth mentioning that SynthesiseStructure works without domain input as well; one can use it to create a «block» of one or more entities, or start on an «empty entity» to build a structure from nothingness.

This function supports the mentioned «rotation framework», and uses "DomainCentroid" as the default anchor points. Additionally, it is possible to add a "RotationMap" that assigns a rotation to one or more domains. This has been utilised to model imperfections at the grain boundaries and mosaicity.

4.2.3 Simulation of diffraction patterns

If one intends to simply visualise the nodes of reciprocal space, using `ReciprocalSpaceSimulation` may be easiest method. We have already seen in Subsection 2.2.3 how this function can be used to readily produce reflection nodes with correct relative positioning. It normally produces a two-dimensional image where the Bragg reflections are represented by disks with a radius and colour signalling its relative intensity. See Figure 4.7 for an example and compare with Figure 2.13a.

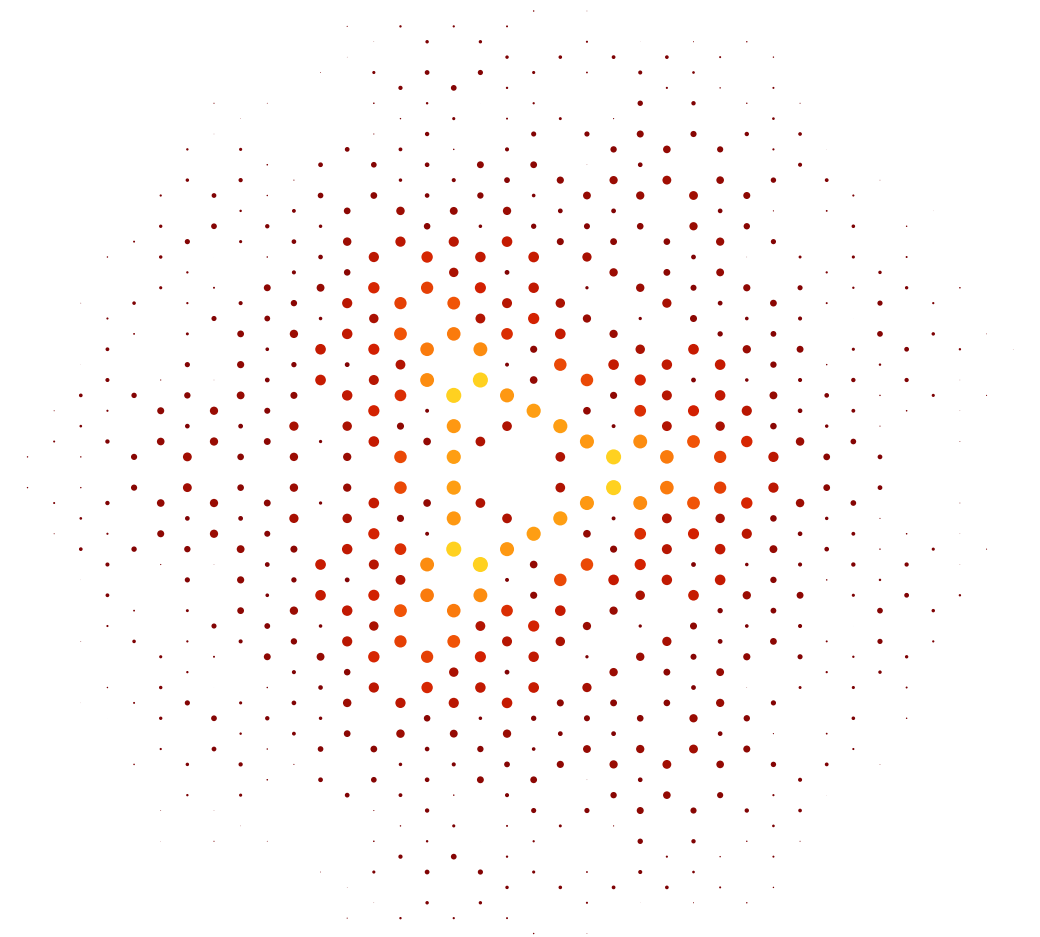


Figure 4.7: The reciprocal lattice of TFIC in the rhombohedral state, as rendered by `ReciprocalSpaceSimulation`. This is of the $hk1$ -plane with a resolution of $d_{\min} = 0.15 \text{ \AA}$. The outermost reflections have at least one Miller index being around 30. Hovering the mouse over a node will display the indices in a tooltip (in the Mathematica notebook).

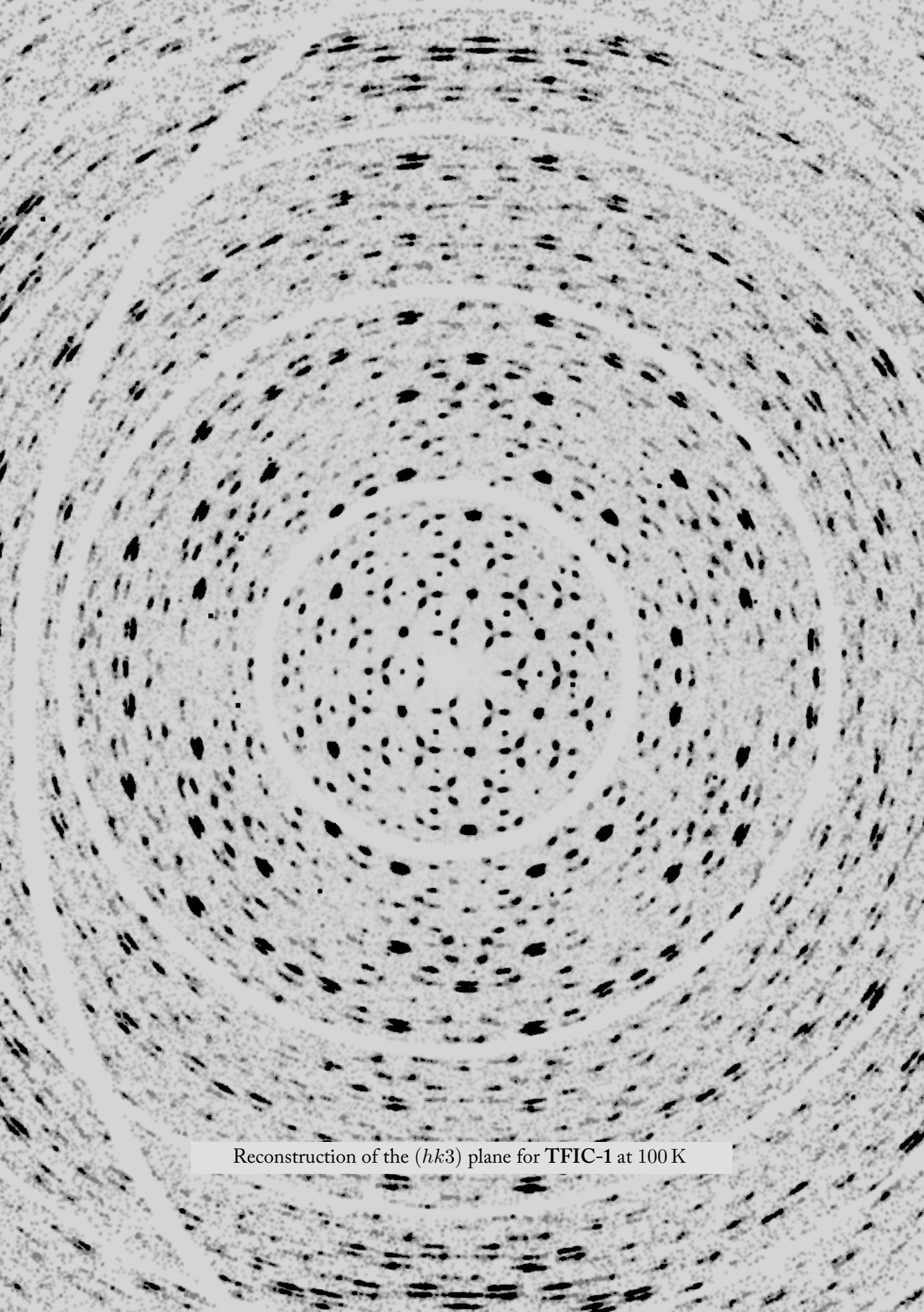
In order to produce a diffractogram of a given entity—and overcome the limitation of shapeless reflections, among others—one inputs that structure label along with the de-

sired external program to use (currently supporting DISCUS^[72] and DIFFUSE^[12]) and the Miller indices of the reciprocal plane to study. MaXrd will automatically handle the export of crystal data to the correct format for the external program, execute the necessary instructions, and collect the resulting image. The function that performs this, `Simulate-DiffractionPattern`, have a few options to control the result, such as the image dimension and intensity scaling factor.[†]

All the produced simulations are visualised in a typical colour-scaled figure where the «warmer» shades of red correspond to higher intensity (such graphical settings are configurable). To validate the output, the produced images were compared with those of a tutorial on DISCUS^[71] to check if the patterns were replicated.

This concludes the «quick tour» of the current simulation capabilities in MaXrd. Since the work with this utility has been so closely linked to our research of the TFIC, the subsequent Chapter 5 is dedicated to this study and contains plenty of usage examples.

[†]For DIFFUSE, one can also relay the setting for its so-called «subtraction mode».



Reconstruction of the $(hk3)$ plane for TFIC-1 at 100 K

Chapter 5

Simulations

From the structure solutions in Chapter 3 it is apparent that the cyclopentadienyl rings pose a challenge, and that a traditional structure solution method only facilitates an understanding of the average structure. We therefore propose an alternative method for investigating the thiourea-ferrocene inclusion compound: a «bottom-up» approach in which an imperfect crystal structure is built with the MaXrd package. This comprises a structure modelling in direct space, followed by a reciprocal space validation through comparison with the experimental diffraction patterns. The ferrocene is too disordered for an adequate «extraction» from the TFIC structure solutions, but the remaining unit cell content, i.e. the thiourea in its host arrangement, was readily exported to another separate «entity», as termed in Chapter 4. Structural information of the ferrocene molecule will therefore be based on our pure sample. These two units comprise the basic building blocks in the modelling and this analysis—with two versions of the thiourea host.

It is our intention in this chapter to first present some very basic models, then move on to comparing models described in the literature, before going beyond these into more advanced and novel models. Simulations presented in this chapter have been produced with either the DISCUS^[72] or ZMC/DIFFUSE^[12] programs through MaXrd 3.0.0. The same random seed[‡] has been used prior to the construction of each model.

Despite the advanced technology of synchrotron diffraction studies, the technique will only provide us with an average description of the structure. Harris^[32] encourages to extend our understanding of the structure by considering distributions of local features of the structure—in position and/or time—for example conformational properties of the guest and interaction between adjacent guest molecules. Simulations of urea–nonadecane indicate that reorientation of the guest molecules couple with movements of the host structure; a lesson that is likely valid for thiourea–ferrocene.

Summary of thiourea-ferrocene honeycomb structure

The conclusion of Section 1.5 is repeated here to serve as a reminder of what discovered features of TFIC are typical and of interest from a modelling perspective. Starting at the lower end of the temperature scale, the ferrocene molecules are essentially static and without the possibility to change orientation. Above 140 K, the thiourea host remains stationary.^[47] The ferrocenes are distributed in almost equally between the parallel and perpendicular types, and there is no tilting. Molecules oriented perpendicular first come

[‡]The code `SeedRandom[1234567]` was run immediately before the making of each model, but this has been excluded from the code listings in this chapter.

«to life» around 150 K as they are now able to switch between the three sub-variants. Somewhere around 150 K to 160 K the ferrocenes gain enough thermal energy to tilt and flip between two main orientations, and the process intensifies with temperature up to circa 225 K, where the average guest orientations appear isotropically disordered.

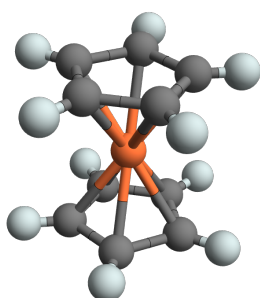
One could imagine that an outward push from the tunnel centres is necessary to uphold the honeycomb structure, and when the number of perpendicular variants falls below a certain threshold at 160 K, the shape of host network deteriorates. Our own structure solutions were unable to settle this question further, since occupancies were fixed at 50 % in order to achieve stability, but the narrative in the literature is that the proportion of parallels increases slightly with lower temperature (see Table 1.1). In a modelling perspective we should therefore bear in mind a coupling between an embedded guest unit and its surrounding host environment (see e.g. model B03).

Preparing the essential modelling elements

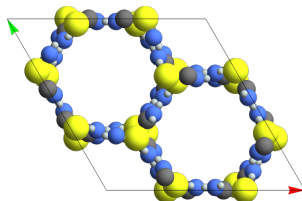
This chapter contains many code blocks with the actual instructions used to generate the TFIC structure models. These are details and illustrate how to solve the various model construction challenges with `MaXrd`, in addition to permitting repeatability. Even if the reader is not fluent in the Wolfram Language, one should hopefully get the general idea of what is done from the variable names and the surrounding paragraphs.

We start by importing the basic constituents required for our modelling: the ferrocene molecule and the (empty) thiourea host structure, one for each of the main phases. Recall that the ferrocene structure has been modelled with two parts, and looks like Figure 3.1 when imported. We therefore start by removing one of the components,

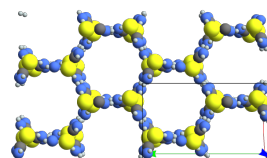
```
1 $CrystalData[["FerroceneMolecule", "AtomData", Range[2, 11]]] = Nothing;
```



(a) Ferrocene molecule.



(b) Rhombohedral (high-temperature) host, shown as a unit cell.



(c) Monoclinic (low-temperature) host, shown as a $2 \times 2 \times 1$ supercell.

Figure 5.1: Essential building blocks extracted from our structure solutions, here displayed using the `CrystalPlot` function. All our upcoming models will in practice be combinations these three entities.

Next we copy the cyclopentadienyl ligand centrosymmetrically over to the other side of the iron atom:

```
2 cyclopentadienyl = $CrystalData[["FerroceneMolecule", "AtomData", 2 ;;]];
3 cyclopentadienyl = MapAt[(1 - #) - 1 &, cyclopentadienyl, {All, "FractionalCoordinates"}];
4 $CrystalData[["FerroceneMolecule", "AtomData"]] = Join[
5   $CrystalData[["FerroceneMolecule", "AtomData"]], cyclopentadienyl];
```

Finally, we rotate the molecule so that it is normal to the **ab**-plane:

```
6 coordinateDataCartesian = GetAtomCoordinates["FerroceneMolecule",
7   "Cartesian" -> True, "GatherElements" -> False];
8 oldCoordinatesCartesian = coordinateDataCartesian[[All, 2]];
9 T = RotationTransform[{{1/3, 1, 1}, {0, 0, 1}}];
10 newCoordinatesCartesian = T /@ oldCoordinatesCartesian;
11 M = Inverse @ GetCrystalMetric["FerroceneMolecule", "ToCartesian" -> True];
12 newCoordinatesCrystallographic = Transpose[M] . # & /@ newCoordinatesCartesian;
13 $CrystalData[["FerroceneMolecule", "AtomData", All, "FractionalCoordinates"]] =
   newCoordinatesCrystallographic;
```

We save this entity for later use.

Next we «punch out» only the thiourea parts from our two TFIC structures. In the following code, we make copies in the `$CrystalData` data dictionary, and remove the atoms belonging to the ferrocenes:

```
14 AppendTo[$CrystalData, "RhombohedralHost" -> $CrystalData["TFIC_HighTemperature"];
15 $CrystalData["RhombohedralHost", "AtomData"] = $CrystalData[["RhombohedralHost", "AtomData", 2 ;; 6]];
```

and

```
16 AppendTo[$CrystalData, "MonoclinicHost" -> $CrystalData["TFIC_LowTemperature"];
17 $CrystalData["MonoclinicHost", "AtomData"] = $CrystalData[["MonoclinicHost", "AtomData", 2 ;; 25]];
```

In Figure 5.1 we see the three basic entities we will be using as «foundations» for our modelling.

From all the trials and errors regarding the modelling of the thiourea–ferrocene inclusion compound, a selection of the most pertinent and noteworthy results will be presented here. The models have been organised into five different categories, which evolve in complexity.

In category A the code is held at an introductory level and not using the available options to a high extent, nor altering the entities too much. Even if the models are of limited interest, the reader will get more familiarised with the function syntax through practical examples.

In category B we study simulations that are tied to descriptions from the literature and to our own solutions. We also make implicit use of the `DistortStructure` function.

In category C we rely on the "Rotations" option of `EmbedStructure` to explore various short-range arrangements.

Next a few models demonstrate how one can recreate the twinned structures in category D.

The final section contains models where the use domains plays a central part, and relies on the `ConstructDomains` function and the auxiliary plotting tool.

5.1 Category A: Simple models

In this first series of models, we begin with rather plain models and basic use of MaXrd to tackle this challenging compound in particular.

Models A01 and A02: Empty thiourea host lattice

It would be instructive to see what the diffraction patterns look like with the ferrocene molecules absent. The host will still be structured the way it is in clathrate composition with the characteristic honeycomb shape, but without any ferrocene guest molecules. First, let us expand the rhombohedral host to $16 \times 16 \times 16$:

```
18 ExpandCrystal["RhombohedralHost", {16, 16, 16},  
19 "IncludeBoundary" -> False,  
20 "NewLabel" -> "RhombohedralHost16"]
```

It is ready to be simulated:

```
21 SimulateDiffractionPattern["DIFFUSE", "RhombohedralHost16", "hk0"]
```

We perform the same simulations with different Miller indices, $hk0$, $hk1$, $hk3$ and $h0l$, and then perform the same steps with the monoclinic variant. Comparisons are displayed

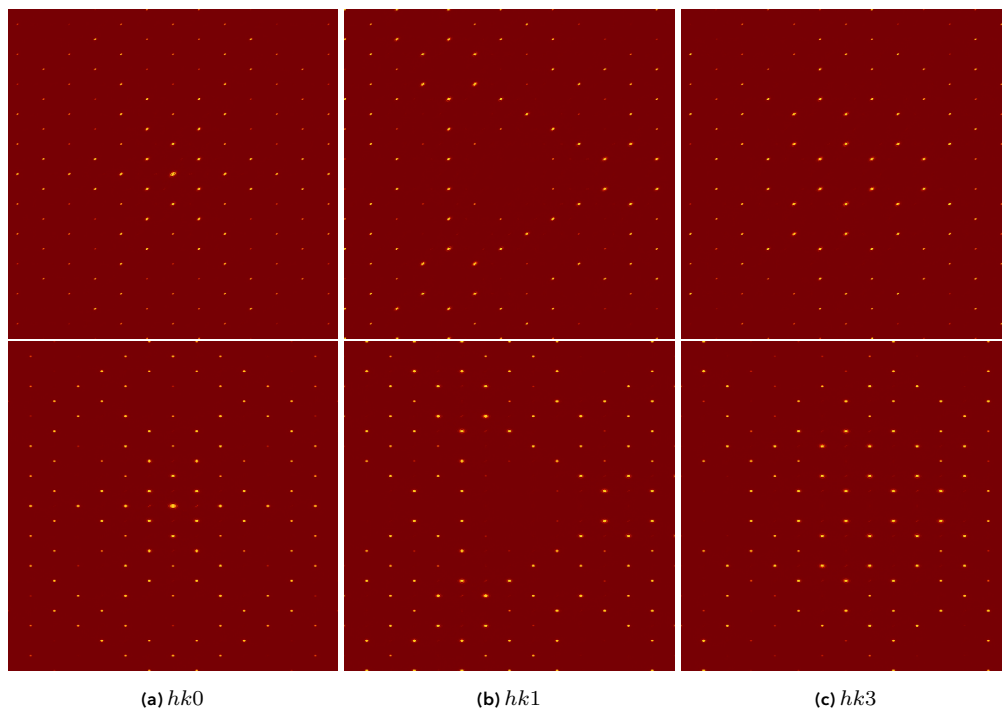


Figure 5.2: Simulated sections of the hk -plane with the top row belonging to the rhombohedral model (A01), and the bottom row the monoclinic version (A02). The $hk1$ - and $hk3$ -layers can be compared with experimental reconstructions in Figure 2.13 (page 45).

in Figure 5.2.

Comparing Figure 5.2a with the real counterpart in Figure 2.9a (page 42), we can see that the diffraction pattern of the lattice itself match, but the intensity distributions differ. Most noticeably we observe that the most intense reflections in the simulation follow a «star shape», which we do not detect in the experimental picture. We should naturally expect a mismatch, as our model is not populated with ferrocene.

In the simulation we also notice a greater intensity difference in alternating reflections around the second circle of reflections from the centre. The brighter reflections are symmetry equivalent to (220), while the dimmer reflections are equivalent to (300).

Model A03: Ferrocene in z -conformation

Now we wish to study the consequences of adding the guest phase. We will be inserting the ferrocene molecules in a straightforward manner, first in the « z -conformation» (molecule axis aligned parallel with the tunnel axis). First, let us get all the positions at which we want to place the iron centre of ferrocene molecules:[†]

```
22 ironPositions = SymmetryEquivalentPositions["R-3c", {0, 0, 1/4}]
```

This returns six positions; two on top of each other in each of the three columns in a single unit cell. We first load the «standard host» created in lines 18–20 to restart with an empty host structure. Since the ferrocene molecules have already been rotated to «point straight up» in the lines 6–13, we embed them into the host directly:

```
23 EmbedStructure[{"FerroceneMolecule"}, ironPositions, "RhombohedralHost16", "NewLabel" -> "Model"]
```

With all the molecules identically placed at the special positions with site symmetry 32 (multiplicity 6), we observe in particular that the reflections (280) and (550), together with their equivalents, differ greatly from the experimental picture by being more or less extinct. We also remark that no differences are seen between model A01 and A03 when comparing the layers with odd l .

Model A04: Perturbation of ferrocene in z -conformation

We now alter the previous model by introducing small vertical shifts of the ferrocene as well as arbitrary rotations about the molecular axes.

```
24 EmbedStructure[{"FerroceneMolecule"}, ironPositions, "RhombohedralHost16", "NewLabel" -> "Model",
25 "Distortions" -> {0, 0, {-0.2, 0.2}},
26 "Rotations" -> {0, 0, {0, 360 Degree}}]
```

The above code signifies a random displacement along the z -axis by (an arbitrarily chosen) magnitude of $\pm 0.2 \text{ \AA}$ and a random rotation about the z -axis. These adjustments are relative to where the guest entities are placed (default setting). No practical difference could be seen between models A03 and A04.

[†]The position used has site symmetry 32.

Model A05: Isotropic ferrocene

In this model, we use the following:

```
27 EmbedStructure[{"FerroceneMolecule"}, ironPositions, "RhombohedralHost16", "NewLabel" -> "Model",
28 "Rotations" -> {#, #, #} &@ {0, 360 Degree}];
```

This rotates each ferrocene molecule in a completely random orientation, and is a simple and favoured high-temperature disorder model.

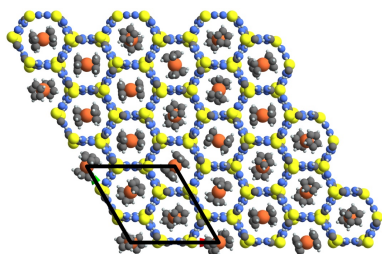


Figure 5.3: A $3 \times 3 \times 1$ illustration of the isotropic ferrocene model, A05. The black frame shows a single unit cell. Only one layer of ferrocenes is shown for clarity, although there are really two molecules stacked in a single tunnel inside a unit cell.

The simulation output from this model is so far our best candidate for matching the experimental counterpart at room temperature. All the Bragg reflections are present, although some are relatively weaker than expected.

We also try a variant where we exchange the rhombohedral host structure with the monoclinic, as seen in Figure 5.1c. The diffraction patterns are by all practical means the same, and they in turn resemble those in Figure 5.2. All reflections present in one model, appears to also be in the other. None of the minor changes in the intensity distribution are characterised to be of any systematic importance.

Model A06: Four ferrocene orientations

In this final model of series A, we make another randomised distribution of the ferrocene molecules. Instead of allowing complete orientational freedom, we restrict the guest molecules to take one in four different positions:

```
29 EmbedStructure[{1/4, 3/4} -> {"FerroceneMolecule", "FerroceneMoleculePerpendicular"},
30 ironPositions, "RhombohedralHost16", "NewLabel" -> "Model",
31 "Rotations" -> {
32 "FerroceneMoleculePerpendicular" -> {0, 0, {0}, {60}, {120}} Degree
33 }];
```

Note that we first specify to have one quarter in the parallel orientation and the rest in the perpendicular. In the rotation option we obtain the three sub-configurations of the perpendicular variant.

Comparing model A06 with A05, we find that in A06 the reflections (440) and (550) are suppressed, in contrast to what is seen in A05 and in the experimental reconstructions.

5.2 Category B: Literature models

In this section we simulate structures collected from the literature.^[18,35,46,47,52] The purpose is to use these structures as they are, or replicate them, then apply the same simulation procedure and compare the results with our proposed models and the experimental images.

Model B01: Distributed ferrocene with tilting

Here we will test the hypothesis that the two main orientations of the ferrocene—parallel and perpendicular—are distributed roughly equal. Moreover, small deviations off the molecular axis has been mentioned; *tilting*. In the perpendicular orientation a tilt of up to 3° can be expected,^[46] while a tilt of around 17° from the tunnel axis has been reported for the other kind.^[46,47]

First, we may simplify some of the work ahead by preparing a separate entity for the ferrocene molecule in the perpendicular setting:

```
34 EmbedStructure[{"FerroceneMolecule"}, {{0, 0, 0}}, "Void",
35   "NewLabel" -> "FerroceneMoleculePerpendicular",
36   "Rotations" -> {90 Degree, 0, 0}]
```

Next, we build the actual model:

```
37 EmbedStructure[{"FerroceneMolecule"}, ironPositions, "RhombohedralHost16", "NewLabel" -> "Model",
38   "RotationAxes" -> {{0, 0, 1}, {1, 0, 0}, {0, 1, 0}},
39   "Rotations" -> {
40     "FerroceneMolecule" -> {{{0}, {120}, {240}}, 17, 0} Degree,
41     "FerroceneMoleculePerpendicular" -> {{{0}, {120}, {240}}, 3, 0} Degree
42   }
43 ];
```

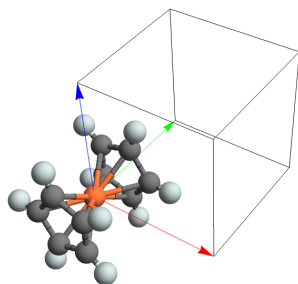


Figure 5.4: The perpendicular ferrocene entity. Since it has been constructed on «Void» the unit cell is $1 \times 1 \times 1 \text{ \AA}^3$, but that does not matter here. The red, green and blue vectors represent the a -, b - and c -axes.

Note in the code above that we specify that the rotations will first be performed about the z -axis (which coincides with the tunnel axis for both orientations) then the x -axis, which tilts them the desired amount. We see that all molecules are given a random orientation among three possible in the «horizontal» plane perpendicular to the tunnels. The results are more or less identical with model A03.

Be aware that in our instructions above, the second rotations (tilting) are precisely 17° and 3° . We have checked the effects of continuous rotations as well by substituting the rotations setting with:

```
44 "Rotations" -> {
45   "FerroceneMolecule" -> {{{0}, {120}, {240}}, {0, 17}, 0} Degree,
46   "FerroceneMoleculePerpendicular" -> {{{0}, {120}, {240}}, {-3, 3}, 0} Degree
47 }
```

No particular effects of continuous rotations were observed.

Model B02: Layered distribution

This model is relatively simple and created in two steps:

```
48 EmbedStructure[{"FerroceneMolecule"}, topIronPositions, "RhombohedralHost16", "NewLabel" -> "Model"];
49 EmbedStructure[{"FerroceneMoleculePerpendicular"}, bottomIronPositions, "Model"];
```

Here, the two parameters `topIronPositions` and `bottomIronPositions` are, as their names suggest, the six positions listed in `ironPositions` split into two parts (not shown here). In this manner, we obtain alternating ferrocene layers as we progress through the tunnels—in one layer, the ferrocenes are all in the parallel orientation, then the perpendicular in the adjacent ones. In this way we avoid the placement of two (perfectly) parallel molecules as vertical neighbours, which is an unlikely configuration.^[37]

The greatest change in the resulting diffraction patterns between the two latest models, is that reflections (410) , (710) , $(5\bar{1}0)$, $(8\bar{1}0)$, $(\bar{5}10)$, $(\bar{8}10)$, $(8\bar{1}0)$ and $(\bar{7}10)$ are visible in model B02 and not B01. In this regard, B02 resembles the experimental data more closely, but still lacks other reflections for an optimal match of the $hk0$ -plane. See also Figure 5.5 for a graphical insight to the mentioned reflections. The underlying code is presented here:

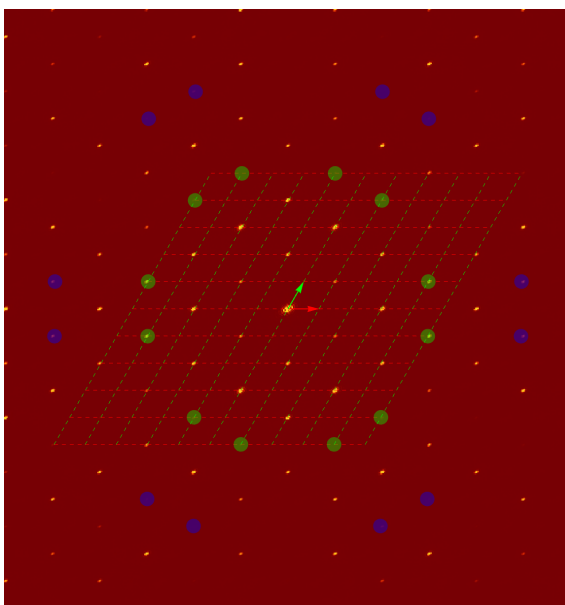


Figure 5.5: Output from the `ReciprocalImageCheck` function produced by the code in the previous code listing (lines 50-55). The background image is a simulation of the $hk0$ -plane of model B02. The green circles show reflection (410) and its symmetry equivalents; the blue circles the same for (710) . The red and green arrows depict the \mathbf{a}^* and \mathbf{b}^* unit vectors, respectively, and the dashed lines are extensions of these cell lengths up to five times in magnitude.

```
50 ReciprocalImageCheck[image, GetLatticeParameters["RhombohedralHost"], {
51   {544, 580, 0, 0, 0}, {724, 580, 3, 0, 0}, {906, 581, 6, 0, 0},
52   {1079, 578, 9, 0, 0}, {542, 685, -1, 2, 0}, {542, 788, -2, 4, 0}
53 },
```

54
55

```
"BackgroundImage" -> True, "LatticeSize" -> 5,  
"HighlightSymmetry" -> "R-3c", "HighlightReflections" -> {{4, 1, 0}, {7, 1, 0}}]
```

The image parameter refers to the simulated $hk0$ -plane of model B02. The six data points on the form $\{x, y, h, k, l\}$ have been collected by looking up arbitrary nodes in the experimental data. They are used to fixate the overlay lattice.

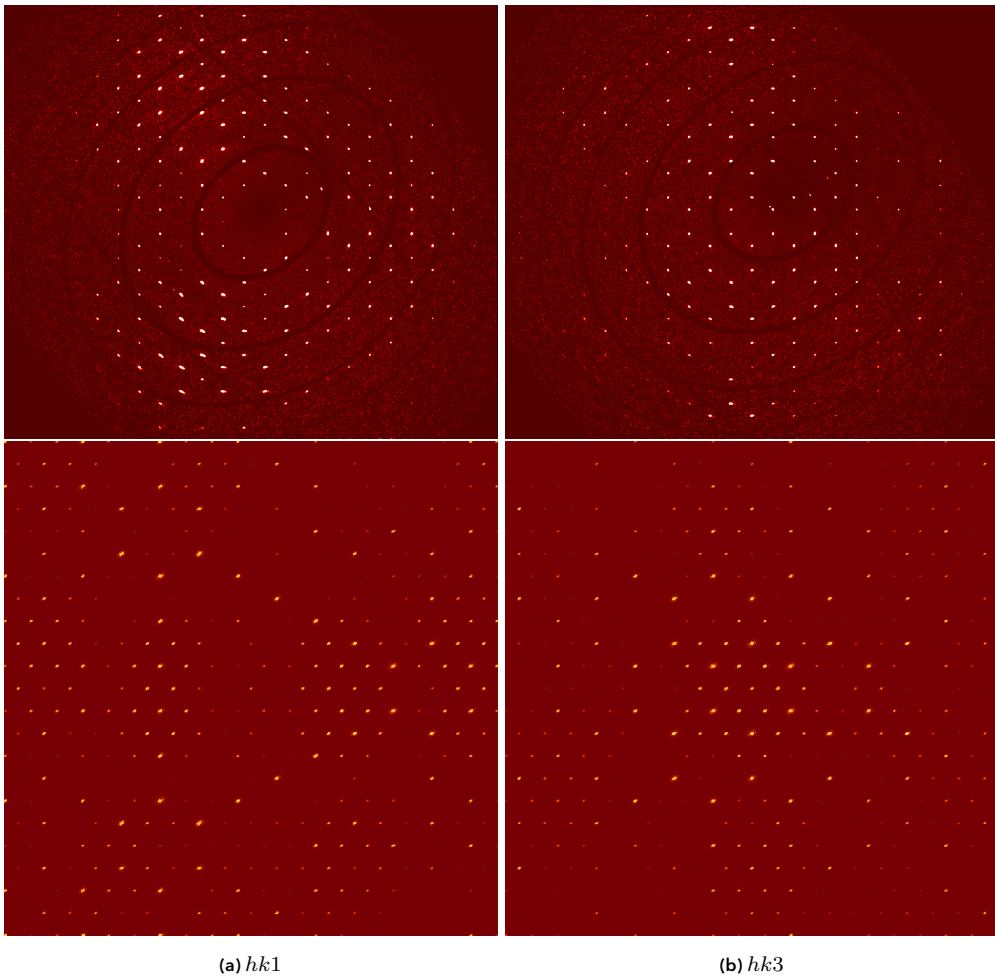


Figure 5.6: Comparison between simulated sections of the B02 model and the experimental counterparts. (a) and (b) show $hk1$ and $hk3$, respectively. The upper row contains experimental images of TFIC-2; the simulations are shown below.

It is nonetheless apparent from the simulated layers $hk1$ and $hk3$ as seen in Figure 5.6 that this is not a well-suited model. Attempts at making the structure more isotropic and randomised were also done by adding the same rotation setting as in lines 44–47 before. Those results were not change for the better and are thus not provided here.

Model B03: Distorted channels

The function `DistortHost` was written to simulate the distortion of the host framework. Later, this was incorporated as an option to `EmbedStructure` so that the targetted embedding positions could follow the overall distortion. In the literature, we find the transitioning to a monoclinic cell described as (1) a distortion of the thiourea «honeycombs» and (2) a somewhat more localisation of the guests.^[48,66] We have attempted to replicate this effect with the following:

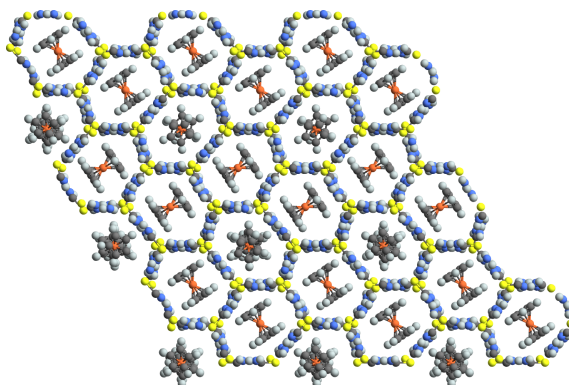


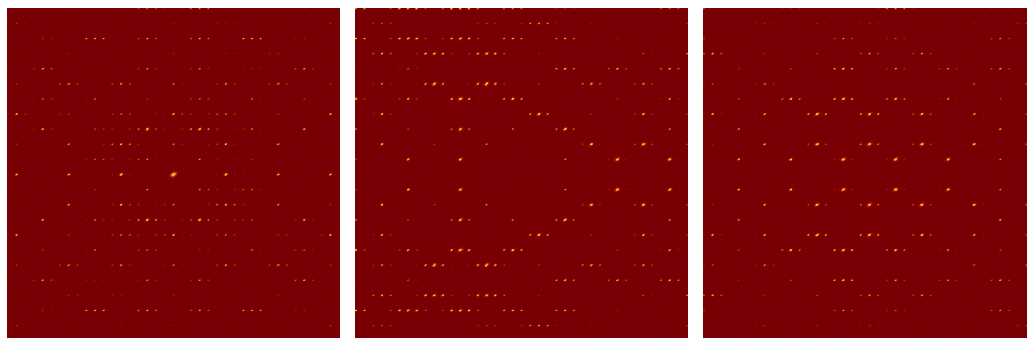
Figure 5.7: A $3 \times 3 \times 1$ segment of model B03. The distortion amplitude has been exaggerated five-fold in this figure to better discern the effects of the triangular wave. Note that the guest molecules are more ordered as well.

```

56 EmbedStructure[{"FerroceneMolecule"}, ironPositions, "RhombohedralHost16",
57   "DistortionType" -> "Crystallographic",
58   "DistortHost" -> (0.025 {TriangleWave[#2/2], 0, 0} &),
59   "RotationAxes" -> {{0, 0, 1}, {0, 1, 0}, {1, 0, 0}},
60   "Rotations" -> {
61     {x_, y_, z_} /; TriangleWave[y/2] > 0 -> {120, 90, 0} Degree,
62     {x_, y_, z_} /; TriangleWave[y/2] < 0 -> {30, 90, 0} Degree,
63     {x_, y_, z_} /; True -> {{{0}, {120}, {240}}, 17, 0} Degree
64   },
65   "NewLabel" -> "Model"
66 ];

```

The setting of `"DistortionHost"` describes an anonymous function which only works along the a direction and is periodically dependent on the y -coordinate (having twice the period).



(a) $hk0$

(b) $hk1$

(c) $hk3$

Figure 5.8: Sections of the B03 model. We see clear indication of the commensurate satellites made by the periodic function perpendicular to the a^* direction.

B03 is evidently not a good match with experimental data, but we will return to distorted host models when using domains.

Model B04: Structure solutions

Lastly in this section, we wish to have a look at how our «unadulterated» structure solutions compare. The cif imports were stored as `TFIC_HighTemperature` and `TFIC_LowTemperature`. These will have to be expanded in the manner we have seen before, e.g. in lines 18–20.

The resulting simulations of Bo_4 resemble those of models Ao_1 and Ao_2 , but lacking some reflections. In that sense, the first two models are more aligned with the actual diffractograms. One should keep in mind that what the structure solutions provide is time-averaged. Finally, one can see that the monoclinic variant contains additional reflection in $hk1$, although faint.

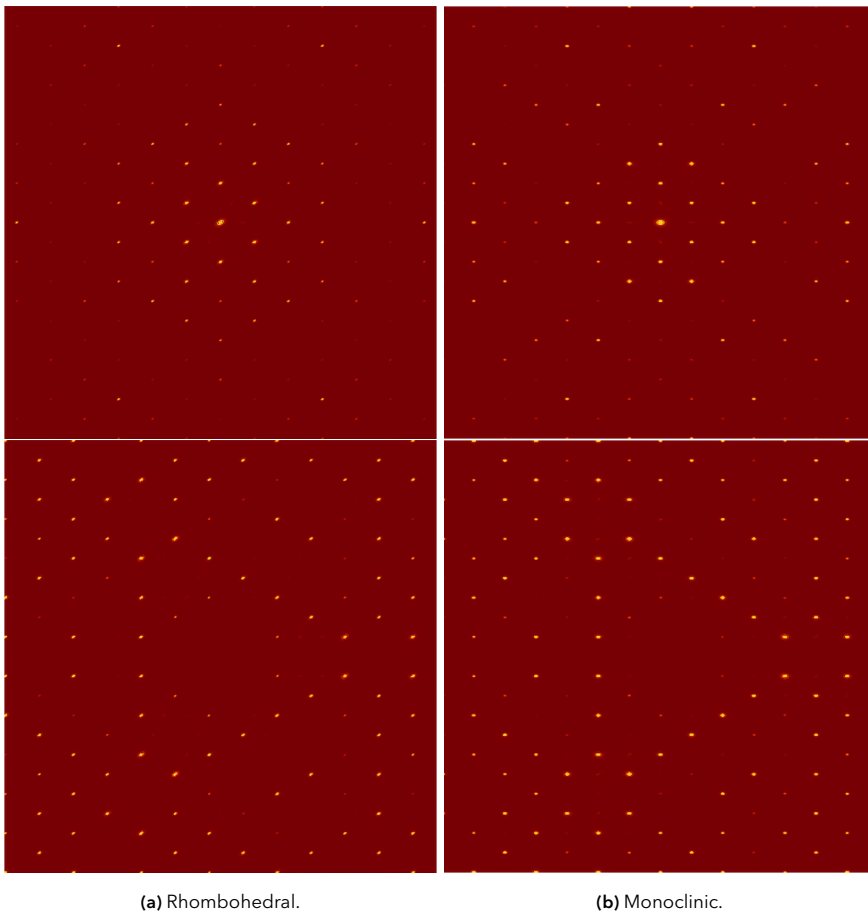


Figure 5.9: Simulations belonging to model B04. Left-side images are made with the rhombohedral structure solution, and monoclinic for the right-side. The top row shows the $hk0$ -plane, and the bottom row $hk1$.

5.3 Category C: Particular orderings

Model C01: Herringbone pattern

We will be making a «herringbone pattern» out of two different configurations of ferrocene, see Figure 5.10. The first type can be made by placing the molecules in an alternating fashion and rotating them like so:

```

67 EmbedStructure[{
68     {x_, y_, z_} /; EvenQ @ Round[x + y] -> "FerroceneMolecule",
69     {x_, y_, z_} /; True -> "FerroceneMoleculePerpendicular"
70 }, ironPositions, "RhombohedralHost16", "NewLabel" -> "Model",
71 "Rotations" -> {
72     {x_, y_, z_} /; EvenQ @ Round[x + y] -> {90, 30, 0} Degree,
73     {x_, y_, z_} /; True -> {0, 0, -30} Degree
74 }
75 ];

```

The second type is made differently, but following the same concept:

```

76 EmbedStructure[{"FerroceneMoleculePerpendicular"}, ironPositions,
77 "RhombohedralHost16", "NewLabel" -> "Model",
78 "Rotations" -> {
79     {x_, y_, z_} /; Mod[3 y, 2] == 0 -> {0, 0, 60} Degree,
80     {x_, y_, z_} /; True -> {0, 0, -60} Degree
81 }
82 ];

```

In both cases, another version where the layers alternate has been carried out. The other layer is identical, except that each guest molecule is rotated 90° compared to the vertical neighbour. The idea is to create a more realistic packing, but we just get images with many satellites which we do not recognise in our data collection (they are not included here).

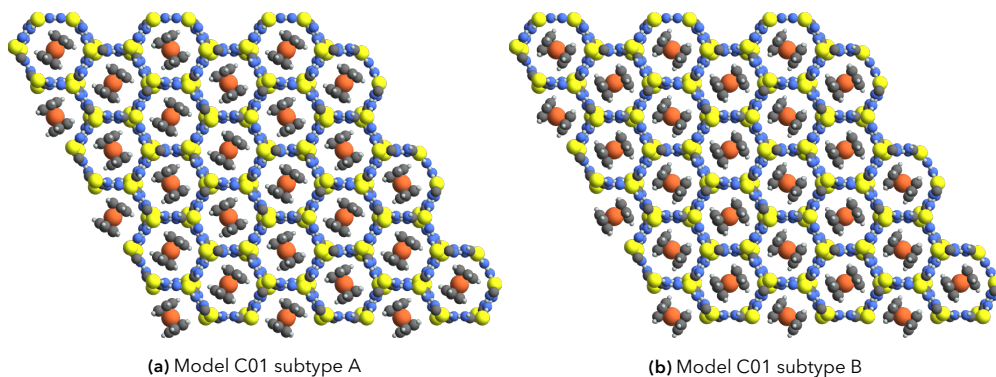
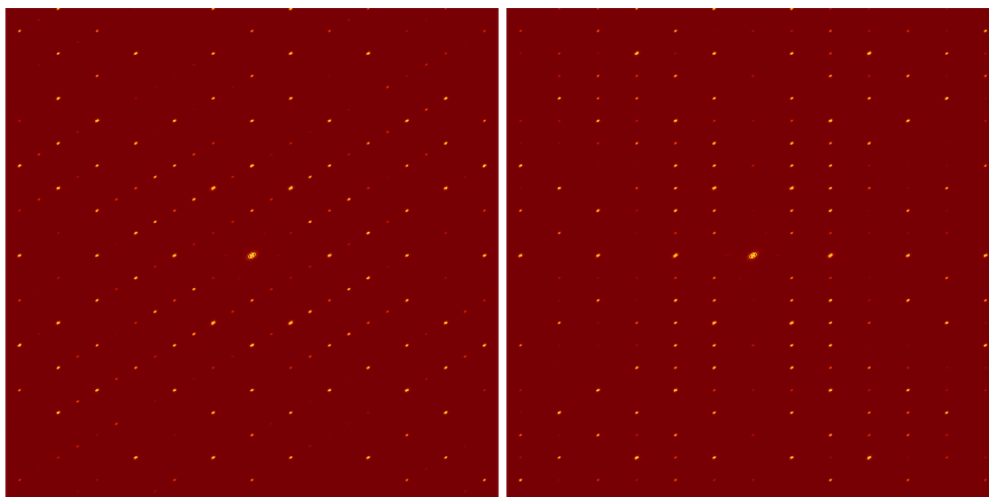


Figure 5.10: Two types of arrangements of the C01 model. In type (a) the ferrocenes are rotated by $\pm 30^\circ$ away from the Cartesian y -direction, and $\pm 60^\circ$ in type (b). Note that in type (a) equal guest orientations follow the «diagonals» (normal to $\mathbf{a} + \mathbf{b}$), while they follow the Cartesian vertical in type (b).

For both types we only spot a difference in the $hk0$ -plane, where satellites have emerged parallel to \mathbf{b}^* in type A and perpendicular to \mathbf{a}^* in type B. See Figure 5.11.

We also tried making stacks of this model in which alternating layers were using rotations angles offset by 90° in order to «fit» vertically neighbouring ferrocene molecules



(a) Model C01, type a

(b) Model C01, type b

Figure 5.11: Comparison between simulated $hk0$ -layers of the C01 model.

more realistically. In doing so, the $hk1$ planes became incorrect. Finally, we tried combinations of the two subtypes and rotating the results to emulate twinned diffraction patterns, but we were unable to obtain results that would deem model C01 as a realistic candidate for the TFIC structure.

Model C02: Layered spiral along tunnel axis

In this model, the idea is to stack each of the four configurations of ferrocene in separate layers along the tunnel. Let us first simplify the work ahead by preparing the α -, β - and γ units. We make one alternate version of the perpendicular by rotating it 60° :

```
83 EmbedStructure[{"FerroceneMoleculePerpendicular"}, {{0, 0, 0}},
84 "Void", "NewLabel" -> "FerroceneMoleculePerpendicular060",
85 "Rotations" -> {0, 0, 60 Degree}
86 ];
```

then another similar one with 120° . Next we prepare a $1 \times 1 \times 2$ block of the host in which we will embed the ferrocenes:

```
87 ExpandCrystal["RhombohedralHost", {1, 1, 2}, "IncludeBoundary" -> False, "NewLabel" -> "HostBlock"];
```

Now the embedding code:

```
88 EmbedStructure[{
89   {x_, y_, z_} /; 0.0 <= z < 0.5 -> "FerroceneMoleculePerpendicular",
90   {x_, y_, z_} /; 0.5 <= z < 1.0 -> "FerroceneMoleculePerpendicular060",
91   {x_, y_, z_} /; 1.0 <= z < 1.5 -> "FerroceneMoleculePerpendicular120",
92   {x_, y_, z_} /; 1.5 <= z < 2.0 -> "FerroceneMolecule"},
93   ironPositions, "HostBlock", "NewLabel" -> "ModelBlock"
94 ];
```

Now we have our building block which we just need to duplicate to a desired size for the simulations. This model resembles B02, but alternates between the four configurations

instead of just two. See Figure 5.12. The duplication is readily done with `SynthesiseStructure`. Recall that this function differs from `ExpandCrystal`, whose purpose is to expand the asymmetric unit to complete unit cell(s). First we should rescale the lattice parameters of our block so it counts as one unit.

As seen in Figure 5.12 the embedding was performed outside the unit cell, so the actual height (lattice parameter c) of the block should be twice as high. We can use `ResizeStructure` without specifying the scaling; the size is detected automatically:

```
95 ResizeStructure["ModelBlock"];
```

Now it is straightforward to make our final model. Note that we specify the size to be $16 \times 16 \times 8$, since the blocks we use constitute two TFIC cells stacked on top.

```
96 SynthesiseStructure[{"ModelBlock"}, {16, 16, 8}, "Model"];
```

In the simulated results of model Co₂, the $h0l$ -plane is deviant with occurrence of primary and secondary satellites of the main reflections. Also the $hk1$ - and $hk3$ -planes are substantially different, showing a hexagonal symmetry not matching our experimental records—not even the obverse–reverse twin. There are too many reflections which ought to be extinct.

Model C03: Leaning columns

Here we consider each tunnel to be populated by ferrocene molecules in exactly the same orientation along it. As seen in the code snippet below we perform the embedding in three passes. This is one way to achieve three individual classes of orientation.

```
97 SetOptions[EmbedStructure, "RotationAxes" -> {{0, 0, 1}, {0, 1, 0}, {1, 0, 0}}];
98 ExpandCrystal["RhombohedralHost", {1, 1, 1}, "IncludeBoundary" -> False, "NewLabel" -> "HostBlock"];
100 EmbedStructure[{{x_, y_, z_} /; x == 0.0 && y == 0.0 -> "FerroceneMolecule"},
101   ironPositions, "HostBlock", "NewLabel" -> "ModelBlock",
102   "Rotations" -> {150, 0, 17} Degree];
104 EmbedStructure[{{x_, y_, z_} /; x == 2/3 && y == 1/3 -> "FerroceneMolecule"},
105   ironPositions, "ModelBlock",
106   "Rotations" -> {-90, 0, 17} Degree];
108 EmbedStructure[{{x_, y_, z_} /; x == 1/3 && y == 2/3 -> "FerroceneMolecule"},
109   ironPositions, "ModelBlock",
110   "Rotations" -> {30, 0, 17} Degree];
112 SynthesiseStructure[{"ModelBlock"}, {16, 16, 16}, "Model"];
```

The results for model Co₃ resemble model Ao₃ to a high degree. Satellites are most visible in the $h0l$ -layer, which may be seen in Figure 5.13b.

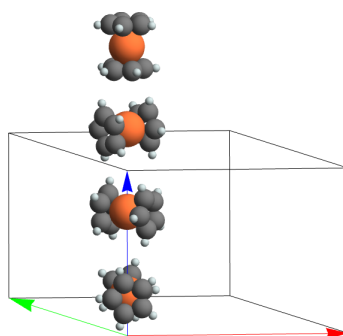
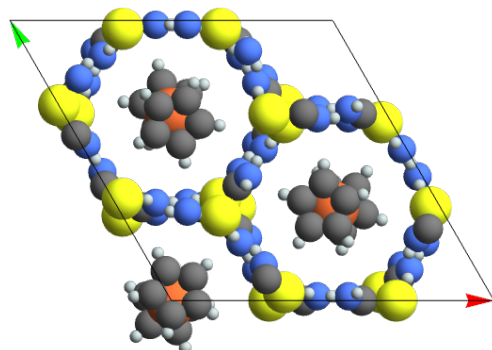
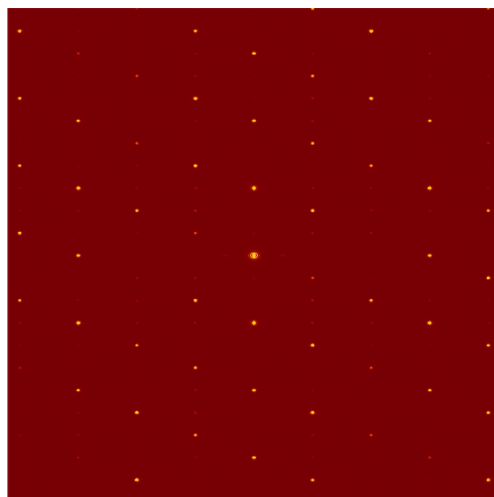


Figure 5.12: One column of ferrocenes as they are stacked in model C02. The other content is not shown here for clarity. Two unit cells are required to fit each of the four configurations.



(a) Populated unit cell of model C03. There are three variants of the tilted ferrocene; each leaning toward their common centre.



(b) Simulated $h0l$ -plane of model C03.

Figure 5.13: An illustration showing a unit cell in direct space in (a) and a picture of the simulated $h0l$ -plane of reciprocal space in (b).

Model C04: Alternating rows

We now try to keep «rows» of guest molecules in the same main type of orientation, i.e. lines of either parallel or perpendicular ferrocenes, see Figure 5.14. To accomplish this, we can think of converting the crystallographic coordinates back to Cartesian, then apply the constraint of being close to whole unit of lattice parameter a . Consider the coordinate conversion:

$$\begin{pmatrix} a & b \cos 120^\circ \\ 0 & b \sin 120^\circ \end{pmatrix} \begin{pmatrix} x \\ y \end{pmatrix} = \begin{pmatrix} ax - by/2 \\ \sqrt{3}/2 by \end{pmatrix} \quad (5.1)$$

This is the background for the condition form in line 115 below. We assume that the "RotationAxes" setting from model C03 remains.

```

114 EmbedStructure[{
115   {x_, y_, z_} /; IntegerQ @ Round[x - y/2, 1/10] -> "FerroceneMolecule",
116   {x_, y_, z_} /; True -> "FerroceneMoleculePerpendicular"
117 },
118 ironPositions, "RhombohedralHost16", "NewLabel" -> "Model",
119 "Rotations" -> {
120   "FerroceneMolecule" -> {{{0}, {120}, {240}}, 0, 17} Degree,
121   "FerroceneMoleculePerpendicular" -> {{{0}, {120}, {240}}, 0, 0} Degree
122 }
123 ];

```

Like model C01 we have created two sub variants. The only difference is the orientation of the «rows». By simply replacing the condition in line 115 with:

```

124 {x_, y_, z_} /; EvenQ@IntegerPart[x + y] -> "FerroceneMolecule"

```

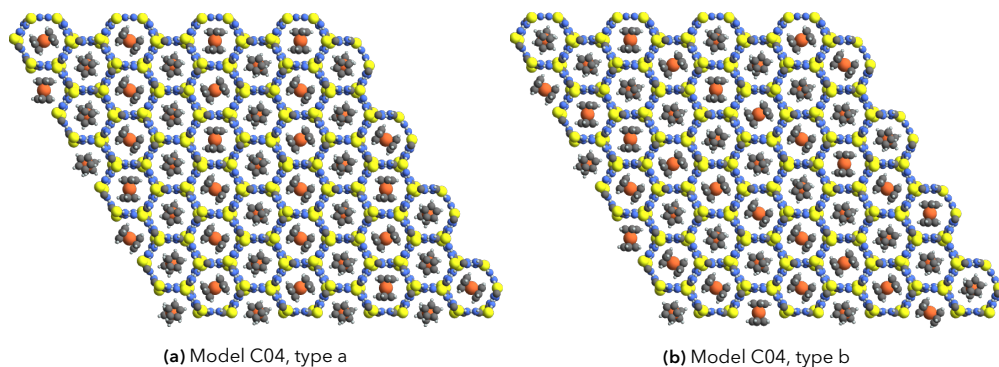


Figure 5.14: Two $4 \times 4 \times 1$ representations of model C04. In type a, each vertical row alternate between the main type, with three sub variants (chosen randomly everywhere). In type b the same effect occurs diagonally instead. Their constructions only differ in line 115.

we embed half the guests diagonally instead.

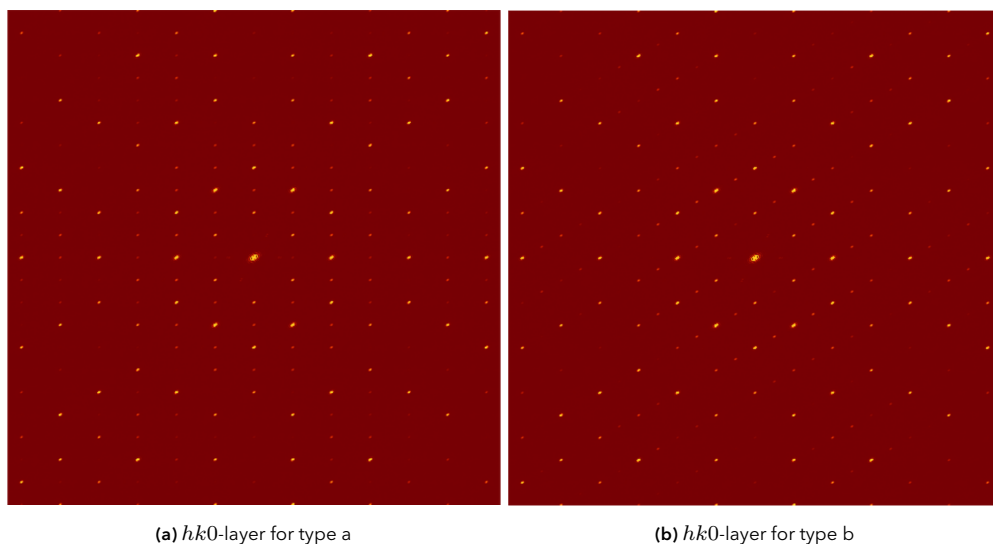


Figure 5.15: Simulated $hk0$ -layers of the C04 model. See Figure 5.14 for the corresponding direct space layouts.

Resulting simulations are presented in Figure 5.15. What we see is promising—if we were to combine the two, we would acquire a set of new reflections comparable to those appearing when we cross the main transition temperature at around 150 K.

Note that model C04b (Figure 5.15b) looks very similar to C01a (Figure 5.11a). We find the intensity distribution, however, to be more correct in C04b, and will investigate this version further.

Before continuing with a merged model, realise that there are (at least) two stacking

strategies for either type. One could either (i) keep the same kind of orientation along the vertical, or (ii) alternate at each layer. The first strategy was used to create Figure 5.15. The second strategy was abandoned, because it produced an $hk0$ -plane with no «extra» reflections, and the $hk1$ -layer was similar to Figure 5.8b. Similar satellites appear in $hk3$, but they are strongest near the centre of reciprocal space.

We proceeded with two $16 \times 16 \times 8$ blocks of each of the two types, using the first stacking strategy, and placed them on top of each other. The resulting $hk0$ -plane is shown in Figure 5.16. Reflections from one kind are stronger than the other, and there are absent reflections along one direction (normal to $[110]$). Since the two types have made new reflections along two directions, it is reasonable to believe a third type of arrangement would complete the last direction.

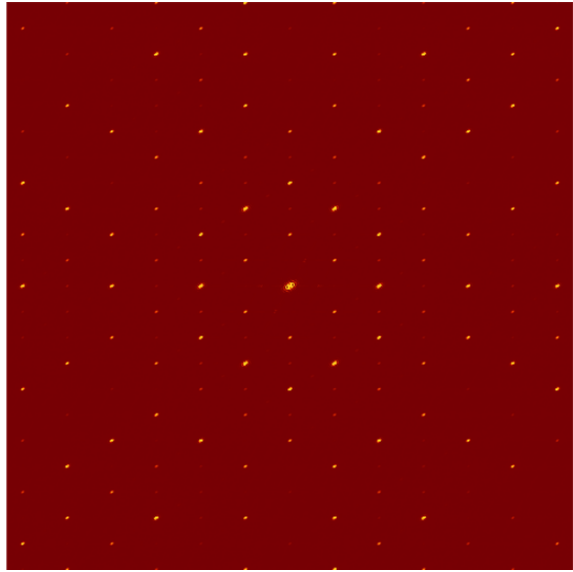


Figure 5.16: The $hk0$ -layer of model C04 after combining the two types. Effectively a «blend» of the images in Figure 5.15.

5.4 Category D: Models of twinning

Model D01: Obverse–reverse twin

We first tried making a copy of the unit cell that is rotated 180° , and then stacked them on top of each other to simulate the twinning operation. The results were not in accordance with expected diffraction patterns.

Then we considered a structure consisting of the same two types of unit cells, but this time combined them in a «chequered» pattern, meaning they each neighbour the other kind. An unexpected error occurs in the simulation process when piping the data through the `DIFFUSE` program; the error is not encountered when using `DISCUS`. Regardless, the resulting diffraction patterns do not resemble the experimental images.

The reason behind using a chequered pattern was to double the effective cell dimensions in the plane, thus hopefully obtain something like the modulated sub-phases of the obverse–reverse twin (page 68).

Model D02: Plesiotwin

Recall that our third TFIC sample was a plesiotwin, i.e. a twin in which the components are rotated by a non-crystallographic amount. To model this, we build our structure in three steps: (1) Make a block of the standard host cell (disregard the guest phase to keep it simple), and embed a rotated version on top of it. (2) «Cut out» an effective repeating unit and make this the «unit cell» of a new structure. (3) Synthesise a new «crystal» by copying the new cell to an arbitrary size. These steps are outlined graphically in Figure 5.17.

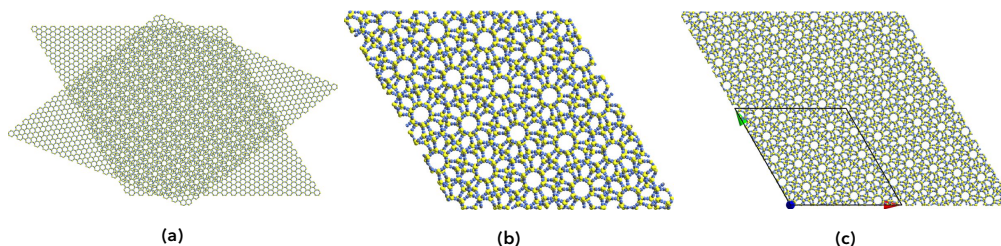


Figure 5.17: The process of making the plesiotwin model. (a): Two identical layers are rotated by the special amount (38.2°). (b): A 7×7 substructure is «cut out», representing the new repeating unit. (c): A larger structure is made with `SynthesiseStructure`, which duplicates the block from (b). Here, a new $2 \times 2 \times 1$ structure is made of the block in (b).

The underlying code is as follows:

```

125 cutoutSize = {cutX, cutY, cutZ} = {7, 7, 14};
126
127 templateSize = {tX, tY, tZ} = cutoutSize * {3, 3, 1/2};
128 ExpandCrystal["RhombohedralHost", templateSize,
129   "NewLabel" -> "RhombohedralCell",
130   "ExpandIntoNegative" -> "PlanarOnly"];
131
132 EmbedStructure[{"RhombohedralCell"}, {{0, 0, tZ}}, "RhombohedralCell",
133   "MatchHostSize" -> False,

```



Figure 5.18: Simulated planes of model D02, made with DISCUS. From left to right: $hk0$, $hk1$ and $hk3$. Compare with Figure 2.15 and Figure 2.20.

```

134 "Rotations" -> {0, 0, 38.2132 Degree},
135 "NewLabel" -> "TwinModel";
136
137 (* Cut out: *)
138 AppendTo[$CrystalData, "ModelCell" -> $CrystalData["TwinModel"]];
139 atomData = $CrystalData["ModelCell", "AtomData"];
140 atomData = Select[atomData,
141   (#FractionalCoordinates[[1]] >= 0 && #FractionalCoordinates[[1]] < cutX) &&
142   (#FractionalCoordinates[[2]] >= 0 && #FractionalCoordinates[[2]] < cutY)
143   &];
144 $CrystalData["ModelCell", "AtomData"] = atomData;
145 $CrystalData["ModelCell", "Notes", "StructureSize"] = cutoutSize;
146
147 ResizeStructure["ModelCell", cutoutSize];
148 SynthesiseStructure[{"ModelCell"}, {2, 2, 1}, "Model"];
149 ResizeStructure["Model", 1/cutoutSize];
    
```

As seen, we start by defining our cutout size (seen in Figure 5.17b). Next we define a template size, which here is effectively three times larger in the ab -plane. The height is halved since we will have half of each of the «twin components». The option `ExpandIntoNegative` is used here to centre the origins to the expanded block, and thereby let the rotation be about the centre as well. The cut out is essentially an extraction of those atoms satisfying the condition $0 \leq x, y < 7$. `ResizeStructure` is first used to gather the whole block as seen in Figure 5.17b into one large unit.

After synthesising the structure, the second use of `ResizeStructure` ensures that the unit cells of the model returns to the proper size, required to have the simulation program DISCUS produce correct results. The same error hindered us from using DIFFUSE as the simulation tool here as well.

As we can see in Figure 5.18, the general pattern of the strongest reflections are recognised when comparing with the experimental reconstructions. The images are, however, limited when it comes to advancing our insight to the structure. We therefore

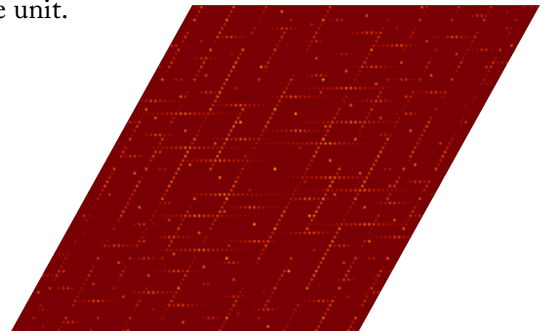


Figure 5.19: Simulated $hk0$ -plane of model D02, but where the host is distorted before adding a rotated «twin» on top.

reproduced the model with a single tweak:

```
150 DistortStructure["RhombohedralCell", (5 * 0.025 {TriangleWave[#2/2], 0, 0} &)];
```

This was added after line 130 to distort the host like in model B03. Alas, the result did not improve to something resembling our experimental records, as one can see in Figure 5.19.

Model D03: Monoclinic triplet

It has been pointed out in the literature that the broadening of powder diffraction rings may be attributed to twinning^[37] (even triplet formation^[46]). In a similar case with *n*-paraffins embedded in urea^[13] it is noted that the diffraction pattern of the colder phase is reconcilable with the superposition of three individuals of the low-temperature cell mutually rotated by 120° about the *c*-axis.[†]

To investigate this process in our case, we may use `ReciprocalSpaceSimulation` to first make a selection of reciprocal lattice points for the monoclinic cell, then combine these with two duplications where the nodes have been rotated 120° and 240°, respectively, about the origin. When also combining this result with the nodes of the high-temperature rhombohedral lattice, we derive an image as seen in Figure 5.20.

Note from the figure that this combination fulfils the third common observation listed in Section 2.3, namely that the new reflections appearing below ca. 150 K are situated midway between the «old» reflections. It must be noted, however, that all the reflections not overlapping with the rhombohedral nodes in Figure 5.20 are very weak. We have around 20 times difference in the magnitude of the structure factors when comparing this group of weak reflections to the next weakest reflection. Looking up the corresponding values in the final structure solution of the low-temperature phase[‡] and comparing ratios yields inconclusive results.

Looking closely at the same figure, note that there are six directions in which none of the monoclinic reflections land. This is in agreement with experimental data at *hk0*—see

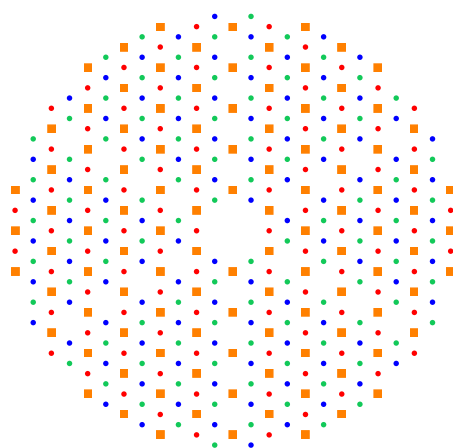


Figure 5.20: Superposition of simulated reciprocal nodes (not to scale) for three mutually rotated monoclinic lattices and a rhombohedral lattice, all of the *hk0*-plane. The red, green and blue dots are of the monoclinic cell; the orange squares of the rhombohedral. The rhombohedral notes completely overlap a subset of one of the monoclinic variants (in this case the blue).

[†]That low-temperature cell could be approximately obtained with one of the hexagonal–orthorhombic relations, much the same the rhombohedral–monoclinic relation in equation (1.1).

[‡]Recall from Subsection 3.2.2 that the low-temperature structure is represented by the primary twin component of TFIC-3 at 140 K.

for instance Figure 2.12a. Repeating this generation of monoclinic triplets for other planes, however, such as $hk2$ and $hk3$, we find that the overall pattern of new reflections fit well, but nonetheless with various reflections not in accord with the experimental images.

We also tried using a rotation angle slightly off 120° to recreate the mosaicity effect of elongated nodes. In that case, not all of the monoclinic reflections are affected, which is contradictory to the observations.

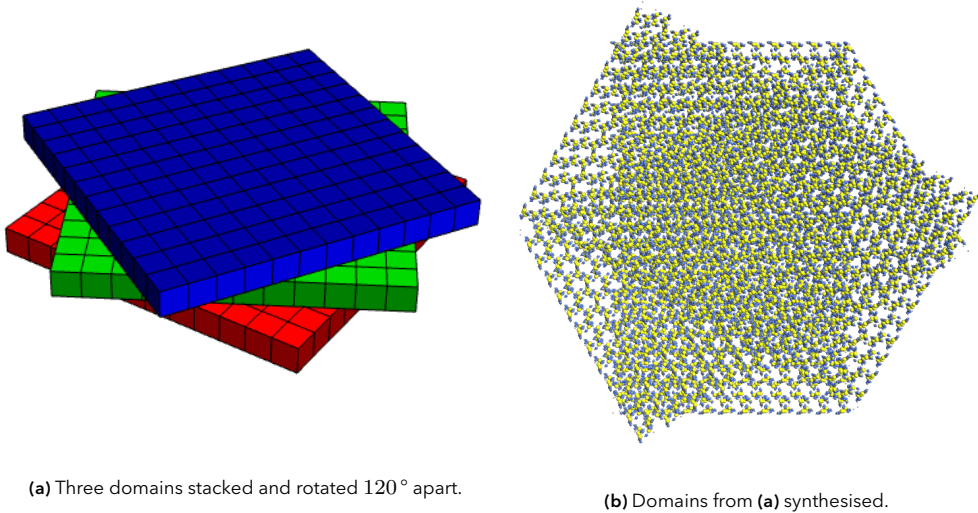


Figure 5.21: Illustrating steps of the model creation. In (b) the domains in (a) have been populated by empty cells of the monoclinic low-temperature version.

It is difficult to imagine how the three monoclinic components would efficiently pack a surface plane. Also keeping in mind that this transformation twinning should be «easily» reversible, we explored the possibility that the twins are stacked along the c direction, as illustrate in Figure 5.21. Unfortunately, the rendered simulations were too poor to enlighten us in our verdict, and are omitted in the thesis.

5.5 Category E: Domains

In this section we present models in which the *domain* functions have been brought forth to help model subgrain- and boundary effects. Recall from Section 4.2 (page 86) that the concept of domains entered MaXrd as a central modelling equipment. We apply rotations in order to model effects of incoherency across the domain boundaries.

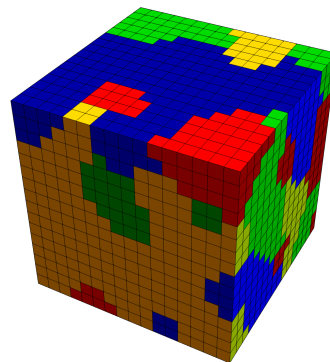


Figure 5.22: A generated structure for model E01 (3D type).

Model E01: Four-coloured domains

In this model we first prepare four unit cells, each containing six ferrocene molecules in one of the four expected directions: either parallel or among the three perpendicular settings. This may resemble model Ao6 in which each embedded ferrocene molecule was in one of the four orientations mentioned. In the code below we follow the naming convention of Sorai et al.^[90].

```

151 ExpandCrystal["RhombohedralHost", {1, 1, 1},
152   "IncludeBoundary" -> False,
153   "NewLabel" -> "EmptyHostCell"];
154
155 Scan[
156   EmbedStructure[#{#1}, ironPositions, "EmptyHostCell", "NewLabel" -> #2] & @@ # &,
157   Transpose[
158     {
159       "FerroceneMolecule",
160       "FerroceneMoleculePerpendicular",
161       "FerroceneMoleculePerpendicular060",
162       "FerroceneMoleculePerpendicular120"
163     }, {
164       "TFIC-cell-z", (* parallel *)
165       "TFIC-cell-a", (* perpendicular, alpha *)
166       "TFIC-cell-b", (* perpendicular, beta *)
167       "TFIC-cell-c" (* perpendicular, gamma *)
168     }
169   ]
170 ]

```

With the instructions above we first create an «empty» thiourea host cell, then embed the various ferrocene guests to make four different populated unit cells. Next we need to create or specify the domains of our model. CreateDomains has been written for this purpose. It employs Monte Carlo methods to gather domains of equal index (at least when using its default settings), and produces an array of indices denoting the domain belonging to each unit cell. The two figures on this page are merely graphical representations of the produced domains; each domain/index is associated with a certain colour. Here we make the characterisation for a $16 \times 16 \times 16$ structure with four domains, where the randomisation process iterates 25 times:

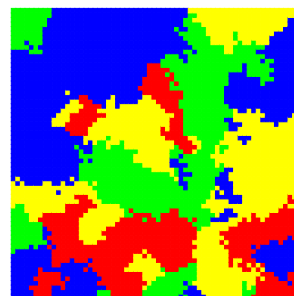
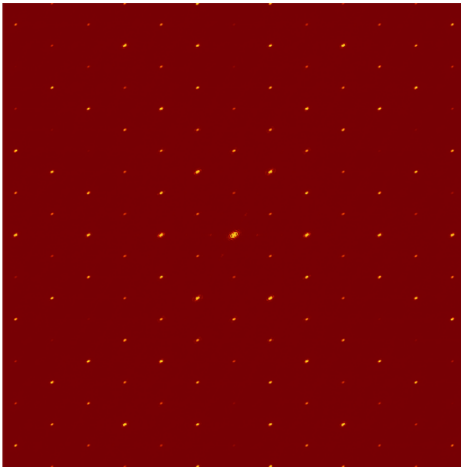


Figure 5.23: A generated structure for model E01 (2D type).

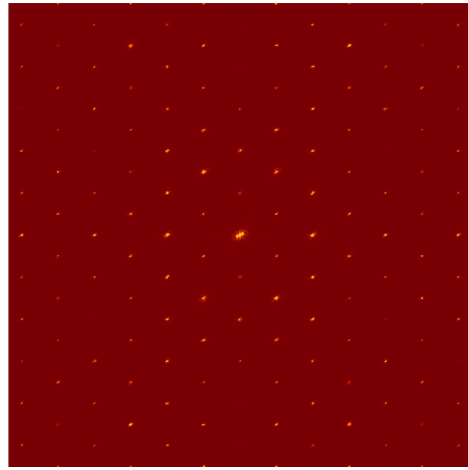
```
170 domain = ConstructDomains[{16, 16, 16}, 4, 25];
```

See Figure 5.22 for a depiction of the output. Then it is to be synthesised into a proper model with:

```
171 SynthesiseStructure[domain, "Model", <|
172   1 -> "TFIC-cell-z", 2 -> "TFIC-cell-a", 3 -> "TFIC-cell-b", 4 -> "TFIC-cell-c"|>]
```



(a) $hk0$ -layer of the E01 model (3D type).



(b) $hk0$ -layer of 2D type E01 model.

Figure 5.24: Comparison of the simulated $hk0$ -layers of the two E01 models, 3D to the left and 2D to the right. The most evident feature of dissimilarity, is that some of the reflections in the 2D version are «ragged».

We also investigate a two-dimensional variant with four different domains. A randomly generated $64 \times 64 \times 1$ structure, iterated 50 cycles, is made with the following:

```
173 ConstructDomains[{64, 64, 1}, 4, 50]
```

See Figure 5.23 for a depiction of the result. The four colours represent the same four types of unit cells, as they are both made into «proper models» with same code in lines 171–172.

Besides being different from Figure 5.22, we might have expected that boundary effects play a role here. Nonetheless, the two images in Figure 5.24 are quite similar to each other. The same reflections are present in both images, just with a different intensity distribution. In the 3D version, the reflections $\{440\}$ and $\{550\}$ are very faint. This was seen in model B02, too, but whereas the $hk1$ - and $hk3$ -layers were unrealistic, we find the simulations of the current model to be quite sensible. Both the 2D- and 3D versions of model E01 are thus on a par with model A05, and should be considered as plausible representations of the high-temperature phase of the TFIC. The apparently greatest difference between the models A05 and E01, is that the $\{440\}$ and $\{550\}$ reflections are more intense in A05, which is more true to the data.[†]

[†]Although the $\{440\}$ reflections are somewhat weaker than the neighbouring reflections in the ex-

Model E02: Sector domains

The motivation for making models where the domains are arranged in a sector-like fashion came from articles in the literature about ferroelastic domains.^[36]

Contrary to the first domain created with `ConstructDomain`, the use of this function with the keyword "SectorRegions" does not make a randomly iterated structure. Instead, one specifies the number of sector pairs, their angular widths and offsets only. The code that generated what is seen in Figure 5.25a is:

```

174 domain = ConstructDomains["SectorRegions", {64, 64, 1}, {
175   {3, 27 Degree, 10 Degree} (* red *),
176   {3, 22 Degree, 2 Degree}  (* green *),
177   {5, 8 Degree, 23 Degree}  (* blue *),
178   (* the rest is taken by yellow *)
179 }]
```

and for model E02 type B we used:

```

180 domain = ConstructDomains["SectorRegions", {64, 64, 1}, {
181   {3, 17 Degree], 7 Degree]} (* red *),
182   {2, 20 Degree], 18 Degree]} (* green *),
183   {1, 50 Degree], 22 Degree]} (* blue *)
184   (* the rest is taken by yellow *)
185 }]
```

They were both made into models with the same code as before (lines 171–172).

We have compiled a series of randomly generated sector domains. These are shown in Figure 5.27, which is split across three pages. The input parameters are varied randomly to generate various $16 \times 16 \times 1$ structures. Up to six domains are generated, but they are populated by the same four types as in model E01.

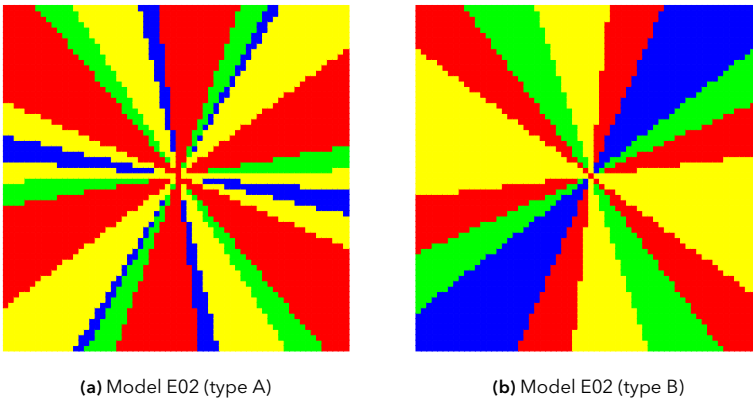


Figure 5.25: Output from `DomainPlot` which represent the various domains of the structure. Types A and B are here characterised by having relatively narrow and wide sectors, respectively. Both are considered variants of the E02 model.

In Figure 5.27 (starting on page 116) the second through fifth columns are all simulations made with `DIFFUSE` just with different settings for the «subtraction mode of Bragg periemntal «unwarps», it is not faint. Study e.g. Figure 2.9a.

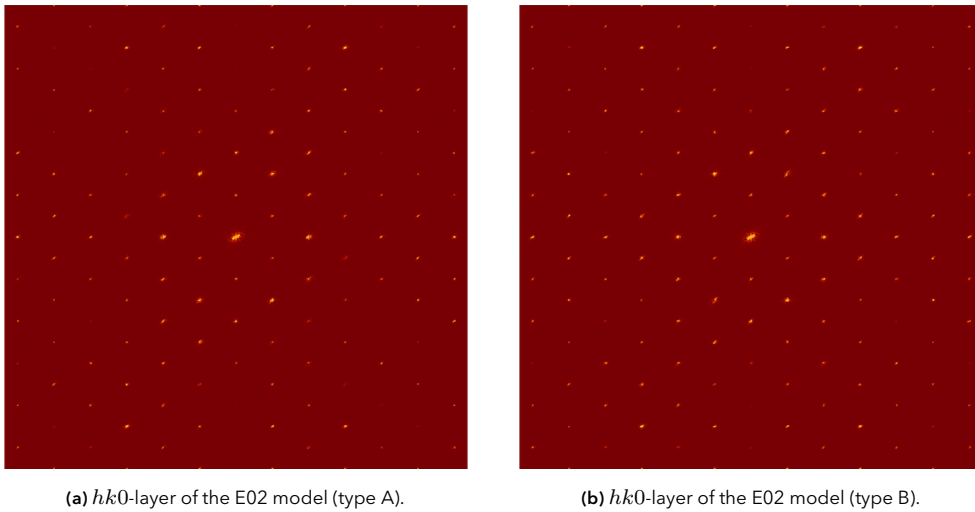


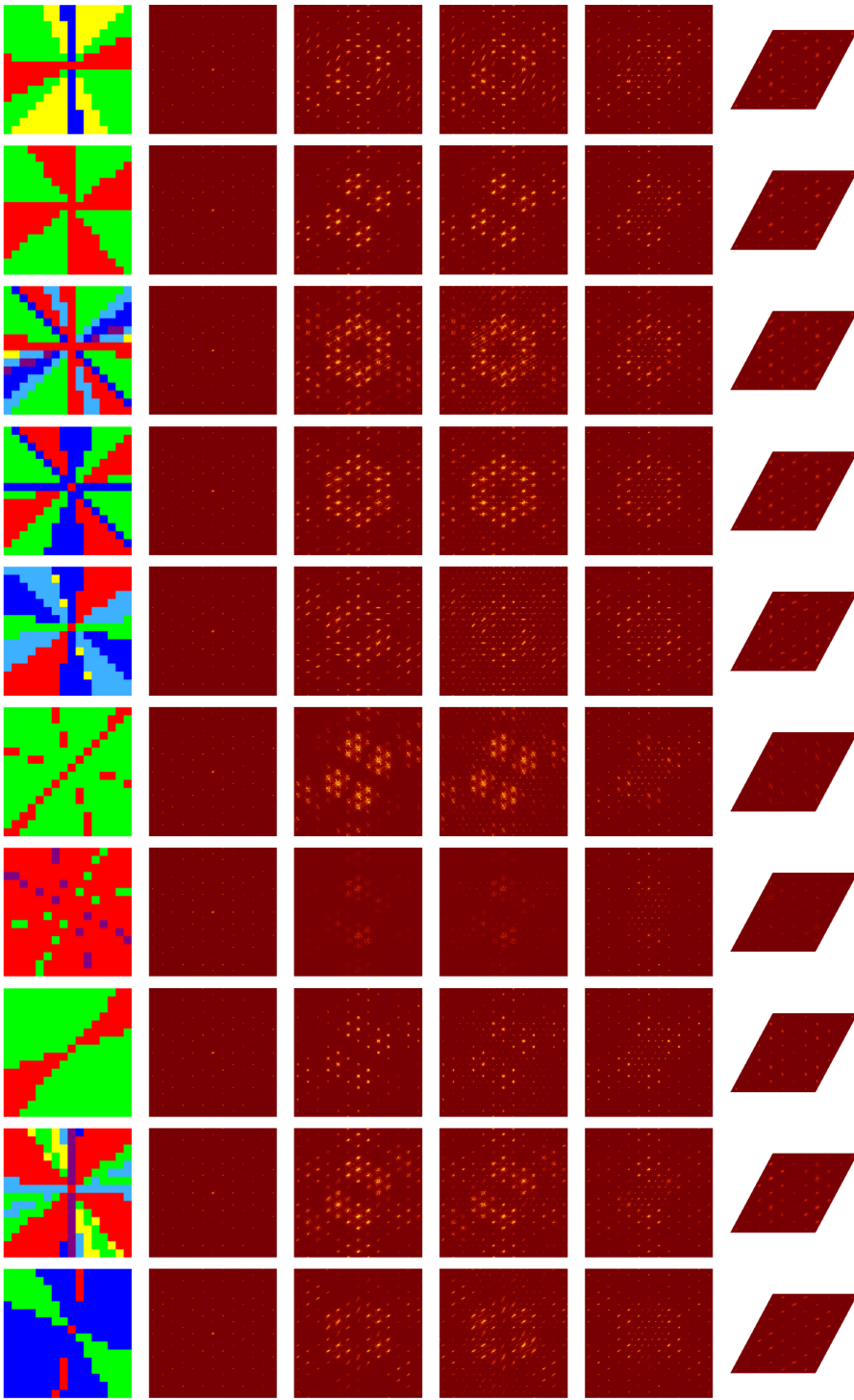
Figure 5.26: Simulations based on model E02, where the domains take the shape of triangular «sectors». Minor differences in some intensities is the only differentiating aspect.

scattering». According to the author^[28] the first result is a «control» where no modification is performed. The next is a less precise calculation of the Bragg scattering from B_{iso} values. The final two have the Bragg scattering subtracted by averages made from the whole and from 5 % of the crystal, respectively, to highlight diffuse scattering.

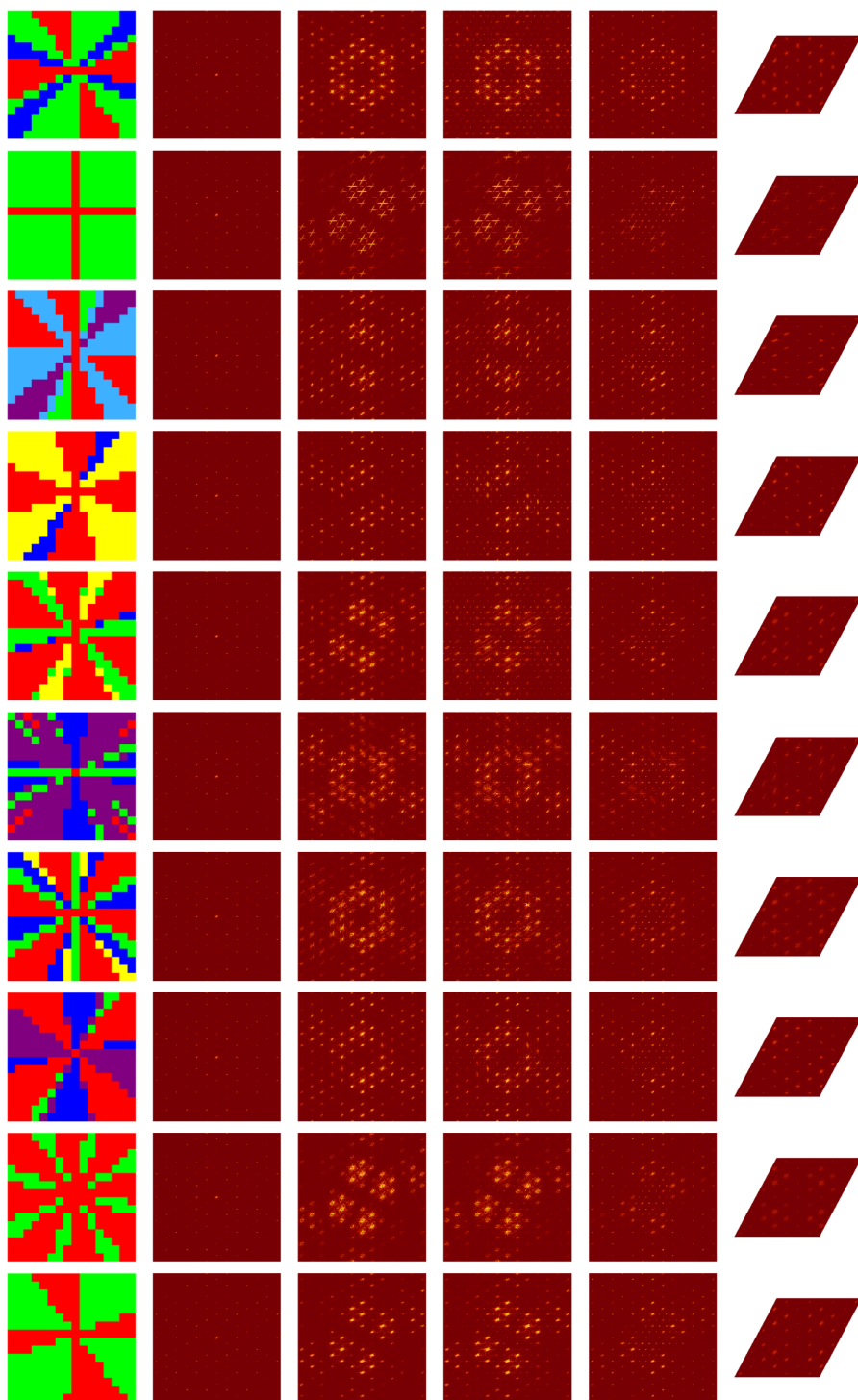
One of the reasons for compiling these was to see if any of the features of the reflections in the low-temperature phase could be reconstructed, in particular the elongation of the nodes along concentric circles. Despite no obvious winning candidate, there are some close cases worth pursuing further—for example the second from the bottom in Figure 5.27c. One may use larger (as well as three-dimensional) structure sizes, and swap out the content with more intricate guest arrangements as we have used in the previous model categories.

In model E02 we have made two variants where one type features narrower sectors. As we are interested in capturing this particular two-dimensional arrangement, we use a structure of size $64 \times 64 \times 1$ instead (same number of cells in total a 16^3 version). Figure 5.25 illustrates how the domains look like, while Figure 5.26 shows the results. The $hk0$ -, $hk1$ - and $hk3$ planes all look quite the same as the previous E01 model. A minor disparity between the two E02 variants, is that type A displays fainter $\{440\}$ reflections as well.

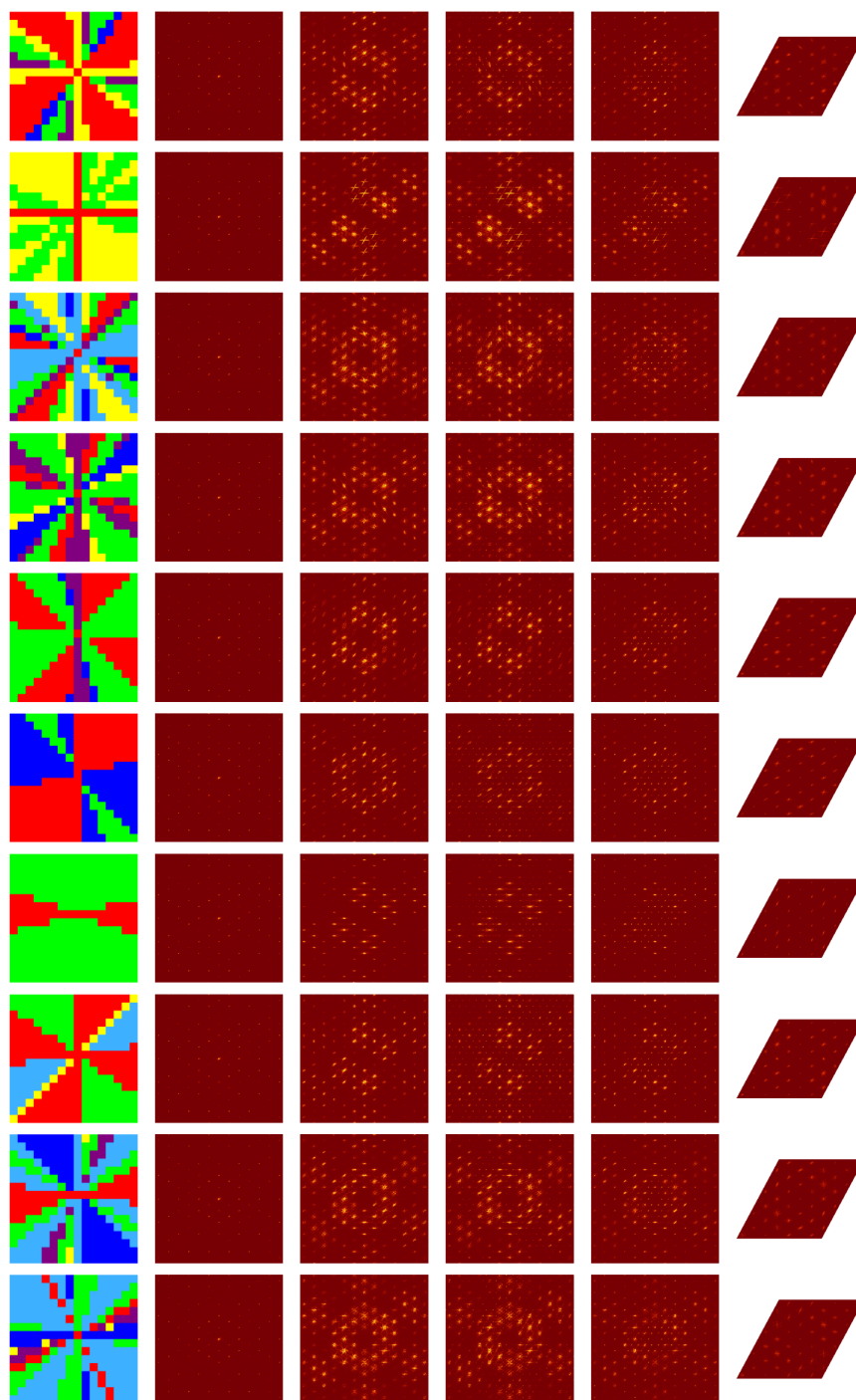
The E01 and E02 models do not give any clear indication of being either correct or wrong. E02 appears similar to A01 and A03, only with slightly different reflection shapes and intensities.



(a) Randomly generated sector domains. Part 1 of 3.



(b) Randomly generated sector domains. Part 2 of 3.



(c) Randomly generated sector domains. Part 3 of 3.

Figure 5.27: A collection of randomly generated sector domains. The leftmost columns show DomainPlot representations. The next four columns are all simulations generated by DIFFUSE, with various subtraction flags used (read more in the text on page 114). The rightmost images are DISCUS simulations. Various colours represent the various ferrocene orientations.

Model E03: Mosaic model

Here we will continue to use `ConstructDomain` to model a structure with a high degree of mosaicity, i.e. imperfectly aligned subgrains. Let us start by viewing how the domains are shaped.

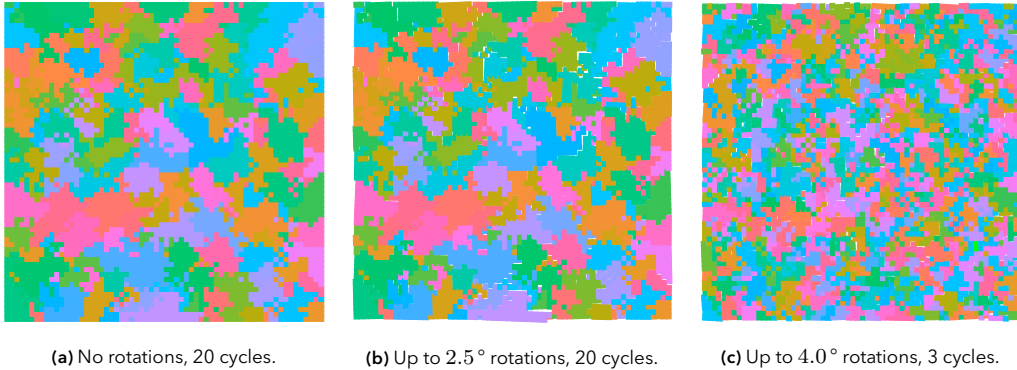


Figure 5.28: Model E03 variants with different values of rotation amplitudes and iteration cycles. The gaps in (b) and (c) come from the small, random rotations of the individual domains, and represent imperfections at the grain boundaries.

In Figure 5.28 we see three variants of the same basic E03 model. They all evolve in the same course (since we set the same random seed beforehand each time), but the rotation amplitudes and number of iteration cycles vary. In Figure 5.28a and Figure 5.28b there are 154 individual domains after 20 cycles,[†] while there are still 755 domains after only three cycles, which is the status in Figure 5.28c.

The code in lines 186–201 below is used to create each form; only the parameters amplitude and cycles in the first two lines are changed. `amplitude` sets the range in which random rotation angles will be drawn, and set to zero first.

```

186 amplitude = 0.0 Degree;
187 cycles = 20;
188
189 structSize = {64, 64, 1};
190 totalSize = Times @@ structSize;
191 domain = ConstructDomains[structSize, totalSize, cycles];
192 rotations = AssociationThread[Range@totalSize -> RandomReal[{-#, #}, totalSize] &@ amplitude];
193
194 indices = DeleteDuplicates@Last@domain;
195 randomMap = AssociationThread[indices -> RandomChoice[
196   {"TFIC-cell-a", "TFIC-cell-b", "TFIC-cell-c", "TFIC-cell-z"},
197   Length@indices]];
198
199 SynthesiseStructure[domain, "Model", randomMap,
200   "RotationMap" -> rotations /. x_Real -> {0, 0, x},
201   "RotationAnchorReference" -> "DomainCentroid"];

```

In line 192 we associate each domain i with a random number, x , which indicates the rotation angle. The same numbers are used in line 200, just converted to the required

[†]154 individual domains averages to 26.6 cells per domain in this case (standard deviation: 18.4).

three-dimensional form, $\{0, 0, x_i\}$. The variable `randomMap` maps each domain index to a TFIC unit cell with ferrocene embedded in one of the four orientations, chosen at random.

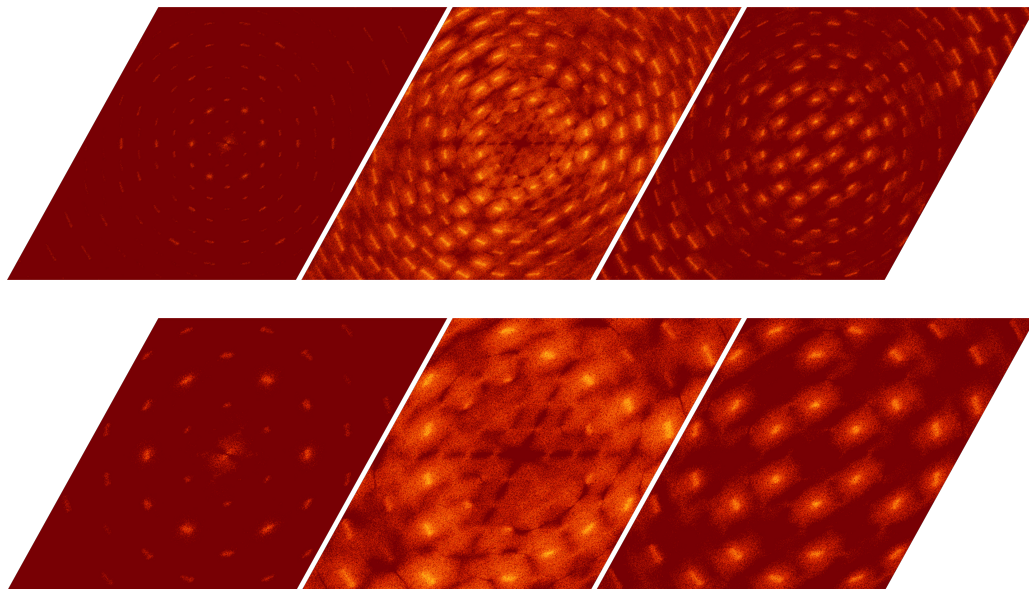


Figure 5.29: Simulated planes of model E03, variant with rotation amplitude 2.5° and 20 iteration cycles. From left to right: $hk0$, $hk1$, $hk3$. The top row has a range of $|h, k| \leq 12.5$ while the bottom row has a range $|h, k| \leq 5.5$. Compare with Figure 2.12a and Figure 2.14.

Figure 5.29 shows the results of the second variant (amplitude at 2.5° and 20 cycles), while Figure 5.30 show just the $hk0$ -planes of the other two variants.

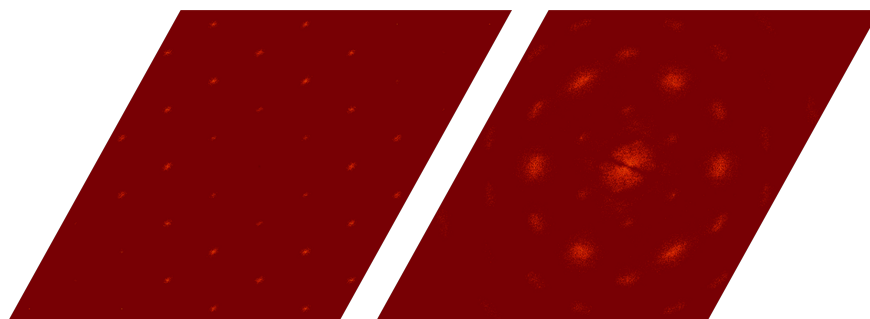


Figure 5.30: Simulated $hk0$ -planes of model E03, the first and third variants.

The first variant is merely a control for the other two, and show no particular features

in any of the reconstructed sections of reciprocal space. The second and third variants display somewhat the same patterns, but the Bragg spots are naturally more delocalised in the latter. The reflections in the experimental recordings are definitely not as diffuse as the last variant suggests; our best bet is currently with the second variant.

The use of «subgrains» accompanied with minor rotations seems to have recreated the «tangential smearing» of reflections. However, emergence of reflections between the others, as if the ab -plane of the unit cell doubles in size, is missing. Further attempts with adjustments of the E03 model will be pursued in the very next model, but first we also try to «pack» the $64 \times 64 \times 1$ structure into the three-dimensional 16^3 equivalent. The code is mostly identical; apart from the `structSize` we change the second argument of `RandomReal` on line 192 to `{totalSize, 3}` in order to generate triplets.

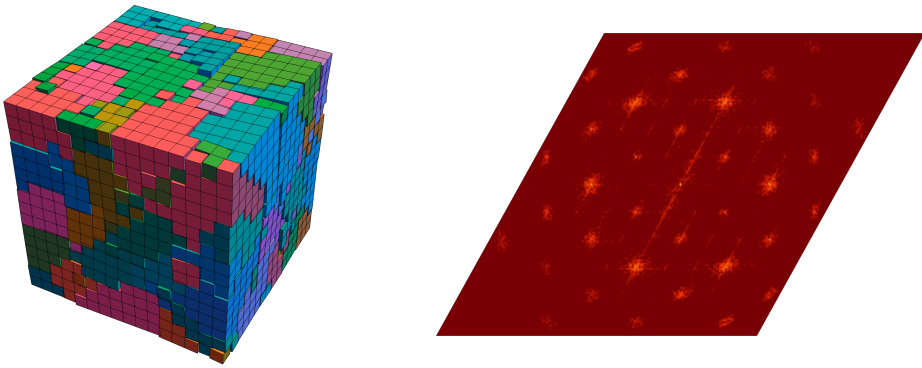


Figure 5.31: A three-dimensional version of model E03 and the simulated $hk0$ -plane. Rotations up to 2.5° , fewer iteration cycles were used to achieve about the same number of domains and average size.

The number of iteration cycles was lowered from 20 to 8 in order to obtain approximately the same domain statistics.[†] The artifact (narrow line) seen in the simulation above is likely due to truncation effects of the Fourier transform. Apart from this, we see that it differs from the «flat» equivalent when it comes to the shape of the reflections. The «flat» model, which was rotated only around the vertical axis, have reflections which are more elongated tangential to circles about the origin (000).

Figure 5.32 on the next page presents miscellaneous «dual domain» structures—with and without rotations—to exhibit some additional trials with simple domains.

[†]Here: 161 individual domains; average: 25.4 cells per domain (standard deviation: 24.8).

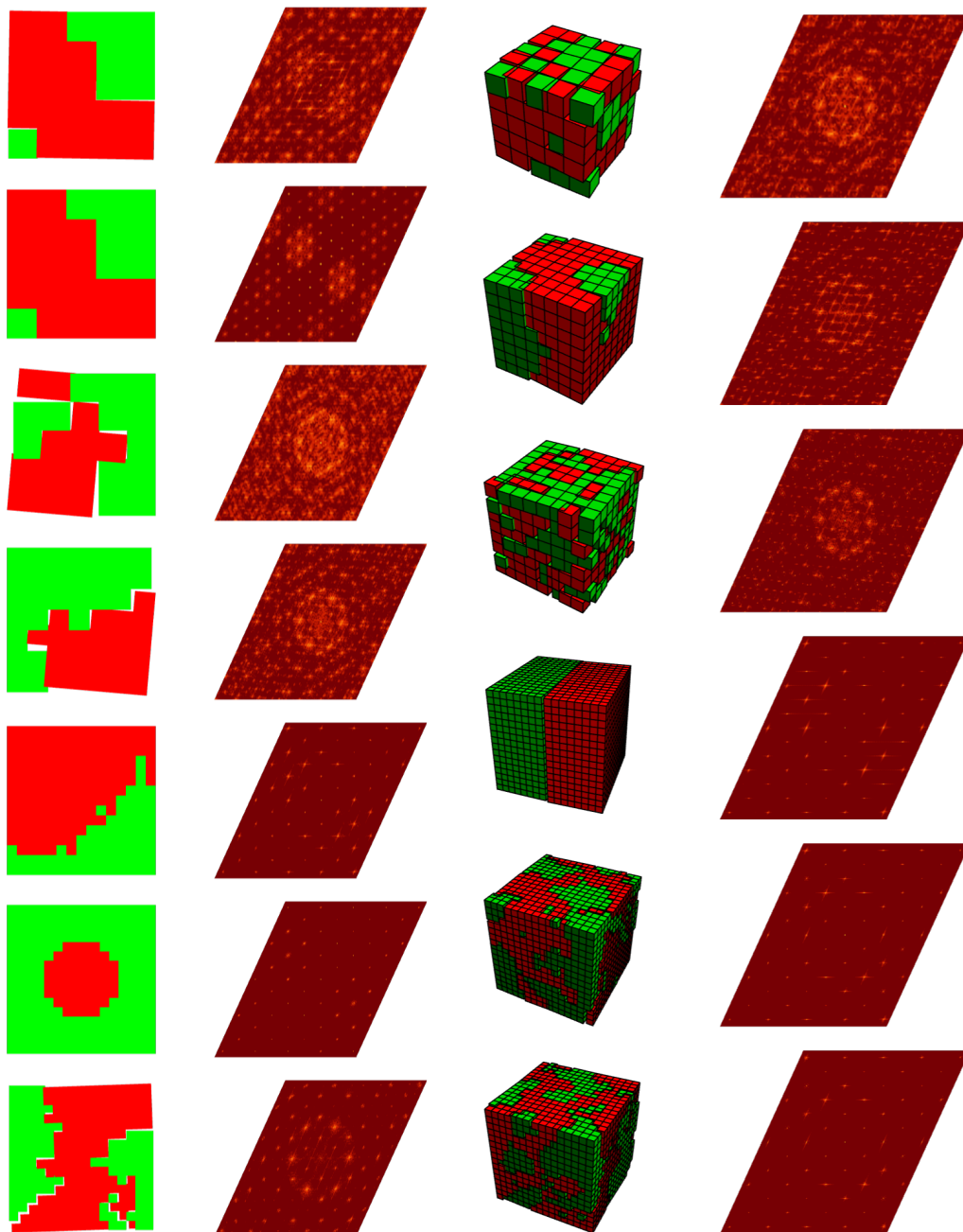


Figure 5.32: A collection of randomly generated domains, most of which have been rotated by a small and random amount. The red and green components are embedded with a parallel and a perpendicular ferrocene variant, respectively.

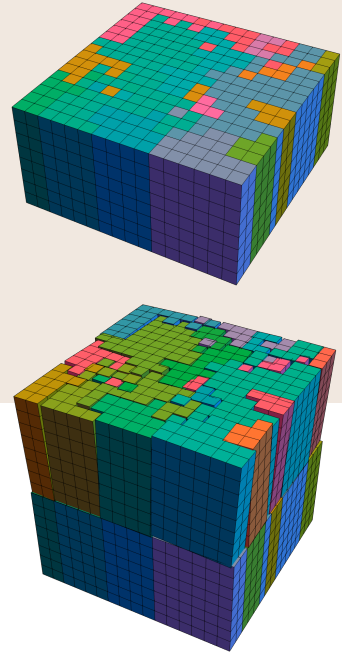
Model E04: Partially distorted

We continue from the essentials of the previous model; we rerun the code in lines 186–201, but reduce the structure size from 64 to 16. Next we run the following:

```

202 bottomPart = MergeDomains[domain, 8];
203 bottomIndices = DeleteDuplicates@Last@bottomPart;
204
205 topPart = bottomPart;
206 shift = Max@bottomIndices;
207 topPart[[2]] += shift;
208 amplitude = 2.5 Degree;
209 rotations = AssociationThread[
210   (bottomIndices + shift) -> RandomReal[{-#, #},
211   {Length@bottomIndices, 3}] &@amplitude];
212
213 merged = MergeDomains[{bottomPart, topPart}];
214 bottomMap = AssociationThread[bottomIndices -> RandomChoice[
215   {"TFIC-cell-a", "TFIC-cell-b", "TFIC-cell-c", "TFIC-cell-z"},
216   Length@bottomIndices]];
217 topMap = KeyMap[# + shift &, bottomMap];
218
219 SynthesiseStructure[merged, "Model", Join[bottomMap, topMap],
220   "RotationMap" -> rotations,
221   "RotationAnchorReference" -> "DomainCentroid"];

```



This first duplicates the generated layer to make a stack eight cells high, resulting in the block seen on top in Figure 5.33. We then make a copy of this block, stack it on top, and prepare a set of random rotations. Note that the top part has all its domain identifiers shifted by a constant amount. This is to help us retain the same content along the vertical, while only applying rotations to domains in the upper half.

A selection of resulting images are shown in Figure 5.34 below. We note that the $h0l$ -plane is quite dissimilar what we see in Figure 2.12b. The reconstructed reflections are mostly «smeared out» in the manner we have seen this before. In the main transition, however, we observe an emergence of new reflections midway between the originals as the primary feature. Also, the fragmentation of reflections in $hk0$ and $hk3$ occur tangentially along circles ¢ric to (000), not radially, as we see in the experimental records.

Inspired by the construction of the last model, we also try creating another form of «partially distorted» structure by «fusing» together a rhombohedral and monoclinic version of the TFIC structure. We choose to let the ferrocene guests be oriented completely random, thus essentially merging the two variants of model A05. The code used to create these submodels contains nothing new, and we «cut out» the final model similar to how we did it with model D02. After preparing one of each system, we perform a trick on the monoclinic variant:

```

222 $CrystalData[["MonoclinicModel", "LatticeParameters", {"\[Alpha]", "\[Beta]", "\[Gamma]"}]] = 90;

```

Figure 5.33: Model E04 construction. The $16 \times 16 \times 8$ «fundamentals» is seen above. A copy is placed on top, which is to house the same entities, only with the domains rotated by small amounts. The final, merged model is seen below.

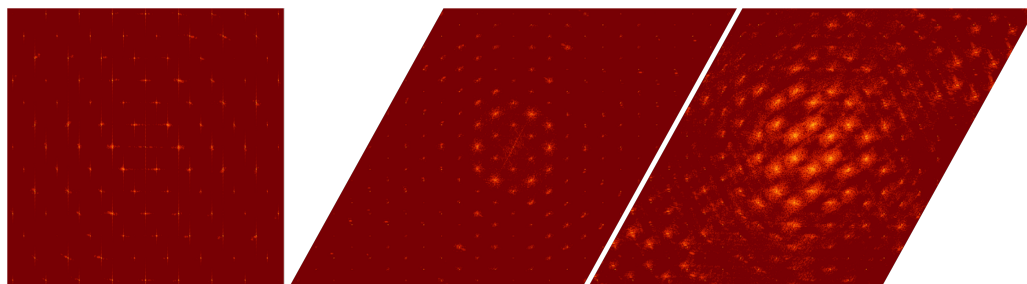


Figure 5.34: Simulated planes of the E04 model. From left to right: $h0l$, $hk0$, $hk3$.

where "MonoclinicModel" is an arbitrary name used for the model in this case. With this we «orthogonalise» the supercell, in order to align the tunnel c -axis with the rhombohedral version. When instructing the embedding, we also rotate the monoclinic structure 30° anti-clockwise in order to align the two b -axes as well. We end up with two $16 \times 16 \times 8$ blocks which we stack together vertically. The whole structure must be «trimmed» at the edges for the two versions to stack nicely. An illustration of the results and a simulation of the $hk0$ -plane may be seen in Figure 5.35.

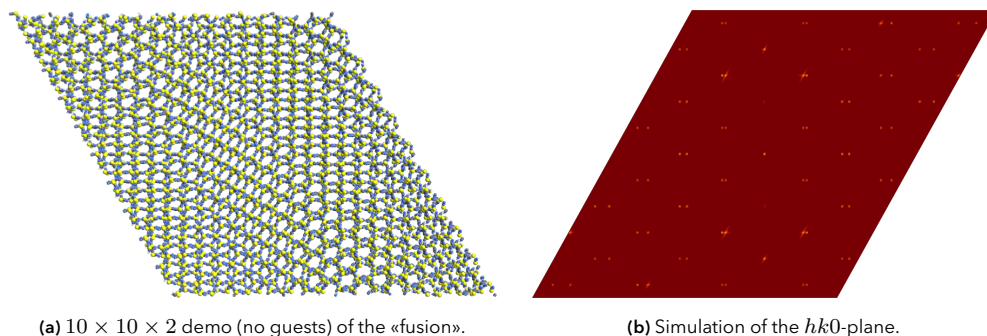


Figure 5.35: A variant of the E04 model where the two halves are made of different crystallographic systems, instead of using rotations to simulate imperfection. (a): Top view of the monoclinic variant on top of the rhombohedral. To avoid cluttering in this figure, no ferrocene was added. (b): DISCUS simulation result showing the $hk0$ -plane.

In the simulations we find obvious indications of twinning, as seen in Figure 5.35a, but not in the fashion we have seen in our experimental «unwarps».

Model E05: Partially shrunk structure

When reflections are «smeared» and split, the emerging reflections seem to mostly be farther out (larger h , k values). This could be interpreted as the cells shrinking due to the drop in temperature. Recall from Subsection 2.2.3 (Figure 2.18) that observations led us to believe that one of the two twin components were affected by the main phase transition before the other, since changes (the smearing and fragmentation) unfold for a subset of reflections. Also, when the crystal returns to 140 K, the structural change seems to linger on in the twin individual that started transitioning first. One possible explanation could be that one of the twin domains is situated in the middle of the structure, somewhat protected from losing heat by the other individual.

We can easily make a naïve model with the code we have used so far. We create a prototype where one part is slightly «shrunk» compared to the other by stacking two identical parts with the «regular» rhombohedral TFIC on top of each other. Before the embedding, we alter the top part simply with:

```
223 $CrystalData["ModelPart_Shrunk", "LatticeParameters", #] *= scaling & /@ {"a", "b", "c"};
```

where "ModelPart_Shrunk" is an arbitrary label, and scaling is a parameter, which we set to 0.95 in our test. The idea resembles Figure 5.33, just where the top half is shrunk instead of rotated. The resulting $hk0$ -plane shows two «sets» of reflections where one kind is slightly further out in reciprocal space, as expected. In $hk1$ and $hk3$ we see the same effect. None of the images have been included here, but are far from a good match with the true diffraction patterns.

Next we attempt to combine this idea with model E03, i.e. a subgrain model where in addition to small rotation perturbations, the domains may experience a slight decrease of the unit cell dimensions. We choose to reuse model E03, the second variant with rotation amplitude set to 2.5° and the number iteration cycles to 20. Recall that we ended up with 154 individual domains. Our strategy is to only alter the randomMap variable (lines 195–197), which was a map of each identifier to a random choice of four TFIC cells, in a way that maps to a completely «prepared» set of cells. Observe the following code:

```
224 AssignShrunkCell[label_String] := Block[{
225   randomScaling, newLabel, copy, newDimensions
226   },
227   If[RandomReal[] < 0.5, Return @ label];
228
229   randomScaling = RandomReal[{0.90, 1.00}];
230   newLabel = label <> "+" <> ToString[randomScaling];
231
232   copy = $CrystalData[label];
233   newDimensions = Values @ copy[["LatticeParameters", {"a", "b", "c"}]]
234     * {randomScaling, randomScaling, 1};
235   copy[["LatticeParameters", {"a", "b", "c"}]] = newDimensions;
236   AppendTo[$CrystalData, newLabel -> copy];
237
238   newLabel
239 ];
240
```

Mapping this function on `randomMap` after defining it, we obtain an «updated» association where about half of the cells have been shrunk by a random amount up to 10 % (all heights are still the same). We also emphasise that `AssignShrunkCell` should not be applied to the very first domain, since we want that one to have «full size». This can be achieved by specifying:

```
241 randomMap = MapAt[AssignShrunkCell, randomMap, 2 ;;]
```

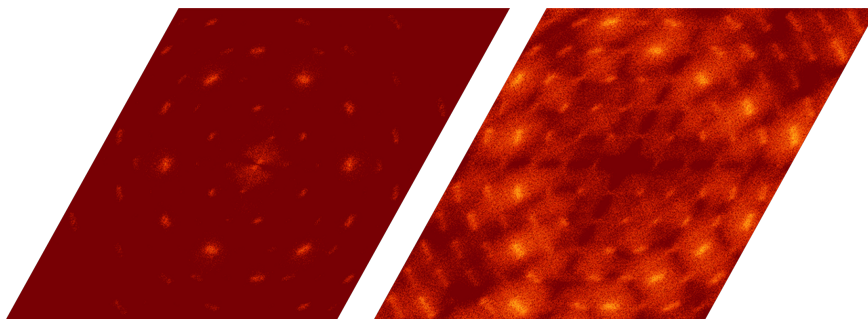


Figure 5.36: Simulated $hk0$ - and $hk1$ -planes of the E05 model. They are similar to Figure 5.29 (model E03), but contain more reflections.

The results, seen in Figure 5.36, are similar to model E03, but with a few additional reflections. This is something we hoped to produce, but unfortunately they are not «midway» between the original reflections as in our empirical images.

5.6 Summary of the modelling results

In the same way the fundamental laws of physics can never be *proven*, our simulations may give insight into which models that appear unrealistic, rather than settling the real question: what does the structure look like on the nanometre scale? After eliminating candidates by comparing diffraction patterns with experimental data, we have are left with more confidence in certain models.

The high-temperature phase

Our simulation results point to A05 as indeed a plausible high-temperature state of the TFIC. This simple and isotropic model, with complete disordered of the ferrocene molecule about the special position of the iron centre, is also favoured above the stricter A06 where the ferrocenes take one of four possible orientations. Keep in mind that the space group symmetry will generate a mess of superimposed molecules regardless of how neatly the ferrocene molecules are positioned in parallel- and perpendicular parts.

We also saw that model E01 gave very similar diffraction patterns. Thus, it is not easy to tell whether the ferrocene orientation is truly isotropic, or just approximately when one considers the structure to be an ensemble of many domains, each with a uniform internal structure. In our simulations, we are unable to find solid, distinguishable features when comparing results of randomly oriented ferrocene contra ferrocene distributed among the four orientations. We are disposed to believe that the latter is correct, since (recall from Section 1.5) Mössbauer spectroscopy indicated a prevalence of either parallel or perpendicular orientations,^[27] especially below 140 K where they are furthermore «locked-in» either parallel or perpendicular to the tunnel axis.^[35] The fully isotropic models seem to emulate the chaotic reshuffling of ferrocene molecules well.

The low-temperature phase

None of the models we have simulated have come close to resemble the intricate patterns seen in all the chapter images and other figures—also taking prototypes not discussed in this chapter into account. This goes for B04, too, which is based directly on the produced `cif` files. Figure 5.9b shows no dramatic changes after transitioning to the monoclinic system.

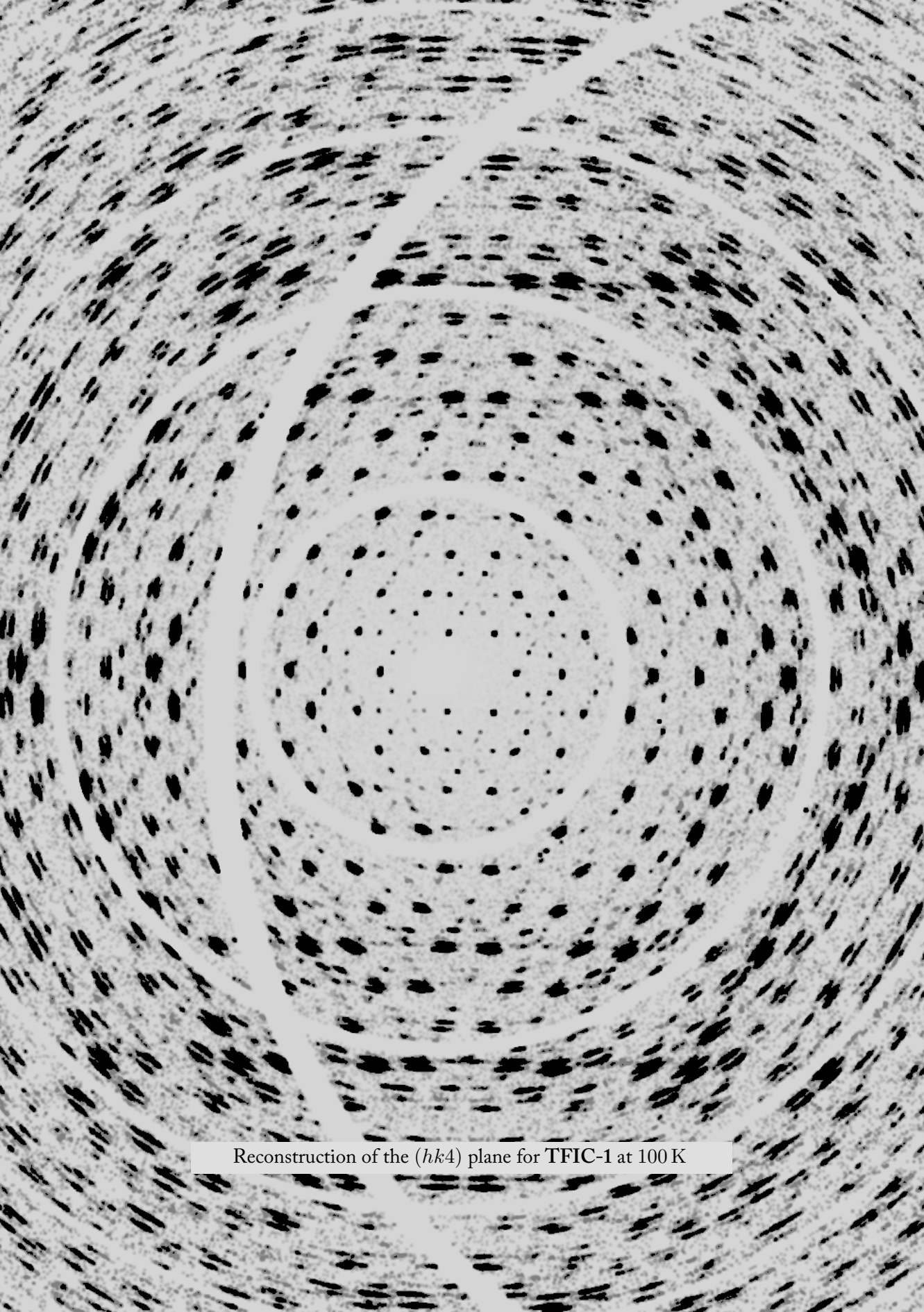
In our endeavour to replicate the diffractograms, we only managed to switch various nodes «on and off» or add satellite reflections. Also when altering the host by distortion (B03), no decent change in the shape of reflections occurred. We had to introduce the concept of domains before seeing any «stretching» of individual nodes. Randomised domains populated with the four ferrocene conformations (E01) only gave some reflections a «ragged» shape. The same can be said for the two variants of the sector-shaped domain models (E02), but variations on the «sector domain» model led us closer to what we were

searching for (Figure 5.27).

We continued by substantially increasing the number of separate domains, but keeping the same four cells with ferrocene. By perturbing the «subgrains» to emulate imperfections at the grain boundaries, we obtained for the first time a result which contained the «smearing effect» on the reflections (E₀₃). Recall that in the D₀₃ model we had attempted rotating the twin components by angles slightly different than 120°, but that did not affect all reflections as required to match experimental records. Based on the results of model E₀₃, we deem it likely that the «grain boundary mismatches» are modelled well as rotations about the tunnel axis only. As in the experimental images, the elongation increases with higher reflection indices, as is normal with high mosaicity. The fact that we had to perturb subgrains of the whole TFIC in order to achieve the «smearing» effect, may indicate that an establishment of short-range order of the ferrocenes does not necessarily alter the structure as a whole—at least not as long as the thiourea host remains unchanged.

New reflections are also another sign of the phase transition. This has not been a difficult criteria to fulfil, but we have struggled to make them appear at the right positions. We have not detected any short-range arrangements of ferrocenes that yielded a recognisable signature in the simulations. In the case with the last model (E₀₄) and most of those before it, whenever we double the planar size of the repeating unit we obtain new nodes that do not fit with what we have seen in the experimental records. Rotation of the lattice has not proven to be the answer. The patterns obtained by models C₀₁ and C₀₄ provided some inspiration to how the «new reflections» could arise, but the monoclinic triplet model D₀₃ seems to be the better candidate, as the pattern fits well with experimental counterparts of $hk0$. Also D₀₃ fall short when it comes to mimic the diffractograms of other planes, such as $hk1$ and $hk2$, when this simple triplet rotation does not situate new reflection midway between the existing ones.

Despite this advancement, one key feature is still missing (see Section 2.3): the fragmentation of reflections. We believed a superposition of multiple structures (rhombohedral, monoclinic) could be to physical basis for this effect, but attempts at combining different systems in the same model (E₀₄) were unsuccessful at recreating the fragmentation.



Reconstruction of the $(hk4)$ plane for TFIC-1 at 100 K

Concluding remarks

The aim of this final chapter is to discuss and compare the findings of this thesis in order to review what we have learned and discovered about the TFIC structure. These remarks include the observations made of reciprocal space in Chapter 2, the learning outcomes from the structure solution in Section 3.2, and from the simulation techniques in Chapter 5. In the end, we discuss what could potentially be included in further research of the TFIC and in future releases of MaXrd.

6.1 Discussion and results

6.1.1 Information conveyed by the data

Structural phases and sample variations

Recall that the choice of temperature points we selected to study originate from the article by Sorai et al.^[90]. It is peculiar that in two of the three samples (TFIC-2 and TFIC-3), no substantial changes were observed between room temperature and the main transition event occurring somewhere around 140 K. Not only are four of the five critical temperatures skipped, the greatest oddity is that the grand transition described by Sorai, Ogasahara and Suga (at 160 K) does not show any signs of change in the reciprocal space, nor in the lattice parameters in the adjacent data sets. In each of our three samples, a rhombohedral description fits well at this temperature, with no apparent transition.

Perhaps an explanation of this lies in the seemingly unique variations from sample to sample, probably due to random events in the growth process. Even though the data reduces to the familiar rhombohedral cell for each crystal (in the high-temperature phase), we know from observing the diffractograms that these specimens are all distinct in some form. We have seen that the main phase transition was both delayed and disproportionately affected in the twin TFIC-3. One can therefore imagine that the particular sample of Sorai et al. possessed another intrinsic substructure that advanced the main phase transition. We note that also Lorson et al.^[46] detected the high-temperature phase at 160 K.

If we consider our TFIC-1, however, we were able to discern four phases when inspecting the $h0l$ -planes along in the range 290 K to 90 K (see Figure 2.5). The first transition, phase 1 to phase 2 in our description, seems to coincide with $T_5 = 220$ K. One of our data points is at 180 K, which is situated six degrees below $T_4 = 186$ K. From what we observe, 200 K and 180 K belong to the same structural phase. Minuscule differences come across as random fluctuations, also when comparing these two temperatures on the return.

The second transition we observe, phase 2 to 3, is first seen at 165 K, and thereby closest to $T_3 = 171$ K. Since the data looks identical at 155 K, however, and if one accepts that Sorai et al.'s particular sample happened to instigate the main transition sooner, we could be looking at the largest $T_2 = 160$ K transition instead (cf. Table 2.2). Concerning the final phase, labelled 4 by us, there is sufficient upheaval in both the hk - and $h0l$ -planes to assert a new phase.

Thus, in the **TFIC-1** scenario, if we allow ourselves to regard the crossings of T_4 and T_3 as minor and elusive alterations of the structure, all of Sorai et al.'s phases have been accounted for, whereas the identical progress for **TFIC-2** and **TFIC-3** only revealed two distinguishable phases. It appears that structural variations from the onset have given **TFIC-1** a different trajectory through the temperature evolution compared to the other samples, giving rise to the four mentioned phases and the peculiar satellite reflections prominent only to this crystal (Figure 2.7), possibly resulting from modulation along the tunnels.

We draw a general conclusion that traits of the individual sample constitute one of many complexity aspects of the TFIC structure. Different structural imperfections may also play a role in this.

6.1.2 The main phase transition event

Normally, at lower temperatures the structure tends to be easier to solve due to a decrease in thermal fluctuations. In the thiourea inclusion compounds, however, the remarkable alteration of the host lattice makes it the opposite. The process has been speculated to be caused by higher mosaicity or (further) reversible twinning with lower symmetry.^[37] Our observations of reciprocal space, our structure solutions and simulations would not favour either of these effects in particular. It has been proposed in the literature that the family of thiourea tunnel inclusion complexes are generally rhombohedral at higher temperatures, and transition to a «distorted version» described as a monoclinic cell with more ordering of the guest molecules.^[15,16,32,39,48,65,66,100] We derived at the same structure solution conclusions, but our study of the other two aspects (reciprocal space and simulations) leaves us with further questions. For instance, if we import the `cif` files we have created and simulate the diffraction patterns (model $B0_4$), we generate images that are in agreement with experimental results, but as Figure 5.9 shows, the low-temperature phase is hardly distinguishable from the high-temperature phase. All our samples show highly complex diffraction patterns below the main transition temperature—also the untwinned **TFIC-2**—a fact which compels us to regard the monoclinic cell as a incomplete (and not considerably better than the rhombohedral) description of the low-temperature phase of the TFIC. Solving the structure alone will not push our understanding further; and the monoclinic triple model ($D0_3$) does not provide explanations for the curious remarks.

It has therefore been important to us to filter out what signatures are truly ascribed to the main phase transition at circa 150 K, which appears to be a common event in all samples. A thorough analysis indicate that the main transition event is characterised by three features as listed in Section 2.3 and repeated here: (1) reflections are «smeared» tangential to circles centred at the origin; (2) reflections are split into two or three fragments; (3) new reflections appear between old ones, as if we have a doubling of the cell dimensions. Bearing these remarks in mind, modelling and simulation capabilities were developed in the MaXrd package, aiming to recreate the complex patterns by trying out various arrangements and perturbations of both the host and guest constituents. Although we were unable find some definite arrangement to capture all effects of the perplexing phase, we have arrived at some conclusions.

A recurrence in the structure solutions was a noticeable «flattening» of the atomic displacement parameters to the *ab*-plane, of both the host and guest, likely connected with the distortion of the «honeycombs». Altogether, we regard the TFIC as devoid of hysteresis effects. While we have observed minor differences between equal temperatures around the phase transition, all the samples «settle» back to the same structure without any permanent changes to our knowledge.

In the high-temperature phase, we find it likely that the ferrocene molecules are either isotropically distorted (model A05), or are found in one of four distinct types of domains, which approximate an isotropic model in totality (model E01).

For the low-temperature phase, we have no particular model to recommend as the sole representative of the phase. We rather note that a mosaic model with about 20–30 cells per domain and with a subgrain boundary mismatch with up to 2.5° seems to capture the broadening of reflections quite well (model E03). Our modelling suggests that the emergence of new peaks between the Bragg reflections of the rhombohedral lattice could be explained by a distortion of the hexagonal channels in a way that is described by a triplet of monoclinic cells (model D03), although we are not sure how the domains are situated relative to each other. We have so far been unable to create a model that could reproduce the fragmentation of reflections as recorded.

A question we ask ourself is whether it is more correct to consider the low-temperature structure as a modulation or perturbation of the high-temperature phase, or as a real transition to the monoclinic system where the «honeycombs» are distorted as seen in Figure 5.1c. The unit cells we ended up with in Chapter 3 are the same as found in the literature, both with and without ferrocene as the guest. Again, presumably several types of imperfections may be simultaneously present, yielding an extremely complex superimposed result, as we record in the experimental pattern. The chaos we see in reciprocal space appears irreconcilable with a simple deformation of the «honeycombs». It seems impossible to explain the grand changes occurring at the main phase transition with reorientation of

the ferrocene molecules alone. Their influence on the host framework must undoubtedly be considered. In addition, below the main transition temperature, most of the curious observations made in Chapter 2 (e.g., Figure 2.8; Figure 2.10) are not accounted for. Even if we have not gained a complete and final understanding of the TFIC structure or dynamics, we have been able to note what features we see in common with sample variety, and shed light on the fact that considering the monoclinic cell derived from solving the structure in a typical manner does not simply give a complete correspondence with what the crystal actually looks like at this temperature stage.

6.2 Future work

The future of the MaXrd package

We have demonstrated the usefulness of both the tools ready in the package, as well as how Mathematica enables one to make swift adaptations. While the We have seen how one is able to make depictions of reciprocal space, either by creating the crystal and compute diffractograms, or by considering the geometric arrangement of reflections as dictated by the space group symmetry and structure factors, even superimposing crystal components. This utilities us to invalidate some models, and inspires us to continue pursuing others. Versatility of MaXrd has been presented with the examples and that it is indeed applicable to other systems.

Regarding the modelling capabilities there are always improvements and extensions that can be made. Incorporating other diffraction producing programs or write a procedure in the Wolfram Language would be a leap forward in overcoming challenges arising with disordered models, where unexpected errors in the DIFFUSE program occur. The `ReciprocalSpaceSimulation` function is completely internal to the package. While it is purely geometrical today, it would be possible to develop an internal Fourier- or Monte Carlo procedure to simulate diffraction images completely inside Mathematica.

Owing to the intricate relations of the host and guest, being able to insert the guests in a way that forces repulsion or contraction of the surroundings upon embedding would be advantageous, causing, for example, the local host structure to locally shrink to adapt to the spatial dimensions of a particular guest molecule.

One should also focus on the technical performance and quality enhancements. The crystal plotting function can always be improved, or even «outsourced» to an external and dedicated tool, or we could make use of an internal molecule plotting function in the Wolfram Language. The way crystal data is stored in the current version (in memory) worked well when we only really considered asymmetric units or very small structures, but it is not suited for the newer modelling stage. We could compress the stored data by not saving each individual atom in the structure, and rather store the instructions that

will be used to expand or build the final structure, or we could move `$CrystalData` over to a proper database structure. With the current model construction capabilities, making new «outputting» functions could be useful, such as performing total energy calculations. There are also exciting times for machine learning, which could perhaps be integrated in pattern recognition tasks.

Adding more examples and tutorials is always a good idea—including development guides for how to contribute to the package—could lift up the content in reachable ways for users and possible collaborators. In time we hope to apply MaXrd on other systems, and continue to work and adapt to new challenges.

Further studies on the thiourea–ferrocene inclusion compound

A model with a higher level of conformity with experimental data, especially in the low-temperature phase, remains to be designed. There is much to learn about what mechanisms that make the obverse–reverse twin acquire the different sub-phase schema compared to the non-twin and plesiotwin, and the peculiarities with the «trefoil» patterns and the 5-fold increase along the *c*-axis that is sometimes observed, requires our attention and should be investigated further. More is to be learned about how the domains are «cracking» and restored, and to what extent the changes are local. It would perhaps be intriguing to conduct new studies in various magnetic- and/or pressure studies to learn more about the phase transitions.

Appendix

The following content is found in the appendix:

- A. Oriented crystal associations (page 138)
- B. MaXrd Change log (page 144)
- C. Poster contribution at the 32nd European Crystallographic Meeting (page 154)

A Oriented crystal associations

Twin nomenclature and classification

Crystals may grow together in various ways, oriented arbitrarily or in a specific manner. Common growth directions tend to be parallel or along known grain- or growth-sector boundaries.

A *twin* is a particular subtype of aggregates/intergrowths of multiple single crystals of the same species having well-defined crystallographic orientation relations – rotations, translations, inversions or reflections.^[31] We may refer to the whole crystal as the (twinned, crystalline, heterogeneous) *edifice*; the constituents called *individuals*, (twin) *components*, *domains* or simply *crystals*[†].

The geometrical transformation (symmetry operation) that would bring one component into coincidence with the other, is called the *twin operation* (or action), k . The lattice nodes are said to be *restored* by a twin operation if they are mapped to nodes of other individuals.^[56]

A set of equivalent twin operations makes a *twin law*, which defines the orientation relation between two individuals. The twin law is in practice represented by a 3×3 matrix indicating how the crystallographic axes transform, bridging reflection indices hkl between two individuals in reciprocal space.^[67] The twin law cannot be contained in the symmetry of the crystal; that would make the individuals indistinguishable and unite them into a single crystal.

A single crystal has an *eigensymmetry*, \mathcal{H} , which is given by its point group and independent of its orientation. The various components of a twinned crystal have the same eigensymmetry and are congruent. The twin operation adds to the eigensymmetry, so the edifice possesses a *composite symmetry*, \mathcal{K} , defined as the extension of \mathcal{H} by k via a coset composition.

$$\mathcal{K} = k_1 \times \mathcal{H} \cup k_2 \times \mathcal{H} \cup k_3 \times \mathcal{H} \cup \dots \cup \underbrace{k_i \times \mathcal{H}}_{\text{one coset}} \quad (1)$$

Conversely, if we let \mathcal{H}_i be the oriented point group of component i in a twin, and the intersection symmetry group

$$\mathcal{H}^* = \cap_i \mathcal{H}_i, \quad (2)$$

then the coset decomposition of \mathcal{K} with respect to \mathcal{H}^* gives the possible twin laws; each coset represents a twin law, which further contains the (equivalent) twin operations.^[95]

The number of different orientation or domain states in a twinned crystal defines its *index*,

[†]The term *single crystal* should always refer to an untwinned crystal.

$[i]$ of \mathcal{H} in \mathcal{K} (also commonly written n or m).

$$[i] = \frac{|\mathcal{K}|}{|\mathcal{H}|} \quad (3)$$

Alternatively, the index is equal to the number of twin laws, or to the ratio of the primitive unit cell volumes of the twin lattice (common sublattice[†]) and the crystal structure.^[44] An index of 1 means there is complete restoration of nodes, while no restoration at all would technically be denoted by ∞ . A low degree of lattice nodes restoration is connected with a high twin index, and vice versa. An algorithm for calculating the index given the twin lattices is given in section «1.3.2. Twin lattices» in the International Tables, volume C.^[44]

Morphology

Simple twins have only one twin law, i.e. there's only two orientation states. Aggregates with three or more are called *repeated* or *multiple twins*.^[31]

Twins have a minimal geometric requirement: there must be at least one common lattice row and one pair of parallel lattice planes, and the crystals should be at least 10 nm to 100 nm in size (informal requirement).^[31] If domains are smaller than that, one would characterise it as disorder instead.

From the first geometric requirement it follows that a set of lattice points are shared between two individuals in a twin, defining a (physical) *boundary* or *twin interface*[‡]. If all twin interfaces are parallel, it is called a *polysynthetic twin*, otherwise a *cyclic twin*.^[44] See also the entry `_twin_morphology` in the Twinning CIF dictionary.^[1]

With every twin operation there is also attached a geometric lattice element (plane, axis or point), defining a *twin element*.^[94] Twin elements are always direct-lattice elements (*Mallard's law*).^[26,57]

In real twins, it may be that an individual is only quasi-perpendicular to a mirror plane. The angular discrepancy defines the *obliquity* ω . A twin lattice quasi-symmetry (TLQS) may also occur with $\omega = 0$, producing instead a small linear deviation called *twin misfit* δ , if the twin operation is a rotation of order higher than 2. Nespolo and Ferraris define it to be

$$\delta = \langle \Delta u \quad \Delta v \quad \Delta w | \mathbf{G} | \Delta u \quad \Delta v \quad \Delta w \rangle^{1/2} \quad (4)$$

where Δu , Δv and Δw are coordinate differences between two quasi-restored nodes that are along the two shortest directions in the twin lattice, and \mathbf{G} the metric.^[57]

[†]Yet another way to view the index: the number of lattice nodes of an individual divided by the number of restored nodes (exactly or approximately).^[50] The index gives an indication of how frequently the individual lattices «meet».

[‡]The interface is sometimes called *composition plane/surface* or *domain boundary/interface*.

Some authors prefer to merge these two quantities into one, making the twin misfit a parallel component of the obliquity.^[50] Obliquities larger than 6° are rare, and so are twin indices larger than 5 or 6.^[54,56]

Formation mechanism

Transformation twins resulting from phase transitions usually have numerous, small twin domains.^[44] A reduction in symmetry may be associated with an alteration to a domain structure. The crystal then consists of variants that have a fixed relation to the high-symmetry phase, but differ from each other, analogous to the different orientations of a twin.^[101]

See also the entry `_twin_formation_mechanism` in the Twinning CIF dictionary.^[1]

Classification

From the «French school» there are four main categories of twinning, described shortly here, and with an overview given in Table 1. See also the entry `_twin_individual_twin_lattice_type` in the Twinning CIF dictionary.^[1]

A *twin by merohedry* is a class of twins where the twin operation belongs to a higher point group of its crystal system, and not the point group of the crystal itself.^[78] This results in lattices (and reflections) that overlap exactly, and a twin of index 1.^[44] Twinning by merohedry is possible when the point group is a subgroup of the Laue group.^[53]

There are two subtypes or classes: (I) The twin operation belongs to the Laue symmetry.^[11] (II) The twin law happens to be the symmetry operator that differs between two Laue groups of the same system, making the crystal appear to be the higher one.^[78] The twin operation belongs to the lattice, but not the Laue symmetry of the crystal.^[11] In the first class the Laue symmetry of the crystal matches the lattice symmetry; in the second it is lower. A consequence is that twin-related reflections have equal intensities in class I, but differ in class II.^[11]

It is also possible that the twin law belongs to another crystal system of higher symmetry; then called twinning by *pseudo-merohedry*. The keyword «pseudo» signals that the cell metric happens to *appear* more symmetric, as reflections are quasi-restored. A common example is monoclinic cells with $\beta \approx 90^\circ$ becoming pseudo-orthorhombic, or an orthorhombic lattice with $a \approx b$ being pseudo-tetragonal.

If parts of the reflections overlap exactly, and others do not, we have twinning by *reticular merohedry*. Systematic absences in one domain may overlap with reflections from another domain[†].^[78] The twin operation is not a symmetry operation of the lattice symmetry, but makes a common twin lattice which overlaps only partially. One can divide between

[†]One of our three TFIC samples were found to be a twin of this kind. See Subsection 2.2.1.

single reflections and *coincident (superimposed) reflections*, depending on whether the twin operation will transform the set of indices to fractions or integers, respectively.^[41]

Finally, it may be that the twin law belongs neither to the crystal class nor to the metric symmetry of the lattice. This *non-merohedric twinning* (or *reticular pseudo-merohedry*) leads to non-overlapping reciprocal lattices, although some reflections may be exactly or partially superimposed.^[86]

Category	Twin operation belongs to		Reflection overlap	Index and obliquity	
	Crystal system	Metric symmetry		n	ω
Merohedry	✓	subgroup	exact overlap	$n = 1$	$\omega = 0$
Pseudo-merohedry	✗ (higher)	subgroup	almost overlap	$n = 1$	$\omega > 0$
Reticular merohedry	✗	✗	not all overlap, but always exact	$n > 1$	$\omega = 0$
Non-merohedry	✗	✗	all possibilities (distinct, partial or exact overlap)	$n > 1$	$\omega > 0$

Table 1: The four classifications of crystal twinning by Georges Friedel.^[58] «Metric symmetry» is also called «lattice symmetry».

Obverse–reverse twinning

There are few known cases of twinning by exact reticular merohedry, and so-called $\Sigma 3$ *obverse–reverse twinning* of rhombohedral and cubic crystals is one of them. These may occur in any rhombohedral crystal, independent of c/a ratio or α angle. There are four different twin laws, although these coalesce into one for point group $\bar{3}2/m$. The simplest to envision, and normally considered, is a twofold rotation parallel to the threefold symmetry axis.[†]

As the name suggests, the twin is composed of differently oriented rhombohedrons, labelled *obverse* and *reverse* in the hexagonal setting, related by the twin operation described in the previous paragraph. Reflection conditions are:

$$-h + k + l = 3N \quad (\text{obverse}) \quad (\text{A.obv})$$

$$h - k + l = 3M \quad (\text{reverse}) \quad (\text{A.rev})$$

for some integers N and M . In all reciprocal layers with $l = 3N$, no single reflections occur.^[41]

Practical consequences

In practice, twinning imposes a complication on the resulting diffraction pattern (and subsequently the structure solution) since contributions from the various domains will be superpositioned in the collected data, revealing the composite symmetry (\mathcal{K}) if volume fractions of all domain states are more or less equal.^[31]

[†]In a rhombohedral setting: around $[111]$ instead of $[001]$ (hexagonal setting).

Owing to the point group nature of twinning, intensities from the different components are simply a weighted sum, and not the structure factors as in the case of disorder.^[78] The distribution of diffracted intensity is directly linked to the volume ratio of the various individuals.

Splitting of the X-ray diffraction spots is an indication of twinning (by the pseudo categories; obliquity^[55]), and more than one orientation matrix is needed to index crystals twinned by non-merohedry.^[44,86]

Non-merohedral twins are the easiest kind to discover by examining the diffraction pattern, but may be challenging to process.

Non-twin definitions

There are classifications that resemble twinning, but deviate slightly from the definition at the start of this appendix. The terms examined in the following are nevertheless linked to the same topic.

In the context of materials science, *polymorphism* refers to the fact that compounds may exist in different crystal structures; *polymorphs*. It is analogous to *allotropy*, but generalises to compounds instead of just a single kind of chemical element.

Polytypes are linear structures where the polymorphs differ in the stacking sequence of layers, and is thus considered a type of polymorphism.^[50] Slight compositional deviations between layers in different polytypes may be permitted,^[21] as well as rotations.^[53]

Coincidence site lattices

If we consider two crystal individuals of a twin and lift the restriction of crystallographic rotation angles, i.e. let rotations about the composition plane be free, there may still exist certain orientations where a subset of reflections are restored – this is a *coincidence site lattice* (CSL). See Figure 2.17 for relevant examples. Technically, twinning by reticular merohedry produce CSLs.^[41] From lattices interfering in this way, Moiré patterns emerge. Physically, the CSLs correspond to special grain orientations.^[25]

Same as for twins, a *coincidence index*, Σ or Ξ , is defined for the superimposed lattice. This is also the ratio of unit cell volumes of the CSL to the underlying lattice. The coincidence index will always be an odd number.^[25] Additionally, a boundary plane of the CSL will have a certain *planar coincidence site density*, Γ , per unit area. A high value of Γ means there are more atoms sharing sites, smaller boundary period, and lower strain field energy. In CSLs, the atomic structure of grain boundaries are relaxed by a shear displacement in a way^[8]

A CSL can itself be displaced in a way that preserve the coincidence. Such displacement vectors make a new lattice, the so-called *displacement shift complete* lattice (DSC). The DSC lattice is reciprocal to CSL, and the coarsest sublattice of the CSL that in-

cludes all atoms somewhere on its lattice. These translation vectors are also the possible Burgers vectors for grain boundary dislocations.^[25]

Miscellaneous terms

Related to polytypes are *allotwins*, which are polytypes of same chemistry with similar but slightly different structures.^[31] The twin operation relating the crystal components may be from the point group of one or both crystals, which is not possible for twins. Allotwin structures are built with a common mesh for the layers, allowing polytypes with different space groups to be grown on top. *Allotwin indices* are defined as the ratio of lattice nodes in one component to the total number of common lattice nodes in the edifice.^[53]

Another phenomenon not quite adhering to the twin definition is the *plesiotwin*, which is when individuals are rotated by a non-crystallographic amount. These are characterised by a low degree of lattice restoration, owing to a large CSL. Nespolo et al.^[54] state three criteria in their definition of plesiotwinning:

1. Usually larger coincidence index than for twins, i.e. $\Sigma \geq 5$.
2. Twin operation is of the common lattice, not the crystal.
3. Twin individuals are rotated by a non-crystallographic amount about the composition plane.

Plesiotwinning happens on a more macroscopic level compared to regular twinning. These form when crystals interact, rotating relative to another and reaching a local energy minimum,^[56] and coherently oriented.^[54]

Retaining an orientational relation in consecutive layers of two crystals of different species is called *epitaxial-* or *epitactic growth (epitaxy)*,^[4] or *oriented overgrowth*.^[53] *Syntaxy* is the three-dimensional equivalent of epitaxy, also called *oriented intergrowth*.^[4] *Topotaxy* is when a parent phase regulates the orientation of a three-dimensional precipitation following a solid-state transformation or chemical reaction.^[4]

B MaXrd Change log

Below is the latest change log file of the project.

MaXrd: Mathematica X-ray diffraction package – change log

Version 2.5.0

New content

- Reintroduced `ReciprocalImageCheck` and `FindPixelClusters`; now more efficiently integrated with MaXrd and more general purposed.
- Created a `GetAtomCoordinates` function which works with crystal labels and crystal plots.
- Changed the name of `EquivalentIsotropicADP` to `TransformAtomicDisplacementParameters` and added a method for transforming atomic displacement parameters given a transformation matrix P .
- Added "AugmentedMatrix" option to `GetSymmetryOperations`; `StructureFactor`, `SystematicAbsentQ` and `ToStandardSetting` updated to comply with changes.
- Added Boolean option "IgnoreTranslations" to `GetSymmetryOperations` in order to simplify use with `SymmetryEquivalentReflections`.
- Added the Boolean option "Radians" to `GetLatticeParameters`.
- Added the Boolean option "Bonds" to `CrystalPlot` along with configuration option "BondRadius".
- Added the option "AtomRadius" to `CrystalPlot` that can be used to set a fixed radius for all atoms. This takes precedence over "AtomRadiusType", but is ignored when it is set to a non-positive number.
- Created `InputCheck["GetAtomData", _]` for querying atom data of crystals.
- Added possibility to plot ellipsoids in `CrystalPlot` using stored ADPs.

Improvements and fixes

- Misspelling of `SchoenfliesSymbol` in `$SpaceGroup[[71]]` (thanks to `ungerade`).
- Fixed a formatting bug on the `SynthesiseStructure` documentation page.
- When using the signature of `SynthesiseStructure` expecting `domain` input, the `map` now recognises more general replacement commands (e.g. `_Integer` \rightarrow "SomeEntity").
- Merged `GetLatticeParameters` with `GetCrystalMetric`, and refactored the latter.
- Refactored `InputCheck["GetCentringVectors", _]` to also accept crystal entries and space group

representations.

- Refactored `SymmetryEquivalentPositions` and `SymmetryEquivalentReflections` to use augmented matrix representations of symmetry operations.
- Altered `InputCheck["GetCrystalSpaceGroup", _]` to accept space group entires and return them.
- Updated `InputCheck["CrystalQ", _]` to also check for temporary crystal data. It now returns the crystal data as well.

Miscellaneous

- Minimised large documentation files by clearing large output cells.
- Removed `SynthesiseStructure::DomainPatternMismatch` error check; input blocks/supercells now replace a single domain cell, regardless of block size.
- Wavelength values assume angstrom by default in the functions `AttenuationCoefficient`, `BraggAngle`, `DarwinWidth`, `ExtinctionLength`, `GetAtomicScatteringFactors`, `GetScatteringCrossSections`, `ImportCrystalData`, `ReciprocalSpaceSimulation`, `ReflectionList`, `StructureFactor` and `StructureFactorTable`; this is now made clear in the documentation pages (thanks to `Sterling Baird` (sgbaird)).
- Changed the way essential data are initialised.

Version 2.4.0

Improvements to `SynthesiseStructure`

- Creating single element (or void) unit cells now possible with `SynthesiseStructure[<chemical symbol>, _, _]`.
- Added "Shuffled" as a possible setting to the "SelectionMethod" option in `SynthesiseStructure`.
- Added Boolean option "Padding" to `SynthesiseStructure` which utilises the `InputCheck["PadDomain", _, _]` snippet.
- Refactored `SynthesiseStructure`; when inputting a list of entities, an appropriate domain representation will be created and relayed to the function expecting a domain signature.
- "UsePlacementBuffer" option of `SynthesiseStructure` deprecated; "Padding" will now be used instead.
- If a domain is not covered in the mapping from in-

tegers to entities in `SynthesiseStructure`, empty cells will now be used instead of throwing an error.

Improvements to `EmbedStructure`

- Enabled the possibility to embed in void (message `EmbedStructure::VoidHost` removed).

Improvements to space group database

- Removed entries such as `HermannMauguinFullAlt` in space groups with multiple origins.
- For rhombohedral space groups, the note specifying obverse setting was moved to the alternative settings section.
- Regenerated `$GroupSymbolRedirect`.
- Minor error corrections.

New `InputCheck` snippets

- Added snippet `InputCheck["GenerateTargetPositions", _]` (currently used in `ConstructDomains`, `DomainPlot`, `EmbedStructure`, `ExpandCrystal` and `SynthesiseStructure`).
- Added snippet `InputCheck["PadDomain", _, _]`.
- Added snippets `InputCheck["ShallowDisplayCrystal", _]` (employed in: `ImportCrystalData`, `UnitCellTransformation`).
- Added snippets `InputCheck["FilterSpecialLabels", _]` and `InputCheck["HandleSpecialLabels", _]` for processing chemical element symbols and "Void".
- Added snippet `InputCheck["CrystalEntityQ", _]`.

Miscellaneous

- Added the option `ImageDimensions` to `SimulateDiffractionPattern` for specifying the width and height of the produced image (`ExportCrystalData` and `InputCheck["GetReciprocalImageOrientation", _]` also updated to comply with this change).
- Appended a missing `_alt` to the CIF definition `_space_group_name_H-M` in the list of space group search keys in `ImportCrystalData`.
- Fixed errors in the `$GroupSymbolRedirect` data file (thanks to Tobias Hadamek for finding this).
- `ImportCrystalData` now takes away tildes (-) if they are present in the chemical formulas.
- Fixed a bug where `GetScatteringCrossSections` would not work on Windows due to different line break implementations (thanks to Tobias Hadamek for discovering this).
- An error is now given when attempting to use a

chemical symbol or "Void" for the name a crystal to be imported from a `cif` file through `ImportCrystalData`.

- `CrystalPlot` will now plot empty structures without errors.
- Demo file `DemoBlocksAB.m` removed (these structures will now be generated on demand).
- Updated code part B.2 in `InputCheck["InterpretSpaceGroup", _]` to find origin choice automatically.

Version 2.3.0

New content

- Option `"ShowProgress"` added to `ConstructDomain`.
- Option `"AtomRadiusType"` added to `CrystalPlot`.
- Added the possibility to filter "Host" or "Guest" atoms only with the `"OpacityMap"` option of `CrystalPlot`.
- Added another example to the `"SectorRegions"` in `ConstructDomains`.
- Added a modulation example to the `DistortStructure` documentation.
- Added the possibility for `ConstructDomains` to store and return the a complete collection of the states in every cycle, and `DomainPlot` to present such a series.

Improvements and fixes

- Fixed broken hyperlinks in the *See Also* section in the documentation of `ExpandCrystal` and `CrystalPlot`.
- Fixed a bug where `ConstructDomains` would finish each iteration after only three cell visits.
- Set a default Windows path for `DIFFUSE` in `SimulateDiffractionPackage`.
- Altered `SimulateDiffractionPattern` to use `discus` through `discus_suite`.
- Fixed a bug in `SimulateDiffractionPattern["DISCUS", _, _]` where the structure size would not be correctly assessed.
- Fixed a bug where `"UnitCellAtomsCount"` would not be correctly updated when using `SynthesiseStructure`.
- Default plot options for `CrystalPlot` in cases of trigonal or hexagonal systems have changed `ViewPoint` to `{0, 0, Infinity}` and `ViewAngle` to `90°` for more intuitive visual representations.
- The use of `EmbedStructure` with guest and host parameters will now store a `"Component"` key in the atom data.
- Default/suggested paths for Linux added to the

- "ProgramPaths" option of `SimulateDiffractionPattern`.
- Fixed a bug in `SimulateDiffractionPattern["DISCUS", _, _]` where the procedure would not halt despite missing the *DISCUS* program.
- Fixed a bug with too long assembly list in `SynthesiseStructure`.
- `ConstructDomains` now exits early if a single domain reaches complete domination.
- Fixed an issue where `InputCheck["ProcessWavelength", _, _]` would not work as expected in combination with `BraggAngle`.
- `CrystalPlot` now exits more gracefully if the atom data list is empty.
- `AtomicMass` was renamed to `StandardAtomicWeight` in `$PeriodicTable` and affected functions updated to comply with this change.
- Minor documentation updates.

Version 2.2.0

- Added the Boolean option "IgnoreSymmetry" to `ExpandCrystal`.
- Fixed a bug in `SynthesiseStructure` that would occur if the input units did not have a *Notes* key.
- Improved assembly performance of `SynthesiseStructure`.
- Fixed bug encountered when using `SynthesiseStructure` with blocks not having size `ixxx`.
- Swapped sections `iC` and `iD` in the internal code for `UnitCellTransformation` to avoid an error for crystals missing notes.
- Added the Boolean option "ReturnData" to `SimulateDiffractionPattern`.
- Fixed a bug in "RelatedFunctionsGraph".
- Added twin example to the documentation pages of `ReciprocalSpaceSimulation`.
- Added coordinate transformation example to the documentation pages of `GetCrystalMetric`.
- `docbuild.xml` file updated to work with both macOS and Windows.
- Updated references (`./Misc/References.bib`)
- `README.md` file updated with a *Functionality* section.
- Minor documentation updates.

Version 2.1.1

- Added more examples to the `SimulateDiffractionPattern` documentation page.
- When specifying a probability distribution of entities with `EmbedStructure`, the procedure now more closely fulfils that distribution instead of us-

- ing `RandomChoice`.
- Updated `ImportCrystalData` to use the data file in the `UserData` directory by default (changed the "DataFile" option).
- Added "DataFile" option to `EmbedStructure` and `ExpandCrystal`.
- Factorised data file operations for `ImportCrystalData`, `EmbedStructure` and `ExpandCrystal` into a `InputCheck` snippet with label "Update\$CrystalDataFile".
- Minor updates in the documentation (`SimulateDiffractionPattern`, `EmbedStructure`) and in the package unit test.

Version 2.1.0

New content

- Added the option "IncludeStructureSizeInfo" to `ExportCrystalData`.
- Added the option "ScalingFactor" to `SimulateDiffractionPattern`.

Improvements and fixes

- Fixed a bug in `SimulateDiffractionPattern` where the use of *DISCUS* would not work correctly.
- Created a `UserData` directory in the package root and moved `CrystalData.m` here. `$CrystalData` and `ResetCrystalData` updated to conform with this change.
- `ImportCrystalData` now returns instead of aborting if user cancels import.
- Improved the package unit test.
- `$MaxXrdPath` updated with support for *Windows*.
- Minor documentation updates.

Version 2.0.0

Changes

- `InputCheck["DomainRotation"]` has been replaced with `InputCheck["RotationTransformation"]`, which is more versatile (now used in `DomainPlot`, `EmbedStructure` and `SynthesiseStructure`) and uses different rotation options ("RotationAnchorReference", "RotationAnchorShift", "RotationAxes").
- Angular input parameters in `BraggAngle`, `DomainPlot`, `EmbedStructure`, `ReflectionList` and `SynthesiseStructure` are now expected to be in radians. This seems to be more universally adopted and makes it clearer when input is in degrees.
- "DISCUSPlot" changed name to `SimulateDiffractionPattern`, as both "DISCUS" and

"DIFFUSE" can now be used to generate simulations.

- Edited `init.m` to print message in case of insufficient *Mathematica* version.
- `InputCheck` declarations reorganised so snippet labels are always the first parameter (affected: `"CrystalQ"`, `"GetCentringVectors"`, `"GetCrystalFormulaUnits"`, `"GetCrystalSpaceGroup"`, `"GetCrystalWavelength"`, `"GetEnergyWavelength"`, `"GetPointSpaceGroupCrystal"`, `"InterpretElement"`, `"InterpretSpaceGroup"`, `"PointGroupQ"`, `"PointSpaceGroupQ"`, `"Polarisation"`).

New content

- Added functionality to `ConstructDomains` that simplifies creation of sector domains/regions.
- `SynthesiseStructure` now has a designated routine for domains.
- `"OpacityMap"` option added to `CrystalPlot`.
- Created the tutorial *Using the rotation options* aimed at the usage of `DomainPlot`, `EmbedStructure` and `SynthesiseStructure`.
- `ExportCrystalData` now supports a new format: `"DIFFUSE"`.
- Implemented `"DIFFUSE"` as an alternative method of producing simulated diffraction patterns (through Darren Goossens' *ZMC* program).
- New snippet `"GetReciprocalImageOrientation"` added to `InputCheck`.
- Created the function `ResetCrystalData`.

Miscellaneous

- `DistortStructure` now checks the dimensions of input.
- Fixed a bug where `GetCrystalMetric` had problems with lattice parameters expressed as quantities.
- Interstitial defect example added to `DistortStructure`.
- Minor documentation updates.
- Corrected misspelling of *AsymmetricUnitCellCount* in `ExpandCrystal`.
- Option `"Flag"` in `ExportCrystalData` changed to `"Detailed"` (now a Boolean type).
- `EmbedStructure` now calculates the (mean) number of atoms per unit cell for the new structure.
- Fixed a bug in `GetSymmetryData` where the label `"Setting"` would not work as expected.
- Renamed error message `GetElements::formula` to `GetElements::InvalidFormula` and `::invalid` to `::InvalidElement`.
- Error messages of `InputCheck` updated.

- A unit test for the package has been written.
- Reorganised internal layout of the package.
- Documentation pages updated.

Version 1.8.0

New content

- Created the function `ConstructDomains`.
- Created the function `DomainPlot`.
- `InputCheck` updated with a `"DomainRotation"` and a `"GetCrystalFamilyMetric"` label.

Improvements to `EmbedStructure`

- If conditional placement is used with `EmbedStructure` and a given coordinate tuple falls through without any match, nothing is inserted here (used to insert last entry in `guestUnits`).
- Fixed a bug with `EmbedStructure` where using `"Rotations"` did not assume numbers in degrees.
- Message is no longer given if conditions or random selections are such that nothing is embedded (`EmbedStructure::OnlyVoid`).
- A host structure is now considered to be placed in positive coordinates as long as no coordinates are below `-1.0` in any direction.
- `EmbedStructure` now updates the `"StructureSize"` of the resulting structure.

Miscellaneous

- `SynthesiseStructure` now also supports the `"RotationMap"` and `"RotationPoint"` options akin to `DomainPlot`. Documentation page updated.
- Second argument of `ExpandCrystal` changed to `structureSize_List: {1, 1, 1}`.
- `ExportCrystalData`: Change third argument `format_String` to `format_String: "DISCUS"` (default value).

Version 1.7.0

New content

- Created the function `SynthesiseStructure`.
- Added the snippet `"Update$CrystalDataAutoCompletion"` to `InputCheck` and factorised functions that update `$CrystalData` to use this (`DistortStructure`, `EmbedStructure`, `ExpandCrystal` and `ImportCrystalData`).

Improvements to `EmbedStructure`

- Option `"ShowProgress"` added to `EmbedStructure`.

- `EmbedStructure` is now capable of dealing with overlapping atoms (new options: `"OverlapPrecedence"` and `"OverlapRadius"`).
- `EmbedStructure` parameter identifiers *source* and *target* were renamed to *guest* and *host*, respectively, to avoid confusion.
- `EmbedStructure` now mutates the *hostCrystal* by default (and uses a new option `"NewLabel"` to create new crystal objects) to be more aligned with the usage of similar functions.

Miscellaneous

- `$MaXrdChangelog` updated to handle headings/subsections in this changelog.
- `$MaXrdPath` updated to prioritise the standard location of packages in *Mathematica* (`.../Mathematica/Applications/`), as it can find the developing directory as well.
- Minor documentation updates.

Version 1.6.0

- `DISCUSPlot` now prints error messages from *DISCUS* if there are any (new option: `DISCUSPrint`).
- Improved structure size recognition for `DISCUSPlot`.
- `EmbedStructure` now recognises symbols of the chemical elements; single atoms of the given type will be used.
- Entries (keys) in `$CrystalData` are now sorted alphabetically after using `EmbedStructure` and `ExpandCrystal`.
- Fixed a bug where `ImportCrystalData` would not save manually created crystal entries.
- `ExportCrystalData` updated to use ADP value of zero if no such data is available.
- Created the function `DistortStructure`.
- Minor documentation updates.

Version 1.5.2

- Removed duplicate entries in the *Mathematica code* sections in the documentation pages.
- Added information on `UnitCellTransformation` option `"CustomP"` in the documentation.
- `DISCUSPlot` now recognises `"Void"` to be used as a vacancy/absence of embedding.
- `MillerNotationToString` now supports string input and supports negative indices written both as negative characters (`Times[-1, "a"]`) and strings where the character is preceded by a dash (`"-a"`).
- Minor documentation updates.

Version 1.5.1

- `DISCUSPlot` now works on *Windows* and checks whether *DISCUS* is installed.
- Minor documentation updates.

Version 1.5.0

- Created the function `DISCUSPlot` which executes diffraction simulation in *DISCUS* automatically and plots the result.
- Fixed `GetCrystalMetric` so that the `"Space"` and `"ToCartesian"` options work when input is a list of lattice parameters.
- Updated `InterplanarSpacing` to use the `"Space"` option of `GetCrystalMetric`.
- Fixed a bug in `MillerNotationToList`. Numerical entries are now outputted as integers instead of strings.
- Fixed a bug where settings of `"Rotations"` in `EmbedStructure` would not work as expected.
- Very small numbers are no longer written in scientific notation in `ExportCrystalData`.
- Any ion charges are not carried through in the output of `ExportCrystalData`.
- Updated `RelatedFunctionsGraph` to comply with new option names in *Mathematica* version 12.
- Minor documentation updates.

Version 1.4.0

- Renamed the options `"RandomDistortions"` and `"RandomRotations"` to `"Distortions"` and `"Rotations"`, respectively, in `EmbedStructure` and made them more general by enabling the choice between set values or ranges.
- Added the option `"DistortionType"` which enables the function to interpret the given distortions either as ångströms in a `"Cartesian"` system or as fractions of the host unit cell in a `"Crystallographic"` setting.
- Added the option `"RotationOrder"` which lets the user specify the order of axes to rotate.

Version 1.3.0

- Updated the example under *Scope* in the `UnitCellTransformation` documentation page to make use of `CrystalPlot`.
- Added `EmbedStructure` to the list in `AutoComplete.nb`.
- Added the option `"Space"` to `GetCrystalMetric` so lattice parameters can be used from either direct or reciprocal space.
- Fixed a bug in `ExportCrystalData[_, _, "DISCUS"]` where the structure size would not be

included in the output file.

- Added the possibility to use `EmbedStructure` with list of conditions that dictate where to place embeddings.
- Updated `ExportCrystalData` with the option "Flag" which can be set to "Simple" (default) or "Detailed".
- Added the Boolean option "ExpandIntoNegative" for `ExpandCrystal` which centres the origin at the middle of the new structure. Updated `EmbedStructure` to detect this change.
- Added the option "TrimBoundary" to `EmbedStructure` enabling a "trimming" of the structure after embedding.
- Created the option "RandomDistortions" for `EmbedCrystal` which can perform a random shift/distortion of units upon embedding.
- Removed `DeleteCrystalData`. Using `KeyDropFrom[$CrystalData, <label_to_delete>]` gives the same result.
- Created the option "RandomRotations" for `EmbedCrystal` analogous to "RandomDistortions".
- Minor documentation updates.
- Changed all `Modules` with `Block` in the definitions for better performance.

Version 1.2.0

- Replaced `Part` brackets with `\[LeftDoubleBracket]` and `\[RightDoubleBracket]` in definition code for better readability.
- Prepend `Global`` to the lattice parameter symbols in `TransformationMatrices.m` to avoid *Mathematica* treating these as `Global`Private``.
- Added an example (with ferrocene) to the `$TransformationMatrices` documentation page.
- Added the option "Space" to `GetLatticeParameters` so lattice parameters can be obtained for both direct and reciprocal space.
- Fixed the `SyntaxInformation` for `SymmetryEquivalentPositions`.
- Minor documentation updates.
- Added the option "ToCartesian" to `GetCrystalMetric` that utilises the appropriate transformation matrix automatically.
- Functions that have options now simply have `OptionsPattern[]` instead of `OptionsPattern@<function_name>` in the definitions.
- Changed the space group of `CalciumFluoride` in `$CrystalData` from `Fd-3m (# 227)` to `Fm-3m (# 225)`.
- Created the function `EquivalentIsotropicADP`.
- Created the function `CrystalPlot`.
- Created the function `ExportCrystalData`.
- Created the function `ExpandCrystal`.

- Created the function `EmbedStructure`.
- Updated `InputCheck[_, "GetPointSpaceGroup-Crystal"]` to handle crystal instances in a temporary `$CrystalData` construct.
- Updated `PacletInfo.m`.
- Removed `Installation.nb` and updated installation instructions in `README.md`.

Version 1.1.0

- `SyntaxInformation` added for relevant functions.
- Minor changes to the guide page (main documentation page) and title of this change log.
- Updated documentation page for `SymmetryEquivalentReflections` (function can be called with one argument).
- Corrected option table for `StructureFactor`.

Version 1.0.2

- Fixed a bug where `ReflectionList` and `ReciprocalSpaceSimulation` would not work with crystals that stored wavelength as a `Quantity`.
- Minor updates and changes in the documentation (thanks to Bianca Eifert for pointing out some of them).
- Added some missing auto-complete suggestions for `$CrystalData` (for the second argument).
- Added the option `AngleThreshold` to `BraggAngle` and `ReflectionList` for more efficient filtering by Bragg angle.

Version 1.0.1

- `Changelog.txt` changed extension to `Changelog.md`.
- Updated `$MaXrdChangelog`.
- The `MaXrd/Kernel/init.m` file was edited to allow for a more general package placement and correct auto-complete version requirement (thanks to Szabolcs Horvát).
- Minor revisions in the `README.md` file.
- Corrected version requirement from `10.0+` to `10.3+`.
- Changed the definition of `$MaXrdPath` to comply with a more general package placement.
- Fixed some hyperlink bugs in the main tutorial page.
- Corrected spelling errors in the documentation.
- Corrected a bug where `MillerNotationToString` did not work as expected with negative indices.

Version 1.0.0

- Package renamed from `Xray` to `MaXrd!`

- Renamed `$XrayFunctions` to `$MaxrdFunctions`, `$XrayChangelog` to `$MaxrdChangelog`, `$XrayPath` to `$MaxrdPath`, `$XrayRedirect` to `$GroupSymbolRedirect` and `$XrayVersion` to `$MaxrdVersion`.
- `GetAtomicScatteringFactor` and `GetScatteringCrossSection` renamed to `GetAtomicScatteringFactors` and `GetScatteringCrossSections`, respectively.

Version 0.9

- Refactored some code in `ImportCrystalData`; updated documentation.
- `GetAtomicScatteringFactor` restructured so to better handle crystal label with reflections input and element(s) with `sinlam` input.
- `InputCheck` procedures with `ProcessWavelength`, `GetCrystalWavelength` and `GetEnergyWavelength` were updated to let `-r` pass through without aborting evaluation.
- `ImportCrystalData` returns a message (but does not abort) if *neutron* radiation type is detected in `.cif` file.
- `InputCheck` with label `InterpretElement` now replaces *D* (deuterium) with *H*.
- Added the Hall symbol `-B 2ydav` to the space group `B 21/d`.
- Adding crystal data manually in dialog windows is now possible with `ImportCrystalData`.
- Completed tutorials.
- Added the option `IgnoreHydrogen` to `CrystalFormulaUnits`.
- `$XrayChangelog` file is now formatted in Markdown language.
- `ImportCrystalData` now also counts the number of `atomsitefract_` to verify subdata length.
- Detailed information on how `fo` and `fi2` data files were restructured for this package is now available in the tutorial page *Applying crystal data*.
- `GetAtomicScatteringFactor` now checks for source specific `sin(theta)/lambda` limits.

Version 0.8

- Merged the separate package-sections into one notebook, and made a `Core` directory for the core elements of the package. The folder `ExampleFiles` could in theory be deleted without affecting the package.
- `$XrayPath` created, which is a path to the main directory of the package. All other paths should be set relative to this.
- Removed `$XrayExamples`. Easy enough to use `$XrayPath`.

- Miscellaneous updates of the documentation.
- Updated `$PointGroups`: The association is now using non-formatted keys, some keys have been adjusted and more symbol variations have been added. Schoenflies symbols and class names information has also been added.
- Miscellaneous updates to `$SpaceGroups`.
- The `XrayChangelog` function was updated. The log is now presented in a new window/notebook.
- Created `ExportCrystalData`.
- Renamed `AddCompoundToDataset` and `RemoveCompoundFromDataset` to `ImportCrystalData` and `DeleteCrystalData`, respectively.
- Updated the default data in `$CrystalData`.
- Added the option "Threshold" to `StructureFactor`.
- Added the option "IgnoreSystematicAbsence" to `StructureFactor`.
- Updated `ReflectionList` to use Tuples. Table will be used if "HoldIndex" option is applied.
- `ScatteringFactor` and `StructureFactor` are now effectively Listable in regards to reflections.
- Added subgroup data to `$PointGroups`.
- Fixed a bug in `SymmetryEquivalentPositions` where the non-centring sub-routine was not working properly.
- Renamed `ScatteringFactor` to `AtomicScatteringFactor`.
- Deleted `$ScatteringFactors`; its functionality has been incorporated with `AtomicScatteringFactor`.
- Fixed a bug in `SymmetryEquivalentPositions` where too many equivalent positions were generated when not taking centring into account.
- Fixed a bug in `StructureFactor`; the multiplicity reduction was incorrect.
- Length- and energy quantities may now be input in `StructureFactor`.
- `$PhysicalConstants` discontinued.
- Created `CromerLieberman.m` from all the anomalous correction dat-files. This is now the default source for calculating corrections to the scattering factor in `AtomScatteringFactor`.
- Information on Wyckoff position and site symmetry has been implemented in `$SpaceGroups`.
- Added `InternationalTablesC(3rd)` as a source for coefficients used for calculating the atomic scattering factor.
- Expanded `WaasmaierKirfel.m` with ions.
- Added tabulated data for calculating atomic scattering factors from the `DABAX` directory found at <http://ftp.esrf.eu/scisoft/DabaxFiles/>.
- `AtomicScatteringFactor` now extracts elements from the atom data and not the chemical formula, and elements from the periodic table may be input

- directly.
- Auto-complete is now updated for `ImportCrystalData` and `DeleteCrystalData` after each successful execution.
 - Added more unconventional space group settings for the monoclinic, tetragonal and trigonal crystal systems.
 - Added scattering cross section data from *xraylib*, which is applied in `AttenuationCoefficient`.
 - Added anomalous scattering factors (correction terms) from *xraylib*.
 - Added the option `RationaliseThreshold` → 0.001 in `SymmetryEquivalentPositions`.
 - Updated local variables in `StructureFactor` to coincide with notation used in coreCIF.
 - `ImportCrystalData` can now store both `SiteSymmetryOrder` and `SiteSymmetryMultiplicity`.
 - Better handling of chemical formulas in `ImportCrystalData`.
 - Added sub routines to `InputCheck` for retrieving formula units stored in `$CrystalData` and converting energy or wavelength input to angstroms.
 - Separated the "development code" from the *Definitions.nb* notebook.
 - Changed name of `ExtinctionDistance` to `ExtinctionLength`.
 - Separated out the geometrical factor of the normal procedure for `ExtinctionLength` and `DarwinWidth` (the experimental angles can also be put in).
 - Removed `AlignUB`, `ErrorPropagation`, `ExportReflectionFile`, `ImgScript`, `ImportReflectionFile`, `IntensityTable`, `MergeLogs`, `MonitorIni`, `LeastSquaresFit`, `PeakTableInspection`, `RefinedValues`, `RoundSignificants`, `UnwarpLayerList` and `WeightedMean` from the package (not considered core functions to X-ray or diffraction topics).
 - `ExtinctionLength` and `DarwinWidth` are now practically listable in terms of reflections.
 - All data sources used in `AtomicScatteringFactor` have been truncated at $\lambda = 2.5$ angstroms.
 - The space groups of the crystals *Copper* and *Aluminium* were changed from *Fd-3m* to *Fm-3m*.
 - Corrected a couple of Hall strings (`C 4 -2a` and `F -4 -2`).
 - `OldHallString` and `OldSymbolAlt` added for space groups 39, 41, 64, 67 and 68.
 - Added label `GetCentringVectors` to `InputCheck`.
 - Added option `UseCentring` to `SymmetryOperations`.
 - The tag `SpaceGroupQ` in `InputCheck` has been replaced with a more thorough `InterpretSpaceGroup`, which will return the interpreted space group symbol and abort with messages if not successful.

- Created `CrystalFormulaUnits`. Some functionality was transferred from `CrystalDensity`.
- `SymmetryEquivalentPositions` is now practically listable in terms of coordinates.
- Crystal names can now be input to `GetElements` in order to return a list of elements in its `ChemicalFormula` or `AtomData`.
- Created `GetScatteringCrossSection`.
- Extended `InputCheck` with the label `InterpretElement`.
- Added "IgnoreIonCharge" option to `ImportCrystalData`.
- Several functions now have the name `Get-` prepended to them: `GetAtomicScatteringFactor`, `GetCrystalMetric`, `GetLatticeParameters`, `GetLaueClass`, `GetScatteringCrossSection`, `GetSymmetryData`, `GetSymmetryOperations`.

Version 0.7.9

- Updated `$SpaceGroups`: Space group entries now have a `Name` sub-key that extends support for more alternative settings.
- Created the function `UnitCellTransformation` for transforming entries in `$CrystalData` to different cell settings.
- Fixed minor formatting bugs in `$SpaceGroups`.
- Added `HermannMauguinFullAlt` entries to rhombohedral space groups (*R*₃, *R*₋₃, *R*₃₂, *R*_{3m}, *R*_{3c}, *R*_{3m}, *R*_{-3c}) that include *:h* or *:r*.
- Also added `SymbolAlt`, `HermannMauguinShortAlt` and `HermannMauguinFullAlt` to space group entries with multiple cell origins.
- Fixed *I 41/a* (no. 88) entry in `$SpaceGroups`.
- `$XrayRedirect` updated to comply with changes of `$SpaceGroup`.
- Fixed a bug in `AddCompoundToDataset`; no `DisplacementParameters` were written if the cif-file were missing such data.
- Added the functionality to find "best fitting" space group formatting with `ToStandardSetting`.
- Fixed a bug in `AddCompoundToDataset` when a `label` was not explicitly given by the user.
- Added support for chemical formulas with decimals in `AddCompoundToDataset`.
- Updated `GetElements` with an option to ignore the charge of ions.
- Updated documentation on `UBtransformation`.
- Added support for string input in the `ToMiller` and `FromMiller` functions.
- Changed names of `SymmetryOperationsNotationA` to `SymmetryOperationsITA` and `SymmetryOperationsNotationB` to `SymmetryOperationsSeitz` in `$PointGroups`.

- Improved `MergeSymmetryEquivalent`.
- Minor fixes and updates in documentation.
- Created documentation on `RoundSignificants` and `ErrorPropagation`.
- Fixed a bug in `RoundSignificants` where output would not have a zero as second significant figure when expected.
- Created `SymmetryData`.
- Added the option `UseCentring` to `SymmetryEquivalentPositions`.
- Updated a bug in `InputCheck` where reflections containing negatives would not pass the function tests.
- Merged `ReflectionSetInspection` and `PeakTableHelper` to `PeakTableInspection`.
- Update documentation on `ReflectionConditionCheck`.
- Fixed bugs in `AddCompoundToDataset`: Procedure for finding the ADPs is now more robust.
- Updated `SymmetryData` with the option `UnambiguousSymbol`.
- Changed the name from `ReflectionConditionCheck` to `ReciprocalImageCheck`.
- Changed the name from `SimulateReciprocalSpace` to `ReciprocalSpaceSimulation`.
- Created the functions `BraggAngle` and `InterplanarSpacing`.
- Created the functions `ExtinctionDistance` and `DarwinWidth`.
- `$XrayRedirect` now supports concatenated versions of short Hermann–Mauguin symbols.
- Added the `HoldIndex` option in `ReflectionList`. Included this option in `ReciprocalSpaceSimulation`.
- Fixed a bug in `ReflectionList` where the incorrect resolution, based on the wavelength, was found.
- Added `CrystallographyToCartesian` to `$TransformationMatrices`.
- Updated `GetElements` with a `Tally` option.
- Created `$PeriodicTable`.

Version 0.7.8

- Minor bug fixes and updated in the documentation.
- It is now possible to set values for the cutoff intensity and group width in `ReflectionSetInspection`.
- Updated `ToMiller` to return output with commas if any index is not an integer.
- New function added to the `Statistics` context: `NonlinearLeastSquares`.
- Fixed an error with `StructureFactor` causing it to not accept wavelength input.
- `AddCompoundToDataset` now adds the site sym-

- metry order for each atom to `$CrystalData`.
- Updates on `StructureFactor` (handles occupation factor and site symmetry differently).
- Updated some functions to also use `InputCheck` for crystal names.

Version 0.7.7

- Updated documentation on `CrystalMetric` and fixed a link in the `Xray` guide.
- Updated documentation on `StructureFactor`.
- Minor fixes in the code.
- Added `P21/n` and `P21/a` to `$XrayRedirect`.
- Contact e-mail added to main guide page.
- Updated documentation on `$ScatteringFactors`. References are now included.
- `Installation.nb` will no longer ask user to save changes.
- If structure factor equals zero, corresponding phases are now displayed as `--` in `StructureFactorTable`.
- `StructureFactor` now has an option for disabling units (the phase). Documentation updated.
- `$PointGroups` and `$SpaceGroups` now have the formatted symbol prepended to each entry.
- Minor bug fixes in `AddCompoundToDataset`. Updated the way output is presented. Changed the way ADP type information is stored in `$CrystalData` – now the various atoms can be of different types.
- `CrystalMetric` updated to support input of lattice parameters directly.
- Introduced a `Limit` and a `Progress` option to `ReflectionList`.

Version 0.7.6

- `$XrayVersion` and `$XrayChangelog` added.
- Minor fixes in documentation.
- Fixed some bugs in `AddCompoundToDataset`.
- Fixed a bug with `StructureFactorTable` that could give unit cell volumes to be imaginary.
- Updated `RefinedValues`. New tag available: `Wavelength`.
- Updated `MergeLogs`.

Version 0.7.5

- Changelog started.
- Documentation on `SystematicAbsentQ` fixed.
- Several functions belonging to the context `Crystallography` have been ascribed the new context `Physics`.
- `$PhysicalConstants` created.
- Wrong coefficients in `$ScatteringFactors` were

- corrected (At, Be, C, Ho, Ni, Tm, Zn).
- The space groups of **Silicon**, **Germanium** and **Diamond** are now set to use the alternative origin in `$CrystalData`.
 - Added new alternative space group entries to `$SpaceGroups` (B₁, C₁, F₁, I₁, P₁, A₋₁, B₋₁, C₋₁, F₋₁, I₋₁). `$XrayRedirect` was also updated.
 - `SymmetryOperations` in `$SpaceGroups` have been flattened to a plain list structure.
 - The following new functions were created: `InputCheck`, `LaueClass`.
 - `StructureFactorTable` now sorts by decreasing structure factor by default.
 - `ReflectionList` now sorts reflections from least to highest digit sum (ignoring sign), and has been extended with a `Keep` option.
 - Added the option `ReflectionListKeep` to `StructureFactorTable`.
 - Updated the documentation on `StructureFactor` and `StructureFactorTable`.
 - Minor bug fixes.

Utilising *MaXrd* in the Study of Inclusion Compounds

Abstract

The Mathematica X-ray diffraction package *MaXrd* [1] has now been expanded with the capability to compose “custom” crystal structures, particularly aimed at facilitating the embedding of a guest phase into a host lattice. After importing the required crystallographic information from a cif file, one can extend the asymmetric unit to a desired number of unit cells while inserting atoms, molecules or other structures in the process. The embedded phase can also be distorted and/or rotated by a specified or random amount when placed into the host. The resulting structure can be visualised in three dimensions in direct space and the information may be utilised automatically by *DISCUS* [2] to obtain a simulated diffraction pattern. A consequence of this technique is that the space group of the guest phase becomes independent of that of the host (essentially having $P1$ symmetry). This gives the means to test hypotheses on the crystal structure and simultaneously investigate reciprocal space for any implied characteristics in a relatively swift and easy manner. This functionality is used in our ongoing study of a thiourea-ferrocene clathrate, which has proven challenging with regard to its phase transitions and the five-fold symmetry of the cyclopentadienyl rings [3, 4].

References

- [1] Ramnes, S., Larsen, H. B. & Thorkildsen, G. (2019). *J. Appl. Cryst.* 52, 214–218. [2] Proffen, T. & Neder, R. B. (1997). *J. Appl. Cryst.* 30, 171–175. [3] Hough, E. & Nicholson, D. G. (1978). *J. Chem. Soc., Dalton Trans.*, 15–18. [4] Lorson, L. C., Tai, O. & Foxman, B. M. (2018). *Crystal Growth & Design*, 18, 409–415. [5] R. Clement, R. Claudi, and C. Mazurek, “Calibration of ferrocene and nickelocene in a thiourea host lattice,” *J. Chem. Soc., Chem. Commun.*, pp. 654–655, 1974. [6] M. Sotai, K. Ogasawara, and H. Suga, “Heat capacity and phase transitions of thiourea-ferrocene channel inclusion compound,” *Molecular Crystals and Liquid Crystals*, vol. 73, no. 3–4, pp. 231–254, 1981. [7] M. G. B. Drew, A. Lind, and D. G. Nicholson, “Molecular modelling studies on the thiourea ferrocene clathrate,” *Supramolecular Chemistry*, vol. 8, no. 3, pp. 197–212, 1997.

Motivation

The thiourea-ferrocene clathrate has been studied since 1974 [5], and its rhombohedral lattice and reversible phase transition at 162 K has been known since then. Four other phase transitions have been reported in 1981 [6]. Nevertheless, the dynamics of ferrocene in this tunnel inclusion complex has been the topic of research papers up to this day. Discussion have mainly revolved around the orientation of ferrocene as a function of temperature, effects of different conformations and the disordered ferrocene’s impact on the overall thiourea structure at the transitions.

We still seek a more complete and intuitive understanding of the low-temperature phase as well as the transition mechanism and overall disorder.

Functionality

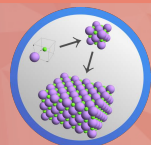
The latest version, *MaXrd 1.7.0*, comes with a handful of functions which simplify the process of building and tweaking a “custom” crystal structure and visualising it in both direct and reciprocal space. A typical workflow starts by using *ImportCrystalData* to import the relevant content of a cif file to *Mathematica*. Next one can use *ExpandCrystal* to grow the asymmetric unit to a desired number of unit cells. At this point one can apply *ImportCrystalData* to the object for an inspection in direct space, or use *DISCUSPlot* which feeds the structural information into *DISCUS* and outputs a 2D plot of a reciprocal space simulation. Interactive examples are found in the documentation.



ImportCrystalData

A straightforward but necessary step is to import the relevant crystallographic information to *Mathematica*.

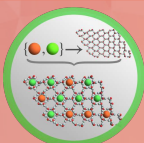
The simplest way is to use this function with a cif file, but one also has the option to enter the required information programatically or through a dialogue window.



ExpandCrystal

With the asymmetric unit, lattice and space group in place, this function will simply grow the structure to a desired number of unit cells.

One of the main purposes is to create the host phase of the structure, and also to prepare the crystal for visualisation. It is flexible for creating both stand-alone structures or pieces that are to be part of a larger or more complicated structure.



EmbedStructure

Once a host structure has been defined, the guest phase can easily be embedded. The targeted positions specified are automatically matching the host size by default. Guest entities can be placed randomly, sequentially or conditionally. Furthermore, the entities can be shifted or rotated—by a constant or random amount—at placement.



DistortStructure

With this function, the user specifies a displacement field that shifts every atom relative to their present location. The flexibility in *Mathematica* makes it easy to configure the vector field to work periodically or in specific domains.

This function works well with the built-in *Manipulate* function to tweak the distortion parameters dynamically.

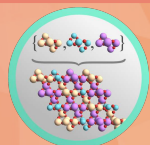


DISCUSPlot

If *DISCUS* is installed, the user needs only input a structure name and Miller indices to obtain a simulated diffraction pattern. This function will automatically generate the input code of *DISCUS* and run it through a terminal/command prompt in the background, then present the resulting plot.

SynthesiseStructure

If the structure is made from a set of smaller substructures, this function can synthesise the overall structure by assembling the blocks automatically. These items can also be placed sequentially or in random order. Normally they are assembled “edge-to-edge”, but there is also an option for using a buffer between them (which may be useful for cubic structures).



CrystalPlot

This plot function can be called on every crystal/structure object to give a simple 3D representation of it. All direct space plots of crystals on this poster (and in the package documentation) have been created using this function.

In this research context it provides an easy way of checking the current status of embedment or distortions.

Simulations

In the literature we find reports of 60/40% distribution of the ferrocene molecules in parallel and perpendicular orientations, respectively [7]. Simulating this is a fitting task for the discussed tools. It is easy to try out different weighting schemes or switching between a random embedding or trying for instance a herringbone pattern. Another idea is to model incommensurability between the guest and host by imposing a random shift in the tunnel direction when placing the ferrocene molecules. Additionally, it is not too difficult to form the ferrocenes in a repeating spiral structure along the tunnel.

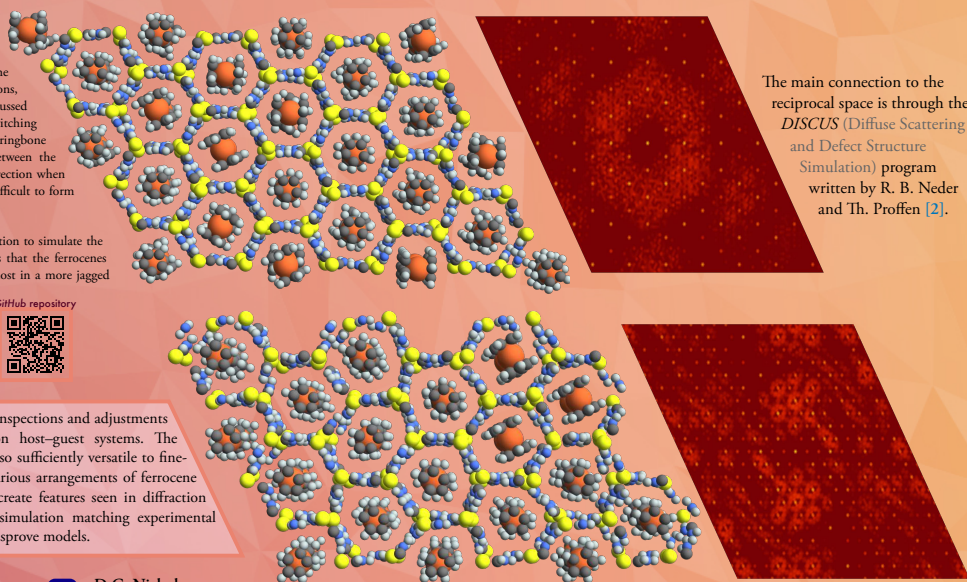
The lower figures demonstrate the use of the distortion function to simulate the lower-temperature phase of the structure. The hypothesis is that the ferrocenes become more static at this point and distorts the thiourea host in a more jagged way, bringing it in to an orthorhombic structure.

GitHub repository



Conclusion

The presented tools enable users to perform simple inspections and adjustments of crystal structures with particular emphasis on host-guest systems. The functions are first and foremost user-friendly, but also sufficiently versatile to fine-tune complex structures. In our case, we try out various arrangements of ferrocene and distortion of the thiourea frame aiming to recreate features seen in diffraction images. We have not yet arrived at a definitive simulation matching experimental records, but believe these tools are useful to test or disprove models.



The main connection to the reciprocal space is through the *DISCUS* (Diffuse Scattering and Defect Structure Simulation) program written by R. B. Neder and Th. Proffen [2].

Publications

Included in this part of the thesis are the manuscripts of the three articles comprising this thesis. A list of the works and abstracts of each paper are repeated here:

- I Stian Ramsnes, Helge Bøvik Larsen and Gunnar Thorkildsen. ‘Using *Mathematica* as a platform for crystallographic computing’. In: *Journal of Applied Crystallography* 52.1 (Feb. 2019), pp. 214–218. DOI: [10.1107/S1600576718018071](https://doi.org/10.1107/S1600576718018071) (see page 156)
- II Stian Penev Ramsnes, Helge Bøvik Larsen and Gunnar Thorkildsen. ‘*MaXrd* updated with emphasis on model construction and reciprocal-space simulations’. In: *Journal of Applied Crystallography* 53.6 (Dec. 2020), pp. 1620–1624. DOI: [10.1107/S160057672001328X](https://doi.org/10.1107/S160057672001328X) (see page 161)
- III Stian Penev Ramsnes et al. ‘Complementary Synchrotron Diffraction and Simulation Studies on a Ferrocene:Thiourea Inclusion Compound’. To be published. 2022

The first paper concerns the release of the *Mathematica* X-ray diffraction package (*MaXrd*). In essence, it contains point- and space group information from the International Tables for Crystallography and tabulated data on scattering factors and cross sections, required for calculations related to X-ray physics. Included are also functions to utilise this data, with a documentation demonstrating their usage. Highlighted functionality includes extraction of symmetry data, data import from *cif* files, calculations of structure factors, linear absorption coefficients and unit cell transformations.

The second article was submitted once a practical structure modelling extension had been sufficiently generalised. The imported *cif* data could now be employed to create and visualise crystal structures. Many additions depended on the original symmetry-related foundation, but a few brought novel concepts into the package, such as the function for making domains. The focus on model construction was motivated by the study of a host-guest complex, hence the ability to embed one crystal entity into another. With the possibility to simulate the diffraction patterns (reciprocal space maps), a way of comparing a customised structure with experimental data was realised.

The third article conveys our findings on the thiourea–ferrocene inclusion compound. Complementary studies have been conducted in three areas: qualitative exploration of reciprocal space, quantitative structure solutions of synchrotron data and various model investigations with the *MaXrd* utility package in *Mathematica*. We discuss both supporting evidence and shortcomings of the prevalent high- and low-temperature phases of the TFIC structure.



Using *Mathematica* as a platform for crystallographic computing

Stian Ramsnes,* Helge Bøvik Larsen and Gunnar Thorkildsen

Department of Mathematics and Physics, University of Stavanger, 4036, Norway. *Correspondence e-mail: stian.p.ramsnes@uis.no

Received 20 September 2018

Accepted 20 December 2018

Edited by Th. Proffen, Oak Ridge National Laboratory, USA

Keywords: *Mathematica*; structure factors; computation; *MaXrd*; CIF.

A comprehensive *Mathematica* package for crystallographic computations, *MaXrd*, has been developed. It comprises space-group representations based on *International Tables for Crystallography*, Vol. A, together with scattering factors from *XOP* and cross sections from *xraylib*. Featured functionalities include calculation of structure factors, linear absorption coefficients and crystallographic transformations. The crystal data used by *MaXrd* are normally generated from external *.cif* files. The package comes with a dynamic documentation seamlessly integrated with the *Mathematica* system, including code, examples, details and options. From the onset, minimal *Mathematica* experience is required to make use of the package. It may be a helpful supplement in research and teaching where crystallography and X-ray diffraction are essential. Although *Mathematica* is a proprietary software, all the code of this package is open source. It may easily be extended to cover user-specific applications.

1. Introduction

At its core, the *MaXrd* (*Mathematica* X-ray diffraction) package is an implementation of point-group and space-group symmetry information from *International Tables for Crystallography*, Vol. A (ITA; Aroyo, 2016), cf. the Bilbao Crystallographic Server (Aroyo *et al.*, 2006), as well as several tables for atomic scattering factors and cross sections from *International Tables for Crystallography*, Vol. C (ITC; Prince, 2004; Maslen *et al.*, 2004; Creagh & Hubbell, 2004; Creagh, 2004), cf. *XOP* and *xraylib* (del Rio & Dejus, 2011; Schoonjans *et al.*, 2011). Relevant crystal data may be imported automatically from any *.cif* file¹ and applied by functions of this package (see Section 4).

Mathematica (Wolfram Research, 2018b) is accessible on Linux, macOS and Windows. This package requires *Mathematica* version 11.3 or later. (See Wolfram's web site for machine requirements.) Renowned for being versatile and spanning many technical and scientific fields, *Mathematica* is an excellent platform in which to facilitate crystallographic computations and subsequent analyses. *MaXrd* is thus embedded in a software system that is continuously maintained and developed.

The package also features a comprehensive documentation. This is constructed to be as dynamic and helpful as the built-in *Mathematica* documentation. A complete collection of definitions may be found in a separate notebook (*Definitions.nb*).

¹ Owing to the many ways data can be formatted in *.cif* files, the user may be prompted with messages or dialogue windows if crucial elements are missing or have an unexpected format.



research papers

The purpose of *MaXrd* is primarily to establish a crystallographic functionality in the *Mathematica* language, which can prove useful for students, scientists and developers alike. It is not intended as a replacement for data reduction software as such, but rather to be a generic tool in pre- and post-processing in various fields of X-ray analysis, broadly speaking. Users' interest in developing similar *Mathematica* content is evident, ranging from simple 3D demonstrations (Wolfram Research, 2018a) and electron density simulations (Delatorre & Azevedo, 2001) to packages for macromolecular crystallography (Ambert *et al.*, 2006) and for plotting crystal structures (Eifert & Heiliger, 2016).

The package comes with several of tutorials that can help familiarize the user with the content provided. It includes demonstrations of how to perform symmetry and crystallographic computations and work with crystallographic data input. Additionally, there are some short tutorials on relevant aspects of *Mathematica* and a reference overview.

2. Crystallographic core

2.1. Point and space groups

The main guide page, as seen in Fig. 1, shows an overview of the content. Point- and space-group information is stored as



Figure 1
The main guide page of the *MaXrd* package. Definitions and examples are provided for all functions in the documentation.

large 'association' structures (in the *Mathematica* language, an association is an 'associative array', similar to the dictionary data type in Python), consisting of 32 and 230 keys, respectively. Symbols for library items start with '\$', and the actual associations have been named `$PointGroups` and `$SpaceGroups`. They are built automatically when the package is launched (`<<MaXrd'`).

Each space-group entry points to a set of sub-associations with the following keys:

```
SpaceGroupNumber, LaueClass, CrystalSystem,
Name, Properties, Setting, SymmetryOperations,
SpecialPositions, AlternativeSettings
```

(The key `AlternativeSettings` only exists for a subset of the space groups.)

The first three items point to obvious values. `Name` points to symbols used to denote the space group: Hermann–Mauguin, Schönflies and Hall symbols. `Properties` holds two boolean statements: `CentrosymmetricQ` and `SohnckeGroupQ`. `Setting` is used to store information on cell centring, cell origin, axis permutation and alternative choices of a unique axis. `SymmetryOperations` points to a list of pairs, `{{<matrix>, <vector>}, ...}`, representing the symmetry operations of the space group. `SpecialPositions` points to the spatial information listed in ITA (Aroyo, 2016): multiplicity, Wyckoff letter, site symmetry and coordinates. Finally, 165 of the 230 space groups are listed with the `AlternativeSettings` key, e.g. *Pmaa* and *Pbmb* are two alternative settings of the space group *Pccm*. The 230 'main keys' point to conventional space-group symbols. `$PointGroups` has a similar structure.

2.2. Extracting elements

There are multiple ways to look up and extract the stored information in `$PointGroups` and `$SpaceGroups`. The code shown in Fig. 2 exemplifies how to retrieve data directly from associations. *MaXrd* comes with functions (starting with `Get`) which simplify extraction of such information:

```
GetAtomicScatteringFactors, GetCrystalMetric,
GetElements, GetLatticeParameters,
GetLaueClass, GetScatteringCrossSections,
GetSymmetryData, GetSymmetryOperations
```

```
in[]:= $SpaceGroups[["Pba2", "AlternativeSettings",
  "AxisPermutationCAB", "SymmetryOperations"]]
Out[]:= {{{{1, 0, 0}, {0, 1, 0}, {0, 0, 1}}, {0, 0, 0}},
  {{{1, 0, 0}, {0, 1, 0}, {0, 0, -1}}, {0, 1/2, 1/2}},
  {{{1, 0, 0}, {0, -1, 0}, {0, 0, -1}}, {0, 0, 0}},
  {{{1, 0, 0}, {0, -1, 0}, {0, 0, 1}}, {0, 1/2, 1/2}}}}
```

Figure 2
A 'direct approach' for obtaining the symmetry operations of *P2cb*, which has a *cab*-axis relation to the standard setting of *Pba2*.

```
In[ ]:= GetSymmetryOperations["P2cb"]
Out[ ]:= {{{{1, 0, 0}, {0, 1, 0}, {0, 0, 1}}, {0, 0, 0}},
          {{{1, 0, 0}, {0, 1, 0}, {0, 0, -1}}, {0,  $\frac{1}{2}$ ,  $\frac{1}{2}$ }},
          {{{1, 0, 0}, {0, -1, 0}, {0, 0, -1}}, {0, 0, 0}},
          {{{1, 0, 0}, {0, -1, 0}, {0, 0, 1}}, {0,  $\frac{1}{2}$ ,  $\frac{1}{2}$ }}}}
```

Figure 3
Extracting the same information as shown in Fig. 2. Note that the permutation of axes is not required, just the alternative space-group symbol.

(cf. Fig. 3 as well). In this example, *P2cb* is an alternative setting not found in ITA. Although ITA is the main source and reference to crystallographic material, other sources have been supplementary, for instance in the completion of symmetry operations for unconventional space groups [see *ctbx* (Grosse-Kunstleve *et al.*, 2002) and *A Hypertext Book of Crystallographic Space Group Diagrams and Tables* (Cockcroft, 2016)].

`GetSymmetryData` mainly serves as an alternative for looking up data elements in `$PointGroups` and `$SpaceGroups`. The remaining functions listed have self-explanatory functionality.

3. User-specific data

Fig. 4 gives a simple overview of how *MaXrd* is organized.

3.1. Atomic scattering factors

Data used in affiliation with the atomic scattering factors [$f^{(0)}$, $f'(E)$, $f''(E)$] are gathered from `.dat` files belonging to *XOP 2.3* located at ESRF's FTP (ESRF, 2013). This information is kept in files located in a separate `Data` directory and imported to the *Mathematica* kernel when the package is loaded, or when needed by relevant functions.

In the retrieved files, data are stored either as the Cromer–Mann coefficients (a , b , c) used in a regression model built as a linear combination of Gaussians,

$$f^{(0)}(s) = \sum_i [a_i \exp(-b_i s^2)] + c, \quad s \equiv (\sin \theta)/\lambda, \quad (1)$$

or as data points, $\{s, f^{(0)}(s)\}$ or $\{E, f'(E), f''(E)\}$, where E denotes energy.

When data points are used, the *Mathematica* function `Interpolation` has been applied to generate interpolation functions. These are stored as associations with element symbols as keys, and saved to a separate `.m` file named according to the `.dat` file used. The default $f^{(0)}$ source (Waasmaier & Kirfel, 1995) or $\{f', f''\}$ source (Cromer & Liberman, 1981)² can be changed by using an optional argument in relevant functions.

² Jensen term set to zero and $f_{\text{cl}}(\infty)$ replaced by values provided by Kissel & Pratt (1990).

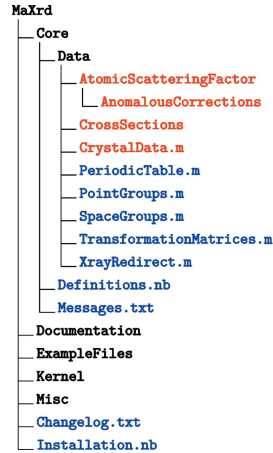


Figure 4
Overview of the most essential directories (black) and files (blue) of the package. The items of Section 3 are coloured red.

3.2. Photoelectric and scattering cross sections

Cross sections (σ_{pe} , σ_{coh} , σ_{incoh} , σ_{tot}) have been generated with *xraylib v3.3.0* (Schoonjans *et al.*, 2011). *Mathematica* bindings were made via the `.NET/Link` integration as described in the *xraylib* documentation, by which cross sections were tabulated for atoms with atomic number $Z \in \{1, 98\}$ in the wavelength range $\lambda \in \{0.001, 3.000\}$ Å, which is adequate in the regime of both synchrotron and conventional sources. The tables are stored in `.dat` files – one for each element – and are read with `GetScatteringCrossSection`, which by default returns total cross sections using the nearest data point in the table.

3.3. Importing crystal data from `.cif` files

In order to make use of *MaXrd* functions, some basic structural input is required. The function `ImportCrystalData` performs the task of extracting this information from a `.cif` file and appending it to `$CrystalData` as well as to a local file tied to this association (`MaXrd/Core/Data/CrystalData.m` by default, which contains some predefined 'crystal' data.)

Initializing a dialogue window for manual input is possible, but normally all the relevant data are automatically extracted from `.cif` files.

When executing the `ImportCrystalData` function, data items are verified.³ Files containing multiple data series can be treated using the `ExtractSubdata` option. Quasicrystals

³ In the current version more than 30 items are scanned. See the documentation on `ImportCrystalData` for details. The procedure can be expanded to include other data items found in `.cif` files; cf. core CIF (IUCr, 2018).

research papers

and modulated structures are currently not supported. Every 'crystal' has at least the following keys:

SpaceGroup, LatticeParameters, AtomData

with AtomData entries containing at least one chemical element and its fractional coordinates. Typically they also include information concerning site occupancy and aniso-

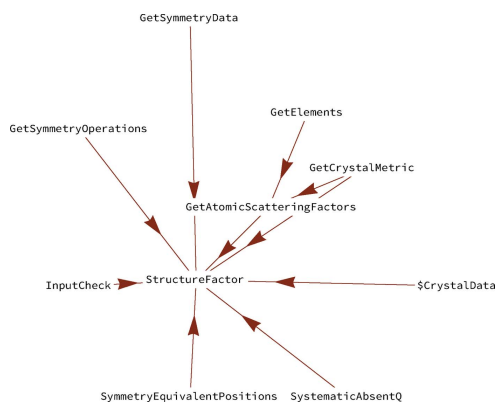


Figure 5
A graph showing which other functions StructureFactor depends on. Generated with RelatedFunctionsGraph.

```
In[1]:= StructureFactor["Silicon", {1, 1, 1}, 0.709317]
Out[1]:= {59.3744, -179.62°}
```

Figure 6
The structure factor (modulus and phase) for the 111 reflection of silicon at $\lambda = 0.709317$ Å.

```
In[1]:= AttenuationCoefficient["GalliumArsenide", 1.1573]
Out[1]:= 615.285/cm
```

Figure 7
Calculation of μ for gallium arsenide at $\lambda = 1.1573$ Å.

```
In[1]:= ImportCrystalData["/tmp/demo_folder/Ferrocene.cif"]
Out[1]:= {ChemicalFormula -> C10H10Fe, FormulaUnits -> 2, SpaceGroup -> P21/n,
  LatticeParameters -> {a -> 5.9285 Å, b -> 7.612 Å, c -> 9.041 Å, alpha -> 90°, beta -> 93.156°, gamma -> 90°},
  Wavelength -> 0.69804 Å, AtomData -> {<<11>>}}
```

```
In[2]:= UnitCellTransformation["Ferrocene", "P21/a"]
Out[2]:= {ChemicalFormula -> C10H10Fe, FormulaUnits -> 2, SpaceGroup -> P21/a,
  LatticeParameters -> {a -> 10.5349 Å, b -> 7.612 Å, c -> 5.9285 Å, alpha -> 90°, beta -> 121.031°, gamma -> 90°},
  Wavelength -> 0.69804 Å, AtomData -> {<<11>>}}
```

Figure 8
The UnitCellTransformation function. Crystallographic data for ferrocene presented in the space group $P2_1/n$ are imported from a .cif file. Transformation to the targeted alternative, $P2_1/a$, is achieved as shown. AtomData is not explicitly depicted.

tropic displacement parameters (ADPs). Other useful data items are the chemical formula and the wavelength from a data collection. At this stage the 'crystal' is ready to be mapped onto functions such as AttenuationCoefficient, CrystalDensity or StructureFactor.

4. Applications

In this section a few selected functions will be elaborated.

4.1. Calculating structure factors

Acquiring structure factors – efficiently and with minimal user interaction – was one of the tasks that initiated the creation of this package. Three inputs are required by StructureFactor: a crystal label, reflection indices and wavelength/energy [if a wavelength accompanies the crystal entry (.cif), this will be used by default].

The graph in Fig. 5 shows which components (other package functions) the function is built upon. Fig. 6 displays a generic input.

4.2. Linear absorption coefficient

The linear absorption coefficient, μ , is calculated with the function AttenuationCoefficient (cf. Fig. 7).

4.3. Unit-cell transformations

UnitCellTransformation is used to transform lattice parameters, atomic coordinates and ADPs to an alternative space-group setting. It is a utility capable of comparing different structure solutions. The function checks whether there is a valid transformation between source and target cell before executing. See Fig. 8 for an example.

5. Conclusion

A *Mathematica* package for crystallography has been launched, containing core elements of crystallographic symmetry and photon-atom interactions. The package is available at <https://github.com/Stianpr20/MaXrd>, where future add-ons will also be published. Crystal data are imported to *Mathematica*

from `.cif` files. Included are functions that can utilize this information, along with a thorough documentation. The scope of some selected functions is considered.

Acknowledgements

A presentation of this package was given at the 31st European Crystallographic Meeting in Oviedo, Spain.

References

- Ambert, N., Vanwinsbergh, J. & Dumas, P. (2006). *Biocrystallographica, a Package for Doing Crystallography with Mathematica*, CCP4 Newsletter on Protein Crystallography, <https://www.ccp4.ac.uk/newsletters/newsletter44/articles/BioCrystallographica.pdf>.
- Aroyo, M. I. (2016). Editor. *International Tables for Crystallography*, Vol. A, *Space-Group Symmetry*, 6th ed. Chichester: Wiley.
- Aroyo, M. I., Perez-Mato, J. M., Capillas, C., Kroumova, E., Ivantchev, S., Madariaga, G., Kirov, A. & Wondratschek, H. (2006). *Z. Kristallogr. Cryst. Mater.* **221**, 15–27.
- Cockcroft, J. K. (2016). *A Hypertext Book of Crystallographic Space Group Diagrams and Tables*, <http://img.chem.ucl.ac.uk/sgp/mainmenu.htm>.
- Creagh, D. C. (2004). *International Tables for Crystallography*, Vol. C, *Mathematical, Physical and Chemical Tables*, 3rd ed., ch. 4.2.6, pp. 241–258. Dordrecht: Springer.
- Creagh, D. C. & Hubbell, J. H. (2004). *International Tables for Crystallography*, Vol. C, *Mathematical, Physical and Chemical Tables*, 3rd ed., ch. 4.2.4, pp. 220–236. Dordrecht: Springer.
- Cromer, D. T. & Liberman, D. A. (1981). *Acta Cryst.* **A37**, 267–268.
- Delatorre, P. & Azevedo, W. F. de Jr (2001). *J. Appl. Cryst.* **34**, 658–660.
- Eifert, B. & Heiliger, C. (2016). *Crystallica: a Package to Plot Crystal Structures*, <http://library.wolfram.com/infocenter/MathSource/9372/>.
- ESRF (2013). *ESRF Anonymous FTP Server*, <http://ftp.esrf.eu/scisoft/xop2.3/DabaxFiles/>.
- Grosse-Kunstele, R. W., Sauter, N. K., Moriarty, N. W. & Adams, P. D. (2002). *J. Appl. Cryst.* **35**, 126–136.
- IUCr (2018). *Core CIF dictionary*, https://www.iucr.org/resources/cif/dictionaries/cif_core.
- Kissel, L. & Pratt, R. H. (1990). *Acta Cryst.* **A46**, 170–175.
- Maslen, E. N., Fox, A. G. & O'Keefe, M. A. (2004). *International Tables for Crystallography*, Vol. C, *Mathematical, Physical and Chemical Tables*, 3rd ed., ch. 6.1.1, pp. 578–580. Dordrecht: Springer.
- Prince, E. (2004). Editor. *International Tables for Crystallography*, Vol. C, *Mathematical, Physical and Chemical Tables*, 3rd ed. Dordrecht: Springer.
- Rio, M. S. del & Dejus, R. J. (2011). *Proc. SPIE*, **8141**, 814115.
- Schoonjans, T., Brunetti, A., Golosio, B., Sanchez del Rio, M., Solé, V. A., Ferrero, C. & Vincze, L. (2011). *At. Spectrosc.* **66**, 776–784.
- Waasmaier, D. & Kirfel, A. (1995). *Acta Cryst.* **A51**, 416–431.
- Wolfram Research (2018a). *Wolfram Demonstrations Project: Crystallography*, <http://demonstrations.wolfram.com/topic.html?topic=Crystallography>.
- Wolfram Research (2018b). *Mathematica*. Version 11.3. Wolfram Research Inc., Champaign, IL, USA.



MaXrd updated with emphasis on model construction and reciprocal-space simulations

Stian Penev Ramsnes,* Helge Bovik Larsen and Gunnar Thorkildsen

Department of Mathematics and Physics, University of Stavanger, 4036 Stavanger, Norway. *Correspondence e-mail: stian.p.ramsnes@uis.no

Received 1 September 2020
Accepted 3 October 2020

Edited by J. Ilavsky, Argonne National Laboratory, USA

Keywords: *Mathematica*; *MaXrd*; inclusion compounds; host–guest systems; simulations.

Supporting information: this article has supporting information at journals.iucr.org/j

A major revision of the *Mathematica X-ray Diffraction Package (MaXrd)* has been undertaken, where developments have focused upon construction of crystal structure models, in particular host–guest systems, and subsequent simulations of reciprocal space through the external programs *DISCUS* and *DIFFUSE (ZMC)*.

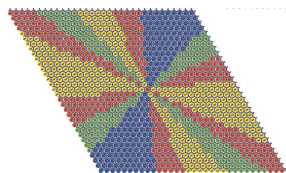
1. Introduction

The initial version of *MaXrd* (Ramsnes *et al.*, 2019) contained the essential symmetry information from *International Tables for Crystallography*, Vol. A (Hahn, 2002). It came with various utilities built around this core, to calculate X-ray diffraction parameters and perform symmetry assessments. *MaXrd* has since acquired new and more specific functionality, which this article intends to summarize.

Inclusion complexes – two-component systems where a distinct guest is enclosed by a host – have a history stretching back over a century (Herbstein, 2005). These host–guest systems are still a broad subject of interest and have motivated recent package improvements. Subcategories are based on the type of cavities the hosts provide. Gas hydrates are examples of clathrates, *i.e.* systems where the host restrains the guest by surrounding it with hydrogen-bonded ‘cages’ (Sloan & Koh, 2008). Another class of hosts form one-dimensional tunnels for the guests to occupy. Here, urea and thiourea are prime examples (Li, 1996). They create a characteristic honeycomb-shaped structure in conjunction with appropriate guests. Dynamic disorder of guest molecules is common at standard conditions as well (Yeo *et al.*, 2001), and transition to a low-temperature phase distorts the tunnel structure of both thiourea (Maris *et al.*, 2001; Pan *et al.*, 2008) and urea (Yeo & Harris, 1997).

When a structure solution failed, presumably due to the individual guests not adhering to the overall space-group symmetry, combined with an anticipated high degree of disorder, the idea of decoupling the clathrated guest molecules from the host phase arose. The adopted procedure permits individual control over guest molecules when adding them into structure components. Instead of representing the whole crystal with a single, average asymmetric unit, an adequately large cluster of customized cells is introduced instead, its final size reflecting a trade-off between level of detail and computational resources. The modelling capabilities of *MaXrd* will be covered in Section 2.

The package also addresses familiar crystallographic subjects such as domains and twinning. The topic of domains arises frequently, often in relation to ferromagnetic materials



© 2020 International Union of Crystallography

computer programs

or phase transitions (Authier, 2013). Utilities for working with domains were considered general enough to be included in *MaXrd*. Their modes of operation will be examined in Section 3.

A goal has been to simulate X-ray diffraction patterns of structural models for comparing observable features with experimental records. *DISCUS* (Proffen & Neder, 1997, 2009), a computer program designed to simulate diffuse scattering from disordered structures, which also supports deviations from a purely average picture, gained attention. An interface was written to pipe crystallographic data through the *DISCUS* software along with the necessary commands to build a diffraction image. A similar program module, *DIFFUSE*, was also implemented through *ZMC* (Goossens *et al.*, 2011) as an alternative. More details are given in Section 4.

Although the code was initially written to model a particular scattering system, the add-ons remain completely general. Providing useful documentation with plenty of examples has still been a priority during the expansion. An overview of new functionalities and their relations to the original version is given in Fig. 1.

2. Structure composition

In the following, *entity* will be used as a collective term for generic atomic constructs, *e.g.* a single chemical element, a molecule, an asymmetric unit, a unit cell or an arbitrarily large collection of cells. This last entity may also be termed a block, a fragment or a supercell. Whole structures or finite crystals also comply with this definition. This section and the next essentially describe how entities can be copied, manipulated and assembled into structure models.

A simple, yet indispensable addition is *CrystalPlot*, which draws the atoms of the input entity along with unit-cell edges of the appropriate crystal system. It is convenient to use for quick visualizations of small molecular systems and geometrical inspections. *CrystalPlot* relies on *Mathematica*'s *Graphics3D* function, thereby inheriting all its relevant options for graphics configurations. There are some additional options related to atom radius and opacity.

2.1. Embedding of guest entities into the host phase

The function *EmbedStructure* was written with host-guest complexes in mind. It has been designed to work effortlessly in the default setting, while also retaining flexibility to cover a variety of modifications. *ExpandCrystal* may be used to 'grow' the asymmetric unit to a unit cell or supercell, suitable for creating a host entity. There are three ways of embedding the guests. (i) A plain list of guest entities will position them sequentially in the given input order. (ii) Joining (i) with a list of occupational probabilities will prepare

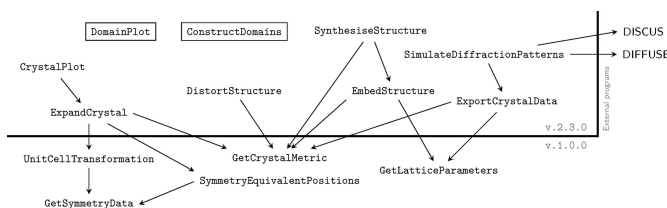


Figure 1
A selection of a few original (version 1.0.0) and new functions (version 2.3.0) separated by the horizontal line, with arrows indicating dependencies. Some additions are not attached to the original code library (framed labels).

a corresponding distribution of the content before a random positioning. (iii) The third option enables the user to make patterned arrangements, by providing conditions on the entities' positions.

In any case, target positions are needed, *i.e.* fractional coordinates in the host's crystallographic coordinate system specifying the positioning of the guests. By default, given coordinates are expanded to match the host's size automatically.

Fine-tuning of the model may be achieved with a couple of perturbative options, one for translations and another for rotations. These can be used to make slight adjustments of the guest entities relative to their targeted locations, with three axes available in either case. Single scalars designate static displacement/rotations, while a pair of numbers indicate a range for random choice.

Rotation axes intersect at some point, an *anchor*, which can be arbitrarily moved in principle. This is managed automatically by *RotationAnchorReference*. Four settings are available: two of them belong to domain structures (see Section 3), the remaining two are for moving the anchor either to the origin of the host or to the target position of each guest. A separate tutorial that covers these options in more depth may be found in the documentation.

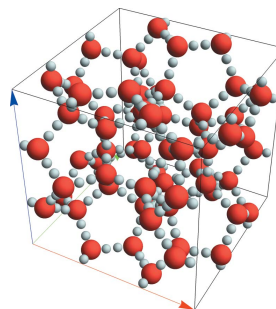


Figure 2
Plot showing the unit cell of cubic ice structure I without any guest molecules. The *a*, *b* and *c* axes are coloured red, green and blue, respectively.

Table 1

To give an idea of approximate computation times, the methane clathrate example was run on four different systems, divided into four parts.

Task 1: construct the host framework. Task 2 (and 3): embed methane into a plain (and perturbed) version. Task 4: render diffraction simulation. *DIFFUSE* was used in the last step, with the output size of the images set to 500×500 pixels. The percentages denote the fraction of time spent preparing the input files for the external program. The Macs were unable to use *DIFFUSE* due to dropped support for 32-bit software.

	PC 1 (Windows)	PC 2 (Linux)	Mac 1	Mac 2
Year	2017	2016	2012	2013
CPU	Quad-core 2.50 GHz Intel Core i5-7500T	Dual-core 2.30 GHz Intel Core i5-6200U	Dual-core 2.50 GHz Intel Core i5-3210M	Dual-core 1.30 GHz Intel Core i5-4250U
RAM	16 GB	8 GB	8 GB	4 GB
Task 1	27 s	22 s	43 s	42 s
Task 2	1 min 55 s	1 min 57 s	2 min 51 s	3 min 11 s
Task 3	3 min 35 s	3 min 5 s	4 min 37 s	4 min 17 s
Task 4	5 min 19 s (36%)	7 min 18 s (18%)	–	–

Embedding a guest into a host structure is summarized in four steps, where steps (ii) and (iii) are optional. (i) The atomic coordinates of a given guest entity are converted to match the system of the host, to be inserted at a site designated by the user. (ii) Rotation is performed on the entity, dictated by three axes and rotation angles, their common point of intersection given a predefined origin as mentioned. (iii) The contents of the entity are shifted by user specifications analogously to the previous step. (iv) The content is merged with the targeted host system.

As an example, consider a simple clathrate hydrate of methane trapped in ice. The host lattice is arranged in the so-called cubic structure I, where guest molecules are entrapped in dodecahedra and tetracaedra formations of water molecules (Kótai *et al.*, 2012). Basic structural data can be imported from a CIF or entered manually from a source, *e.g.* Sloan & Koh (2008). The ice structure may then be assembled by calling `ExpandCrystal`; a single unit cell is shown in Fig. 2. The centres of the cavities will serve as target positions for the guest entities. Since the methane molecules are weakly bound to the ice (Lenz & Ojamäe, 2011), we choose to include random perturbations of each methane molecule in our model, using both the translational and rotational options. A small extract of the resulting structure is shown in Fig. 3.

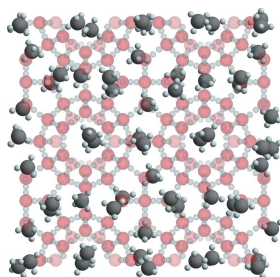


Figure 3
A $4 \times 4 \times 1$ section of the modelled clathrate, where the methane is shifted up to 0.85 \AA from the targeted position and with complete rotational freedom. The host atoms have been made transparent for clarity.

The diffraction pattern of this particular system may be compared with one having a different arrangement of methane. Fig. 4 shows a pixel-wise difference map based on two simulations with slightly different guest distributions. The crystal size has been set to 16^3 unit cells, and a uniform scaling has been applied to clarify the diffuse parts. Readers should also consult Table 1 for some benchmarks.

3. Domains and customization

To make models more realistic, the concept of domains was included. `ConstructDomains` helps in designing a structure with a chosen number of domains. It operates with a structure of *abstract* cells: objects on the lattice that are to be replaced by entities. An integer is associated with each cell that identifies a particular domain. The function reorders these identifiers by a process yielding a structure representation. This may be input to `SynthesizeStructure` for assembling entities into a model, or relayed to `DomainPlot` for a 2D or 3D depiction.

Functions and concepts encountered so far may be used to build entities, replicated to an arbitrarily large structure. The role of these domain-related functions is to provide a way of engineering the model on a higher level. Domains may be accompanied by rotation instructions as well to model, for

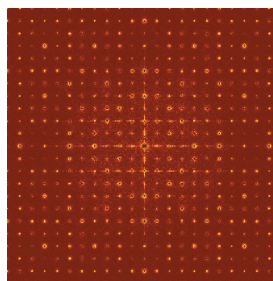


Figure 4
Difference map of simulated diffraction intensities of two clathrate models. Methane is embedded identically in every cell in one model, but perturbed randomly in the other (as in Fig. 3). *DIFFUSE* was used, outputting images with dimensions of 500×500 pixels.

computer programs

instance, interface effects at grain boundaries or mosaicity (continued in Section 3.2).

3.1. Methods of generating domains

`ConstructDomains` has two main modes of operation. The most generic one starts with a randomized structure and employs Monte Carlo methods to reorganize the domain identifiers of the abstract unit cells. The procedure works by traversing through each cell in a random order, completing one *cycle* when all cells have been visited. At each visit, the number of neighbouring cells sharing the same identifier is counted and mapped into a probability. This decides whether the visited cell will have its identifier reassigned. The mapping is governed by the option `TransitionProbabilities`, whose default values are suitable for aggregation of equal domains.

The numbers of distinct domains and iteration cycles are set by the user. When the final cycle is done, a structure representation is returned. It is also possible to capture the state at each cycle and return a complete list of generated structures.

The second type of operation is run with the keyword `SectorRegions`. This generates domains with sector-like boundaries when viewing the structure perpendicular to its domain walls. The user specifies the number of sector pairs, their angular widths and optionally an initial offset angle. It is proposed to model features observed in ferroelastic inclusion compounds (Hollingsworth *et al.*, 2005), a reconstruction of

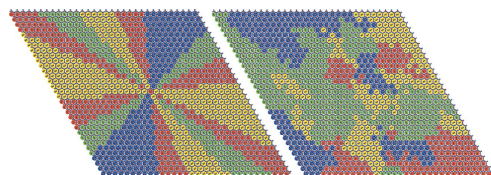


Figure 5
Two $32 \times 32 \times 3$ structures with four distinct domains, each signifying a different orientation of the guest molecule 2,10-undecanedione in a host network of urea. Both are created with `ConstructDomains` and illustrated with a combination of `CrystalPlot` and `DomainPlot`.

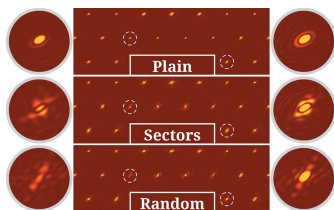


Figure 6
Extracts of X-ray simulations through *DIFFUSE* belonging to the structures of Fig. 5 in addition to a plain variant consisting entirely of a single type of guest orientation. Subtle variations in the shape of the reflections can be seen; a couple of outlined reflections have been enlarged.

which may be seen in Fig. 5 together with a model created by a regular Monte Carlo process for comparison.

That particular example incorporates 2,10-undecanedione as guest molecule, included in a host matrix of urea at a commensurate ratio of 2:3. The guests are crystallographically related by a twofold screw axis and have an orientational freedom about the tunnel axis. Each domain identifier represents a certain orientation in the model construction. Commensurability and guest adjustments are straightforwardly handled using the `EmbedStructure` function (see the supporting information for source code details).

Three associated diffraction patterns are shown in Fig. 6, one belonging to a 'plain' structure, consisting of just one type of guest orientation, while the other two correspond to the systems presented in Fig. 5.

3.2. Perturbations

Final adjustments to the model may require small rotations. It is recalled from Section 2.1 that *MaXrd* has four settings for rotation anchors. In addition to the two mentioned choices (fixing the anchor to the host or the individual guests), rotations about the origins or centroids of the domains are also possible. In all the relevant functions, the amount of rotation is controlled by the `RotationMap` option, which associates any domain index with a rotation instruction. These are to be used with `DomainPlot` or `SynthesiseStructure`.

Using `ConstructDomains` with many domains and few cycles will result in a model with numerous small domains. By applying minuscule rotations about domain centroids, a resemblance to a crystal of subgrains may be obtained.

Another function, `DistortStructure`, applies a given vector field to the atoms of an input structure. The flexibility in *Mathematica* allows for easy configuration of displacement fields that work periodically or in specific domains. Thus, point defects, modulation by displacement waves or interfaces of various degrees of coherency, including misfit dislocations, may be simulated. Presently, the function is predominantly used for illustration purposes.

3.3. Assembly

`SynthesiseStructure` is used to produce a crystalline model from an abstract domain pattern and a map between identifiers and entities. It works without any domain input as well; in the clathrate hydrate example, the host framework construction was followed by an embedding of methane molecules, resulting in a relatively small structure, or 'block'. To make a superlattice or a complete model, spanning perhaps 64^3 blocks, a list of entities representing building units in the assembly must be provided. These will be duplicated automatically to pack the structure, and their distribution on the lattice may be sequential or random.

4. Simulating diffraction patterns

Whereas the original *MaXrd* release only had a primitive function for displaying the diffraction patterns of a given

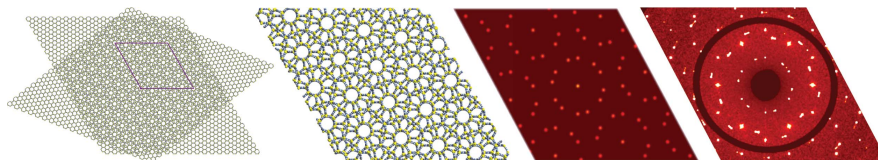


Figure 7

Reconstruction of a twin along with simulation and experimental image of reciprocal space. From left to right: the first image shows two $21 \times 21 \times 1$ slabs of thiourea stacked on top of each other, rotated 38.2° about the vertical through the centre. This thiourea lattice is that of an inclusion compound host, but with guests omitted for clarity. A $7 \times 7 \times 2$ substructure is extracted as representative of the twinned structure, and shown in the second image. The third image is a simulated diffraction pattern made with *DISCUS* and the rightmost image is a reconstruction from a real experiment.

structure, the package now relays this task to external programs, either to *DISCUS* or to *DIFFUSE*. The whole procedure of `SimulateDiffractionPattern` is designed to require only the minimum of user input: the program of choice, the crystal structure to simulate and which reciprocal plane to display.

It first exports the structure to separate file(s) (using `ExportCrystalData` internally), formatted to match the chosen program. Necessary instructions are generated for the external program, and these are executed in the background via the command shell of the system. The simulated diffraction image is finally imported to *Mathematica*. All file processing takes place in a temporary directory.

The objective of `SimulateDiffractionPattern` is to connect crystallographic data (from CIFs) with reciprocal-space maps; intermediate stages are facilitated by *MaXrd* as described. With *Mathematica* chosen as the working environment, an extensive range of functionality is at the user's disposal for further processing.

In a final example, a combination of functions is used to model the structure of the thiourea–ferrocene inclusion compound, currently under investigation. Experimental data indicate non-merohedral twinning by rotation about the *c* axis, which coincides with the hexagon-shaped-tunnel axis. Geometrical manipulations of domains are used to emulate twin operations: a supercell is copied to the top of the original, followed by a rotation. See Fig. 7 for details.

5. Conclusion

A structure composition extension has been added to the *MaXrd* package, improving its practicability. Tools are developed to build custom structures, especially targeted at clathrated host–guest systems, allowing for flexible post-processing on the *Mathematica* platform. Constructions of crystalline models aim to produce realistic reciprocal-space mappings for comparison with experimental results.

In this paper, we have elucidated some applications of the new tools through examples. Source code used to generate the figures may be found in the supporting information. Models have been made with the specific topics of inclusion

compounds, domains and twinning in mind. The package is available at <https://github.com/Stianpr20/MaXrd>.

Parts of this work were presented at the 32nd European Crystallographic Meeting in Vienna, displaying updated features at that time, and a demonstration notebook has been contributed to Wolfram's upcoming Notebook Archive (<https://notebookarchive.org>).

Acknowledgements

The authors wish to thank David Graham Nicholson for helpful chemical insight regarding the thiourea host network.

References

- Authier, A. (2013). Editor. *International Tables for Crystallography*, Vol. D, *Physical Properties of Crystals*. Chichester: Wiley.
- Goossens, D. J., Heerdegen, A. P., Chan, E. J. & Welberry, T. R. (2011). *Metall. Mater. Trans. A*, **42**, 23–31.
- Hahn, T. (2002). Editor. *International Tables for Crystallography*, Vol. A, *Space-Group Symmetry*, 5th ed. Dordrecht: Kluwer Academic Publishers.
- Herbstein, F. H. (2005). *Crystalline Molecular Complexes and Compounds: Structures and Principles*. Oxford University Press.
- Hollingsworth, M. D., Peterson, M. L., Rush, J. R., Brown, M. E., Abel, M. J., Black, A. A., Dudley, M., Raghothamachar, B., Werner-Zwanziger, U., Still, E. J. & Vanecko, J. A. (2005). *Cryst. Growth Des.* **5**, 2100–2116.
- Kótai, L., Bálint, S., Gács, I., Lakatos, G., Angyal, A. & Mehrotra, R. N. (2012). *Z. Anorg. Allg. Chem.* **638**, 648–651.
- Lenz, A. & Ojamäe, L. (2011). *J. Phys. Chem. A*, **115**, 6169–6176.
- Li, Q. (1996). PhD thesis, The Chinese University of Hong Kong.
- Maris, T., Henson, M. J., Heyes, S. J. & Prout, K. (2001). *Chem. Mater.* **13**, 2483–2492.
- Pan, Z., Desmedt, A., MacLean, E. J., Guillaume, F. & Harris, K. D. M. (2008). *J. Phys. Chem. C*, **112**, 839–847.
- Proffen, Th. & Neder, R. B. (2009). *Diffuse Scattering and Defect Structure Simulation. A Cook Book Using the Program DISCUS*. International Union of Crystallography Texts on Crystallography 11. IUCr/Oxford University Press.
- Proffen, Th. & Neder, R. B. (1997). *J. Appl. Cryst.* **30**, 171–175.
- Ramsnes, S., Larsen, H. B. & Thorkildsen, G. (2019). *J. Appl. Cryst.* **52**, 214–218.
- Sloan, E. D. & Koh, C. A. (2008). *Clathrate Hydrates of Natural Gases*, 3rd ed. Boca Raton: CRC Press.
- Yeo, L. & Harris, K. D. M. (1997). *Acta Cryst.* **B53**, 822–830.
- Yeo, L., Harris, K. D. & Kariuki, B. M. (2001). *J. Solid State Chem.* **156**, 16–25.

References

- [1] (IUCr) *Twinning CIF dictionary*. URL: https://www.iucr.org/resources/cif/dictionaries/cif_twinning (cit. on pp. 139, 140).
- [2] Takanao Asahi, Katsuhiko Hasebe and Akira Onodera. 'Crystal Structure of the High Pressure Phase VI of Thiourea'. In: *Journal of The Physical Society of Japan - J PHYS SOC JPN* 69 (Sept. 2000), pp. 2895–2899. DOI: [10.1143/JPSJ.69.2895](https://doi.org/10.1143/JPSJ.69.2895) (cit. on p. 23).
- [3] Jerry L. Atwood and Jonathan W. Steed, eds. *Encyclopedia of Supramolecular Chemistry*. Marcel Dekker Inc, 2004 (cit. on pp. 22–24).
- [4] S. W. Bailey et al. 'Report of the International Mineralogical Association (IMA)–International Union of Crystallography (IUCr) Joint Committee on Nomenclature'. In: *Acta Crystallographica Section A* 33.4 (July 1977), pp. 681–684. DOI: [10.1107/S0567739477001703](https://doi.org/10.1107/S0567739477001703) (cit. on p. 143).
- [5] Jean-François Berár et al. 'New low-temperature crystalline phase of ferrocene: Isomorphous to orthorhombic ruthenocene'. In: *The Journal of Chemical Physics* 73.1 (July 1980), pp. 438–441. DOI: <http://dx.doi.org/10.1063/1.439894> (cit. on p. 21).
- [6] J.S. Bodenheimer and W. Low. 'An experimental study of the phase transition in ferrocene'. In: *Physics Letters A* 36.4 (1971), pp. 253–254. DOI: [https://doi.org/10.1016/0375-9601\(71\)90494-4](https://doi.org/10.1016/0375-9601(71)90494-4) (cit. on p. 20).
- [7] Robert K. Bohn and Arne Haaland. 'On the molecular structure of ferrocene, Fe(C₅H₅)₂'. In: *Journal of Organometallic Chemistry* 5.5 (1966), pp. 470–476. DOI: [https://doi.org/10.1016/S0022-328X\(00\)82382-7](https://doi.org/10.1016/S0022-328X(00)82382-7) (cit. on p. 21).
- [8] Robert W. Cahn and Peter Haasen, eds. *Physical Metallurgy*. 4th ed. Amsterdam: Elsevier Science, 1996 (cit. on p. 142).
- [9] Stuart Cantrill. *An iron-clad structure*. July 2014. DOI: <https://doi.org/10.1038/nature13357>. URL: <http://www.nature.com/milestones/milecrystal/full/milecrystalho.html> (visited on 24/04/2016) (cit. on p. 19).
- [10] S. Carter and J.N. Murrell. 'The barrier to internal rotation in metallocenes'. In: *Journal of Organometallic Chemistry* 192.3 (1980), pp. 399–408. DOI: [https://doi.org/10.1016/S0022-328X\(00\)81232-2](https://doi.org/10.1016/S0022-328X(00)81232-2) (cit. on p. 20).
- [11] M. Catti and G. Ferraris. 'Twinning by merohedry and X-ray crystal structure determination'. In: *Acta Crystallographica Section A* 32.1 (Jan. 1976), pp. 163–165. DOI: [10.1107/S0567739476000326](https://doi.org/10.1107/S0567739476000326) (cit. on p. 140).
- [12] E. J. Chan and D. J. Goossens. 'A method to perform modulated structure studies using the program ZMC'. In: *Journal of Applied Crystallography* 50.6 (Dec. 2017), pp. 1834–1843. DOI: [10.1107/S1600576717015023](https://doi.org/10.1107/S1600576717015023) (cit. on pp. 88, 91).
- [13] Y. Chatani, Y. Taki and H. Tadokoro. 'Low-temperature form of urea adducts with *n*-paraffins'. In: *Acta Crystallographica Section B* 33.1 (Jan. 1977), pp. 309–311. DOI: [10.1107/S0567740877003501](https://doi.org/10.1107/S0567740877003501) (cit. on p. 110).
- [14] Rene Clement, Renee Claude and Charles Mazieres. 'Clathration of ferrocene and nickelocene in a thiourea host lattice'. In: *J. Chem. Soc., Chem. Commun.* (16 1974), pp. 654–655. DOI: [10.1039/C39740000654](https://doi.org/10.1039/C39740000654) (cit. on pp. 23, 27, 28).
- [15] R. Clément et al. 'Phase changes and molecular motion in the thiourea-cyclohexane inclusion compound'. In: *The Journal of Chemical Physics* 67.11 (1977), pp. 5381–5385. DOI: [10.1063/1.434645](https://doi.org/10.1063/1.434645) (cit. on pp. 28, 29, 73, 132).
- [16] A. Desmedt et al. 'Phase transitions and molecular dynamics in the cyclohexane/thiourea inclusion compound'. In: *Phys. Rev. B* 64 (5 July 2001), p. 054106. DOI: [10.1103/PhysRevB.64.054106](https://doi.org/10.1103/PhysRevB.64.054106) (cit. on pp. 29, 30, 132).
- [17] Oleg V. Dolomanov et al. 'OLEX2: a complete structure solution, refinement and analysis program'. In: *Journal of Applied Crystallography* 42.2 (Apr. 2009), pp. 339–341. DOI: [10.1107/S0021889808042726](https://doi.org/10.1107/S0021889808042726) (cit. on pp. 57, 60).
- [18] Michael G. B. Drew, Astrid Lund and David G. Nicholson. 'Molecular Modelling Studies on the Thiourea/ Ferrocene Clathrate'. In: *Supramolecular Chemistry* 8.3 (1997), pp. 197–212. DOI: [10.1080/10610279708034937](https://doi.org/10.1080/10610279708034937) (cit. on pp. 23, 26, 28, 97).
- [19] Jack David Dunitz and L. E. Orgel. 'Bis-cyclopentadienyl Iron: a Molecular Sandwich'. In: *Nature* 171.4342 (1953), pp. 121–122 (cit. on p. 19).
- [20] Jack David Dunitz, L. E. Orgel and A. Rich. 'The crystal structure of ferrocene'. In: *Acta Crystallographica* 9.4 (Apr. 1956), pp. 373–375. DOI: [10.1107/S0365110X56001091](https://doi.org/10.1107/S0365110X56001091) (cit. on pp. 19, 20).
- [21] S. Durovic, P. Krishna and D. Pandey. 'Layer stacking'. In: *Mathematical, Physical and Chemical Tables*. Ed. by Edward Prince. 3rd ed. Vol. C. International Tables for Crystallography. Springer, 2004. Chap. 9.2, pp. 752–773. DOI: <https://doi.org/10.1107/9780955360206000103> (cit. on p. 142).
- [22] Vadim Dyadkin et al. 'A new multipurpose diffractometer PILATUS@SNBL'. In: *Journal of Synchrotron Radiation* 23.3 (May 2016), pp. 825–829. DOI: [10.1107/S1600577516002411](https://doi.org/10.1107/S1600577516002411) (cit. on p. 34).
- [23] J. W. Edwards, G. L. Kington and R. Mason. 'The thermodynamic properties of ferrocene. Part 1.—The low-temperature transition in ferrocene crystals'. In: *Trans. Faraday Soc.* 56 (0 1960), pp. 660–667. DOI: [10.1039/TF9605600660](https://doi.org/10.1039/TF9605600660) (cit. on p. 20).
- [24] Philip Frank Eiland and Ray Pepinsky. 'X-Ray Examination of Iron Biscyclopentadienyl'. In: *Journal of the American Chemical Society* 74.19 (Oct. 1952), pp. 4971–4971. DOI: [10.1021/ja01139a527](https://doi.org/10.1021/ja01139a527) (cit. on p. 19).
- [25] Helmut Föll. *Defects in Crystals*. URL: https://www.tf.uni-kiel.de/matwis/amat/def_en/index.html (visited on 10/2019) (cit. on pp. 142, 143).
- [26] Georges Friedel. *Leçons de Cristallographie*. Paris: Berger-Levrault, 1926 (cit. on p. 139).
- [27] T C Gibb. 'Anisotropic relaxation of the electric field gradient tensor in the 57 Fe Mossbauer spectra of a thiourea-ferrocene clathrate'. In: *Journal of Physics C: Solid State Physics* 9.13 (July 1976), pp. 2627–2642. DOI: [10.1088/0022-3719/9/13/022](https://doi.org/10.1088/0022-3719/9/13/022) (cit. on pp. 25–27, 127).
- [28] D. J. Goossens et al. 'Monte Carlo Modelling of Diffuse Scattering from Single Crystals: The Program ZMC'. In: *Metallurgical and Materials Transactions A* 42 (2011), pp. 23–31. DOI: [10.1007/s11661-010-0199-1](https://doi.org/10.1007/s11661-010-0199-1) (cit. on p. 115).
- [29] Arne Haaland and J.E. Nilsson. 'The Determination of Barriers to Internal Rotation by Means of Electron Diffraction. Ferrocene and Ruthenocene'. In: *Acta Chemica Scandinavica* 22 (1968), pp. 2653–2670. DOI: [10.3891/acta.chem.scand.22-2653](https://doi.org/10.3891/acta.chem.scand.22-2653) (cit. on p. 21).
- [30] Theo Hahn, ed. *Space-Group Symmetry*. 5th. Vol. A. International Tables for Crystallography. Kluwer Academic Publishers, 2002 (cit. on p. 73).

- [31] Theo Hahn and H. Klapper. 'Twinning of crystals'. In: *Physical Properties of Crystals*. Ed. by Edward Prince. 2nd ed. Vol. D. International Tables for Crystallography. Wiley, 2013. Chap. 3.3, pp. 413–483. doi: <http://dx.doi.org/10.1107/9780955360206000113> (cit. on pp. 138, 139, 141, 143).
- [32] Kenneth D. M. Harris. 'Towards a Fundamental Understanding of Urea and Thiourea inclusion Compounds'. In: *Journal of the Chinese Chemical Society* 46.1 (1999), pp. 5–22. doi: <https://doi.org/10.1002/jccs.199900002> (cit. on pp. 24, 27, 72, 91, 132).
- [33] Kenneth D.M. Harris. 'Investigation of a time-dependent "nondiscrete" component of X-ray scattering from monohalocyclohexane/thiourea inclusion compounds'. In: *Journal of Solid State Chemistry* 84.2 (1990), pp. 280–288. doi: [https://doi.org/10.1016/0022-4596\(90\)90326-S](https://doi.org/10.1016/0022-4596(90)90326-S) (cit. on p. 30).
- [34] Frank H. Herbstein. *Crystalline Molecular Complexes and Compounds: Structures and Principles*. Oxford University Press, 2005 (cit. on pp. 22–24).
- [35] Stephen J. Heyes, Nigel J. Clayden and Christopher M. Dobson. 'Ferrocene molecular reorientation in the (thiourea)₃-ferrocene inclusion compound as studied by deuteron NMR spectroscopy'. In: *The Journal of Physical Chemistry* 95 (Feb. 1991), pp. 1547–1554. doi: [10.1021/j100157a009](https://doi.org/10.1021/j100157a009) (cit. on pp. 23, 26, 27, 97, 127).
- [36] Mark D. Hollingsworth et al. 'Memory and Perfection in Ferroelastic Inclusion Compounds'. In: *Crystal Growth & Design* 5.6 (Nov. 2005), pp. 2100–2116. doi: [10.1021/cg050347j](https://doi.org/10.1021/cg050347j) (cit. on p. 114).
- [37] Edward Hough and David G. Nicholson. 'X-Ray crystallographic studies on ferrocene included in a thiourea host lattice'. In: *J. Chem. Soc., Dalton Trans.* (1 1978), pp. 15–18. doi: [10.1039/DT9780000015](https://doi.org/10.1039/DT9780000015) (cit. on pp. 22, 26–28, 34, 98, 110, 132).
- [38] Jürg Hulliger, Olaf König and Ralf Hoss. 'Polar inclusion compounds of perhydroptriphénylene (phtp) and efficient nonlinear optical molecules***'. In: *Advanced Materials* 7.8 (1995), pp. 719–721. doi: [10.1002/adma.19950070807](https://doi.org/10.1002/adma.19950070807) (cit. on p. 23).
- [39] Matthew J. Jones, Ian J. Shannon and Kenneth D. M. Harris. 'Temperature-dependent structural properties of the chlorocyclohexane/thiourea inclusion compound investigated by synchrotron X-ray powder diffraction'. In: *J. Chem. Soc., Faraday Trans.* 92 (2 1996), pp. 273–279. doi: [10.1039/FT9962000273](https://doi.org/10.1039/FT9962000273) (cit. on pp. 28, 29, 73, 132).
- [40] Thomas J. Kealy and Peter L. Pauson. 'A New Type of Organo-Iron Compound'. In: *Nature* 168.4285 (1951), pp. 1039–1040. doi: [10.1038/1681039b0](https://doi.org/10.1038/1681039b0) (cit. on p. 19).
- [41] H. Klapper and Th. Hahn. 'The application of *eigensymmetries* of face forms to X-ray diffraction intensities of crystals twinned by 'reticular merohedry''. In: *Acta Crystallographica Section A* 68.1 (Jan. 2012), pp. 82–109. doi: [10.1107/S0108767311032454](https://doi.org/10.1107/S0108767311032454) (cit. on pp. 48, 49, 141, 142).
- [42] Thomas Kluyver et al. 'Jupyter Notebooks – a publishing format for reproducible computational workflows'. In: *Positioning and Power in Academic Publishing: Players, Agents and Agendas*. Ed. by Fernando Loizides and Birgit Schmidt. Netherlands: IOS Press, 2016, pp. 87–90 (cit. on p. 79).
- [43] Donald E. Knuth. 'Computer Programming as an Art'. In: *Commun. ACM* 17.12 (Dec. 1974), pp. 667–673. doi: [10.1145/361604.361612](https://doi.org/10.1145/361604.361612) (cit. on p. viii).
- [44] E. Koch. 'Twinning'. In: *Mathematical, Physical and Chemical Tables*. Ed. by Edward Prince. 3rd ed. Vol. C. International Tables for Crystallography. Springer, 2004. Chap. 1.3, pp. 10–14. doi: <https://doi.org/10.1107/9780955360206000103> (cit. on pp. 139, 140, 142).
- [45] N. R. Kunchur and Mary R. Truter. '517. A detailed refinement of the crystal and molecular structure of thiourea'. In: *J. Chem. Soc.* (o 1958), pp. 2551–2557. doi: [10.1039/JR9580002551](https://doi.org/10.1039/JR9580002551) (cit. on p. 23).
- [46] Logan C. Lorson, Onkei Tai and Bruce M. Foxman. 'Use of Topotactic Phase Transformations To Obtain Solutions of the Crystal Structures of Highly Disordered Materials'. In: *Crystal Growth & Design* 18.1 (2018), pp. 409–415. doi: [10.1021/acs.cgd.7b01406](https://doi.org/10.1021/acs.cgd.7b01406) (cit. on pp. 24–28, 64–66, 71, 72, 97, 110, 131).
- [47] Michael D. Lowery et al. 'Dynamics of ferrocene in a thiourea inclusion matrix'. In: *Journal of the American Chemical Society* 112.11 (May 1990), pp. 4214–4225. doi: [10.1021/ja00167a017](https://doi.org/10.1021/ja00167a017) (cit. on pp. 25–27, 91, 97).
- [48] T. Maris et al. 'Investigations of the Phase Transitions in Thiourea Inclusion Compounds with Cycloheptane, Cyclooctane, and Cyclooctanone'. In: *Chemistry of Materials* 13.8 (July 2001), pp. 2483–2492. doi: [10.1021/cm991173u](https://doi.org/10.1021/cm991173u) (cit. on pp. 28, 29, 100, 132).
- [49] Samuel A. Miller, John A. Tebboth and John F. Tremaine. '114. Dicyclopentadienyliron'. In: *J. Chem. Soc.* (o 1952), pp. 632–635. doi: [10.1039/JR9520000632](https://doi.org/10.1039/JR9520000632) (cit. on p. 19).
- [50] Annibale Mottana et al., eds. *Micas: Crystal Chemistry & Metamorphic Petrology*. Berlin, Boston: De Gruyter, 2018. doi: <https://doi.org/10.1515/978151509070> (cit. on pp. 48, 139, 140, 142).
- [51] Peter Müller et al. *Crystal Structure Refinement: A Crystallographer's Guide to SHELXL*. Ed. by Peter Müller. Oxford University Press, 2010 (cit. on p. 61).
- [52] T. Nakai et al. 'A ¹³C NMR study of the dynamic structure of the thiourea-ferrocene inclusion compound'. In: *Chemical Physics Letters* 132.6 (1986), pp. 554–557. doi: [https://doi.org/10.1016/0009-2614\(86\)87123-8](https://doi.org/10.1016/0009-2614(86)87123-8) (cit. on pp. 26, 27, 97).
- [53] M. Nespolo, T. Kogure and G. Ferraris. 'Allorwinning: oriented crystal association of polytypes – some warnings on consequences'. In: *Zeitschrift für Kristallographie – Crystalline Materials* 214.1 (Jan. 1999), pp. 5–8. doi: <https://doi.org/10.1524/zkri.1999.214.1.5> (cit. on pp. 140, 142, 143).
- [54] M. Nespolo et al. 'Plesiotwinning: oriented crystal associations based on a large coincidence-site lattice'. In: *Zeitschrift für Kristallographie – Crystalline Materials* 214.7 (Jul. 1999), pp. 378–382. doi: <https://doi.org/10.1524/zkri.1999.214.7.378> (cit. on pp. 48, 140, 143).
- [55] Massimo Nespolo. *MaThCryst: Crystal twinning – International Union of Crystallography, Commission on Mathematical and Theoretical Crystallography*. URL: <http://www.crystallography.fr/mathcryst/twins.htm> (visited on 03/02/2009) (cit. on p. 142).
- [56] Massimo Nespolo. 'Plesiotwins versus diperiodic twins'. In: *Acta Crystallographica Section A* 74.4 (July 2018), pp. 332–344. doi: [10.1107/S205327318005351](https://doi.org/10.1107/S205327318005351) (cit. on pp. 138, 140, 143).
- [57] Massimo Nespolo and Giovanni Ferraris. 'Overlooked problems in manifold twins: twin misfit in zero-obliquity TLQS twinning and twin index calculation'. In: *Acta Crystallographica Section A* 63.3 (May 2007), pp. 278–286. doi: [10.1107/S0108767307012135](https://doi.org/10.1107/S0108767307012135) (cit. on p. 139).
- [58] Massimo Nespolo and Giovanni Ferraris. 'The derivation of twin laws in non-merohedric twins. Application to the analysis of hybrid twins'. In: *Acta Crystallographica Section A* 62.5 (Sept. 2006), pp. 336–349. doi: [10.1107/S0108767306023774](https://doi.org/10.1107/S0108767306023774) (cit. on p. 141).
- [59] Fischer E. O. and Pfäb W. 'Cyclopentadien-Metallkomplexe, ein neuer Typ metallorganischer Verbindungen'. In: *Zeitschrift für Naturforschung B* 7 (1952), pp. 377–379. doi: [10.1515/znbb-1952-0701](https://doi.org/10.1515/znbb-1952-0701) (cit. on p. 19).

- [60] Kouji Ogasahara, Michio Sorai and Hiroshi Suga. 'New finding of a stable low-temperature phase in ferrocene crystal'. In: *Chemical Physics Letters* 68.2 (Dec. 1979), pp. 457–460. doi: [https://doi.org/10.1016/0009-2614\(79\)87237-1](https://doi.org/10.1016/0009-2614(79)87237-1) (cit. on pp. 20, 21).
- [61] Jun Okuda. 'Ferrocene – 65 Years After'. In: *European Journal of Inorganic Chemistry* 2017.2 (2017), pp. 217–219. doi: [10.1002/ejic.201601323](https://doi.org/10.1002/ejic.201601323) (cit. on p. 19).
- [62] P. Seiler and J. D. Dunitz. 'Low-temperature crystallization of orthorhombic ferrocene: structure analysis at 98 K'. In: *Acta Crystallographica Section B* 38.6 (June 1982), pp. 1741–1745. doi: [10.1107/S0567740882007080](https://doi.org/10.1107/S0567740882007080) (cit. on pp. 20, 21).
- [63] Damian Paliwoda et al. 'U-Turn Compression to a New Isostructural Ferrocene Phase'. In: *The Journal of Physical Chemistry Letters* 4.23 (2013), pp. 4032–4037. doi: [10.1021/jz402254b](https://doi.org/10.1021/jz402254b) (cit. on pp. 20, 21).
- [64] Benjamin A. Palmer et al. 'An incommensurate thiourea inclusion compound'. In: *Chem. Commun.* 47 (13 2011), pp. 3760–3762. doi: [10.1039/C0CC05477A](https://doi.org/10.1039/C0CC05477A) (cit. on p. 72).
- [65] Benjamin A. Palmer et al. 'Structural Rationalization of the Phase Transition Behavior in a Solid Organic Inclusion Compound: Bromocyclohexane-/Thiourea'. In: *Crystal Growth & Design* 12.2 (Feb. 2012), pp. 577–582. doi: [10.1021/cg201656y](https://doi.org/10.1021/cg201656y) (cit. on pp. 28, 29, 71, 72, 132).
- [66] Zhigang Pan et al. 'Structural Properties of Low-Temperature Phase Transitions in the Prototypical Thiourea Inclusion Compound: Cyclohexane-/Thiourea'. In: *The Journal of Physical Chemistry C* 112.3 (2008), pp. 839–847. doi: [10.1021/jp076706y](https://doi.org/10.1021/jp076706y) (cit. on pp. 28–30, 100, 132).
- [67] Simon Parsons. 'Introduction to twinning'. In: *Acta Crystallographica Section D* 59.11 (Nov. 2003), pp. 1995–2003. doi: [10.1107/S0907444903017657](https://doi.org/10.1107/S0907444903017657) (cit. on p. 138).
- [68] Peter L. Pauson. 'Ferrocene—how it all began'. In: *Journal of Organometallic Chemistry* 637–639 (2001), pp. 3–6. doi: [https://doi.org/10.1016/S0022-328X\(01\)0126-3](https://doi.org/10.1016/S0022-328X(01)0126-3) (cit. on p. 19).
- [69] Fernando Pérez and Brian E. Granger. 'IPython: a System for Interactive Scientific Computing'. In: *Computing in Science and Engineering* 9.3 (May 2007), pp. 21–29. doi: [10.1109/MCSE.2007.53](https://doi.org/10.1109/MCSE.2007.53) (cit. on p. 79).
- [70] Václav Petrášek, Michal Dušek and Lukáš Palatinus. 'Crystallographic Computing System JANA2006: General features'. In: *Zeitschrift für Kristallographie - Crystalline Materials* 229.5 (2014), pp. 345–352. doi: [doi:10.1515/zkri-2014-1737](https://doi.org/10.1515/zkri-2014-1737) (cit. on p. 68).
- [71] Thomas Proffen and Reinhard B. Neder. *Diffuse Scattering and Defect Structure Simulations: A Cook Book Using the Program DISCUS*. International Union of Crystallography Texts on Crystallography. Oxford University Press, Jan. 2009 (cit. on p. 88).
- [72] Thomas Proffen and Reinhard B. Neder. 'DISCUS: a program for diffuse scattering and defect-structure simulation'. In: *Journal of Applied Crystallography* 30.2 (Apr. 1997), pp. 171–175. doi: [10.1107/S002188989600934X](https://doi.org/10.1107/S002188989600934X) (cit. on pp. 88, 91).
- [73] *Queen star bands in science PhD*. Aug. 2007. URL: <http://news.bbc.co.uk/1/hi/entertainment/6929290.stm> (visited on 03/08/2007) (cit. on p. ix).
- [74] Stian Ramsnes. 'Aspects of X-Ray Diffraction Using Mathematica'. MA thesis. University of Stavanger, June 2016 (cit. on pp. 33, 34, 59).
- [75] Stian Ramsnes, Helge Bøvik Larsen and Gunnar Thorkildsen. 'Using Mathematica as a platform for crystallographic computing'. In: *Journal of Applied Crystallography* 52.1 (Feb. 2019), pp. 214–218. doi: [10.1107/S1600576718018071](https://doi.org/10.1107/S1600576718018071) (cit. on pp. xiii, 82, 84, 155).
- [76] Stian Penev Ramsnes, Helge Bøvik Larsen and Gunnar Thorkildsen. 'MaXrd updated with emphasis on model construction and reciprocal-space simulations'. In: *Journal of Applied Crystallography* 53.6 (Dec. 2020), pp. 1620–1624. doi: [10.1107/S160057672001328X](https://doi.org/10.1107/S160057672001328X) (cit. on pp. xiii, 155).
- [77] Stian Penev Ramsnes et al. 'Complementary Synchrotron Diffraction and Simulation Studies on a Ferrocene:Thiourea Inclusion Compound'. To be published. 2022 (cit. on pp. xiv, 155).
- [78] Herbst-Irmer Regine. 'Twinning in chemical crystallography – a practical guide'. In: *Zeitschrift für Kristallographie - Crystalline Materials* 231 (2016), pp. 573–581. doi: [10.1515/zkri-2016-1947](https://doi.org/10.1515/zkri-2016-1947) (cit. on pp. 140, 142).
- [79] Heiko Röss and Martin Zimmermann. *High Resolution X-ray Diffractometry*. www.bruker-webinars.com. Mar. 2011 (cit. on p. 43).
- [80] Rigaku OD. *Crysalis PRO*. Rigaku Oxford Diffraction. Yarnton, England, 2015 (cit. on pp. 34, 60).
- [81] Anabel Morte Ródenas. 'Solid-State Studies of Inclusion Compounds and Other Organic Materials'. PhD thesis. Cardiff University, Feb. 2011 (cit. on p. 24).
- [82] E. A. Seibold and L. E. Sutton. 'Structure of Ferrocene'. In: *The Journal of Chemical Physics* 23.10 (1955), p. 1967. doi: [10.1063/1.1740629](https://doi.org/10.1063/1.1740629) (cit. on p. 21).
- [83] P. Seiler and J. D. Dunitz. 'A new interpretation of the disordered crystal structure of ferrocene'. In: *Acta Crystallographica Section B* 35.5 (May 1979), pp. 1068–1074. doi: [10.1107/S0567740879005598](https://doi.org/10.1107/S0567740879005598) (cit. on p. 20).
- [84] P. Seiler and J. D. Dunitz. 'Redetermination of the ruthenocene structure at room temperature and at 101 K: molecular internal motion'. In: *Acta Crystallographica Section B* 36.12 (Dec. 1980), pp. 2946–2950. doi: [10.1107/S0567740880010588](https://doi.org/10.1107/S0567740880010588) (cit. on p. 21).
- [85] P. Seiler and J. D. Dunitz. 'The structure of trislinic ferrocene at 101, 123 and 148 K'. In: *Acta Crystallographica Section B* 35.9 (Sept. 1979), pp. 2020–2032. doi: [10.1107/S0567740879008384](https://doi.org/10.1107/S0567740879008384) (cit. on pp. 20, 21).
- [86] Madhumati Sevvana et al. 'Non-merohedral twinning: from minerals to proteins'. In: *Acta Crystallographica Section D* 75.12 (Dec. 2019), pp. 1040–1050. doi: [10.1107/S2059979819010179](https://doi.org/10.1107/S2059979819010179) (cit. on pp. 141, 142).
- [87] George M. Sheldrick. 'A short history of SHELX'. In: *Acta Crystallographica Section A* 64.1 (Jan. 2008), pp. 112–122. doi: [10.1107/S0108767307043930](https://doi.org/10.1107/S0108767307043930) (cit. on p. 57).
- [88] George M. Sheldrick. 'Crystal structure refinement with SHELXL'. In: *Acta Crystallographica Section C* 71.1 (Jan. 2015), pp. 3–8. doi: [10.1107/S205329614024218](https://doi.org/10.1107/S205329614024218) (cit. on p. 60).
- [89] George M. Sheldrick. 'SHELXT – Integrated space-group and crystal-structure determination'. In: *Acta Crystallographica Section A* 71.1 (Jan. 2015), pp. 3–8. doi: [10.1107/S2053273314026370](https://doi.org/10.1107/S2053273314026370) (cit. on p. 60).
- [90] Michio Sorai, Kouji Ogasahara and Hiroshi Suga. 'Heat Capacity and Phase Transitions of Thiourea-Ferrocene Channel Inclusion Compound'. In: *Molecular Crystals and Liquid Crystals* 73.3–4 (1981), pp. 231–254. doi: [10.1080/00268948108072337](https://doi.org/10.1080/00268948108072337) (cit. on pp. 25, 27, 33, 36, 38, 42, 43, 53, 54, 112, 131, 132).

- [91] M. R. Srinivasan et al. 'Studies on the phase transitions in thiourea'. In: *Ferroelectrics* 21.1 (1978), pp. 539–541. DOI: [10.1080/00150197808237322](https://doi.org/10.1080/00150197808237322) (cit. on p. 23).
- [92] F. Takusagawa and T. F. Koetzle. 'A neutron diffraction study of the crystal structure of ferrocene'. In: *Acta Crystallographica Section B* 35.5 (May 1979), pp. 1074–1081. DOI: [10.1107/S0567740879005604](https://doi.org/10.1107/S0567740879005604) (cit. on p. 21).
- [93] Hanna Tomkowiak and Andrzej Katrusiak. 'High-Pressure Transformations and the Resonance Structure of Thiourea'. In: *The Journal of Physical Chemistry C* 122.9 (Mar. 2018), pp. 5064–5070. DOI: [10.1021/acs.jpcc.8b00452](https://doi.org/10.1021/acs.jpcc.8b00452) (cit. on p. 23).
- [94] *Twin element - Online Dictionary of Crystallography*. URL: https://dictionary.iucr.org/Twin_element (visited on 20/11/2017) (cit. on p. 139).
- [95] *Twin operation - Online Dictionary of Crystallography*. URL: https://dictionary.iucr.org/Twin_operation (visited on 28/10/2020) (cit. on p. 138).
- [96] Srivathsa Vaidya. 'Clathrates —An exploration of the chemistry of caged compounds'. In: *Resonance* 9.7 (2004), pp. 18–31. DOI: [10.1007/BF02903573](https://doi.org/10.1007/BF02903573) (cit. on p. 23).
- [97] Geoffrey Wilkinson et al. 'The Structure of Iron Bis-Cyclopentadienyl'. In: *Journal of the American Chemical Society* 74.8 (1952), pp. 2125–2126. DOI: [10.1021/ja01128a527](https://doi.org/10.1021/ja01128a527) (cit. on p. 19).
- [98] B. T. M. Willis. 'Three-dimensional neutron diffraction study of ferrocene'. In: *Acta Crystallographica* 13.12 (Dec. 1960), p. 1088. DOI: [10.1107/S0365110X60002430](https://doi.org/10.1107/S0365110X60002430) (cit. on p. 21).
- [99] Ralph Walter Graystone Wyckoff and Robert B. Corey. 'The Crystal Structure of Thiourea'. In: *Zeitschrift für Kristallographie - Crystalline Materials* 81 (Oct. 1932), pp. 386–395 (cit. on p. 23).
- [100] Lily Yeo, Kenneth D.M. Harris and Benson M. Kariuki. 'Temperature-Dependent Structural Properties and Crystal Twinning in the Fluorocyclohexane/Thiourea Inclusion Compound'. In: *Journal of Solid State Chemistry* 156.1 (Jan. 2001), pp. 16–25. DOI: <https://doi.org/10.1006/jssc.2000.8951> (cit. on pp. 28, 29, 39, 132).
- [101] Z. Zikmund. 'Symmetry of domain pairs and domain twins'. In: *Czechoslovak Journal of Physics B* 34.9 (1984), pp. 932–949. DOI: [10.1007/BF01589823](https://doi.org/10.1007/BF01589823) (cit. on p. 140).

List of symbols

<p>[<i>i</i>] (twin) index (alternative symbol) 139</p> <p>δ twin misfit 139</p> <p>Γ density of coincidence sites per unit area 142</p> <p>ω obliquity 139</p> <p>Σ coincidence index 142</p> <p>Ξ coincidence index (alternative to Σ) . . . 142</p> <p>k twin operation 138</p> <p>m (twin) index (alternative symbol) 139</p> <p>n (twin) index (alternative symbol) 139</p> <p>ADP atomic displacement parameters 58</p>	<p>CSL coincidence site lattice 142</p> <p>DSC displacement shift complete 142</p> <p>ESRF European Synchrotron Radiation Facility 34</p> <p>TFIC thiourea–ferrocene inclusion compound 22</p> <p>TFIC-1 (-2, -3) reference to our three TFIC crystal samples 34</p> <p>TLQS twin lattice quasi-symmetry 139</p> <p>\mathcal{H} eigensymmetry 138</p> <p>\mathcal{H}^* intersection symmetry group 138</p>
---	---

Index

- A**
allotwin indices I43
allotwinning I43
- B**
binary adduct 22
block 84
BraggAngle 82
- C**
clathrate 22
coincidence index I42
coincidence site lattice 47, I42
coincident reflection I41
composite symmetry I38
composition plane/surface *see* twin interface
ConstructDomains 86
crystallographic binary file 34
CrystalPlot 83
cyclic twin I39
- D**
displacement shift complete I42
DistortStructure 85
domain 86
domain boundary/interface *see* twin interface
DomainPlot 86
double cone structure *see* sandwich compound
- E**
edifice I38
eigensymmetry I38
EmbedStructure 84
entity 83
epitaxy I43
ExpandCrystal 83, 84
- F**
ferrocene 19
fragment *see* block
- G**
GetAtomCoordinates 82
GetSymmetryData 82
grain 86
- I**
ImportCrystalData 82
inclusion compound 22
index *see* twin index
- M**
mallard's law 139
- maxrd 79
merohedry *see* twin by merohedry
metallocene 19
molecular complexes 22
molecular compounds 22
mosaicity II9
multiple twins I39
- N**
non-merohedric twinning I41
- O**
obliquity I39
obverse–reverse twinning I41
oriented intergrowth *see* syntaxy
oriented overgrowth *see* epitaxy
- P**
pentafulvalene 19
planar coincidence site density I42
plesiotwin I43
polymorphism I42
polysynthetic twin I39
polytype I42
premature optimisation viii
pseudo-merohedry I40
pseudo-orthorhombic I40
pseudo-tetragonal I40
- R**
repeated twin *see* multiple twin
ResetCrystalData 82
restored (lattice nodes) I38
reticular merohedry I40
reticular pseudo-merohedry I41
- S**
sandwich structure 19
simple twins I39
SimulateDiffractionPattern 88
single crystal I38
single reflection I41
soft host 23
subgrain 86
supercell *see* block, 86
syntaxy I43
SynthesiseStructure 86
- T**
thiourea 23
thiourea–ferrocene inclusion compound 22
topotaxy I43
transformation twins I40
trefoil pattern 41, 43

tunnel inclusion complex 22

twin 138

twin action *see* twin operation

twin boundary *see* twin interface

twin by merohedry 140

twin element 139

twin index 139

twin interface 139

twin law 138

twin misfit 139

twin operation 138

U

unwarp 33

W

Wolfram Language 79

